Universidad de Oviedo

TESIS DOCTORAL
Programa de Doctorado en Energía y Control de Procesos

Alternativas de Métodos de Control para Plantas Fotovoltaicas Híbridas de Nueva Generación con Almacenamiento de Energía

Daniel del Rivero Peña

Gijón, Diciembre 2024

Universidad de Oviedo

Departamento de Ingeniería Eléctrica, Electrónica, de Comunicaciones y de Sistemas

Programa de Doctorado en Energía y Control de Procesos

Alternativas de Métodos de Control para Plantas Fotovoltaicas Híbridas de Nueva Generación con Almacenamiento de Energía

Daniel del Rivero Peña

Director: Pablo García Fernández.
Departamento de Ingeniería Eléctrica, Electrónica,
de Comunicaciones y de Sistemas
Director: Ángel Navarro Rodríguez.
Departamento de Ingeniería Eléctrica, Electrónica,
de Comunicaciones y de Sistemas

Gijón, Diciembre 2024

Universidad de Oviedo

RESUMEN DEL CONTENIDO DE TESIS DOCTORAL

1.- Título de la Tesis	
Español: **Alternativas de Métodos de Control para Plantas Fotovoltaicas Híbridas de Nueva Generación con Almacenamiento de Energía**	Inglés: **Control Method Alternatives for Next Generation Hybrid PV Plants with Energy Storage**

2.- Autor	
Nombre: **Daniel del Rivero Peña**	
Programa de Doctorado: **Energía y Control de Procesos**	
Órgano responsable: **Centro Internacional de Postgrado**	

RESUMEN (en español)

La adopción masiva de sistemas de generación distribuida en los sistemas de potencia responde tanto a la lucha contra el cambio climático como a la necesidad de reducir la dependencia de los combustibles fósiles. Este impulso hacia soluciones energéticas más sostenibles y respetuosas con el medio ambiente se refuerza por la creciente concienciación sobre la reducción de emisiones de gases de efecto invernadero y la madurez tecnológica de fuentes renovables como la fotovoltaica (PV) y la eólica. A medida que estas tecnologías avanzan, sus costos disminuyen, lo que ha facilitado su implementación a gran escala en los sistemas de generación de energía.

No obstante, la transición hacia estas tecnologías renovables conlleva ciertos desafíos, especialmente en términos de estabilidad de las redes eléctricas. A diferencia de los generadores síncronos tradicionales, que aportan inercia y amortiguamiento gracias a su masa rotante, los recursos basados en inversores (IBR) de potencia carecen de estos atributos. Esto puede hacer que las redes eléctricas sean más vulnerables ante perturbaciones. La falta de inercia y amortiguamiento ha impulsado el desarrollo de tecnologías que puedan emular estas características, habitualmente mediante el uso de sistemas de almacenamiento de energía. Esta emulación de inercia se consigue aplicando el concepto de Generador Síncrono Virtual (VSG).

A lo largo de los años, se han desarrollado diversos sistemas VSG. Sin embargo, esta tesis se centra en un sistema específico, el Synchronous Central Angle Controller (SCAC), que presenta un enfoque distribuido. En este sistema, un controlador central ubicado en el punto de conexión (PoC) gestiona de forma remota varios generadores distribuidos mediante controladores locales. Esto permite que los generadores actúen como un solo ente, ajustando parámetros en el PoC para garantizar un funcionamiento coordinado.

En esta tesis, primero se realiza una revisión de las necesidades del sistema para la implementación de este tipo de controladores, así como de las alternativas existentes en la actualidad. Una vez se establezca el panorama de las alternativas, se procede a una explicación exhaustiva del SCAC.
Posteriormente, se aplica este sistema de control a un sistema de generación distribuido, adaptando el SCAC para su uso en convertidores comerciales, lo que permitirá verificar su comportamiento bajo diversas condiciones. Esta evaluación considera también los retrasos de comunicación entre el controlador central y los locales, los cuales son compensados mediante métodos basados en el predictor Smith. El sistema es validado tanto en simulaciones como experimentalmente, utilizando sistemas en tiempo real, Hardware-in-the-Loop, Power-Hardware-in-the-Loop y montajes de laboratorio a escala.

Después de la validación, el uso del SCAC se extiende a otras aplicaciones, como la compensación de rampas en la generación solar. Las rampas de generación, que se originan principalmente por variaciones climáticas, pueden causar inestabilidades en la red y dar lugar a penalizaciones por parte de los operadores de red. La solución propuesta incluye el uso de almacenamiento energético conectado a las plantas solares para compensar dichas rampas y así mantener la estabilidad del sistema.

Finalmente, el sistema SCAC es adaptado para funcionar en una configuración Grid-Forming, con el objetivo de crear una red aislada para la producción de hidrógeno verde. Este sistema aprovecha la generación solar para alimentar un electrolizador, y se implementa un controlador droop dual para que el electrolizador se comporte como una carga flexible, ajustando su consumo en función de la potencia y energía disponible. La solución es probada considerando también los retrasos de comunicación entre el controlador central y los locales, asegurando así la estabilidad y eficiencia del sistema bajo condiciones realistas.

Además, se implementa el sistema de control en una simulación con una red externa, aprovechando las ventajas introducidas por sistemas de simulación ofrecidos por OPAL-RT, permitiendo y explicando el funcionamiento de una cosimulación entre dos simuladores usando dominios de simulación diferentes.

En resumen, con todos estos experimentos y simulaciones, se valida la eficacia del sistema SCAC para gestionar redel eléctricas distribuidas, proporcionando resultados satisfactorios, incluso con la inclusión de los retrasos de comunicación, demostrando ser una solución robusta y flexible para la gestión de redes distribuidas con alta penetración de energías renovables como son los generadores PV híbridos, coordinando varios generadores de forma centralizada.

RESUMEN (en inglés)

The massive adoption of distributed generation systems in power systems responds to both the fight against climate change and the need to reduce dependence on fossil fuels. This drive towards more sustainable and environmentally friendly energy solutions is reinforced by the growing awareness of greenhouse gas emissions reduction and the technological maturity of renewable sources such as photovoltaic (PV) and wind. As these technologies advance, their costs are decreasing, which has facilitated their large-scale deployment in power generation systems.

However, the transition to these renewable technologies brings with it certain challenges, especially in terms of grid stability. Unlike traditional synchronous generators, which provide inertia and damping due to their rotating mass, inverter-based resources (IBRs) lack these attributes. This can make power grids more vulnerable to disturbances. The lack of inertia and damping has driven the development of technologies that can emulate these characteristics, typically through the use of energy storage systems. This inertia emulation is achieved by applying the Virtual Synchronous Generator (VSG) concept.

Over the years, several VSG systems have been developed. However, this thesis focuses on a specific system, the Synchronous Central Angle Controller (SCAC), which presents a distributed approach. In this system, a central controller located at the point of connection (PoC) remotely manages several distributed generators via local controllers. This allows the generators to act as a single entity, adjusting parameters at the PoC to ensure coordinated operation.

In this thesis, first a review of the system requirements for the implementation of this type of controller is performed, as well as the currently existing alternatives. Once an overview of the alternatives is established, a comprehensive explanation of the SCAC is provided. Subsequently, this control system is applied to a distributed generation system, adapting the SCAC for use in commercial converters, which will allow verifying its behavior under various conditions. This evaluation also considers the communication delays between the central controller and the local ones, which are compensated for by methods based on the Smith predictor. The system is validated both in simulations and experimentally, using real-time systems, Hardware-in-the-Loop, Power-Hardware-in-the-Loop and scaled laboratory setups.

Universidad de Oviedo

After validation, the use of SCAC is extended to other applications, such as ramp compensation in solar generation. Generation ramps, which are mainly caused by weather variations, can cause instabilities in the grid and lead to penalties by grid operators. The proposed solution includes the use of energy storage connected to the solar plants to compensate for such ramps and thus maintain system stability.

Finally, the SCAC system is adapted to operate in a Grid-Forming configuration, with the objective of creating an isolated grid for the production of green hydrogen. This system takes advantage of solar generation to feed an electrolyzer, and a dual droop controller is implemented so that the electrolyzer behaves as a flexible load, adjusting its consumption according to the available power and energy. The solution is tested considering also the communication delays between the central controller and the premises, thus ensuring the stability and efficiency of the system under realistic conditions.

In addition, the control system is implemented in a simulation with an external network, taking advantage of the benefits introduced by simulation systems offered by OPAL-RT, allowing and explaining the operation of a co-simulation between two simulators using different simulation domains.

In summary, with all these experiments and simulations, the effectiveness of the SCAC system to manage distributed power grids is validated, providing satisfactory results, even with the inclusion of communication delays, proving to be a robust and flexible solution for the management of distributed grids with high penetration of renewable energies such as hybrid PV generators, coordinating several generators in a centralized way.

SR. PRESIDENTE DE LA COMISIÓN ACADÉMICA DEL PROGRAMA DE DOCTORADO EN ENERGÍA Y CONTROL DE PROCESOS

A mi querido difunto padre, a mi madre, hermanos, familia, amigos y compañeros. . .

Agradecimientos

Quisiera agradecer en primer lugar a mis tutores, Pablo García Fernández y Ángel Navarro Rodríguez, ya que sin ellos nada de esto hubiera sido posible, así como a otros profesores que me han acompañado durante este largo camino. Gracias por apoyarme, enseñarme y aguantarme durante todos estos años.

Por supuesto a mis padres Antonio y Tere, que me han dado todo lo que ha tenido para llegar tan lejos y siempre han confiado en mí. En especial, mi querido padre que espero que estés orgulloso de mi, allá donde estés. A mis hermanos Juanma, Maite, Cuca, Carlos y Eva, así como mi difunto hermano Toñin, que siempre me han animado a seguir adelante. Sin olvidar mencionar a todos mis cuñados y cuñadas. También a todos mis sobrinos, Tania, María, Romina, Bea, Raquel, Juanma, Catherine, Ainhara y Andrea, que siempre han sido como hermanos pequeños para mí, y realmente hemos disfrutado y crecido juntos. Y como no al resto de mis primos y tíos. No menos importante son mis amigos, en especial a Henar, David, Ángel y Miguel, por todo su apoyo y consejos, así como todo el tiempo de calidad vivido juntos.

A mis grandes compañeros de universidad, Rafa y Tania, así como todos los compañeros de doctorado con los que he compartido buenos momentos y no tan buenos, como son Gleisson, Mhret, Irene, Rand, Carlos, Sarah y Geber. donde su ayuda ha sido crucial para superar esta aventura. Por último y no menos importante, a toda la gente de Luxemburgo (LIST), quienes me recibieron como uno de los suyos, especialmente a Gregg, Shailendra y Pedro.

Acknowledgements

I would first like to thank my tutors, Pablo García Fernández and Ángel Navarro Rodríguez, without whom none of this would have been possible, as well as other teachers who have accompanied me along this long journey. Thank you for supporting me, teaching me and putting up with me during all these years.

Of course to my parents Antonio and Tere, who have given me everything they have had to get this far and have always trusted me. Especially, my dear father who I hope you are proud of me, wherever you are. To my siblings Juanma, Maite, Cuca, Carlos and Eva, as well as my late brother Toñin, who have always encouraged me to keep going. Without forgetting to mention all my brothers and sisters-in-law. Also to all my nieces and nephews, Tania, María, Romina, Bea, Raquel, Juanma, Catherine, Ainhara and Andrea, who have always been like little siblings to me, and we have really enjoyed and grown up together. And of course the rest of my cousins and aunts and uncles. No less important are my friends, especially Henar, David, Ángel and Miguel, for all their support and advice, as well as all the quality time we have spent together.

To my great university classmates, Rafa and Tania, as well as all my fellow PhD students with whom I have shared good and not so good moments, such as Gleisson, Mhret, Irene, Rand, Carlos, Sarah and Geber, where their help has been crucial to get through this adventure. Last but not least, to all the people in Luxembourg (LIST), who welcomed me as one of their own, especially Gregg, Shailendra and Pedro.

Resumen

La adopción masiva de sistemas de generación distribuida en los sistemas de potencia responde tanto a la lucha contra el cambio climático como a la necesidad de reducir la dependencia de los combustibles fósiles. Este impulso hacia soluciones energéticas más sostenibles y respetuosas con el medio ambiente se refuerza por la creciente concienciación sobre la reducción de emisiones de gases de efecto invernadero y la madurez tecnológica de fuentes renovables como la fotovoltaica (PV) y la eólica. A medida que estas tecnologías avanzan, sus costos disminuyen, lo que ha facilitado su implementación a gran escala en los sistemas de generación de energía.

No obstante, la transición hacia estas tecnologías renovables conlleva ciertos desafíos, especialmente en términos de estabilidad de las redes eléctricas. A diferencia de los generadores síncronos tradicionales, que aportan inercia y amortiguamiento gracias a su masa rotante, los recursos basados en inversores (IBR) de potencia carecen de estos atributos. Esto puede hacer que las redes eléctricas sean más vulnerables ante perturbaciones. La falta de inercia y amortiguamiento ha impulsado el desarrollo de tecnologías que puedan emular estas características, habitualmente mediante el uso de sistemas de almacenamiento de energía. Esta emulación de inercia se consigue aplicando el concepto de Generador Síncrono Virtual (VSG).

A lo largo de los años, se han desarrollado diversos sistemas VSG. Sin embargo, esta tesis se centra en un sistema específico, el Synchronous Central Angle Controller (SCAC), que presenta un enfoque distribuido. En este sistema, un controlador central ubicado en el punto de conexión (PoC) gestiona de forma remota varios generadores distribuidos mediante controladores locales. Esto permite que los generadores actúen como un solo ente, ajustando parámetros en el PoC para garantizar un funcionamiento coordinado.

En esta tesis, primero se realizará una revisión de las necesidades del sistema para la implementación de este tipo de controladores, así como de las alternativas existentes en la actualidad. Una vez se establezca el panorama de las alternativas, se procederá a una explicación exhaustiva del SCAC.Posteriormente, se aplicará este sistema de control a un sistema de generación distribuido, adaptando el SCAC para su uso en convertidores comerciales, lo que permitirá verificar su comportamiento bajo diversas condiciones. Esta evaluación considerará también los retrasos de comunicación entre

el controlador central y los locales, los cuales serán compensados mediante métodos basados en el preditor Smith. El sistema será validado tanto en simulaciones como experimentalmente, utilizando sistemas en tiempo real, Hardware-in-the-Loop, Power-Hardware-in-the-Loop y montajes de laboratorio a escala.

Después de la validación, el SCAC se extenderá a otras aplicaciones, como la compensación de rampas en la generación solar. Las rampas de generación, que se originan principalmente por variaciones climáticas, pueden causar inestabilidades en la red y dar lugar a penalizaciones por parte de los operadores de red. La solución propuesta incluye el uso de almacenamiento energético conectado a las plantas solares para compensar dichas rampas y así mantener la estabilidad del sistema.

Finalmente, el sistema SCAC será adaptado para funcionar en una configuración Grid-Forming, con el objetivo de crear una red aislada para la producción de hidrógeno verde. Este sistema aprovechará la generación solar para alimentar un electrolizador, y se implementará un controlador droop dual para que el electrolizador se comporte como una carga flexible, ajustando su consumo en función de la potencia y energía disponible de forma dinámica. La solución será probada considerando también los retrasos de comunicación entre el controlador central y los locales, asegurando así la estabilidad y eficiencia del sistema bajo condiciones realistas.

Abstract

The massive adoption of distributed generation systems in power systems responds to both the fight against climate change and the need to reduce dependence on fossil fuels. This drive towards more sustainable and environmentally friendly energy solutions is reinforced by the growing awareness of greenhouse gas emission reduction and the technological maturity of renewable sources such as Photovoltaic (PV) and wind. As these technologies advance, their costs are decreasing, which has facilitated their large-scale deployment in power generation systems.

However, the transition to these renewable technologies brings with it certain challenges, especially in terms of grid stability. Unlike traditional synchronous generators, which provide inertia and damping due to their rotating mass, Inverter-based resources (IBRs) lack these attributes.. This can make power grids more vulnerable to disturbances. The lack of inertia and damping has prompted the development of technologies that can emulate these characteristics, typically through the use of energy storage systems (ESS). This inertia emulation is achieved by applying the Virtual Synchronous Generator (VSG) concept.

Over the years, several VSG systems have been developed. However, this thesis focuses on a specific system, the Synchronous Central Angle Controller (SCAC), which presents a distributed approach. In this system, a central controller located at the point of connection (PoC) remotely manages several distributed generators via local controllers. This allows the generators to act as a single entity, adjusting parameters at the PoC to ensure coordinated operation.

In this thesis, a review of the system requirements for the implementation of this type of controller, as well as the currently existing alternatives, will be carried out first. Once the overview of the alternatives is established, a comprehensive explanation of the SCAC.Subsequently, this control system will be applied to distributed generation sources, adapting the SCAC for use in commercial converters, which will allow verification of its behavior under various conditions. This evaluation will also consider the communication delays between the central controller and the local ones, which will be compensated by means of specific methods. The system will be validated both in simulations and experimentally, using real-time, Hardware-in-the-Loop, Power-Hardware-in-the-Loop and laboratory-scale set-ups.

After validation, SCAC will be extended to other applications, such as ramp compensation in solar generation. Generation ramps, which are mainly caused by weather variations, can cause grid instabilities and lead to penalties by grid operators. The proposed solution includes the use of energy storage connected to the solar plants to compensate for such ramps and thus maintain system stability.

Finally, the SCAC system will be adapted to operate in a Grid-Forming configuration, with the aim of creating an isolated grid for the production of green hydrogen. This system will take advantage of solar generation to feed an electrolyzer, and a dual droop controller will be implemented to make the electrolyzer behave as a flexible load, adjusting dynamically its consumption according to the available power and energy. The solution will be tested considering also the communication delays between the central controller and the premises, thus ensuring the stability and efficiency of the system under realistic conditions.

Abbreviations and Acronyms

ac	Alternating Current
ADN	Active Distributed Network
AVR	Automatic Voltage Regulator
BDC	Bidirectional Converters
CNG	CINERGIA SL
dc	Direct Current
DEG	Distributed Energy Generation
DER	Distributed Energy Resources
ESS	Energy Storage Systems
FRF	Frequency Response Function
FRT	Fault Ride Through
GFD	Grid-Feeding
GFL	Grid-Following
GFM	Grid-Forming
GM	Gain Margin
GPC	Generalized Predictive Control
GS	Grid-Supporting
HE	Hydrogen Electrolyzer
HIL	Hardware-In-The-Loop
HPG	Hybrid Power Generator
IBR	Inverter-Based Resources
LCOE	Levelized Cost of Electricity
LPF	Low Pass-Filter
MPC	Model Predictive Control

MPP Maximum Power Point
MPPT Maximum Power Point Tracking
PE Pôwer Electronics
PHIL Power-Hardware-In-The-Loop
PI Proportional Integral Controller
PLC Power Loop Controller
PLL Phase-Locked Loop
PM Phase Margin
PMS Power Management System
PoC Point of Connection
PPC Power Plant Controller
PQ Power Quality
PR Proportional Resonant Controller
PV PhotoVoltaic Panel
PVPP PhotoVoltaic Power Plant
PWM Pulse Width Modulation
RES Renewable Energy Sources
RMS Root Mean Squared
RR Ramp-Rate
RT Real-Time
SCAC Synchronous Central Angle Controller
SG Synchronous Generator
SO System Operator
SOC State of Charge
SP Smith Predictor
SPC Synchronous Power Controller
SRF Synchronous Reference Frame
TSO Transmission System Operator
VCO Voltage Controller Oscillator
VSG Virtual Synchronous Generator
VSM Virtual Synchronous Machine
V2G Vehicle-To-Grid
WG Wind Generator
WPG Wind Power Generator

Definitions

- **Active Distributed Network (ADN)**: is an electricity grid that integrates distributed generation sources, storage and controllable loads, actively managing the flow of energy and improving system stability and efficiency through decentralized, bi-directional control.

- **Distributed Energy Generation (DEG)**: electricity generation systems based on distributed sources, i.e. generators that are located close to the point of consumption instead of large centralized plants.

- **Distributed Energy Resources (DER)**: is broader than DEG, and encompasses not only distributed generation, but also other types of resources that can provide or manage energy. It includes DERs, ESS, demand-side management and electric vehicles (V2G).

- **Energy Management System (EMS)**: it is a software system that optimizes energy use in installations, monitoring, controlling and managing energy consumption and production to maximize efficiency and reduce costs, especially in grids that integrate renewable sources.

- **Energy Storage System (ESS)**: is a technology designed to store energy and release it when needed. These systems are key to managing the intermittency of renewable sources such as solar and wind, improving grid stability and optimizing energy use. They can be batteries, flywheels, supercapacitors, among others.

- **Hybrid Power Generator (HPG)**: it is a renewable energy generation plant that combines multiple renewable sources, such as solar and wind, with energy storage systems, such as batteries. This makes it possible to manage the intermittency of renewable generation, storing excess energy when production is high and releasing it when production is low, improving the stability and reliability of the electricity supply.

- **Inverter-Based Resource (IBR)**: refers to a power generation or storage system that uses power electronics, specifically inverters, to convert dc current into ac current for integration into the electrical grid. IBRs are typically used in renewable energy systems, such as solar panels and battery storage, and are essential for maintaining grid stability in systems with high renewable penetration.

- **Microgrid**: is a local electricity grid that can operate independently or connected to the main grid, integrated by distributed generation sources such as renewable, storage systems and loads. Microgrids are capable of autonomously managing energy supply, optimizing efficiency and improving resilience to failures in the main grid.

- **Power Management System (PMS)**: a system responsible for managing the distribution and flow of electrical energy in networks or plants, balancing demand and supply, and ensuring grid stability in the face of fluctuations in generation or consumption.

- **Power Plant Controller (PPC)**: a device or system that coordinates and regulates the operations of a power generation plant, controlling parameters such as frequency, voltage, active and reactive power to ensure the efficient and safe operation of the plant.

- **Virtual Synchronous Generator (VSG)**: is a technology that allows electronic converters to mimic the behavior of conventional synchronous generators, providing inertia and support to the grid. VSGs improve frequency and voltage stability by reacting to changes in the grid, enabling renewable sources and energy storage systems to contribute to grid control more efficiently.

Contents

List of Figures

List of Tables

Chapter 1

Introduction

1.1 Background and Motivation

Currently there is a major problem on a global scale related to the increasingly real climate change, due to the massive electricity generation through the use of traditional generation sources such as coal or gas in recent years. Due to the growing global awareness of the need for a change, as well as the difficulty and limitation in the extraction of these raw materials and the large emission of greenhouse gases, have fortunately made the need for a transition to a more sustainable and environmentally friendly global electricity generation.

In recent years, Distributed Energy Generation (DEG) systems, which are based on renewable energy sources such as Photovoltaic (PV) or wind power generation systems, have been introduced on an increasingly massive scale. The democratization of these technologies due to the large investment and research, have driven to obtain much more affordable systems, offering improved Levelized Cost Of Electricity (LCOE). This has increased their economic viability and attractiveness to investors.

Due to the high variability of the power output of these generation systems, the introduction of energy storage systems (ESS), such as batteries, is also necessary. With all this, advanced control techniques have to be designed and implemented to help maintain grid stability, taking into account the high penetration of these types of systems. These control systems would help to mitigate such variability. This is all the more so given that the inclusion of these generation systems will mean a potential weakening of the electricity systems, given that, until now, energy generation was based on traditional generation plants with synchronous generators (SGs), with a rotating mass (rotor), which provides a certain inertia to the system, which helps to maintain grid stability in the event of possible disturbances in the grid.

Renewable generation systems are interconnected to the grid for energy injection through the use of Inverter-Based Resources (IBR), which lack inertia or damping, raising concerns about system security and stability of the power system. Therefore, when considering a massive inclusion of Distributed Energy Resources (DERs), with large volumes of generation, the inclusion of some alternative, to try to emulate inertia, must be mapped out. Considering this, this is where the concept of Virtual Synchronous Generator (VSG) arises. These systems offer an innovative solution by emulating the dynamic properties of traditional synchronous generators, whether real or arbitrary, in the DEG power converters.

Typically, the concept of virtual inertia is implemented by using ESS with power converters, and using a suitable control mechanism, thus providing a controlled amount of virtual inertia to the power system (typically ranging from milliseconds to several dozen seconds depending on the system). Traditionally, storage systems are used for inertia emulation, but certain control techniques can also be applied to renewable generation systems to emulate a certain level of inertia in their generation.

Most of the traditional power generation will be eventually replaced by these kind of systems. Considering this, VSG techniques create the basis for a large-scale implementation of renewable energy source (RES) systems, without compromising grid stability.

There are several VSG structures in use today, as well as still under development, presented in the literature, which will be discussed in Chapter 2, but this work will be mainly based on one of them, called Synchronous Central Angle Control (SCAC). This technique proposes to simultaneously control several power converters, emulating the behavior of a single SG at the Point of Connection (PoC), resulting in an aggregated VSG system. Thus presenting a system where a virtual rotor with its inertia is emulated at the PoC, where the electromechanical model of the SG is considered, and several stators at converter level, which would inject the necessary power, controlling all of them from a central controller.

The motivation of this thesis lies in the incorporation of this distributed control system in a close-to-reality application. However, the distributed nature of this approach poses additional challenges to ensure its effectiveness and stability in real operating environments. One of the first challenges is the need to establish effective communication between the central controller and the distributed converters, which are at some distance from the central controller. This communication, essential for the correct operation of the system, often introduces certain delays, which can affect system response and stability. Therefore, it is crucial to try to minimize such delays, as well as to look for techniques that minimize or mitigate the effect of such delays. In addition, there is also the challenge of integrating commercial converters used in the system. These converters usually have certain limitations in terms of control capability, as they generally only accept active and reactive power commands, restricting access to their internal control systems. Therefore, it is necessary that the control system used takes full advantage of the limited capabilities of these converters, and adapt to this case. Furthermore, in some cases, the use of measurement sensors is not contemplated, unless it is strictly necessary, having only access to the internal information of the power converters, accessible through communication protocols, in the case of this thesis, MODBUS TCP. All these capabilities are tested in real-time simulation, either by using the system with external hardware, performing Hardware-In-the-Loop simulations, or by integrating the system in a bigger grid, by using a co-simulation structure.

The control system will be implemented in different configurations. Initially, it will operate according to its original design, using grid-following (GFL) with supporting capabilities, allowing arbitrary injection of power into the system or injection/absorption of power in response to grid frequency variations. Subsequently, due to the possible variations in generation due to environmental changes, the system will be adapted to handle ramp compensation in solar generation plants. Finally, a grid-forming (GFM) model will be implemented to operate in an isolated grid, feeding a green hydrogen production plant, as an innovative case of application of the system.

In summary, this thesis proposes to address the implementation of distributed inertia and damping emulation for grid support control systems, considering the interoperability of different commercial converters, considering communication delays and their compensation, implementing different control strategies of the power converters.

1.2 Thesis Objectives

The main objective of this thesis is to address the analysis and implementation of a distributed control system based on VSG, in order to manage several DEG systems simultaneously. This system, known as SCAC, is in charge of coordinating and controlling multiple converters from a central controller located in the PoC through communications. This technique allows the creation of an aggregated VSG system that emulates a single virtual rotor, considering the electromechanical models of the SG, and several stators at converter level to deliver the demanded power. In this way, it is possible to emulate the inertia and damping response in the PoC, providing stability to the electrical system, and acting as a power source on demand, acting as a grid feeding system, and even as a grid forming system for isolated systems. In addition to the main objective, there are other equally important objectives guiding this research:

I. Review of the state of the art relating the motivation of the thesis to its objectives. This review will be framed within the broad spectrum of Power Plant Controllers (PPC), where the VSG controller used in this thesis must be located, for an industrial implementation. Within this objective, the following aspects will be considered:

   - A review of the different PPCs for DEG plants will be carried out, in order to give an introduction and a context of the need for the implementation of these control systems. This will be justified by explaining the existing regulations, which require the implementation of these systems to be increasingly demanding for safety and stability reasons.

- ☐ Subsequently, a review is made about the different parts of the grid interface of the distributed generation plants, bearing in mind that these can operate with grid-forming, grid-feeding (GFD) or grid-following and grid-supporting (GS) structures. This explanation is very necessary to be clear on the fact that, depending on each one, an DEG system can behave in very different ways. In addition, with this classification in mind,the different control layers as well as a review and explanation of different synchronization methods, which are essential for its operation, are also given.
- ☐ An analysis of the different strategies used to emulate inertia in power systems will be carried out, focusing specifically on VSG control systems. This will provide an in-depth understanding of the operation of these control systems and the characteristics they share. Furthermore, an attempt will be made to identify the qualities of each of them, providing a global vision of why a distributed system such as the one addressed in this thesis (SCAC), may be the most suitable for a massive implementation in the current context.
- ☐ Furthermore, due to SCAC system uses communication channels, which can be subject to significant delays, negatively impacting the stability and performance of the system. Therefore, a review of the state of the art of different methods of communication delay compensation is included, justifying the selection of the Smith predictor (SP) based compensator.
- ☐ Finally, as the SCAC system is applied in some industrial applications, a review of the most used ramp-rate compensation methods are done, as well as a review of the control systems for green hydrogen generation.

Hence, through this objective it is hoped to obtain a solid and complete understanding of the current state of research on VSG systems, as well as to lay the theoretical foundations necessary for the development of this doctoral thesis.

II. The detailed development of the SCAC distributed controller, explaining each of its parts, in order to ensure a correct understanding of its operation. This explanation will be done by explaining its operation in the way it was designed, taking into account its behavior as grid-following with grid supporting capabilities, but also adapting the control for its operation in grid forming configuration. This is supported by its mathematical development, in order to improve its understanding. This will lead to a better understanding of its behavior under different operating conditions, which will facilitate the design and implementation of effective control strategies.

III. Investigating the limitations of commercial converters, which are usually restricted to receive only active and reactive power commands. To address this objective, certain modifications will be made to the original control system, in order to achieve a successful implementation of the control system in commercial converters, taking full advantage of its capabilities, and minimizing possible limitations. This is intended to advance the development and adoption of this type of technology more rapidly. Thus, achieving a better understanding of the system, helping to facilitate its industrial implementation, in a simple way, which can even be done on a massive scale.

IV. The validation of the control system through testing in both real-time simulation and laboratory setup experimentation. This process will include the use of industrial converters and will consider the effects of communication delays and their compensation. The ability of the system to inject active and reactive power according to demand, and to compensate for frequency variations where necessary, will be assessed. The main objective of these tests is to demonstrate the feasibility of the system implementation, ensuring its correct operation in environments that simulate real conditions. To achieve this validation, various simulations, validation tools and methodologies will be employed. Initially, tests will be performed in real-time (RT) simulation environments, using platforms such as Matlab and Speedgoat. Subsequently, the system will be implemented using real hardware through the Power-Hardware-In-The-Loop (PHIL) technique, which connects the control system with physical hardware. This will allow simulations to be carried out under realistic operating conditions, evaluating the behavior of the system in a controlled environment closer to reality.

    The combination of these tests in simulation and experimentation will allow the control system to be validated in various scenarios, ensuring its reliability and efficiency. In addition to the validation at converter level, the control system will also be tested in a real-time co-simulation environment, interconnecting two simulators via a Dolphin interface. In this context, OPAL-RT simulators will be used: one in the time domain (eMEGASIM) to simulate the distributed converters, and one in the phasor domain (ePHASORSIM) to simulate the electrical system where the DERs are connected. This comprehensive approach will provide a complete validation of the control system, both at the simulation level and under experimental conditions, ensuring its operability in practical applications.

    These validations help to understand better how distributed VSG can work, specially the SCAC control system, when it is used in different applications.

V. New operating modes are incorporated into the control system in order to increase its versatility. One of these modes focuses on the challenge of generation ramps in PV systems, seeking to take advantage of the available resources to mitigate this problem. These ramps arise due to abrupt changes in solar generation, caused by the significant variability of RES, such as fluctuations in temperature and irradiance. It is essential to note that, according to grid operator regulations, these fluctuations are unacceptable and can result in penalties. Therefore, the use of the SCAC system is proposed for mitigation, given its hybrid nature that includes ESS. This resource will be adjusted by modifying its set-points to ensure that it remains within the limits set by the grid operator in grid-tied applications, thus improving the stability and reliability of the control system, complying with regulations and generating economic savings.

Another mode of operation envisages the adaptation of the SCAC system to grid-forming systems in off-grid applications. This approach will be used to power a local load based on an electrolyzer for green hydrogen production. It will explore how the SCAC system can efficiently manage energy production in such grids, maintaining stability under various conditions.

These are two examples of the implementation of the SCAC system industrially, for applications related to solar generation. Either for a plant working on GFL or another one working on GFM for green hydrogen generation. This is an example of the versatility of the SCAC based control.

1.3 Thesis Contributions

The following list presents the main contributions of this thesis as derived from the stated objectives:

1. **Control System Adaptation and Communication Delay Compensation *(JP1, CP1)*:** this contribution addresses the adaptation of the control system for implementation in commercial power converters, which are typically limited to receive active and reactive power commands. This process involves modifications to the control system to ensure its operation within these constraints without compromising its efficiency and responsiveness. A key part of this application lies in the optimal utilization of the information available through the communication port of the converters. This information includes RMS voltage and current values, as well as the developed active and reactive power, and the frequency of the network. This data is used to reconstruct these variables in the time domain, which is an innovative and effective approach to reduce the costs associated with the installation and maintenance of additional sensors, although with certain limitations.

   On the other hand, the problem of communication delays in distributed systems, which are controlled from a central controller located in the PoC, is addressed. These delays can arise due to the physical distance between the converters and the controller, as well as the latency existing in the communication networks, which can generate instabilities in the control and in the power system. Therefore, a study of the existing delays in the system is carried out, selecting a compensation system, based on prediction as the SP, taking into account the characteristics of the system. This contribution is expected to boost the development of effective strategies for the management of modern power systems, where communication plays an important role in the coordination and control of distributed systems. Thus, facilitating their implementation on a large scale.

2. **Ramp compensation in PV generation *(CP2)*:** this contribution addresses the problem of generation ramps in PV generation systems, and it proposes to

use the system that occupies this thesis for its compensation. Generation ramps appear due to abrupt changes in solar energy production, which can occur due to the natural variability of these systems, such as changes in temperature or solar irradiance caused, for example, by a cloud passing. According to grid operator regulations, such abrupt changes in power generation are not acceptable and may be subject to penalties.

Therefore, the ability of the SCAC system to mitigate such generation ramps is investigated. Since the SCAC is hybrid and has batteries, the possibility of using this system to start the generation ramps and reduce their impact on the electricity system is exploited. This would be achieved by adjusting the power output of the batteries to start sudden variations in solar generation and keep the production within the limits allowed by the grid operator.

Hence, it aims not only to ensure compliance with grid operator regulations, but also to maximize the efficiency and stability of the electricity system. By mitigating generation ramps, it is expected to reduce the costs associated with possible penalties and ensure a reliable and secure electricity supply for end-users. Furthermore, this research is expected to contribute to the advancement of the use of distributed systems for the efficient management of renewable energy generation in modern power systems.

3. **Green hydrogen generation by using distributed VSG *(CP3)*:** this contribution explores another control mode for power converters by implementing the same distributed VSG system, but moving from a grid following/supporting scheme to a grid forming configuration. This approach aims to create an isolated grid capable of generating energy autonomously, which will be used for the production of green hydrogen through the use of an electrolyzer. This electrolyzer implements an external control system based on a dual droop, both voltage and frequency, in order to improve the stability of the system in the face of various disturbances. An example of its usefulness is when the generation of one of the distributed generation units is reduced, or when the storage units cannot meet the demand. This generates a mismatch in the generation, which modifies the voltage and frequency value, causing the system to adapt dynamically, reducing the power and guaranteeing the stability of the system.

   In addition, because this system uses the SCAC system, which is structured in a central controller that coordinates different local controllers, the system is subject to communication delays between them. To mitigate its effects, an SP-based compensation system is implemented, improving the stability of the system.

   Therefore, this contribution, by combining a grid-forming model with an autonomous system for green hydrogen generation and the implementation of a dual droop control with delay compensation mechanisms, represents an important research window to obtain distributed energy systems capable of operating in isolated grids under various dynamic conditions.

4. **Power system co-simulation using distributed VSG *(CP4)*:** in this contribution, the SCAC VSG system has been implemented operating under a grid-following and grid-supporting structure in a real network, with parameters and characteristics of a real converter, including the consideration of its switching behavior. The simulation has been performed in a real-time environment, provided by the OPAL-RT simulators, where a real-time co-simulation has been run, combining two different simulation domains: the time domain (through the eMEGASIM simulator) and the phasor domain (through the ePHASORSIM simulator).

   In the time domain, two distributed SCAC converters have been simulated, while in the phasor domain a two-area Kundur network has been modeled, where the connection point of the converters corresponds to a bus of this network. This configuration has made it possible to analyze the interaction between the converters and the network, evaluating their behavior and response under real conditions.

   Furthermore, a detailed explanation of the process to perform a real-time co-simulation using both OPAL-RT simulators is included. This process is based on the synchronization of the simulations through the use of a Dolphin synchronization cable, which allows coordinating the exchange of data between the different simulation domains. Hence, the contribution not only highlights the results obtained, but also provides guidance for the implementation of complex real-time co-simulations, opening up new possibilities for the validation and testing of distributed control systems in high-precision experimental environments.

1.4 Thesis Publications

1.4.1 Peer-Reviewed Journal Papers

JP1 ***D. del Rivero***, *P. García, C. Blanco and Á. Navarro-Rodríguez, "Control of Aggregated Virtual Synchronous Generators for PV Plants Considering Communication Delays", in IEEE Transactions on Industry Applications, doi: 10.1109/TIA.2024.3377169*

1.4.2 Peer-Reviewed Conference Papers

CP1 ***D. del Rivero***, *P. G. Fernández, C. Blanco and Á. Navarro-Rodríguez, "Control of Aggregated Virtual Synchronous Generators Including Communication Delay Compensation," 2022 IEEE Energy Conversion Congress and Exposition (ECCE), Detroit, MI, USA, 2022, pp. 1-7, doi: 10.1109/ECCE50734.2022.9947466.*

CP2 ***D. del Rivero***, *I. Peláez, P. G. Fernández, C. Blanco and Á. Navarro-Rodríguez, "Integration of Ramp-Rate Compensation in a Distributed Virtual*

Synchronous Generator Schema for Hybrid PV Plants", 2023 IEEE Energy Conversion Congress and Exposition (ECCE), Nashville, TN, USA, 2023, pp. 1122-1128, doi: 10.1109/ECCE53617.2023.10362955.

CP3 ***D. del Rivero***, *Á. Navarro-Rodríguez, C. Gomez-Aleixandre, C. Blanco, P. García, and P. Rodríguez, "Control of Green Hydrogen Production on Isolated Hybrid Solar Plants Considering the Effect of Communications", 2024 IEEE Energy Conversion Congress and Exposition (ECCE), Phoenix, AZ, USA, 2024, pp. 1122-1128, doi: 10.1109/ECCE53617.2024.10362955.*

CP4 ***D. del Rivero***, *S.Singh, P. García, and P. Rodríguez, "Real-Time Cosimulation of Power Systems: Integration of eMEGASIM and ePHASORSIM Using OPAL-RT Simulators". 2024 IEEE Power Electronic for Distributed Generation Systems (PEDG), Luxembourg, LU, 2024, pp. 1122-1128, doi: 10.1109/PEDG61800.2024.10667403.*

1.4.3 Other Contributions

CP5 M. Crespo, C. Gómez-Aleixandre, Gleisson Balen, ***D. del Rivero***, *Á. Navarro-Rodríguez, C. Blanco, P. García, "Integration of Modular Energy Storage Solutions in the Distribution Grid", 2024 IEEE Power Electronic for Distributed Generation Systems (PEDG), Luxembourg, LU, 2024, pp. 1-7, doi: 10.1109/PEDG61800.2024.10667453.*

1.5 Thesis Outline

This thesis comprises six chapters, structured to cover the main topics in the following order:

- Chapter 1: the context and driving factors for this thesis are presented, which help establish its fundamental objectives. The contributions that support the thesis are also outlined, along with a listing of the various publications derived from the thesis work. To aid in comprehension, the structure of the document is described.
- Chapter 2: this chapter provides a comprehensive review of the current status of PPCs, which are essential for the efficient and safe operation of power plants. It analyses the evolution of these systems in response to increasingly stringent regulations imposed by electricity system operators, which have developed new grid codes. To better understand this regulatory context, the current codes and their implications for power plant operation are examined in detail. Although the system presented in this thesis would be more in line with the operation of a Power Management System (PMS), as it is not studied on the basis of grid codes,

for its industrial implementation, its operation on the basis of these codes must be ensured. In addition, the chapter includes a review of the network interfaces, with all the controllers available in an DEG system, with a detailed classification of the types of controllers, such as grid-forming, grid-feeding and grid-supporting, which are essential for the interaction of the plant with the grid, as well as the different control loops available. The importance of integrating VSG systems is then discussed, describing some of the main models used. This section also introduces the different methods to compensate for communication delays, an important challenge since VSG strategies, such as the one used in this thesis, rely on communication systems that may be subject to delays, affecting the stability of the control system. In addition, because the system used is applied to two industrial applications, the most commonly used methods of ramp compensation and the different ways of generating green hydrogen are reviewed.

- Chapter 3: a detailed explanation of the Synchronous Central Angle Controller (SCAC) control system is provided, which is the approach used in this thesis for the control of DEG systems. A detailed description of each of the components that make up this control system is provided, addressing both its operation and its structure. This formulation covers the different operating modes of the units, including grid-following with grid-supporting capabilities and grid-forming modes, explaining how this system is adapted to efficiently control the plants under different grid connection scenarios. This provides a comprehensive overview of the control of DEG in various operating contexts.

- Chapter 4: explains the modifications made to the control system to adapt it to commercial converters, taking advantage of its internal characteristics, such as the use of its registers and internal variables. These modifications allow the system performance to be optimized and reduce the need for external sensors. Additionally, a communication delay compensation method based on the Smith Predictor is implemented, which helps to mitigate the effects of transmission delays in the control loop. The control system, with all these adaptations, is evaluated in different scenarios, including local real-time simulations and experimental tests with external hardware. These tests allow verifying the performance of the system under realistic conditions, ensuring its correct operation and stability in different operational situations.

- Chapter 5: it presents two industrial applications of the SCAC concept, applied to PV generation solutions, one focusing on the compensation of solar generation ramps, and the other on the creation of an isolated grid for green hydrogen generation.

  As it has been commented, the first part of the chapter presents the concept of ramp compensation in solar generation, with the aim of avoiding grid instabilities and possible penalties imposed by system operators. To achieve this, a control system is implemented within the SCAC framework, which has been developed and studied throughout this thesis, with certain specific modifications to suit the ramp control requirements. The explanation of this system will be complemented by the use of simulations that will allow to analyze its behavior under different operating conditions. In addition, an economic analysis will be carried out, whose purpose is to determine the viability and convenience of integrating this type of control system in solar plants, evaluating in which situations its implementation is profitable or justifiable.

The second part of the chapter is focused in the application of the distributed SCAC system for the creation of an isolated grid dedicated to the production of green hydrogen by means of an electrolyzer. The implementation of SCAC in this context will allow not only the efficient operation of the grid, but also an effective management of the associated technical challenges, such as communication delays. To mitigate these delays, compensation strategies will be considered to ensure a fast and accurate system response. In addition, a dual droop controller is introduced at the electrolyzer level, which will dynamically adjust the load in a flexible manner. This approach ensures that the electrolyzer demand adapts to fluctuations in power generation, thus improving the stability of the created grid. In this sense, the SCAC system will allow both generation and storage resources to interact in a coordinated manner to optimize the green hydrogen production process, ensuring the operational efficiency and stability of the electricity system.

- Chapter 6: the SCAC system is implemented in a real-time co-simulation, integrating with a real network to support the operation of one of its nodes. This chapter deals with the methodological aspects of the system, showing its applications and the different ways in which it can be tested. The simulation is carried out using two OPAL-RT real-time simulators: eMEGASIM, which handles the time domain simulation of the converter, and ePHASORSIM, which handles the phasor domain simulation of the network. Both simulators are synchronized by means of a DOLPHIN cable, which allows stationary results to be obtained from the phasor analysis, but including the dynamics of the time domain. The results obtained are detailed in this chapter, while the experimental setup is described in appendix A.

- Chapter 7: presents a complete synthesis of the main contributions and results achieved throughout this doctoral thesis. Through an exhaustive analysis, the most relevant conclusions derived from the research work are highlighted, linking each one of them with the initially stated objectives. It is discussed how each chapter contributes in an integral way to the development of the SCAC system and its application in the management of distributed electricity grids and renewable generation. In addition, a prospective vision for future research in this field is offered. Clear recommendations are provided to further explore emerging lines of research that were partially addressed in this study. These suggestions include the improvement of communication delay compensation mechanisms, the optimization of the distributed control system and the implementation of the proposed solutions in experimental and real environments. In this way, further progress is invited in the search for solutions that ensure stability and efficiency in modern power systems, with a more robust integration of renewable energies and emerging technologies.

Considering the different objectives of the thesis, the contributions and the outline of the document, Table 1.1 shows the relation between them for better understanding.

Objective	Obj. 1	Obj. 2	Obj. 3	Obj. 4	Obj. 5
Contribution	All	JP1, CP1	JP1, CP1	JP1, CP1, CP4	CP2, CP3
Chapter	2	3	4	4, 6	5

Table 1.1: Relation between objectives, contributions and chapters.

Chapter 2

Literature Review and State of the Art

2.1 Introduction

This thesis focuses on the study of a distributed VSG control system designed to add virtual inertia to DEG systems, emulating the electromechanical behavior of a synchronous generator. Although the main focus is on hybrid PV plants (PV plant with ESS), the proposed system has a wide spectrum of applications in distributed generation.

To justify the implementation of the distributed VSG system, this initial chapter provides a fundamental review of distributed power systems and PPCs that are used to regulate plant performance and meet the regulatory demands of grid regulators. These increasingly stringent regulations seek to improve the efficiency and stability of distributed generation systems, especially in an energy environment that is increasingly reliant on renewable sources. The review will include a detailed description of power plant control structures, addressing grid-forming, grid-following and grid-supporting approaches, which are the main control structures for IBR to maintain synchronization and stability with the power system. Grid-synchronization methods, which are indispensable for the efficient and safe operation of distributed plants in increasingly dynamic power grids, will also be reviewed.

Subsequently, an in-depth analysis of the most commonly used inertia emulation systems will be carried out, highlighting the distributed system SCAC, which is the core of this research. This system has the ability to control from the PoC the behavior of all the distributed generation units connected to it, providing a unified and efficient control strategy.

Finally, a critical issue for the stability of distributed VSG systems will be addressed:

communication delays. Since SCAC relies on communication links to coordinate the control of distributed units, these delays can compromise the stability and performance of the system. Therefore, various techniques and systems will be reviewed to compensate for such delays, ensuring that the system maintains stable and efficient operation, even under adverse communication conditions. This analysis will ensure the feasibility of the proposed system in a real environment and provide practical solutions to improve its performance.

2.2 Distributed Energy Resources

The world's power generation system is evolving towards a more sustainable and environmentally friendly approach, moving from a centralized generation system based mainly on fossil fuels and large power plants to a distributed energy generation system based mainly on RES. Renewable energy is generated from natural renewable resources such as sunlight, wind, ocean, hydropower, biomass, geothermal resources, bio-fuels and hydrogen. Their contribution to energy systems is growing because most of them are becoming more mature and cheaper, such as PV and wind generators (WG), which are becoming more affordable and offer better Levelized Cost Of Electricity (LCOE) ratios [2.1]. Their implementation contributes to the diversity of the energy supply portfolio, reducing the risks of continuing/expanding the use of fossil fuels and nuclear energy [2.2]. Such DEG systems are generation systems generally located close to consumption points, which can be connected to the grid or work in off-grid mode. These DEG systems usually work together with other energy resources, such as energy storage systems (ESS), dedicated or auxiliary systems such as batteries, ultra-capacitors, even electric vehicles in their vehicle-to-grid (V2G) controller mode, among others. These systems, along with DEGs, are grouped under the concept of Distributed Energy Resources (DER). [2.3].

PV Power Plants (PVPP) and Wind Power Generators (WPG) generate renewable energy that is used to supply grid loads, working with ESS or not. These DERs, through maximum power point (MPP) methodologies, obtain the maximum available energy that must be adapted to be injected into the grid. There are several maximum power point tracking (MPPT) methods for both systems, although taking into account that this thesis is based on solar generation, the most important ones can be found in [2.4–2.6].

When local loads are connected to DER systems, either in off-grid or grid-tied conditions, the system can be considered as an active distribution network (ADN). These systems require precise and coordinated control to avoid grid stability problems. This not only improves local stability, but also optimizes power quality (PQ) through more efficient voltage control, and can reduce the cost associated with power generation [2.7, 2.8].

The control of these DER systems can be approached in two ways: centralized or decentralized [2.7, 2.9–2.14]. In the centralized approach [2.7, 2.10], a central controller

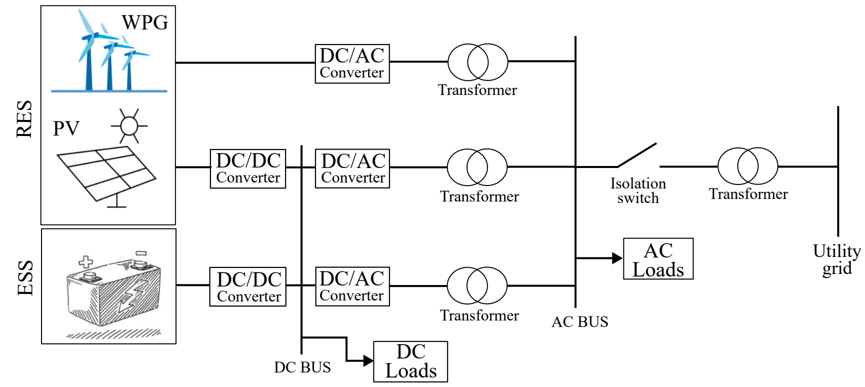

Figure 2.1: General ADN scheme with local generation and local loads. It can work in grid-tied or grid off modes.

is responsible for determining the amount of power that the different distributed units must exchange with the loads or the grid. This controller evaluates the conditions of both the main grid and the loads, optimizing the power flow to ensure operational stability and efficiency. On the other hand, the decentralized approach [2.10–2.12] delegates control to each distributed unit. In this case, each generator performs local control, adjusting its output according to local demand and market conditions. This approach allows power generation to be optimized and, where possible, surplus power to be exported to the main grid, maximizing economic benefits.

Currently, the decentralized approach is more commonly used due to limitations in communications and computing capacity between different systems, as well as the diversity in generation capacity of different generation devices. These limitations often make management more practical and adaptable to changing grid and market conditions. However, with improvements in communications in terms of speed and latency, it is intended to move to a centralized distributed system, where each distributed generation can be safely and efficiently controlled from a central controller, thus improving the performance of the power system.

Figure 2.1 illustrates an example of a ADN-DEG system connected to the main grid, which includes several distributed generators and several local loads. The interconnection and control of these elements is essential to ensure the stability and security of the system as a whole.

To manage these distributed systems effectively, advanced control elements are necessary to ensure the safe and stable operation of the ADN. One of these key elements is the power plant controller (PPC). PPCs enable optimal and safe control of DEGs, ensuring compliance with established regulations and optimizing the integration of the ADN with the wider power system. The different PPC are explained in Section 2.3.

PVPP and WPGs are able to provide the electrical power to supply a grid load. The energy conversion systems provided by wind turbines and PVs enable to extract the maximum wind/solar power, obtaining the electrical power that must be adapted to be injected into the grid, by means of methodologies to track the MPP. These power plant, normally are used beside ESS, building hybrid power systems (HPG), in order to reduce possible RES power variations, resulting from the variable nature of the energy source.

2.3 Power Plant Controllers

In this section, the main functionalities necessary for the management of a plant are explained, in order to understand the systems used in this work, which can be managed by a Power Management System (PMS), which is applied in a variety of energy contexts, such as microgrids, ADNs, HPG, etc [2.15, 2.16]. These PMS manage energy sources and their control, optimizing production and consumption dynamically [2.16]. However, these systems are not always subject to grid regulations, being this done by PPCs, which are designed to comply with the regulation of the grid to which they are connected. The work in this thesis is related to these PMS systems, since, in the development, no work has been done on the network codes. However, it is necessary to point out that for an application of the system they must be taken into account, implementing the control system in a Power Plant Controller, which allows to comply with the current regulations. Therefore, the different functionalities of these PPCs, which must be fulfilled for a real grid-connected application, must be explained [2.17–2.19].

The increasing penetration of renewable energies, leading to a more decentralized system, presents the system operator with the challenge of keeping the system as stable and reliable as possible. To this end, PPCs are introduced in the control system of power plants, in order to regulate and control the different inverters, devices and equipment connected to the grid of renewable energy plants, such as photovoltaic plants and wind generation plants. Although these systems are used for different types of DEG systems, in this thesis document, the focus will be on those used in PVPP. These PPC systems are necessary for several reasons:

1. Grid stability improvement. This is because PV systems generate power intermittently, which can cause grid instabilities if they are not properly managed. Therefore, they ensure that the power generated is kept within the operating limits set by the grid operator.

2. Efficiency. Improve efficiency by optimizing the operation of PVPPs by controlling the output of the plant to meet the demands of the grid. Thus ensuring that the plant generates the maximum amount of energy while maintaining efficiency, reducing costs.

3. Safety. Protects PVPPs and the grid from possible damage, ensuring the safety of personnel and equipment by automatically disconnecting the grid in the event of abnormal operating conditions, such as overvoltage or undervoltage.

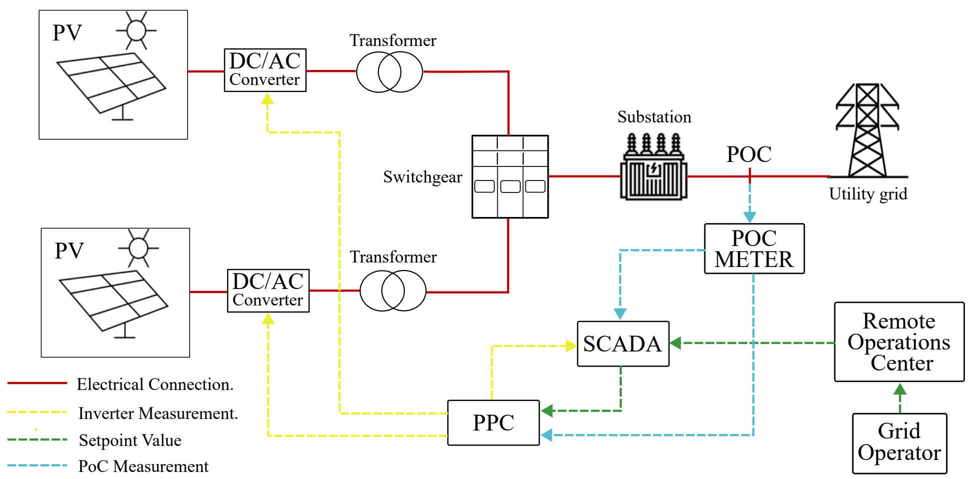

Figure 2.2: DER power plant with PPC, SCADA and TSO interface to control the system.

4. Revenue compliance. Grid operators require the plant controller to ensure that the PVPP complies with the regulations and standards set by the authorities. Ensuring that the plant operates within voltage and frequency limits and complies with grid codes, thus avoiding possible penalties. These DEG systems, like PV, are increasingly integrated into power systems, making it more and more difficult for grid operators to maintain stability. This forces the creation and enforcement of grid codes, making compliance very important.

Considering the DER system schematic shown in Figure 2.2, it is possible to observe a little of how these controllers work. To do this, the grid operator sends specific set-points in order to change some network parameter in the PoC. These parameters are sent to the Remote Operations Center, which communicates with the Supervisory Control and Data Acquisition (SCADA) system. This SCADA system has available the electrical readings at the connection point as well as the values collected from the individual inverters. Considering these values and measurements, the set-points are sent to the PPC system, which will execute the relevant operating mode to comply with the different grid codes. Therefore, the PPC interacts with the system operator, which dynamically defines and transmits the operating control modes and associated set-points. As TSOs do not monitor power at the inverter level, the DER system is considered as a whole, the focus being on the electrical data of the PoC.

Therefore, in relation to grid codes, requested control mode and measurement In the PoC, the DER relies on the PPC to execute control algorithms and send commands in an intelligent way to the available DEG equipment, complying with the different network codes.

In order for these PPC systems to perform efficiently and optimally, they must be selected with several factors in mind:

1. Scalability: the PPC hardware selected must be scalable to accommodate future expansions or increases in capacity. The plant may need to be expanded in the future to meet increased energy demand, so this component must be able to handle additional capacity from the PVPPs, either through vertical or horizontal scaling.

2. Reliability: the hardware selected must be highly reliable and have a long service life. Since the PPC is key to ensure continuous and efficient operation, any failure could lead to significant losses in productivity and profits. It is therefore essential that the equipment has a high level of reliability and is able to withstand adverse conditions in its operating environment.

3. Compatibility: the hardware selected must be compatible with the other PVPP systems. It is essential that the PPC integrates seamlessly with the infrastructure already in place and is able to communicate efficiently with other systems, ensuring coordinated and optimized operation of the entire plant.

4. Security: it is key to select hardware that offers a high level of security to prevent any unauthorized access, which could lead to a security breach. The choice of the PPC should ensure that the system has robust protection mechanisms to safeguard the integrity of the plant and avoid potential vulnerabilities.

5. Cost: the PPC hardware must be cost-effective and fit within the budget allocated for the solar plant. The main objective is to maximize the return on investment while ensuring that costs are kept under control.

6. Maintenance: select a hardware system that is easy to maintain and has accessible spare parts.

7. Performance: the PPC is responsible for managing and optimizing the generation of electricity in the PV plant. Therefore, it is essential to choose a hardware system that is able to support the load and provide high performance.

Considering all the above, these PPCs, in order to comply with the different regulations, according to the measurements carried out in the PoC, must comply with the drivers shown in Figure 2.3, which are the active power control, reactive power control, power factor control, ramp-rate control, grid support (voltage, frequency and fault ride-through), and power plant start up/shutdown.

2.3.1 Active Power Control

Active power control is a strategy used to manage the active power reserve, allowing the power output of a PVPP to be limited. This control is implemented within the range of the nominal power of the plant or according to established contractual limits. The active power generated in the PVPP is restricted to a predefined limit in the PoC by different curtailment methods. The PoC has the function to maintain the active

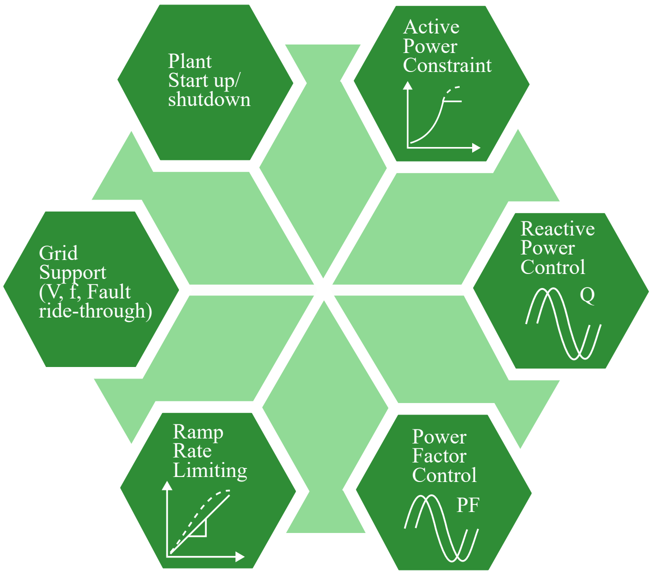

Figure 2.3: Power Plant Controller functions scheme.

power output at the set-point or to respond to reduction orders issued by the operators or the TSO. To carry out these curtailments, the dc bus voltage is generally limited, moving the system away from the MPP. There are three main functions to reduce the active power:

1. Absolute power restriction: protects the system against overloads. In this case, the set-point defines an active power value that the RES cannot exceed.

2. Delta output restriction: maintains a constant active power reserve proportional to the available power, limiting the active power output.

3. Relative power output restriction: reduces the active power as a function of the available active power, according to a pre-defined ratio.

2.3.2 Reactive Power Control

Through the measurements taken at the PoC, it is possible to observe the level of reactive power generation by the inverters. Reactive power control is closely linked to power factor control, which is another management mode that PoCs can perform. When inverters generate and supply reactive power to the grid, the voltage of the power system increases, which raises the power factor and drives it towards a forward state. On the PPC interface, this phenomenon would be represented by a positive sign next to the reactive power values, indicating that the plant is generating reactive power. Conversely, if the inverter absorbs reactive power from the grid, the reactive power value will be negative, indicating a lagging power factor.

It is important to note that reactive power does not generate direct revenue, as utilities generally only remunerate active power, which is the power that produces useful work. However, proper management of reactive power is crucial to maintain the stability and quality of voltage in the grid.

TSO can require a specific reactive power exchange between the DEG and the grid through two main approaches. One is to set a specific set-point of reactive power to be generated or absorbed by the plant. The other method is to set a target power factor value in the PoC, which will depend on the amount of active power generated. This power factor control can be essential to comply with grid codes and optimize the performance of the power system as a whole.

2.3.3 Power Factor Control

Power factor correction is a fundamental aspect of reactive power control and is often an additional requirement to ensure that the plant remains within acceptable power factor limits in the PoC. This control is crucial because it helps to reduce the losses that occur during power transmission over long distances, caused by the presence of reactive power components in the ac circuits. By correcting the power factor, the amount of reactive power in the system is decreased, which in turn reduces transmission losses and improves overall energy efficiency.

From a regulatory point of view, many utilities impose strict regulations that require maintaining a power factor within a specific range when the plant is connected to the grid. Failure to comply with these requirements can result in penalties or financial penalties, which adds a layer of importance to effective power factor control.

In addition to avoiding penalties, power factor correction also has operational benefits for PV power plants. By optimizing the use of active power and minimizing reactive power, the plant can operate at higher capacity, allowing it to generate and sell more power to the grid. This not only improves the profitability of the plant, but also contributes to meeting the growing demand for renewable energy sources, making the plant more competitive and efficient in the energy market.

2.3.4 Ramp-rate Control

The ramp-rate control is tied to active power control, which would generate an active power set-point. These PPCs are able to manage the ramp rate of the active power produced, a functionality that provides smooth variations in the active power output that improve grid stability. This is because RES typically exhibit intermittent behavior, largely influenced by weather conditions. In the case of PV systems, variations in irradiance and temperature can cause abrupt changes in output power. These fluctuations can cause significant power quality (PQ) problems, especially during rapid changes where the TSO has limited capacity to respond effectively. These fluctuations can exceed allowable limits, which can lead to frequency or voltage stability problems. Weather forecasting can predict changes in irradiance allowing proactive reduction of the active power produced to avoid large fluctuations. However, this approach may not maximize the injection of active power into the grid.

The integration of ESS with RES offers a promising solution for advanced ramp rate (RR) control. The combination of PPC-managed active power ramping and ESS-managed seeding ramping significantly mitigates grid instability caused by RES power fluctuations. In addition, the ESS enables additional ancillary services, such as providing fast frequency reserves with minimal impact on the active power sold. In fact, once the ESS is charged, renewable energy can convert as much wind or solar power as possible into electrical energy.

2.3.5 Grid support: Voltage, Frequency, Fault Ride-Through

Grid support features are fundamental to any PPC. These functions are essential for maintaining voltage and frequency stability, responding quickly to grid disturbances and compensating for any Fault Ride-Through (FRT) events. This ensures that the system can absorb and react to sudden failures, contributing to the overall stability of the power system and minimizing negative impacts on renewable energy generation.

2.3.5.1 Voltage control

The voltage regulation system is, from the system operator's perspective, the most relevant reactive power control mode, as it ensures automatic stabilization of the local voltage. This control is normally performed by an Automatic Voltage Regulator (AVR) integrated in the PPC. According to the grid codes, this voltage regulation system usually employs a voltage droop control mechanism, which includes a deadband around the set point, as illustrated in Figure 2.4a). The control algorithm must be configured to meet the requirements of the grid code, in terms of sensitivity, which refers to the slope and deadband settings, as well as the speed of response, which depends on the parameters set in the controller.

Grid-connected PV inverters behave like voltage-controlled asynchronous generators. With this voltage regulation system, whose characteristics and technical specifications are defined in the grid codes, the PVPP is adjusted to maintain the voltage within an allowed range, thus contributing to grid stability. This regulation is essential as it helps to reduce voltage fluctuations in the grid, allowing to compensate for voltage changes caused by variations in solar irradiance.

This ensures that the voltage at the PoC remains continuously within the reactive power limits and the kVA specified on the nameplate of the inverters, ensuring the correct operation of the PV plant and the stability of the power system.

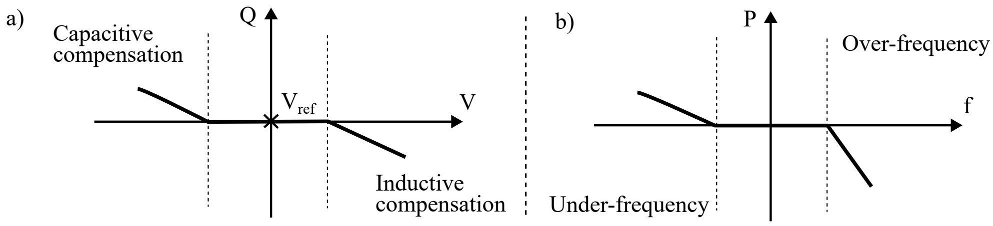

Figure 2.4: a) Voltage control mode. b) Frequency control mode.

2.3.5.2 Frequency control

Frequency response is designed to support the system to the power system by balancing power generation and power consumption. The better balanced the system, the lower the frequency deviation. Different grid codes set different underfrequency and overfrequency modes, each (usually) with a different frequency response. In addition, a deadband is set to avoid large fluctuations. All these parameters are usually set during the design and commissioning of the PPC and can be adjusted to comply with the most demanding network codes. It is important that the frequency response acts as fast as possible to provide real time active power response.

In case of frequency deviations below the lower limit of the deadband, the active power produced must be increased. To realize this control the PPC must be able to manage an active power reserve, and the power inverters must be able to operate at reduced active power.

On the other way around, with frequency deviations above the upper limit, the active power produced must decrease. Normally, the slope of the overfrequency drop is steeper than the underfrequency drop, as can be seen in Figure 2.4b.) If the frequency exceeds the limits set by the System Operator (SO), the generator may trip.

A complementary function can be used to avoid active power fluctuations during frequency swings. The principle involves setting an active power set-point corresponding to the lowest frequency (in the case of underfrequency) or the highest frequency (in the case of overfrequency). The frequency must then return to the admissible range to restore normal operation.

2.3.5.3 Fault Ride-Through

The Fault Ride-Through capability in the PPC allows PV systems to continue operating even when the grid experiences disturbances such as voltage sags or spikes, zero voltages, or frequency fluctuations in both low and high ranges.

This function ensures that the PV system remains operational and has the ability to withstand brief grid events, allowing for continuous operation during short-term faults. To manage these situations, it is essential to have a power quality analyzer that can capture short duration grid events, as these fluctuations typically last only 1-2 seconds. The PPC must be able to react quickly and take appropriate measures to mitigate the effects of these disturbances.

Temporary grid failures are common and cause unavoidable variations in voltage, current and frequency, so it is crucial that the system is able to adapt quickly. This functionality is especially important during critical situations such as natural disasters, where grid fluctuations and failures are frequent, and the ability of the PPC to keep the system operational can be vital to the stability of the plant and the power grid in general.

2.3.6 Plant start up/shutdown

Another standard functionality of PPCs is their ability to efficiently manage PVPP during start-up and shut-down processes [2.20, 2.21]. At start-up, the PPC coordinates the activation sequence of the different elements of the plant, ensuring that inverters, generators and other equipment start up gradually and safely, avoiding current peaks or voltages that could damage components or generate instabilities in the grid. This precise control allows the plant to start up smoothly, minimizing stress on equipment and ensuring smooth integration with the grid.

During shutdown, the PPC also plays an important role in coordinating the orderly disconnection of the plant. This process ensures that inverters and other systems are disconnected from the grid in a controlled manner, avoiding abrupt interruptions or failures that could damage equipment or compromise grid stability. Proper control during shutdown is essential to protect the infrastructure and optimize the lifetime of components.

In addition, the PPC allows the system's behavior to be adjusted based on specific operating conditions or TSO commands. For example, in low demand situations or scheduled maintenance events, the PPC can initiate a partial or total plant shutdown in an efficient manner, ensuring that the plant complies with regulations and operational constraints without compromising grid security. In this way, the PPC contributes to the operational flexibility and stability of the power system, both during the start-up and shut-down phase of the PV plant.

2.4 Grid Standards

The massive inclusion of DEG systems based in RES into the grid challenges the system operators to maintain a stable and reliable system. In order to face those challenges, it has forced the need to create some grid codes in order to ensure the stability to benefit renewable plant capabilities, maintain the stability and good functioning of the different power grids. These grid codes are constantly under development and changing due to the evolution of the technology. Besides many of them are specified locally since the grids around the world differ in different manner. There are many countries that have not grid codes, and the ones which have them, they are changing quickly.

In view of the need to establish a common framework for network codes, some transmission system operators (TSOs) in Europe formed the European Network of Transmission System Operators for Electricity (ENTSO-E). This body has developed European standards, such as EN-50459-1 and EN-50459-2 [2.22, 2.23], which focus on requirements for the connection of distributed generators in distribution networks.

In addition, there are international standards, such as IEC-61727 [2.24] and IEC-62116 [2.25], which address the connection and protection requirements for grid-connected PV systems, as well as methods for anti-islanding protection in these systems. Depending on the country, whether inside or outside Europe, some countries have specific regulations for such systems. For example, in the United States, the IEEE-1547-2020 standard [2.26] applies, while in Japan, the Grid Code for Connecting Renewable Energy Sources [2.27], based on IEEE-1547, is used.

In Spain, the EN 50459 standards have been adapted to the local context and are reflected in the UNE-206007-1 [2.28] and UNE-206007-2 [2.29] standards.

Although these are the most relevant standards for the connection and operation of distributed generation systems, there are also other standards, such as the IEC-61000 series [2.30], which are important for aspects related to power quality.

The RES connected to grids with grid codes must comply with them. If any failure to comply with the grid code would lead to serious financial consequences. This means that after the RES plant construction, it must get a grid compliance certificate in order to enter in the market. In addition, while RES is operating, failure to comply with the grid code could result in RES owner being assigned with penalties, and also plant disconnection requests.

Considering the main European grid codes, some of the most advanced and important grid codes are going to be explained.

The first type of grid code requirements is the voltage and frequency operation ranges in continuous and transient way. These grid codes define the voltage and frequency profiles the RES plant must operate. It is more explained in Subsection 2.4.1.

The second of requirements has to do with the active and reactive control modes. The active power control mode is composed of a frequency response system, curtailment to avoid equipment overload and active power reserve management. It is also necessary to manage the active power rate of change to avoid rapid power changed that could lead to frequency instability. Besides the reactive power control modes is important to manage the voltage on the power system. There are three main types of control modes: reactive power control, power factor control and voltage control. Also, in [2.22, 2.23, 2.31] new power control modes are described. It is more explained in Subsection 2.4.2.

The third requirement is about the contribution to voltage support required by TSO, modifying the reactive power at the output of the distributed plant or at PoC level. It is explained in Subsection 2.4.3.

The fourth type of requirements concerns to the RES response during disturbances. This requirement is probably the most constraining in terms of speed response. The level of injected reactive current is proportional to the voltage system deviation. It is more explained in Subsection 2.4.4.

The essential requirements highlighted in this section are fundamental to ensure the stability, security and efficiency of the electricity grid, especially when integrating distributed and renewable generation resources. In addition to these key aspects, the regulation covers a variety of more detailed technical requirements that must be met to ensure regulatory compliance in various operational situations. Nevertheless, there are other, more specific requirements detailed within the regulations.

2.4.1 Normal Operation Range

2.4.1.1 Continuous Operating Voltage

When a power plant is connected and generating power, it must be capable to operating without problems when the voltage at PoC stays within the range of 90% to 110% of the rated voltage. In the case of a voltage reduction under 95% of the rated voltage, a reduction of the apparent power to maintain the current limits of the generating power is allowed. The management of the plant must take into account the typical voltage rises and drops within the power plant design.

There are other standards, such as EN 50160 which allows the voltage in Medium Voltage (MV) distribution systems to decrease until 85% of rated voltage during a limited time. However, the operational capability of the power plant in that condition must be taken into consideration by the manufacturers and the operator of the power plant.

2.4.1.2 Operating Frequency Range

A connected DEG plant shall be capable of operating continuously when the frequency at PoC stays within the range of 49 to 51 Hz. In case of a wider range from 47 to 52 Hz, the generating plant should be capable of operating until the interface protection trips. Hence the power plant shall at least be capable of operating in the frequency ranges following the requirements of Table 2.1.

A DEG must be able to cope with frequency reductions at the point of connection, minimizing the active power reduction as much as possible. The allowable active power reduction due to low frequency is limited by the solid line in Figure 2.5, which indicates a maximum allowed reduction of 10% of the power per Hz when the frequency drops below 49.5Hz. In some cases, the TSO may require a higher power reduction, although

Frequency range	Time period for operation minimum requirement	Time period for operation stringent requirement
47.0-47.5 Hz	not required	20 s
47.5-48.5 Hz	30 min [a]	90 min
48.5-49.0 Hz	30 min [a]	90 min [a]
49.0-51.0 Hz	Unlimited	Unlimited
51.0-51.5 Hz	30 min [a]	90 min
51.5-52.0 Hz	not required	15 min
[a] Respecting the legal framework, it is possible that longer time periods are required by the responsible party in some synchronous areas		

Table 2.1: Minimum time periods for operation in under-frequency and over-frequency situations

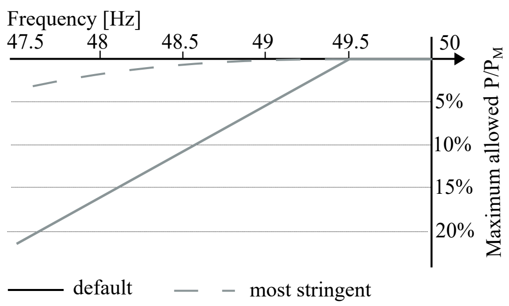

Figure 2.5: Maximum allowable power reduction in case of under-frequency.

this requirement is expected to be limited to that shown by the dashed line in Figure 2.5, which states a 2% maximum power reduction per Hz for frequencies below 49 Hz.

2.4.2 Active Power Response to Frequency Changes

In this subsection the requirements and control modes relative to active and reactive power management are described.

2.4.2.1 Power Response to Over-Frequency

RES plants must be capable of activating active power response to over-frequency events at a programmable threshold f_1 at least between and including 50.2 to 52 Hz with a programmable droop in a range of at least 2 to 12%. Being the droop reference P_{ref}, unless defined different by the TSO. Droop controllers as it will be seen in Section 2.5 is a widely used control methods which respond to SO set-points, not only with active power, but also reactive power.. $P_{ref} = P_{max}$, in the case of synchronous generating technologies and ESS. $P_{ref} = P_M$, the actual AC output power at the instant when the frequency reached the threshold f_1, in the case of all other non-synchronous generating technologies.

The power value is calculated according the droop, getting the maximum power limit. This means, for instance, if the available primary power decreases during a high frequency period below the power defined by droop function, lower power values are permitted. The maximum power limit is described in the next equation.

$$P_{max-limit} = P_M + \Delta P \tag{2.1}$$

$$\Delta P = \frac{1}{droop}\frac{(f_1 - f)}{f_n}P_{ref} \tag{2.2}$$

with f the actual frequency.

The RES plant should be capable of activating active power response to over-frequency as fast as technically feasible with an intrinsic dead-time that shall be short as possible with a maximum of 2 s. After activation, the active power frequency response shall use the actual frequency at any time, reacting to any frequency increase or decrease according to the programmed droop with an accuracy of ± 10 % of the nominal power. Also, the resolution of the frequency measurement shall be ± 10 mHz or less. The accuracy is evaluated within a 1 min average value. At PoC, load if present in the grid, might interfere with the response of the generating plant. However, their effect is not considered in the accuracy evaluation.

If the power plant reaches their minimum regulating level during a frequency increase, they shall maintain the power levels constant unless the TSO requires to disconnect the complete plant or some parts of it. This power response will be deactivated if the frequency is recovered bellow the frequency threshold f_1. Besides, TSO could program another deactivation threshold frequency f_{stop}, in the range of at least 50 Hz to f_1. If f_{stop} is configured to a frequency below f_1, there is not response according to the droop in case of frequency decrease. In this situation, the output power is maintained constant until the frequency falls below f_{stop} for a configurable t_{stop}. Deeper explanation with some figures is performed in EN-50549 [2.23] to better understand the concept, if needed.

2.4.2.2 Power Response to Under-Frequency

Generating power plants shall must be capable to respond adequately against under-frequency events as well. This feature shall be provided when the following conditions are met:

- The generating unit is operating under its maximum generating power (P_{max}) and its available active power (P_A).
- The voltages at PoC of the power plant are within the continuous operating voltage range.

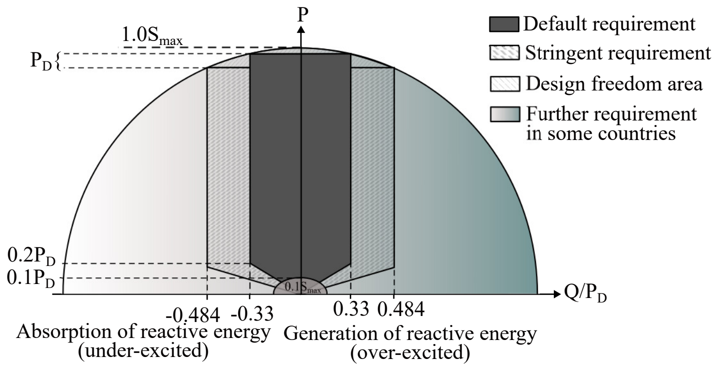

Figure 2.6: Reactive power capability at nominal voltage.

- The operating current is under the current limit.

In case of a ESS as a generator unit, active power response to under-frequency shall be provided in both, charging/generating modes, considering the SOC.

The active power response to under-frequency must be delivered at a programmable frequency threshold f_1, at least between 49.8 and 46 Hz with a programmable droop in a range of at least 2 to 12 %. The droop reference P_{ref} is P_{max}. If the available primary power of a local set values increases during an under-frequency period above the power defined by the droop function, higher power values are allowed. The power values calculated according to the droop is therefore a minimum limit, calculated with the same equations (2.1) and (2.2) than over-frequency case.

The generating unit shall be capable of activating the active power response to under-frequency as fast as possible, taking into account the intrinsic dead-time, that must be as short as possible (less than 2 s) with a step response time of 30 s, unless another value is defined by the TSO. Deeper explanation is performed in EN-50549 [2.23] to better understand the concept.

2.4.3 Reactive Power Response to Voltage Changes

When the contribution to voltage support is required by the TSO, the RES plant shall be designed to have the capability of managing reactive power according to the following requirements.

2.4.3.1 Voltage Support by Reactive Power

RES generating plants shall not lead to voltage changes out of acceptable limits, normally defined by national regulation. Therefore, these generation plant shall be able to contribute to meet the requirements during normal grid operation. Throughout the continuous operating frequency and voltage range, explained in 2.4.1, the power plant is able to deliver the power following the requirements below. Outside these ranges, the generating plant shall follow the requirements as better as possible although there is no specified accuracy.

In Figure 2.6, a graphical representation of the minimum and optional capabilities at nominal voltage are depicted. The power plants shall be able to operate with reactive power provision as defined by the TSO. As it can be seen, the default reactive power requirement Q is up to 33% of P_D over-excited and under excited when the active power is above 20%. If the active power is below P_D, the reactive power shall be provided as shown in Figure 2.6 to a minimum active factor of 0.52. The stringent reactive power requirement Q is up to 48.4% of P_D over and under excited, when the active power is above 20% P_D. While is operating at a active power below 20% P_D reactive power shall be provided according to Fig. 2.6 to a minimum active factor of 0.38.

The reactive power capability shall be evaluated at the terminals of each generating unit or at PoC.The reactive power of generating plants with S_{max} above a power threshold to be defined by the TSO shall be evaluated at PoC. Deeper explanation is performed in EN-50549 [2.23] to better understand the concept.

2.4.3.2 Control Modes

Where necessary, the TSO must specify how voltage control should be contributed. This control can be applied at the terminals of the DER or at the PoC, depending on the size of the generating plant. These plants must be able to operate in the following control modes, which are exclusive (only one can be active at a time):

- Set-point control modes: This mode allows setting a reactive power (Q) or power factor (cos φ) reference, controlling the reactive power and the output power factor according to the defined set-point.
- Voltage related control mode: In this mode, the reactive power is adjusted according to the voltage value, controlling the reactive power Q(U).
- Power related control mode: Here, the reactive power Q(P) or the power factor cos φ(P) is adjusted according to the value of the active power output.

A more detailed explanation of these control modes can be found in EN50459 [2.23].

2.4.4 Disturbance Operation

In general, generating plants should contribute to overall power system stability by providing immunity towards dynamic voltage changes unless safety standards requires a disconnection.

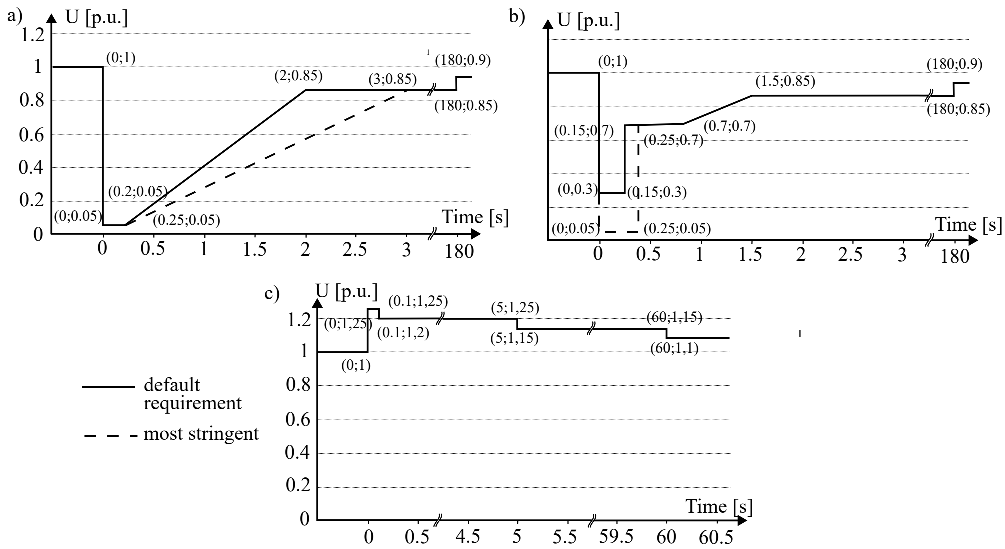

Figure 2.7: a) Under-voltage ride through capability for non-synchronous generating technology. b) Under-voltage ride through capability for synchronous generating technology. c) Over-voltage ride through capability.

In the following subsections the required immunity for power plants considering the connection technology of the generating modules are described. They provide the withstand capabilities regardless the interface protection.

The described immunity requirements are independent of the interface protection settings. Disconnection settings of the protection relay always overrule technical capabilities. So, whether the generating plant will stay connected or not, will also depend on those settings.

2.4.4.1 Rate Of Change Of Frequency Immunity

Rate Of Change Of Frequency (ROCOF) immunity of a power generating plant means the generating modules in this plant, stay connected to the distributed network and they can operate when the frequency on the distribution network changes with a specific ROCOF. The generating units and all elements in the power plant might cause their disconnection or impact their behavior having the same level of immunity.

The generating modules in a generating plant must have ROCOF immunity to ROCOF equal or exceeding the values specified by the TSO. If no ROCOF immunity value is specified, at least 2 Hz/s shall be applied. The ROCOF immunity is defined with a sliding measurement of 500 ms.

2.4.4.2 Under-Voltage Ride Through (UVRT)

Power plants must comply with the following requirements, excluding CHP, fuel cell, rotating machinery and less than 50 kW. These requirements are applied for all kind of faults (1ph, 2ph and 3ph). Besides the requirements changes a little for non-synchronous and synchronous generating technology.

Generating modules may be capable of remaining connected to the distribution network as the voltage at PoC remains above the voltage time curve (Figure 2.7 a) for non-synchronous power plant and Figure 2.7 b) for synchronous power plants), being the voltage relative to the rated voltage at PoC. The smallest phase to neutral voltage, or if no neutral is present, the smallest phase to phase voltage shall be evaluated.

The TSO may define a different UVRT characteristic. Nevertheless, this requirement is expected to limited to the most stringent curve as indicated in Figure 2.7 a) and Figure 2.7 b). This implies the whole generating plant must meet the UVRT requirements. This includes all elements of the generating plant (generation units and disconnection elements).

For a generating unit, this requirement is considered satisfied if it remains connected to the distribution grid as long as the voltage at its terminals stays above the specified voltage-time curve.

After the voltage returns to continuous operating voltage, 90% of pre-fault power or available power whichever is the smallest shall be resumed as fast as possible, but at the latest within 1 s for non-synchronous generating units and 3 s for synchronous generating units, unless the TSO requires another value.

2.4.4.3 Over-Voltage Ride Through (OVRT)

Generating modules must be capable of remaining connected to the distribution grid as long as the voltage at PoC stays below the voltage time curve specified in Figure 2.7c). The highest phase to neutral voltage, or if no neutral is present, the smallest phase to phase voltage shall be evaluated. However, if the pre-fault voltage is below nominal and a voltage step exceeds 25% of the rated voltage, disconnection is permitted.

This means that not only the generating units shall comply with this OVRT requirement but also all elements in a generating plant that might cause its disconnection. Excluding CHP, fuel cell, rotating machinery and hydro below 50 kW.

2.4.4.4 Phase Jump Immunity

Phase jump immunity in a power generating plant means that the generating modules remains connected to the distribution grid, and they continue operating during and after a phase jump occurs. All generating units and components within the plant that could cause a disconnection or affect the performance must maintain the same level of immunity.

The generating modules must have phase jump immunity of at least 20° in the event of a symmetrical phase jump. After a phase jump, 90% of the pre-fault power or available power, whichever is lower, must be restored as fast as possible, but no later than 3 s for synchronous generating technologies and 1 s for non-synchronous generating technologies.

2.5 Grid Interface

Power converters used in DEG systems play an essential role in connecting these systems to the grid. Although there are different control strategies, these converters generally follow certain common principles to ensure their correct operation and integration into the grid. These principles are based on a hierarchical control architecture to manage both current injection and grid support under various operating conditions. Generally speaking, power converters are equipped with several control layers that operate in a coordinated manner, as it can be seen in Figure 2.8. At the core of this structure is the current control, whose main function is to regulate the current injection demanded by the system, ensuring that the converter meets the grid requirements in terms of stability and power quality. This control is key for any grid connection strategy [2.32, 2.33]. Power converter control alternatives can be divided into three main categories: grid-forming, grid-feeding or grid-following and grid-supporting, each with a different approach to grid interaction. Depending on the control strategy used, there will also be a voltage controller, in order to set the voltage commanded or calculated by the control system.

In these converters/grid interfaces, synchronization methods play a key role in their operation. Synchronization ensures that the converter operates in perfect coordination with the grid, allowing precise injection of current in phase with the network parameters. There are two main approaches to synchronization. The first includes methods that rely on a Phase-Locked Loop (PLL), common in GFD systems and, in some cases, in GFM systems. The second approach corresponds to Power Synchronization [2.34], used mainly in grid-forming systems, where synchronization is achieved intrinsically by means of controllers such as droop or VSG, since these systems are responsible for setting the grid parameters.

In summary, power converters used in DER systems must meet certain criteria to ensure a safe and efficient connection to the grid. Depending on the control strategy employed, these converters can simply inject power into the grid, provide active support or even form a grid in off-grid applications. The choice of the appropriate control strategy and synchronization methods is crucial to ensure the correct functioning of the system under different operating conditions. Throughout the following subsections, these concepts will be discussed in depth, explaining how they are implemented

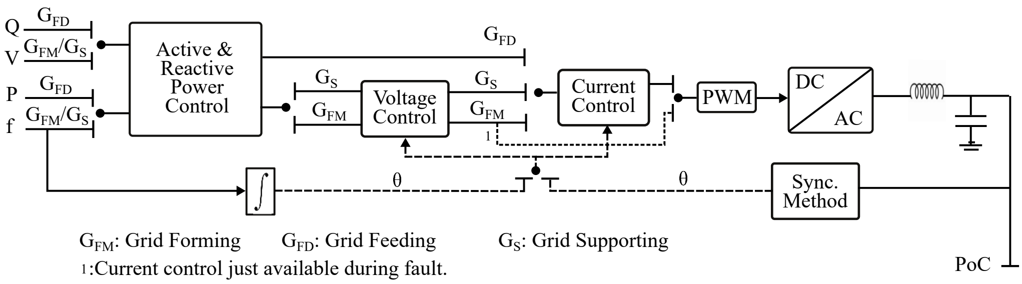

Figure 2.8: Control layers typically utilized for hierarchical control of DEGs [2.35].

Table 2.2: Quick comparison among systems.

Feature	Grid-Forming	Grid-Feeding	Grid-Supporting
Frequency Control	Yes	No	Partial (support)
Voltage Control	Yes	No	Partial (support)
Islanded Mode	Yes	No	No
Virtual inertia	Normally yes	No	Sometimes
Typical application	Grid-tied, grid-off	PV/ WG grid-tied	DEGs with high RES ratio

in converters and how they interact with the grid to meet the established technical requirements.

2.5.1 Power Converter Control Alternatives

Advancements in power electronic devices, from the material level to flexible control strategies, have significantly increased the use of power converters in interfacing distributed generation systems with the grid. These converters facilitate energy conversion between alternating current (ac) and direct current (dc) sources [2.36–2.38]. These converters in ac power systems can operate in islanded or grid-tied modes. Furthermore, these power converter are categorized into three main categories, such as GFM, GFD and GS converters, depending on their working principle and control [2.39]. In Table 2.2 a small comparison among power converter control alternatives are shown, with the main characteristics and differences.

2.5.1.1 Grid-Forming

Power converters with grid-forming control structures are crucial for modern power systems, specially due to the increasing of DEG/RES, as well as the need to maintain the stability and power quality of the grid. These converters are a key part for the standalone operation, because they can create and maintain the power grid guaranteeing specific levels of ac voltage and frequency [2.33].

Essentially, grid-forming converters are controlled in closed loop to work as an ideal ac voltage source with an amplitude E and frequency ω. Normally, these systems have a low output impedance, therefore they need an accurate synchronization system for working in parallel with other grid-forming converters (in Figure 2.9 a), an example is depicted). This control system regulates the active and reactive power injected into the grid throughout the magnitude and phase voltage control at the PoC, working as ideal voltage source with a small impedance which results in a highly dynamic behavior during transients. These transients, as well as the power exchanged, will depend on the value of their output impedances.

Depending on the characteristics of the grid, power converter with grid-forming control strategies can work as a slack bus in islanding operation, or as a power source by using additional loops, which adapt active and reactive power injection to provide voltage and frequency voltage. Besides, the generated ac voltage for these converters in a microgrid, it is used as a reference for other grid-feeding converters connected to this grid. A practical example of this kind of control is a stand-by UPS system, which is normally disconnected to the grid when the operation conditions are normal, and it is activated when there is a failure, in order to create the grid. The control structures of these converters can be divided into three levels: primary, secondary and tertiary. Figure 2.10 shows a concise scheme valid for GFM.

1. Primary control: voltage and frequency control by emulating the behavior of traditional synchronous generators with real or synthetic inertia, adjusting the voltage and frequency, using VSG or droop control systems [2.40–2.42] .

2. Secondary control: voltage and frequency restoration, correcting deviations caused by the primary control, restoring to nominal values. Furthermore, it ensures coordinated and conflict-free operation between multiple grid forming converters [2.43–2.45].

3. Tertiary control: operational optimization, focusing on long-term optimization, considering economic and operational aspects in energy dispatch, minimizing expenses and better management of renewable energy and storage [2.44, 2.46, 2.47].

Hence, these strategies allow RES power converters, such as wind generation or PV panels, to operate in an automatic or semi-autonomous way, even in the absence of a connection to a traditional grid, without completely depending on a network to establish the operating frequency and voltage, generating its own reference signals.

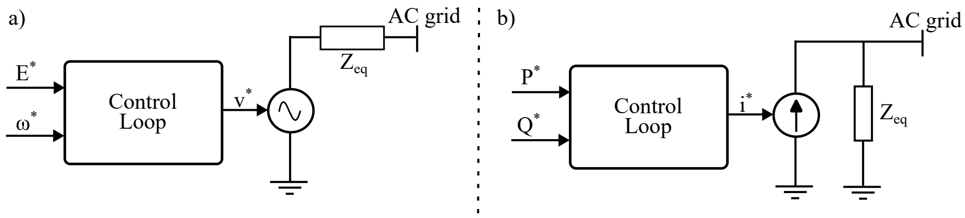

Figure 2.9: a) Grid-forming power converter scheme. b) Grid-feeding power converter scheme.

2.5.1.2 Grid-Feeding

Power converters with a grid-feeding structure are essential for injecting electrical energy into the grid. Normally, converters under this control scheme are modeled as a current source, with a parallel admittance, allowing the operation beside other grid feeding converters connected to the grid, as it can be seen in Figure 2.9 b).

These power converters regulate the power injection by controlling the active and reactive currents, adjusting to the grid voltage magnitude and frequency. It is important to highlight grid feeding converters cannot operate in island mode per se; they need a power grid to connect to, created by another grid-forming converter or a traditional synchronous generator, that establishes the frequency and voltage amplitude of the grid. For that, these converters need a synchronization system in their control system. In addition, an external control loop can be implemented to adjust the power set-points, providing additional frequency and voltage regulation at the connection point, becoming a grid supporting converter as it can be seen in Section 2.5.1.3.

As grid feeding structures, the control structures of these converters can be divided into three levels. Figure 2.10 shows a concise scheme valid for GFD.

1. Primary control: responsible of the instantaneous response of the converter, by controlling the injected current into grid, complying with active and active requirements, normally through the use of synchronous reference frames (d-q axis). Besides, it uses MPPT methods to optimize the energy capture of RES, adjusting the conditions of the operation [2.40, 2.48].

2. Secondary control: in a longer scale, it corrects any deviation from primary control. For that, it adjust the active and reactive power developed for fulfilling the grid conditions, improving the stability and power factor. Furthermore, it is responsible for coordinating with the grid, synchronizing with the grid frequency and phase [2.44, 2.45].

3. Tertiary control: improve energy planning and transmission, reduce costs and efficiency and thus increase system reliability [2.47].

Summarizing, grid-feeding converters have an important role to play in the transition to more sustainable and efficient energy systems. They provide a stable and

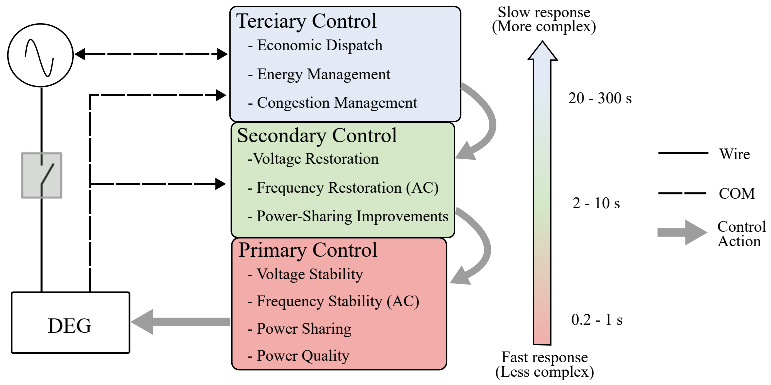

Figure 2.10: Control layers typically utilized for hierarchical control of DEGs [2.35].

controlled connection to RES sources, ensuring the quality of the energy supplied and contribute to the stability and efficiency of the power system.

2.5.1.3 Grid-Supporting

Finally, grid-supporting power converters, are quite important for the regulation and stability of power systems, due to they not only inject power into the grid, but also help maintaining the stability of the system's voltage and frequency, providing essential auxiliary services. They are widely used in DEG system, based in PV systems and wind generation, in order to improve the efficiency in the available power injection. Notice this explanation is considering the traditional grid-supporting concept. Lately, grid-supporting is being considered part of an outer loop of a GFM or GFD scheme [2.49], contributing to voltage and frequency regulation.

There are two main types of grid-supporting converters. The first type is controlled as a current source, based on to the grid-feeding structure, where the objective is not only to feed the loads connected to the grid, but also adjusts the injected energy to contribute to the regulation of the amplitude and frequency of mains voltage. In Figure 2.11 a), a simple scheme is drawn. This feature is quite common in wind generation DEG, which must provide some energy for regulatory purposes. The second type uses an ac voltage source connected with a link impedance (which can be real or virtual), which is based on a grid-forming scheme (see Figure 2.11 b). This kind of of converters can play in the frequency and amplitude voltage regulation, in both grid-connected and off-grid mode, without a grid forming converter connected to the grid.

The control of these converters, as the other structures, is organized in several levels to guarantee the security and stability of the grid. Figure 2.10 shows a concise scheme valid for GS.

1. Primary control: regulating the instantaneous response of the power converter

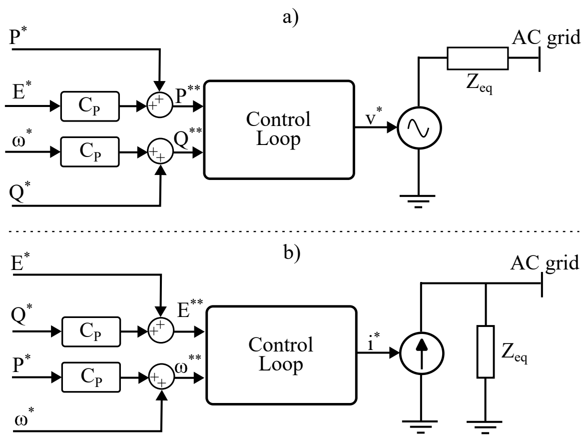

Figure 2.11: Grid-supporting power converter schemes.

according to the grid conditions, managing the injected currents, in order to fulfill with the active and reactive power requirements, while maintaining the output voltage within acceptable limits and avoiding disturbances [2.48] .

2. Secondary control: it acts on a higher time scale, correcting possible deviations caused by the primary control, restoring the nominal values of frequency and voltage after the disturbance, in addition ensuring the coordinated operation between power converters [2.45].

3. Tertiary control: optimizing energy scheduling and dispatch, minimizing costs and maximizing efficiency, thus improving system reliability [2.47].

Therefore, these converters are so important for the grid stability, ensuring the coordination among converters, the efficiency and stability.

2.5.2 Power Control

Considering the structure of the interface of DER systems with the grid, shown in figure 2.8, power controllers are very important in order to manage the interaction between the converter and the grid, ensuring proper control of active and reactive power according to operational needs. There are several control methodologies, each of which can be applied to different types of DER system connection, be it GFM, GFD or GS.

2.5.2.1 Direct Control by Regulator

This strategy, mainly used in GFD topologies, is based on classical controllers such as PI or proportional controllers [2.50]. It is shown in Figure 2.12 a). The desired active

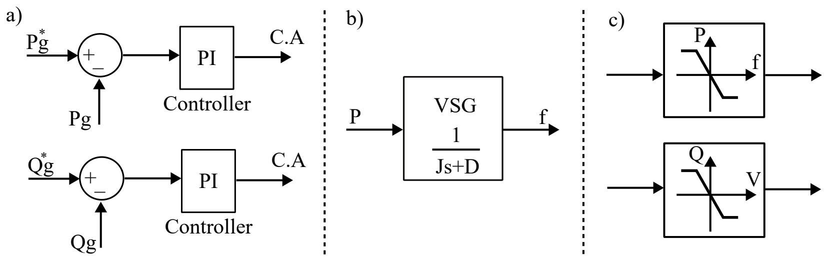

Figure 2.12: a) Power control by traditional regulators. b) Power control by VSG. c) Power control by droop controllers.

or reactive power is set as a reference and compared with the measured values. The resulting error is used to adjust the control action of the converter. Although it is a simple and efficient methodology, it is limited in its ability to respond to disturbances. It can also be applied in other systems, such as reactive power control in GFM and GS.

2.5.2.2 VSG Controller

The VSG emulates the dynamic behavior of a conventional synchronous generator, providing converters with the ability to simulate inertia and damping [2.51]. Figure 2.12 b) shows a small schematic of the VSG. This system is key for frequency control in the grid, which makes it an ideal solution for GFM systems. For the reactive power control, a direct regulator or a droop controller are normally used. In addition, it allows power injection on demand, ensuring dynamic and efficient support in grids with high renewable penetration. In Section 2.6, it is explained in much more detail, as it is key to the development of this thesis. Although its implementation is more complex, its versatility makes it applicable in all control topologies (GFM, GFD and GS).

2.5.2.3 Droop controller

Droop control is a widely used technique in decentralized distributed generation systems. This controller adjusts the active power as a function of frequency variations (P-F droop) and the reactive power as a function of voltage variations (Q-V droop), as can be seen in Figure 2.12 c). If, for example, the frequency decreases, the inverter injects more active power to stabilize it; if the voltage decreases, the reactive power is increased. Although it is simple to implement and works well in GS systems [2.32], its main limitation is the lack of inertia and damping, which makes it less robust than the VSG. Despite this, droop is considered a particular case of VSG, as explained in [2.51].

2.5.3 Voltage Control

Voltage controllers in power converters are fundamental to managing how these devices interact with the power grid. Depending on the control strategy used, such as grid-forming, grid-feeding or their supporting version, voltage control plays a different role [2.52, 2.53].

In the case of the grid-forming strategy, the converter creates its own grid, setting both voltage and frequency, which is essential in grid-off systems such as microgrids. Here, the converter continuously adjusts these parameters to maintain stability. This is usually controlled via a PI loop or a droop control.

In the grid-feeding strategy, the converter does not generate the grid, but connects to an existing grid, simply injecting the generated power. It does not usually need a specific voltage controller, as it is based on current control.

Moreover, the grid-supporting version of GFM or GFD, IBR also contributes to grid stability by providing reactive and active power in response to voltage and frequency fluctuations, respectively, when disturbances occur. Such a voltage regulator is designed to cope with grid variations. Such a regulator is usually controlled by a droop control or directly by a PI.

2.5.4 Current Control

Correctly tuning the current controller in a power converter is so important to ensure optimal performance in the upper control loops, as this controller must have a significantly faster response than the others. Although this thesis does not focus specifically on current control strategies, the most commonly used controllers in this area will be considered, which are the basis on which this work is based. One of the most common methods is the PI controller in the synchronous reference frame, widely adopted for the control of grid-connected power converters. This approach requires the conversion of the current variables to the synchronous reference frame, which involves the use of a synchronization system, such as a PLL. The advantage of this type of control is its simplicity and efficiency in current regulation under normal operating conditions.

Another option is the Proportional Resonant Controller (PR) controller in the stationary reference frame $\alpha\beta$, which makes it possible to maintain a zero error in steady state without the need to transform the current variables [2.36, 2.54]. This type of controller is particularly useful in applications where harmonic compensation is required, as it can be adjusted to operate at different harmonic frequencies, offering more flexible control in systems where harmonic distortion is a problem.

Although current control can be used in all converter control structures, in the case of GFM, this controller may not be necessary, or may only be activated in fault conditions [2.55]. This is because this control would be activated to protect the converter as well as the connected equipment, as the current would be very high. Under normal conditions, the control priority is on voltage and frequency, which allows the converter to regulate the power injected or absorbed without being limited by the magnitude of the current. There are several methods where even in the absence of active current control, auxiliary control is applied during faults [2.56, 2.57]. In countries such as the United Kingdom (UK), their grid codes [2.58] explicitly prohibit this current control loop under normal conditions.

2.5.5 Synchronization System

Grid synchronization methods can be important and necessary to avoid connections and disconnections that compromise the operation of renewable energy sources, reduce penalties and losses of generation units, assist in the performance of power converters and determine the mode of operation of power converters, helping to comply with certain grid code regulations.

For this purpose, such a synchronization system must monitor and estimate grid parameters such as amplitude, frequency and angle of the grid voltage. These systems are mainly based on PLL structures, which are closed-loop controlled and can be used for single-phase and three-phase systems [2.59, 2.60]. They offer fast response speed to voltage disturbances, as well as harmonic rejection. To mention an example of such disturbances, these systems help to provide the necessary power system capacities in power systems by maintaining the grid fault connection, improving the stability of the power system [2.61, 2.62].

Therefore, for an accurate response, in compliance with current regulations, converters must have a robust control, with a fast, efficient and safe synchronization system.

However, the need for synchronization systems such as PLLs depends on the control structure used in DER. As mentioned, in some configurations of both GFD and GFM systems, the use of a PLL is essential to synchronize IBR with the grid. However, there are certain GFM systems where it is not necessary to employ a PLL, as these systems internally generate the reference frequencies, angles and voltages to operate in island mode. In addition, they can employ Power Synchronization [2.34] on external loops when grid support is required.

The need for a PLL depends not only on the control structure of the DEG, but also on the type of power controller implemented. For example, in controllers such as VSG-based controllers [2.63], direct current control [2.64], energy-based control [2.65] or reactive power control [2.48], the use of synchronization systems is not as important.

Although in some cases not strictly necessary, synchronization systems may still be useful to improve system stability and performance. The following is a review of the most common synchronization methods, detailing the one most commonly used in the industry.

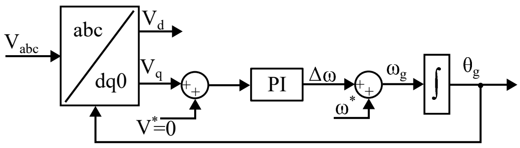

Figure 2.13: SRF-PLL basic structure.

2.5.5.1 Synchronization Methods

The synchronization unit is dedicated to extracting information from the network, which will be used later in the control loops, mainly by reading the voltage. This is a subject that has been studied and referenced many times in the literature, and there are many different methodologies, improving different aspects of system operation. Some existing methods are $\alpha\beta$ PLL, FPD, $d\alpha\beta PLL$, adaptive d$\alpha\beta$ PLL, MSHDC PLL, DN$\alpha\beta$ PLL, PMAFPLL, $\alpha\beta$ EPMAFPLL, EPMAFPLL Type 2, LPNPLL, FFTPLL, EPLL, DSOGI-PLL and DSOGI-FLL [2.66, 2.67] while in [2.33, 2.59, 2.68, 2.69] some comparison and benchmark of the newest methods are done. However, this text is going to focus on the more widely used methodology, with a great ease of use and an improved version, which is able to reject some unbalances from the grid voltage. The first method is based on the transformation of the mains voltage into a synchronous reference frame, and the PLL can be controlled with a simple PI controller, which is known as Synchronous Reference Frame PLL (SRF-PLL). The second also uses the synchronous reference frame, but decomposing and decoupling the voltage into positive and negative sequences [2.68, 2.70, 2.71]. This system is known as Decoupled Double Synchronous Reference Frame PLL (DSRF-PLL).

2.5.5.2 Synchronous Reference Frame Phase-Locked Loop

This PLL technology has been widely used in grid-connected power converters by using the mains voltage. In three-phase systems, the SRF-PLL is the most commonly used, shown in the figure. This system converts the instantaneous three-phase voltage at the abc reference frame into a rotating dq system by using the Park and Clark transformations. The angular position of this dq reference frame is controlled by the closed loop, making the V_q component zero, estimating the Δw value. In addition, the nominal frequency value is included in the control loop in order to improve the dynamics of the theta estimation, which is obtained by integrating Δw. The basic SRF-PLL scheme is shown in Figure 2.13). Since the synchronous frame is rotating with positive angular velocity, the SRF-PLL works accurately in balanced systems. However, in the presence of unbalanced faults its performance deteriorates. This happens due to the presence of doubled line frequency oscillations that are induced by the negative voltage sequence.

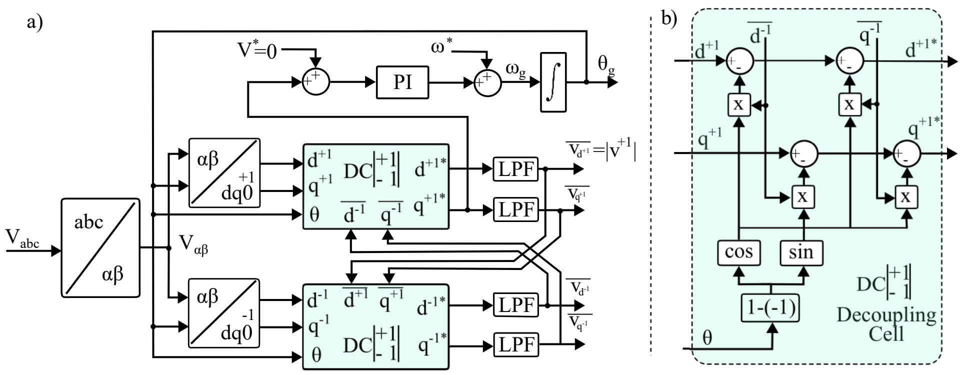

Figure 2.14: a) DDSRF-PLL basic structure. b) Decoupling cell description. The one shown in the picture is for the positive sequence.

2.5.5.3 Decoupled Double Synchronous Reference Frame Phase-Locked Loop

SRF-PLL performance, as it was aforementioned, it is not perfect under unbalance grid conditions. These issues are overcome by the implementation of DDSRF-PLL, where the coupling between positive (+1) and negative(−1) sequences is gone. For its implementation the grid voltage must be converter into the positive and negative synchronous reference frames, as it can be seen in Fig. 2.14 a). Therefore, two SRF are used, one for the the positive sequence and the another for the negative, rotating at their corresponding angular speed. Following the transformation, the decoupled grid is used for canceling the effect that positive and negative sequences have on each other. Once the sequences are extracted and separated, the SRF-PLL algorithm is used to estimate the grid phase angle.

In order to estimate both sequences, two decoupling cells (DC) are used, as it can be seen in Fig.2.14 a) and b). Those components are mainly dc components which can be sued for computing the voltage grid magnitude through a LPF, in order to remove any oscillation in the voltage vector estimation.

The q component of the positive sequence is passed through the phase extraction algorithm of the SRF-PLL, with the PI controller to make it zero, and estimate the phase angle. Due to the decoupling, DDSRF-PLL ensures satisfactory operation under unbalanced grid faults. Because DDSFR uses the SFR algorithm in the phase extraction, it exhibits high frequency and over oscillation during faults. Furthermore, it is not perfect, as in the presence of harmonics, it does not perform equally well.

2.6 Virtual Synchronous Generator

In traditional power systems, the generation elements used to be run, mainly by traditional synchronous machines. However, due to climate change awareness, global generation is migrating towards more sustainable and environmentally friendly alternatives. This is done through the use of DEG systems, based on RES, which replace fossil fuels that have a high environmental cost (such as greenhouse emissions, lack of source material, etc.). However, these DEG/RES elements have virtually no rotating mass, which is the main source of inertia and damping in power systems. This inertia is provided by the kinetic energy of the rotor, just as damping is provided by friction, stator losses, as well as damper winding, in conventional SGs. However, in DEG/RES systems, there is no such machine/grid interface, which is provided by a power converter with switched elements, restricting a very important function in generation systems in terms of grid stability [2.72].

With the growth of these DEG/RES systems, their impact in terms of low inertia and damping on the grid dynamics increases, weakening the system. Therefore, different solutions have been studied to implement such inertia in a virtual way. One of these solutions is the implementation of these systems through the use of ESS next to the power converters, as well as an appropriate control mechanism, providing a specific amount of inertia for a specified time (typically between a few milliseconds to a dozen seconds).o a very important function in generation systems in terms of grid stability [2.51, 2.73, 2.74]. This concept is known as VSG. With the implementation of this idea, these units can operate similarly to a synchronous generator, exhibiting inertia and damping properties for short periods of time [2.2].

In summary, the virtual inertia concept is based on three main components: energy storage, power inverters and control mechanisms. The VSG acts as an interface between the main energy source and the grid, emulating the dynamic function of a synchronous generator and adjusting system power according to grid conditions and variations in energy demand. This approach provides a solid basis for integrating a large number of DEG/RES systems into future power grids without compromising their stability, as has been extensively documented and discussed in the literature [2.51], [2.75].

For this purpose, the VSG block emulates the dynamic function of a SG, based on the swing equation of a synchronous generator, which is used to mimic the dynamic behavior of a real synchronous generator in an electrical system. The swing equation is a fundamental differential equation, commonly used for transient analysis of a generator, which can be expressed with the following equation, as [2.2] explains.

$$P_{in}(t) - P_{out}(t) = J\omega_m(t)\frac{d\omega_m(t)}{dt} + DP_{base}\frac{\omega_m(t) - \omega_g(t)}{\omega_o} \tag{2.3}$$

where P_{in} is the virtual shaft power determined by the governor, P_{out} is the measured output power, P_{base} is the power rating of DEG, J is the virtual inertia, D is the virtual damping factor, ω_m is the virtual rotor angular frequency, ω_g is the angular

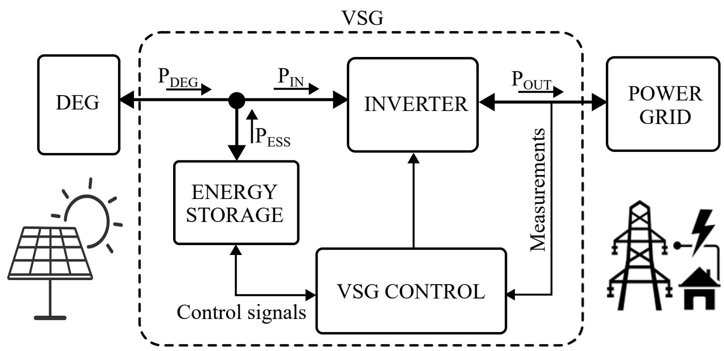

Figure 2.15: Conceptual structure of VSG.

frequency of the point where the voltage sensor is installed, and ω_o is the nominal angular frequency.

In this equation the values of J and D are extremely important, because they are the parameters that can be extracted from a real synchronous machine. J is the inertia characteristic, given by equation (2.4).

$$J = 2HS_0/\omega_o^2 \tag{2.4}$$

where H is the machine inertia constant, S_0 is the nominal apparent power of the machine and ω_o is the system frequency. The parameter H, known as the inertia constant, defines the duration for which a machine can sustain its nominal load using only the energy stored in its rotating mass. A system with a higher H value, meaning a larger time constant, provides a slower response to disturbances but experiences a smaller frequency deviation. Although H depends on the machine's size and power, in typical synchronous machines, it generally ranges between 2 and 10 seconds.

In Fig. 2.15, the block "governor model" is depicted, which is basically a ω-P droop controller that can be represented as:

$$P_{in}(t) = P_o - k_p P_{base} \frac{\omega_m(t) - \omega_o}{\omega_o} \tag{2.5}$$

where P_o is the normal value of the active power and k_p is the droop coefficient in per unit.

By substituting $k_p = (k_p P_{base})/\omega_o$, and $D = (DP_{base})/\omega_o$, and eliminating P_{in} from (2.3) and (2.5):

$$P_o - k_p(\omega_m(t) - \omega_o) - P_{out}(t) = J\omega_m(t)\frac{d\omega_m(t)}{dt} + D(\omega_m(t) - \omega_g(t)) \tag{2.6}$$

Here, $\omega_g(t)$, which is a measured parameter to provide the synchronous frequency for damping power calculation, is replaced by a constant value, that is, nominal frequency

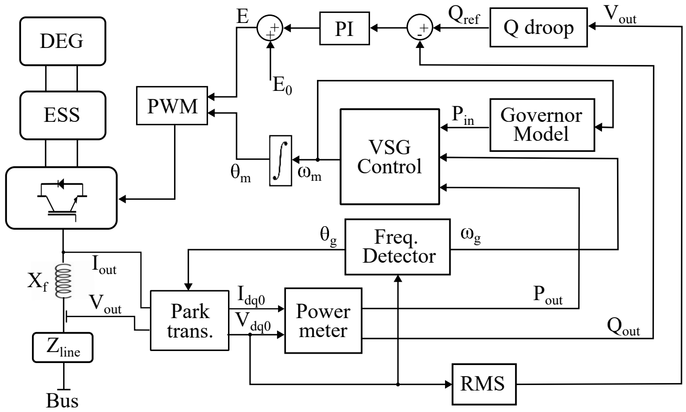

Figure 2.16: Conceptual structure of VSG.

ω_o. Thus, the damping factor D is equivalent to droop coefficient k_p. Besides the grid frequency is obtained through a PLL control algorithm. Through this modification, a simpler model is obtained. Hence the dedicated governor can even be removed. Nevertheless, in this case, no damping effect cased by damper winding is emulated, which might result in larger output power oscillations.

Considering the scheme of Fig.2.16 as the basic VSG control model, once the VSG equation (2.3) is demonstrated, the other elements of the scheme are going to be explained. The main control scheme is done in synchronous reference frame, by using the park transformation [2.76]. This transformation is performed by using the transformation matrix explained in equation (2.7).

$$\begin{bmatrix} d \\ q \\ 0 \end{bmatrix} = \frac{2}{3} \begin{bmatrix} sin(\theta) & sin(\theta - \frac{2\pi}{3}) & sin(\theta + \frac{2\pi}{3}) \\ cos(\theta) & sin(\theta - \frac{2\pi}{3}) & cos(\theta + \frac{2\pi}{3}) \\ \frac{1}{2} & \frac{1}{2} & \frac{1}{2} \end{bmatrix} \begin{bmatrix} a \\ b \\ c \end{bmatrix} \tag{2.7}$$

The grid frequency is detected through the frequency detector block, which is based in a PLL method, such as the one explained in Section 2.5.5. Notice the frequency at output voltage can vary during transients if the line impedance (Z_{line}) is too big, although this is not usually a problem in a microgrid. In case of the block "Power meter", the active and reactive powers are computed by using the output voltage and current of the inverter, by transforming the read voltage and current by using equation (2.7) into the synchronous reference frame by using the equations (2.8) and (2.9).

$$P_{out} = \frac{3}{2}(v_d i_d + v_q i_q + 2v_0 i_0) \tag{2.8}$$

$$Q_{out} = \frac{3}{2}(v_q i_d - v_d i_q) \tag{2.9}$$

In order to calculate the root mean square (RMS) of the output voltage, calculated through the "RMS" block, (2.10) is used.

$$V_{out} = \sqrt{v_d^2 + v_q^2} \tag{2.10}$$

In the case of the block "Governor model", shown in (2.11), it is basically a $\omega - P$ droop controller where ω_o is the nominal angular frequency, P_o is the set active power, k_p is the $\omega - P$ droop coefficient, and T_d is the time constant of the governor, which emulates the mechanical response.

$$P_{in} = P_o - \frac{k_p}{1 + T_d s}(\omega_m - \omega_o) \tag{2.11}$$

The "Q droop block" is the voltage-reactive power droop controller, where E_0 is the nominal voltage, Q_o is the set reactive power and k_q is the V-Q droop coefficient.

$$Q_{ref} = Q_o - k_q(V_{out} - E_0) \tag{2.12}$$

Taking into consideration the Governor model and the Q-V droop blocks, the relation between active power to frequency and the relation between reactive power and voltage is done, respectively. The PI controller of Figure 2.16 is used to control the reactive power set-point calculated by the Q-V droop controller, obtaining the necessary voltage, which when added to the nominal voltage (E_0), gives the voltage to be applied to the PWM block of the inverter.

This basic VSG scheme is working as a voltage source, but supporting an existing grid, so it can be classified as a grid-supporting scheme, as the one explained in Section 2.5.1.3.

Once the basic operation of the VSG has been explained, and considering its wide development by the scientific community and its application in real systems, several strategies for its implementation have been proposed. In this section, some of the most common VSG strategies will be reviewed, with the aim of exploring the different options available in the market [2.63, 2.77]. These control techniques are not only limited to the use of the swing equation (2.3), as there are also alternative approaches to add inertia to the system based in other techniques. Figure 2.17 presents a schematic with different topologies [2.78–2.81].

2.6.1 KHI VSG Topology

Kawasaki Heavy Industries (KHI) VSG topology has been designed for grid-connected converters, using impedance models based on phasor diagrams of SG [2.82]. This topology is particularly effective in ensuring proper operation under different types

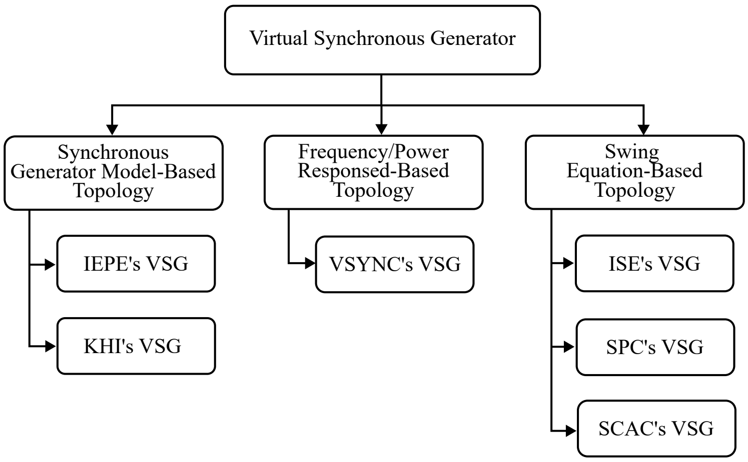

Figure 2.17: Virtual Synchronous Generator categories and topologies [2.77].

of loads, including unbalanced and non-linear loads. The system employs a current control loop that generates the current references according to the SG phasor diagram, as shown in Figure 2.18.

To simulate the behavior of a synchronous generator, a governor model is implemented, which adjusts the angular velocity of the virtual rotor as a function of the active power deviation. This model seeks to emulate the dynamic behavior of a traditional generator, achieving efficient regulation under various operating conditions.

Additionally, an AVR is used, which adjusts the voltage references as a function of reactive power deviation. The AVR is accompanied by a droop control, which allows the system to respond stably to reactive power fluctuations, ensuring more robust operation in challenging load scenarios.

This combination of current control, the governor model and the AVR gives the VSG topology the ability to integrate converters efficiently into the grid, mimicking the behavior of conventional synchronous generators, but taking advantage of the flexibility of modern converters [2.75, 2.81, 2.82].

2.6.2 IEPE's VSG Topology

The main idea of the Institute of Electrical Power Engineering (IEPE) is based on the dynamics of an ideal, linear model of a synchronous generator, which gives inertia to the system. The basic control structure of this VSG technique is shown in Figure 2.19a). In this model, parameters such as active/reactive power, inertia, and damping effect can be adjusted by modifying variables such as virtual torque and excitation.

Figure 2.19b) shows the control scheme of the system the simplified model of the generator to produce the reference current from the grid voltage signals. The param-

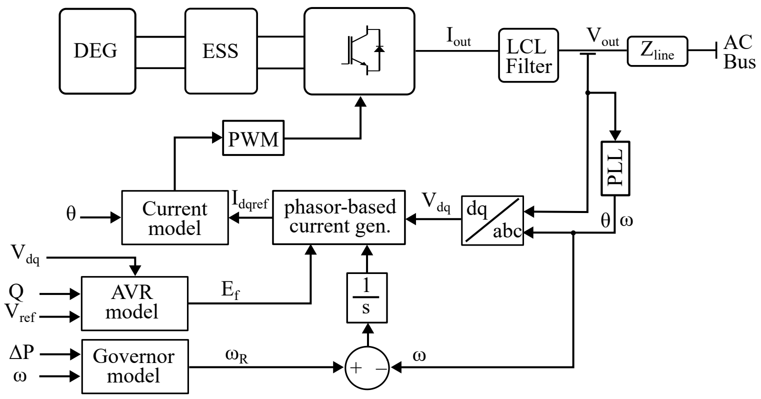

Figure 2.18: The VSG block diagram developed by KHI.

eters include J as the inertia moment, R_s as the stator resistance, L_s as the stator inductance, K_p as the damping factor, $\varphi(s)$ as the phase compensation, ω as the angular velocity), θ as the rotation angle, and T_e and T_m are the electrical and mechanical torques, respectively.

The phase compensation term counteracts any oscillation of the rotor. Despite the simplification in the excitation winding, the induced electromotive force (EMF) is obtained by the adjustable amplitude E_p and the angle θ. This topology generates a voltage reference for the PWM modulator, depending on the output current of the DEG, and uses an algorithm to improve the voltage quality in isolated microgrids. However, this technique has limitations in the numerical calculation and in the management of transient currents during the synchronization period [2.75, 2.78, 2.81].

2.6.3 VSYNC VSG Topology

The VSYNC research group developed the VSG concept, based on the ROCOF, to bring virtual inertia to the power system. The VSG includes an energy storage unit connected to a DC link and an inverter with LCL filter, typically used as a current source. The operation of the PLL is key in this structure, as it generates the reference currents (i_{ref}) from the grid voltage (V_g), emulating the electromechanical characteristics of a SG. A simple scheme of VSYNC topology is depicted in Figure 2.20. The PLL output drives the inverter through PWM modulation, providing the phase angle that allows control in the SRF [2.83].

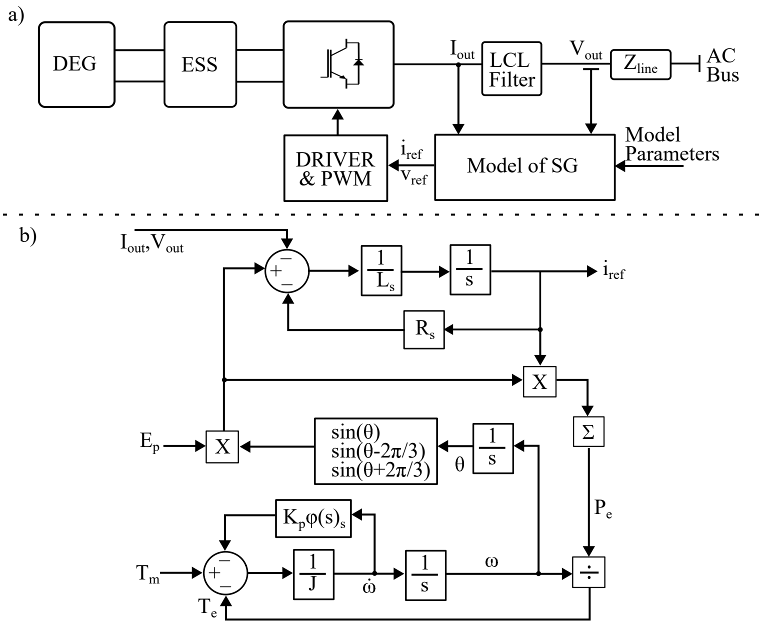

Figure 2.19: VSG structure based on current–voltage (voltage–current) model of SG: a) VSG topology, b) current–voltage model of SG.

$$\begin{cases} P_{ref} = K_{SOC} + K_i \frac{\mathrm{d}f_g}{\mathrm{d}t} + K_p Delta_f \\ Qref = K_q \Delta V \\ i_{dref} = \frac{V_d P_{ref} - VqQ_{ref}}{(Vd - Vq)^2} \\ i_{qref} = \frac{V_d Q_{ref} - VqP_{ref}}{(Vd - Vq)^2} \\ Iref = \frac{K_i \frac{\mathrm{d}f_g}{\mathrm{d}t} + K_p \Delta f}{V_{DC}} \end{cases} \tag{2.13}$$

Where K_{SOC} indicates the input power considering the SOC, i_d, i_q, V_d, V_q are the d and q axis current and voltages respectively.

According to equations (2.13), the generated currents depend on the ROCOF, SOC of the batteries, and the active and reactive powers. The active power is adjusted to match the nominal power of the generator when there are load variations, while the reactive power is modified to ensure that the generator produces its maximum power in case of voltage deviations. These optimizations improve efficiency and system stability in microgrids and distributed power systems. In subsequent studies, system improvements were implemented using advanced control algorithms [2.84, 2.85].

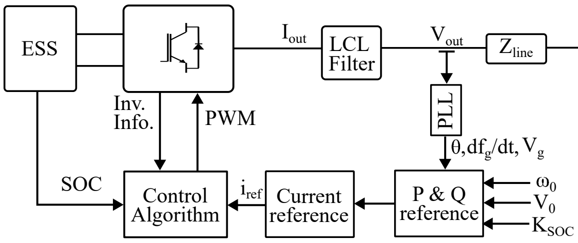

Figure 2.20: VSG structure using PLL to emulate the synchronous generator behavior.

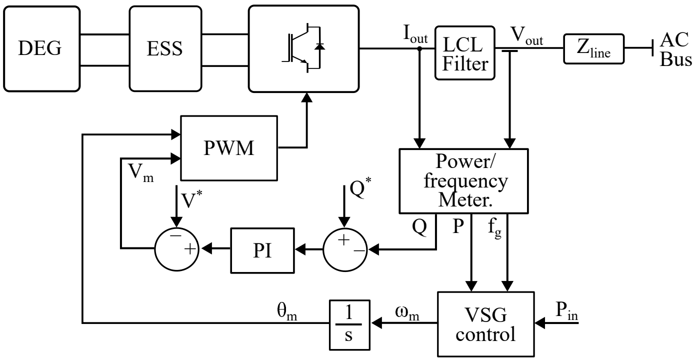

Figure 2.21: ISE's lab VSG structure.

2.6.4 ISE Lab's Topology

The VSG structure proposed by the Information Systems Engineering (ISE) Lab uses the well-known swing equation (2.3) of a SG in the heart of the VSG to regulate the power-frequency relationship [2.86]. By solving equation (2.3) in each control cycle, the instantaneous frequency is calculated, and by integrating it, the virtual mechanical phase angle (θ_m) is obtained. This angle is essential for generating the PWM modulation signals in the inverter. As illustrated in Figure 2.21, the output power and frequency are calculated through the power/frequency block. The virtual angular velocity deviation ($\Delta\omega_m$) is obtained based on the oscillation equation, and the θ_m is used as the phase command to control the inverter through PWM.

This structure enables efficient frequency and power regulation in power systems, emulating the dynamic behavior of synchronous generators, which improves stability in power grids with connected converters [2.75, 2.81, 2.86].

2.6.5 SPC Topology

The Synchronous Power Control (SPC) architecture is characterized by two main blocks: the electromechanical emulation block (outer loop) and the virtual admittance

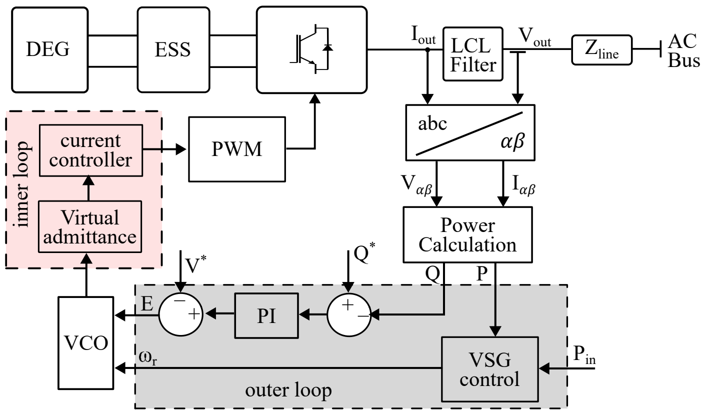

Figure 2.22: SPC VSG structure with the outer control loop emulating the electromechanical characteristic and the inner for the electrical emulation .

block (inner loop), described respectively in [2.39, 2.87–2.89]. Figure 2.22 shows the general control scheme.

In the outer loop of the control, the active and reactive powers are calculated. The active power is based on the emulation of the electromechanical equations of a synchronous generator by means of the swing equation (2.3) in the VSG block, which provides references for the rotor frequency (ω_r), achieved through the proper design of the Power Loop Controller [2.87]. The reactive power, on the other hand, is calculated by a PI controller, which generates voltage references (E).

These signals are sent to a VCO, which provides the references for the inner control loop. In this inner loop, the output impedance of the synchronous generator is emulated through a virtual admittance. This admittance generates the current references that are controlled by the inverter, thus allowing a more stable and efficient operation of the power system. This scheme ensures precise control of both frequency and voltage, emulating the behavior of a real synchronous generator and optimizing interaction with the grid.

The use of virtual admittance allows the system not only to respond to variations in the grid, but also to improve its stability, making this architecture ideal for distributed generation applications and grid-connected converter-based systems.

2.6.6 SCAC Topology

The SCAC control system is based on the SPC scheme, introducing a major improvement by distributing control between central controller and local controllers. While SPC focuses on the inverter connection point, SCAC seeks to control the parameters of PoC, separating the control into two layers, as explained by [2.90], delivering the power by each of the distributed generators, being able to work in any of the GFM,

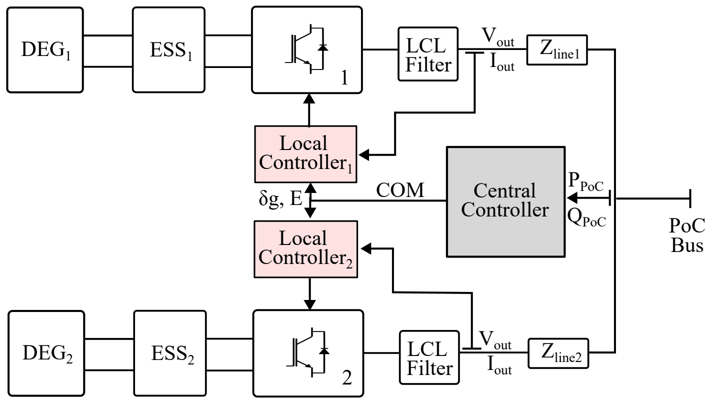

Figure 2.23: SCAC VSG general structure with central controller for emulating the electromechanical characteristic and the local controller for emulating the electrical behavior.

GFD or GS control schemes. In Figure 2.23, the general control scheme of the SCAC, working as a GFD, is represented.

The central controller manages the active and reactive power, comparing them with reference values and sending common voltage magnitude and load angle signals to several distributed converters. This approach makes it possible to create an aggregated VSG system independent of the line impedances of each distributed generation unit. The local controller, in turn, calculates the specific load angle for each distributed generator and performs the electrical emulation through a virtual admittance, allowing synchronization, voltage support and power sharing between different generators.

One of the main advantages of SCAC allows control of an entire DEG plant from a single point, adding a certain level of inertia and damping to the system, at the PoC and not at the output of the inverters as the decentralized control systems discussed above do. This would help to improve control in order to meet grid code requirements. In addition, the total power level handled by this system is the aggregate power of each of the distributed generators. However, given that the reference signals are sent through communication protocols, it is very important to take into account the possible communication delays that can impoverish the stability margins of the system, and it is necessary to compensate for them. In spite of this, as communications technologies improve year by year, with ever better speeds and latencies, the future implementation of this type of system is assured, improving the performance of the power system.

Each distributed generator has its own local controller, which ensures that the critical functions of synchronization and grid support are fulfilled. This control system is the basis of the work developed in this thesis, and its operation will be discussed in more detail in Chapter 3.

2.7 Delay Compensation Methods

As it has been mentioned, the control method of the distributed converters selected for the development of this thesis is the SCAC. This distributed method with central controller has the particularity that it relies on communication systems to send the central load angle references and the voltage module, calculated by the central controller. However, the existence of communications results in communication delays. These delays, depending on the system and their value, can worsen the performance of the control system, or even make it irreversibly unstable. Therefore, such delays must be dealt with and compensated for as efficiently and as simply as possible. Therefore, in this section, we will review the state of the art of communication delay compensation methods, in order to select the most appropriate one for the application. The methods to be reviewed will be the Linear Predictor [2.91, 2.92], Predictive Control [2.93, 2.94], Scattering Transformation [2.95, 2.96], Smith Predictor [2.97, 2.98]. Besides the commented methods, there are many more such as the Model-based Predictive Control [2.99], the state predictor method [2.100, 2.101] or robust control for delay compensation [2.102, 2.103].

2.7.1 Linear Predictor

The linear predictor is one of the best known methods for compensating time delays, which has been proposed and analyzed in [2.92], and is based on an extrapolation technique. If the time to be compensated is T_d, the transfer function $L(z)$ can be expressed as equation (2.14).

$$L(z) = 1 + \frac{T_d}{T_s} - \frac{T_d}{T_s} z^{-1} \tag{2.14}$$

Figure 2.24 shows the structure of the linear predictor, where R is the original modulation signal, while C is the signal compensated through equation (2.14) and the delay. This signal C can be derived as equation (2.15) and equation (2.16). However, for the use of this method it is very necessary to know the exact delay, which is not always possible. Moreover, it is often used for computational delays, which are usually small.

$$\frac{C(z)}{R(z)} = (1 + \frac{T_d}{T_s} - \frac{T_d}{T_s} z^{-1}) = (1 + \frac{T_d}{T_s}) - \frac{T_d}{T_s} z^{-2} \tag{2.15}$$

$$c(k) = (1 + \frac{T_d}{T_s}) r(k-1) - \frac{T_d}{T_s} r(k-2) \tag{2.16}$$

Hence, the Linear Predictor is relatively simple to implement and computationally efficient, making it ideal for systems with short, stable delays. However, its effectiveness is limited in dynamic environments, as it is not robust to rapid fluctuations or unexpected disturbances. While it doesn't require a detailed model of the system, its

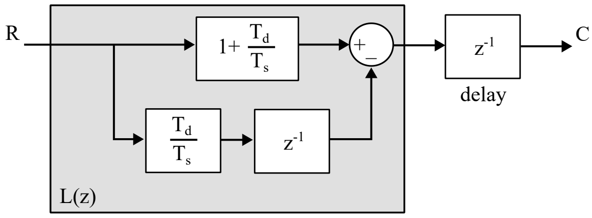

Figure 2.24: Block structure diagram for the linear predictor L(z).

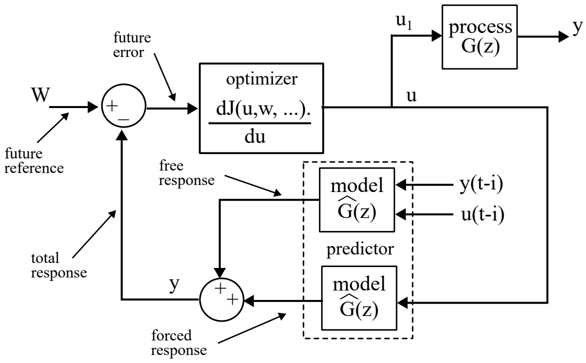

Figure 2.25: Block structure diagram for the predictive control scheme (GPC).

performance can be less suitable in systems with more complex dynamics. The need of short and constant delays and simple dynamics are the main reasons for its discarding in this thesis work.

Despite these limitations, it remains a useful tool for systems where computational resources are limited, though its application in more unpredictable or nonlinear scenarios is constrained.

2.7.2 Predictive Control

There are several predictive methods, but this subsection will focus on Generalized Predictive Control (GPC), which generates a sequence of signals at each sampling interval to optimize the control system and predict the future and thus, in the case of this thesis, try to compensate for communication delays, as [2.93] explains.

Figure 2.25 shows the schematic of the GPC concept. It can be seen that the output prediction system is based on two different components. One is known as the 'free response', which represents the predicted behavior of the output $t(t+j)$ (in the range from $t+1$ to $t+N$), based on native outputs $(y-i)$ and inputs $u(t-i)$, assuming a control action of zero. The 'forced response' represents the output component resulting from the optimization criterion.

The total prediction is the sum of both components, in the case of linear systems. These components with the reference values, the future errors can be calculated by (2.17).

$$e(t+j) = w(t+j) - y(t+j) \tag{2.17}$$

With j counting from 1 to N. Caused by these future errors, future control signals are calculated to force the output to the desired reference value.

However, the main drawback of Predictive Control lies in its high computational cost, especially when applied in real-time systems. The method requires solving complex optimization problems at each control step, which can significantly strain computational resources, particularly in large-scale or fast-response systems. Despite this, MPC remains a powerful tool for handling systems with constraints and dynamic behavior, offering potential for future improvements in computational efficiency or parallelization techniques. This is the main reason for its discarding in this thesis work.

2.7.3 Scattering Transformation

The original idea of this scattering transform comes from the description of the behavior of electrical networks (mostly operating at radio frequency) when subjected to various steady-state stimuli by electrical signals. In the original idea [2.104, 2.105], the term ‘scattering’ refers to the way in which currents and voltages travel into a transmission network that are affected when they encounter a discontinuity caused by the insertion of a network into the transmission line [2.106].

For the definition of the scattering matrix (S) parameters, it must be understood that a network can contain any component as long as the network behaves linearly with small incident signals. It can also include many components or ‘blocks’ typical of communication systems, such as amplifiers, filters etc. An electrical network to be described by S-parameters can have any number of ports. These ports are the points where signals enter or leave the network. Ports are usually pairs of terminals with the requirement that the current flowing into their terminal is equal to the current flowing out of the other.

This tool would be used for the compensation of communication delays in networked control systems. The dispersion matrices, by means of a transformation, would passivate the communication channel by emulating the behavior of a lossless transmission network. This is achieved by transmitting through the communication channel (with delays), instead of the voltage or current signal, its corresponding dispersion signal. This dispersion signal is the signal encoded by the dispersion transform, before being inverted to obtain the value of the real signal. The design would be completed by interfacing the line to a simple PI controller, which is also passive. Passivity is understood as the fundamental property of many physical systems of not generating energy, or in other words as a system that cannot store more energy than is supplied by its input, the energy dissipated being the difference between the energy stored and supplied by the source [2.107, 2.108].

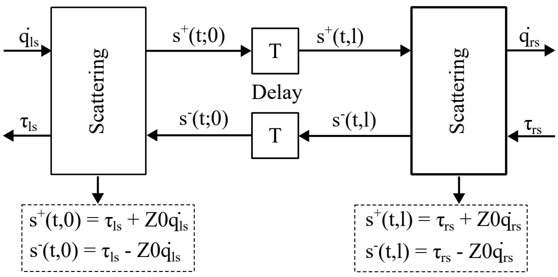

Figure 2.26: Emulation of the transmission line by sending the scattering variables.

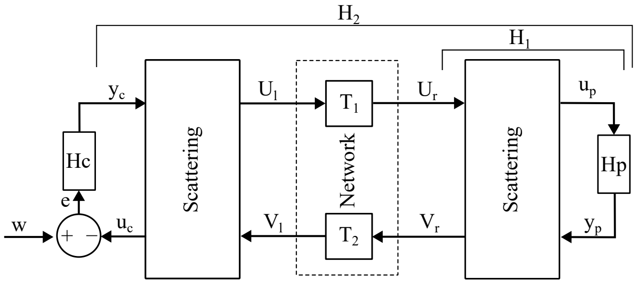

Figure 2.27: Control system with scattering transformation.

To transform the communication delay into a transmission line, one would proceed as follows. First, however, the so-called dispersion variables would have to be defined.

$$\begin{bmatrix} S^+(t,x) \\ S^-(t,x) \end{bmatrix} = T \begin{bmatrix} v(t,x) \\ i(t,x) \end{bmatrix} \tag{2.18}$$

Where v and i, would be the voltage and current associated with the transmission line modeled in [2.107]. Furthermore T=[1 z_0;1 $-z_0$] and z_0=$\sqrt{L/C}$ is the impedance of the transmission line. Furthermore, the transmission variables satisfy:

$$\begin{bmatrix} S^+(t,l) \\ S^-(t,l) \end{bmatrix} = T \begin{bmatrix} s^+(t-T,0) \\ s^+(t-T,0) \end{bmatrix} \tag{2.19}$$

Where $T = l\sqrt{LC}$ is the propagation delay.

Taking into account the phenomenon of wave reflection, which deforms the transmitted signals and degrades the performance of the transmitted signal, because the line termination impedance is different from the line impedance. Since the transmission line is virtual, the coefficient z_0 can be arbitrarily selected. Therefore, it is more convenient to work with a normalized implementation of (2.18), which would give us the notation used in most of the literature, where the dispersion transform is used [2.95, 2.109], as it can be seen in (2.20a).

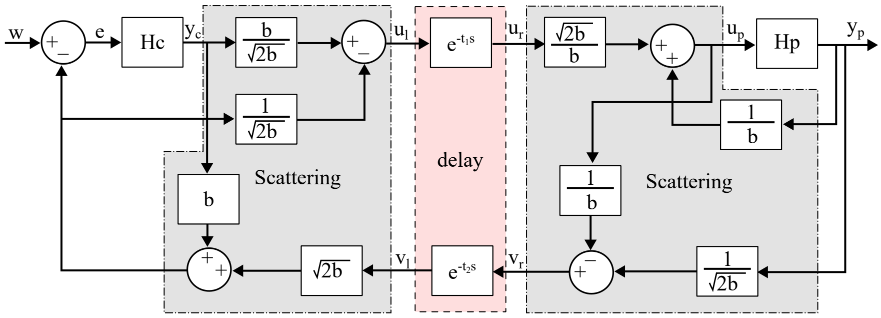

Figure 2.28: Extended block diagram of Scattering transformation.

$$\begin{bmatrix} S^+ \\ S^- \end{bmatrix} = \frac{1}{\sqrt{2}} \begin{bmatrix} I & bI \\ I & -bI \end{bmatrix} \tag{2.20}$$

Where $b > 0$ is the virtual impedance and I is the identity matrix. This ubiquitous transformation has been used in other fields such as network control and in Port-Hamiltonian systems to obtain stability independent of delay, etc. In the case where the communication delay of the network is bidirectional, it can be modeled by a two-port network with delays T_1 and T_2, in the forward and backward paths, as shown in Figure 2.27. In this figure, the H_P block indicates the plant and the H_C block indicates the controller, both SISO (single-input-single-output) LTI (linear-time-invariant) systems. In addition, the scattering transformation blocks are also indicated.

Such a scattering transformation manages to omit/passivate the power generation that creates the communication channel with communication delay, using the equations shown in equation (2.21), which are still the ones shown in equation (2.20), developed in a scalar form and with a small change in notation [2.95].

$$\begin{aligned} U_l &= \frac{1}{\sqrt{2}}(u_c + by_c) \\ V_l &= \frac{1}{\sqrt{2}}(u_c - by_c) \\ U_r &= \frac{1}{\sqrt{2}}(y_p + bu_p) \\ V_r &= \frac{1}{\sqrt{2}}(y_p - bu_p) \end{aligned} \tag{2.21}$$

As shown, the relationship between the left and right-hand side of the dispersion variables is as follows $u_r(t) = u_l(t - T_1)$ and $v_l(t) = v_r(t - T_2)$. These equations are shown in Figure 2.28, with a direct application for a SISO, with a controller and the plant, considering different time delays for sending and receiving.

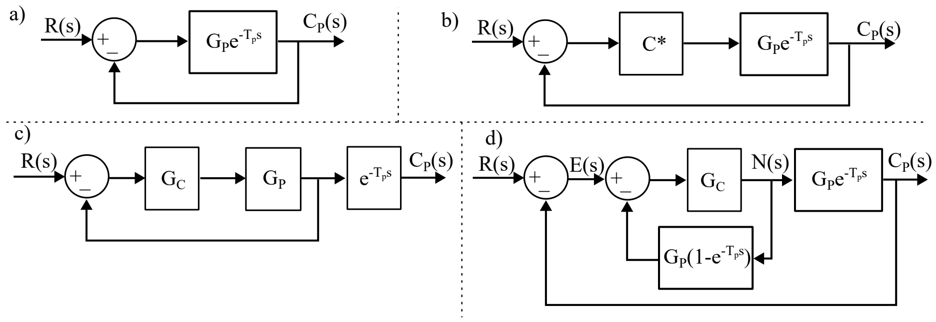

Figure 2.29: Smith predictor development. a) Closed loop control system with delay component. b) Compensator added to the system. c) The updated structure of the system due to the addition of compensator C*(s). d) The Smith Predictor general structure for delay compensation.

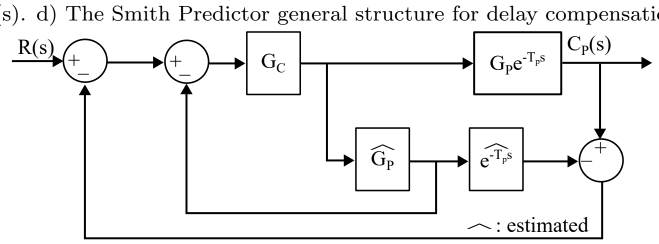

Figure 2.30: The Smith Predictor with process parameter estimation.

Although the Scattering Transformation is an interesting approach for the application in this thesis, it could be applicable to the system, but it requires a great understanding for its application, with a big computational effort due to the non-linearities of the control system. However, this method remains a promising research avenue, as acknowledged in the Future Work section. Its robustness against communication delays and uncertainties could offer significant benefits, making it a valuable area for further exploration and potential future implementations once these challenges are addressed.

2.7.4 Smith Predictor

The Smith Predictor [2.91, 2.92] is a technique used to eliminate the delay component in a control system by incorporating a model of the delay in communications and an accurate model of the plant. Thus, by compensating for the delay, the stability of the system is improved. In this text, the basic SP is explained, however it has several modifications which improve its performance [2.97, 2.98].

In a control scheme with delay, as shown in Figure 2.29 a), it is intended to incorporate a controller (C^*) that eliminates the delay, as shown in figure 2.29 b). This allows the delay to be removed from the closed loop of the system, obtaining the equivalence between the systems shown in Figures b) and c). Through equations (2.22), (2.23) and (2.24), it is shown how it is possible to eliminate the delay and improve the behavior of the system.

$$\frac{C^*(s)G_P(s)e^{-T_ps}}{1+C^*(s)G_P(s)e^{-T_ps}} = \frac{C^*(s)G_P(s)}{1+C^*(s)G_P(s)}e^{-T_ps} \tag{2.22}$$

$$C^*(s)G_P(s)e^{-T_ps}(1+G_c(s)G_P(s)) =$$
$$G_C(s)G_P(s)e^{-T_ps}(1+C^*(s)G_P(s)e^{-T_ps}) \tag{2.23}$$

$$C^*(s) = \frac{G_C(s)G_P(s)e^{-T_ps}}{G_P(s)(1+G_C(s)G_P(s))e^{-T_ps} - G_C(s)G_C^2(s)e^{-2T_ps}} =$$
$$\frac{G_C(s)}{1+G_C(s)G_P(s)(1-e^{-T_ps})} \tag{2.24}$$

$$\frac{N(s)}{E(s)} = \frac{G_C(s)}{1+G_C(s)G_P(s)(1-e^{-T_ps})} \tag{2.25}$$

$$\frac{C_P(s)}{R(s)} = \frac{\frac{N(s)}{E(s)}\frac{C(s)}{N(s)}}{1+\frac{N(s)}{E(s)}\frac{C(s)}{N(s)}} \tag{2.26}$$

$$\frac{C_P(s)}{R(s)} = \frac{\frac{G_C(s)G_P(s)e^{-T_ps}}{1+G_C(s)G_P(s)(1-e^{-T_ps})}}{1+\frac{G_C(s)G_P(s)e^{-T_ps}}{1+G_C(s)G_P(s)(1-e^{-T_ps})}} \tag{2.27}$$

$$\frac{C_P(s)}{R(s)} = \frac{\frac{G_C(s)G_P(s)e^{-T_ps}}{1+G_C(s)G_P(s)(1-e^{-T_ps})}}{\frac{1+G_C(s)G_P(s)(1-e^{-T_ps})+G_C(s)G_P(s)e^{-T_ps}}{1+G_C(s)G_P(s)(1-e^{-T_ps})}} \tag{2.28}$$

$$\frac{C_P(s)}{R(s)} = \frac{G_C(s)G_P(s)e^{-T_ps}}{1+G_C(s)G_P(s)(1-e^{-T_ps})+G_C(s)G_P(s)e^{-T_ps}} \tag{2.29}$$

$$\frac{C_P(s)}{R(s)} = \frac{G_C(s)G_P(s)e^{-T_ps}}{1+G_C(s)G_P(s)} \tag{2.30}$$

Figure 2.29 d) represents the ideal structure of the Smith predictor, where the transfer function of the predictor exactly compensates for the delay ($G_P(1-e^{-T_ps})$. The associated equations show how the effect of the delay in the loop is canceled. This can be demonstrated by developing and demonstrating the transfer functions as shown below.

However, the compensation of the delay shown in figure d would require the exact estimation of the plant transfer function and the delay, which is not always possible. In the case of implementing Smith predictor in a real application, both the plant G_P and the delay must be estimated as accurately as possible. Therefore, by estimating these components, the structure of the system would be represented by Figure 2.30. Furthermore, the Smith predictor transfer function can be obtained as follows.

$$\frac{C_P(s)}{R(s)} = \frac{\frac{G_C G_P e^{-T_p s}}{1+G_C \hat{G_P}(1-e^{-\hat{T}_p s})}}{1 + \frac{G_C G_P e^{-T_p s}}{1+G_C \hat{G_P}+G_C(G_P e^{-T_p s}-\hat{G_P} e^{-\hat{T}_{p s}})}} \tag{2.31}$$

$$\frac{C_P(s)}{R(s)} = \frac{G_C G_P e^{-T_p s}}{1 + G_C \hat{G_P} + G_C(G_P e^{-T_p s} - \hat{G_P} e^{\hat{T_p} s})} \tag{2.32}$$

Equation (2.32) shows that, if the process parameters can be modeled without error, the transfer function of the system in Figure 2.30 is equivalent to the transfer function of the system in Figure 2.29c). This implies that, under perfect modeling, the behavior of the system would be identical in both configurations, which reinforces the effectiveness of the Smith predictor in compensating for delay. However, in practice, the accuracy of the plant and delay model determines how well this equivalence can be achieved.

Considering the operation of the Smith Predictor, due to the simplicity and its reliability, this method is the selected method for compensating the different communication delays in this thesis.

2.7.5 Comparison between described models

In this subsection, a short comparison of the communication delay compensation methods described in this section of the document will be made in order to justify the use of SP as a compensation method [2.110–2.112].

Speaking of the Linear Predictor, it is a relatively easy to implement method, which calculates the future evolution, considering past data. It is useful for scenarios with short and stable delays, with a light computational load, which makes it suitable for applications that do not require large resources. However, it is not very robust to perturbations or rapid fluctuations. This makes it less accurate in complex dynamic systems, as it does not require a very detailed model of the system. This lack of detail limits its use in more complex and variable systems.

In the case of Predictive Control, it is an advanced method that models and predicts the future dynamics of the system, based on mathematical modeling, considering certain restrictions and optimization objectives. Its main advantage is its versatility when handling systems with variable delays and non-linear systems, as it integrates delay compensation directly into its formulation. However, it has a high computational cost, especially for real-time implementation, requiring precise modeling. This makes it more complex and costly to implement than other methods.

Scattering transformation is a very robust method in situations of uncertainty or variability in communication delays. Unlike other traditional methods, the delay is not compensated directly, but transformed to another domain using mathematical techniques, preserving the stability of the system, even with highly variable delays. This

Table 2.3: Comparison between the four compensation methods.

Method	Advantages	Limitations
Linear Predictor	Easy to implement, low computational cost	Not robust for rapid fluctuations.
Predictive Control	Versatile for complex systems.	Hight computational cost.
Scattering Transformation	Robust against uncertainties.	Difficult to implement, requires fine-tuning.
Smith Predictor	Effective under low variability delays. Easy implementation	Sensitive to model errors.

robustness makes it very useful in applications with distributed networks or telecommunications systems. However, it is less intuitive and difficult to implement than more traditional methods. Its effectiveness depends heavily on parametrization and its incorrect implementation can generate suboptimal results, which requires more attention in its initial configuration compared to other methods, such as the Smith Predictor or Predictive Control.

Finally, the Smith predictor is a widely used technique to compensate for communication delays in control systems. Its main advantage is ease of implementation, as well as system efficiency, especially for constant and known communication delays. By modeling system behavior and delay separately, the Smith Predictor can significantly improve stability and performance, even under long delays, without altering the dynamics of the main system. In addition, the SP minimizes oscillations and enables good closed-loop response. However, it is highly dependent on the system model and the delay implemented, and can worsen its performance under varying delays and highly non-linear systems. Compared to other methods such as scattering transformation and predictive control, this one offers a simpler implementation and low computational cost.

Considering the analysis in this subsection, as well as the summarized information from Table 2.3, the Smith Predictor has been chosen as the most suitable delay compensation method for the control system used in this thesis. Its simplicity and reliability improve system stability, as will be demonstrated in later chapters. Although the method is less effective for variable communication delays, as previously discussed, the system compensates for these delays adequately. This is achieved by modeling and characterizing the variable delays using a statistical function, ensuring that the overall performance remains stable and effective despite these variations.

2.8 Ramp-Rate Methods

Renewable energy generation, particularly in PV systems, is characterized by its intermittent and weather-dependent nature. These fluctuations, when rapid and pro-

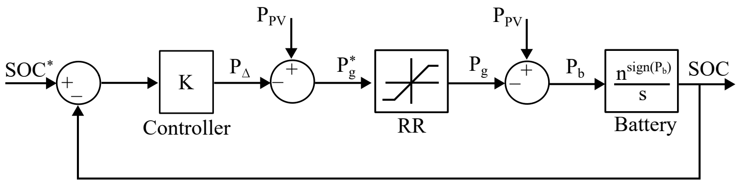

Figure 2.31: Classical ramp-rate control.

nounced, can compromise the stability of the power grid, generating variations in frequency and voltage that operators cannot always adequately manage. Therefore, as discussed in Section 2.4, PPCs must implement ramping control systems, as some grid codes already include regulations to mitigate this problem. Although ramp variation control is not explicitly addressed at the European regulatory level, some countries such as Germany [2.113], Ireland [2.114] and the UK [2.58] have incorporated these regulations into their grid codes.

To meet these regulatory requirements and to improve the stability of the power system in the face of solar generation integration, various compensation methods have been developed. The most common are classical ramp-rate control [2.115] and moving average filtering [2.115, 2.116], both of which are designed to smooth power variations and reduce the impact on the grid. However those are not the only ones, in [2.115], the Clear sky-dark sky method, with and without prediction is addressed. In [2.116] the Moving average is addressed taking into account SOC control and also the Step-Rate Control Strategy.

2.8.1 Classical Ramp-Rate Control

This strategy adjusts the power injected into the grid (P_g) in each sampling period so that the rate of change does not exceed the predefined RR. During P_{PV} ramp-rate violations, the power P_g follows a linear trajectory with a constant gradient RR, which guarantees a smooth evolution of the injected power [2.116].

$$\left| \frac{\Delta P_g}{\Delta t} \right| \leq RR \tag{2.33}$$

Figure 2.31 shows the complete control diagram. The difference between P_{PV} and P_g is handled by the battery as balance power (P_b). To stabilize the state of charge SOC, the control loop sets a reference (E_b) centered at 50% of the battery capacity. This is done to mitigate discharge due to adverse weather conditions and to ensure that the battery can absorb or inject energy (E_{wf}) when needed [2.117]. Thus, the minimum battery capacity ($C_{0,min}$) must comply with [2.116].

$$C_{0,min} = 2E_{wf} \tag{2.34}$$

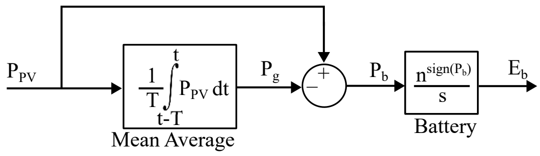

Figure 2.32: Moving average control.

The control loop includes a proportional controller that adjusts the power required (P_Δ) to follow the reference. The difference between P_{PV} and P_Δ defines the desired injected power (P_g^*), which is limited to ensure that the RR is not exceeded. With this system, the battery is only used when strictly necessary, i.e. when the RR is exceeded, thus protecting the battery and reducing unnecessary cycling.

2.8.2 Moving Average Filtering

The moving average method is one of the most representative among the filter-based strategies for smoothing the injected power [2.118]. The control diagram is shown in Figure 2.32, where the power injected to the grid (P_g) is calculated as the average value of the power generated (P_{PV}) in a time window T. The battery manages the power difference (P_b), absorbing or injecting power as needed. The requirement of this method has been analyzed in [2.119], establishing that, in order to obtain the desired RR value, the time window T must be at least equal to that indicated in equation (2.35). As the time window increases, the fluctuations of the injected power become more smooth.

$$T = \frac{\Delta P_{max}}{RR} \tag{2.35}$$

The minimum battery capacity (C_{1min}) is determined according to the equation (2.36) [2.119]:

$$C_{1,min} = \frac{\Delta P_{max}}{2}(N-1)\Delta t \tag{2.36}$$

Where N represents the number of samples included in the time window T and Δt is the sampling period.

The main merit of this strategy over the classical method is that it requires approximately half the battery capacity. However, the disadvantage is that the battery cycles excessively due to the excessive smoothing introduced by the moving average filter [2.116, 2.118]. In addition, the delay between P_g and P_{PV} can lead to deep discharge cycles even on clear days, which affects the lifetime of the battery.

2.9 Green Hydrogen Production

One of the major discussions worldwide is the production of clean fuels, such as hydrogen, from RES systems (PV and WG), which could facilitate the complete decarbonization of the energy system [2.120], and create a synergy between different sectors, such as the transport, energy and industrial sectors. Currently, the green electrolysis of hydrogen from these renewable systems is in the spotlight as a carbon neutral fuel [2.16, 2.121, 2.122].

Such green hydrogen production is based on the exclusive use of RES systems to power the electrolysis processes and decompose water into hydrogen and oxygen. These systems use Hydrogen Electrolyzers (HE), which are mainly based on two technologies, the Proton Exchange Membrane (PEM) unit [2.123] and alkaline [2.124]. However, to develop this process, it is necessary to develop an energy infrastructure that integrates renewable generation systems in an efficient and reliable way, besides ensuring the efficiency in the hydrolysis process.

Such infrastructures can have different types of couplings, the most common being dc-coupling and ac-coupling. The dc coupling involves connecting PV systems directly to the HE, which would avoid the losses derived from the ac system [2.125, 2.126], but with the disadvantage of the difficulty in the design of this coupling.

The ac coupling would use a system of inverters and rectifiers to create the grid and consume the energy, making it easier to use another renewable source such as WG. For this, it would be necessary to create an isolated ADN grid (or peninsula for security reasons [2.127]. This grid provides great flexibility to manage generation and consumption at the local level, dynamically configuring the variability of the energy source. In this context, one of the biggest challenges is to minimize the impact of this intermittency on the operation of the HE, which require as constant an energy supply as possible to maximize their efficiency and prolong their useful life. It is this ac-coupled system that will be the focus of this thesis work.

As shown in Figure 2.33, these ADN are based on a RES generation system, with ESS, due to the variability of the energy source, and one or more HE-based loads. Both generation and load systems have controllers necessary for the stability and proper functioning of the grid. In the following sections we will review the different generation and load controllers.

2.9.1 Green Hydrogen ADN Control

Controllers on the generation side are used to manage the grid created, with GFM control systems providing the control layers discussed in Section 2.5. There are several methods and techniques to efficiently implement power generation for hydrogen generation. These techniques can be applied to centralized or distributed control systems.

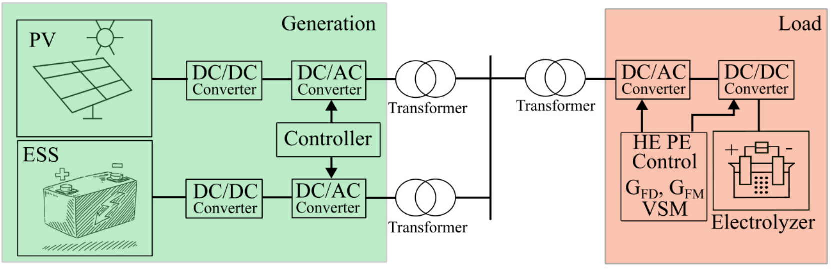

Figure 2.33: Green Hydrogen Interface.

2.9.1.1 Predictive Control

Model Predictive Control (MPC) is an advanced control technique used in green hydrogen production that optimizes the use of renewable energy by anticipating system fluctuations. Using a mathematical model, MPC predicts variations in renewable energy generation, allowing HEs to operate efficiently despite the intermittency of sources such as solar and wind. It also optimizes the use of energy storage systems, storing excess energy at times of high production and releasing it when generation is low. This improves system stability and efficiency, reducing operating costs and ensuring continuous hydrogen production. In short, the MPC allows the complexity of green hydrogen systems to be managed, ensuring more efficient and sustainable operation [2.128, 2.129]. In terms of converters control, a GFM strategy is needed for creating the power system to feed the loads.

2.9.1.2 Virtual Synchronous Generator

VSGs are important for the stabilization of isolated power grids such as those used in green hydrogen plants operating with intermittent renewable energy sources such as solar or wind. These plants are often located in grids that lack the inertia of traditional generators, which can cause stability problems. VSGs emulate the inertia of synchronous generators by automatically regulating the frequency and voltage of the grid, allowing them to respond quickly to fluctuations in generation and consumption. This is important to protect electrolyzer from power fluctuations and improve the efficiency and lifetime of the equipment. In addition, VSGs facilitate the integration of energy storage systems, which improves flexibility and ensures a continuous supply of stable energy for electrolysis. Within this category, any of the existing VSG methods could be included, although in the context of this thesis work, the SCAC system is the one chosen. With it, the different RES generators used can be controlled from a central controller, which can be perfectly located near the HE, by means of communication systems, adjusting the electrical variables of the PoC for an optimal performance of the HE. In short, VSGs improve the operational stability of green hydrogen plants, enabling more efficient and safer hydrogen production. As it was reviewed in Section 2.6, any of the VSG control systems can be applied to green hydrogen generation [2.130], using this control system for the grid creation in this work.

2.9.2 Hydrogen Electrolyzer Control

Due to the variable nature of the generation sources, the system must be as flexible as possible, integrating into units capable of incorporating ESS, managing demand or providing back-up power services. In this context, green hydrogen generation networks have focused much of their efforts on HE control systems to contribute to grid stability. These systems introduce functionalities traditionally found at the generation levels. Adaptive load control schemes can be divided into two main categories: responsive load and grid forming load.

2.9.2.1 Grid-Forming Load

Flexibility in demand control is especially relevant for those loads that can be adjusted according to the needs of the system, and there are several types of loads that are suitable for this purpose [2.131]. In the particular case of HEs, their ability to modify output in less than a second has sparked interest in their use within the power system, particularly through the control of the inverters that make up their interface. These inverters, as explained by [2.132], could be controlled in such a way that the load behaves like a GFM system. Instead of following the voltage and frequency values of the grid, it would be the load itself that would generate these magnitudes, enabling the possibility of creating islanded grids. This would allow the generators connected to the grid created by the load to operate in GFL mode, maximizing power extraction, operating at MPP, without the need to worry about the provision of reserve power.

This approach is particularly suitable for flexible loads that can operate around a scheduled operating point, either by the user or by the grid operator. However, it is important to note that GFM systems depend on the generators connected to the created grid being able to supply the necessary power to maintain system balance.

There are various strategies for controlling these systems, as discussed in [2.133], but a key aspect of grid-forming load-based grids is their ability to regulate voltage and frequency, providing a form of synthetic inertia through Virtual Synchronous Machine (VSM) control schemes. This type of control has the potential to reduce generation or storage requirements elsewhere in the system, as it actively contributes to grid stability. Although these solutions are still under study, the concept of grid-forming loads has the potential to transform the control paradigm of many DER [2.131], providing new ways to manage increasingly decentralized and renewable energy-based electricity grids. This approach not only improves operational flexibility, but also contributes to the dynamic stability of the system, which is very important in scenarios with high penetration of intermittent renewable.

2.9.2.2 Responsive Load

HEs operating as responsive loads, particularly those connected via GFL mode inverters, can play an important role in grid stability. These systems have the ability to adjust their power demand based on generation availability or according to TSO indications. This dynamic adjustment allows balancing supply and demand, acting as flexible loads that contribute to the efficient management of energy resources. One of the main benefits that HEs bring to the grid is frequency regulation. In situations of excess generation, such as during periods of high renewable production, HEs can increase their energy consumption, helping to reduce grid frequency by absorbing excess energy [2.134, 2.135]. Conversely, when generation is insufficient, HE can decrease their demand, thus helping to keep the frequency stable. In addition, these systems are able to absorb renewable generation peaks, avoiding energy waste and facilitating further integration of RES into the grid.

In addition to their ability to regulate frequency, HE can also contribute to voltage regulation, which further improves the operational stability of the system [2.136, 2.137]. Some studies, such as the one presented in [2.133], show that it is possible to add a level of synthetic inertia through VSM based control schemes. This implies that electrolysers are not only active consumers of energy, but can also participate in the dynamic stabilization of the grid, helping to mitigate the effects of fluctuations in renewable generation and reducing the need for storage or conventional back-up generation.

The ability of HE to act as flexible loads is especially valuable in contexts with high RES penetration, where fluctuations in generation can be significant and difficult to manage. By dynamically adjusting to grid conditions, HEs enable better integration of RES, contributing to a more balanced energy balance and a more robust and resilient system. It is precisely this type of system that has been used in this thesis to address contribution CP3 [2.130], highlighting its role in improving the stability and flexibility of electricity grids with high renewable energy penetration.

2.10 Summary and Research Opportunities

Currently, a large part of the scientific literature is based on the control of distributed generation systems in a decentralized manner, although with the improvement of communication systems, research is currently being carried out on how to centralize control at one point, in order to remotely control DER systems, taking into account the PoC parameters. This is why this thesis highlights the use of distributed VSG systems but controlled from a central controller, focusing on the SCAC controller that allows the coordination of multiple generation units from a central controller. This facilitates unified operation and response to frequency and voltage variations, supporting the grid, and helping to ensure its stability. For a better understanding, this chapter reviews the PPCs that must be used in DER systems in order to comply with the different grid codes in a real industrial application. In addition, a review is made of the different forms of interface of the converters used in these systems, for a correct operation of the grid, reviewing from power control to current control, reviewing the synchronization systems for when they are necessary.

Moreover, as the SCAC system used in this thesis uses communication systems, this can generate instabilities in the performance of the system, so it is necessary to compensate them, thus improving safety and reliability. That is why a review of the different compensation methods most used or promising is made, justifying the choice of the SP method. Considering that these systems are applied to RES, such as PVs, which suffer from the natural variability of their energy source, a small review of ramp compensation systems is made, in order to help the stability of the system. And finally, since the control system is applied to green hydrogen generation in one of its industrial applications, the different control methods applicable to this type of system are also discussed. However, there is no established rule for them yet, as there is still much work to be done in defining these generation plants.

Regarding the different research areas, several promising areas can be identified:

Although the SCAC system is the system proposed in this thesis work, it is not a perfect control system, as it has its small limitations that need to be overcome, so further research has to be done in the line of VSGs, trying to achieve a similar and improved system. One line of improvement to this system could be the elimination of local controllers, carrying out all the control from the central controller, and remotely sending the power commands directly to the converters. This would simplify the control system by managing everything from a single point, allowing for complete control of the plant. However, this generates other problems that must be overcome, such as the management of local variable readings, which must be used in the central system, having to take into account communication delays, among others. This is linked to another of the lines of improvement in these systems. One of the main research opportunities lies in improving the efficiency and robustness of the SCAC system in environments with variability of distributed energy resources. The current SCAC implementation is based on the use of communication channels that are subject to delays, which can affect the stability of the system. Although the use of Smith predictor is proposed to mitigate these effects, there is a wide field of research in terms of improving delay compensation methods. The used SP is not perfect, as its performance is hindered by potential variable communication delays. Hence, the development of new techniques that allow for more effective compensation of these delays, such as Dispersion Transformation, Predictive Control or even some new modification of the SP, could improve the stability and efficiency of the system under real conditions.

The integration of SCAC with energy storage systems also offers significant research opportunities, especially in the compensation of generation ramps in solar plants. The inherent variability of renewable sources, such as solar power, poses the challenge of avoiding abrupt fluctuations in generation that can cause grid instabilities. While SCAC can mitigate these ramps by dynamically adjusting generated and stored power, new strategies can be investigated to improve the system's ability to respond more quickly and efficiently to these changes. In addition, research on how to optimize the use of storage systems to compensate for variations in renewable generation could lead to improvements in operational stability and efficiency, as well as reduced costs associated with penalties for grid instabilities.

Considering all this, another area for improvement is the parametrization of the SCAC system for its use in PPC systems, in order to strictly comply with the different grid codes, respecting the regulations established in Section 2.4.

Furthermore, the development of technologies and control systems for green hydrogen generation networks still offers significant room for improvement, with numerous opportunities for research and innovation in this field, as it is a relatively recent topic. The production of green hydrogen, obtained from renewable sources such as solar and wind energy, presents several technical challenges that require advanced solutions in terms of control, storage, and optimization of the electrolysis process efficiency. This control not only involves managing the generation plant, which can be implemented in various ways as discussed in Section 2.9, but also considers the control of the HE itself, which could shift the control paradigm of the grid. Green hydrogen will not only be key to decarbonizing sectors like transportation and industry, but is also expected to play a fundamental role in the future of electrical energy systems.

References

[2.1] F. Durakovic, "Levelized cost of electricity of renewable energy technologies as a criterion for project prioritization," 2021.

[2.2] H. Bevrani, B. François, and T. Ise, *Microgrid dynamics and control.* John Wiley & Sons, 2017.

[2.3] U.S. Department of Energy, *Using Distributed Energy Resources: A How-To Guide for Federal Facility Managers.* Washington, D.C.: Office of Energy Efficiency and Renewable Energy (EERE) Federal Energy Management Program (FEMP), 2002, dOE/GO-102002-1520. [Online]. Available: https://www.eren.doe.gov/femp/

[2.4] A. K. Podder, N. K. Roy, and H. R. Pota, "Mppt methods for solar pv systems: a critical review based on tracking nature," *IET Renewable Power Generation*, vol. 13, no. 10, pp. 1615–1632, 2019.

[2.5] B. Bendib, H. Belmili, and F. Krim, "A survey of the most used mppt methods: Conventional and advanced algorithms applied for photovoltaic systems," *Renewable and Sustainable Energy Reviews*, vol. 45, pp. 637–648, 2015.

[2.6] M. A. Eltawil and Z. Zhao, "Mppt techniques for photovoltaic applications," *Renewable and sustainable energy reviews*, vol. 25, pp. 793–813, 2013.

[2.7] L. Meng, M. Savaghebi, F. Andrade, J. C. Vasquez, J. M. Guerrero, and M. Graells, "Microgrid central controller development and hierarchical control implementation in the intelligent microgrid lab of aalborg university," in *2015 IEEE Applied Power Electronics Conference and Exposition (APEC).* IEEE, 2015, pp. 2585–2592.

[2.8] B. Khan and Z. M. Ali, "Chapter 3 - active electric distribution network: Smart and active," in *Active Electrical Distribution Network*, S. Padmanaban, B. Khan,

O. P. Mahela, H. H. Alhelou, and S. Rajkumar, Eds. Academic Press, 2022, pp. 29–41. [Online]. Available: https://www.sciencedirect.com/science/article/pii/B9780323851695000198

[2.9] L. L. Grigsby, *Power system stability and control.* CRC press, 2007.

[2.10] N. Hatziargyriou, *Microgrids: architectures and control.* John Wiley & Sons, 2014.

[2.11] L. Li, Y. Sun, Z. Liu, X. Hou, G. Shi, and M. Su, "A decentralized control with unique equilibrium point for cascaded-type microgrid," *IEEE Transactions on Sustainable Energy*, vol. 10, no. 1, pp. 324–326, 2018.

[2.12] S. Ghosh and S. Chattopadhyay, "Three-loop-based universal control architecture for decentralized operation of multiple inverters in an autonomous grid-interactive microgrid," *IEEE Transactions on Industry Applications*, vol. 56, no. 2, pp. 1966–1979, 2020.

[2.13] M. Hossain, J. Lu, M. Mahmud, and T. Aziz, "Advanced decentralized der control for islanded microgrids," in *2014 Australasian Universities Power Engineering Conference (AUPEC).* IEEE, 2014, pp. 1–5.

[2.14] Y. Han, K. Zhang, H. Li, E. A. A. Coelho, and J. M. Guerrero, "Mas-based distributed coordinated control and optimization in microgrid and microgrid clusters: A comprehensive overview," *IEEE Transactions on Power Electronics*, vol. 33, no. 8, pp. 6488–6508, 2017.

[2.15] F. Katiraei and M. R. Iravani, "Power management strategies for a microgrid with multiple distributed generation units," *IEEE transactions on power systems*, vol. 21, no. 4, pp. 1821–1831, 2006.

[2.16] C. Natesan, S. K. Ajithan, S. Chozhavendhan, and A. Devendiran, "Power management strategies in microgrid: a survey," *International journal of renewable energy research*, vol. 5, no. 2, pp. 334–340, 2015.

[2.17] J. Brun and C. Durand, "Renewable management system plant controller to manage grid codes and contribute to the grid stability."

[2.18] E. Bullich-Massagué, R. Ferrer-San-José, M. Aragüés-Peñalba, L. Serrano-Salamanca, C. Pacheco-Navas, and O. Gomis-Bellmunt, "Power plant control in large-scale photovoltaic plants: design, implementation and validation in a 9.4 mw photovoltaic plant," *IET Renewable Power Generation*, vol. 10, no. 1, pp. 50–62, 2016.

[2.19] L. M. Díaz and J. M. Mauricio, "Controladores de potencia de plantas (ppc)," *Economía Industrial*, vol. 431, no. 1, pp. 145–154, 2024.

[2.20] M. Morjaria, D. Anichkov, V. Chadliev, and S. Soni, "A grid-friendly plant: The role of utility-scale photovoltaic plants in grid stability and reliability," *Power and Energy Magazine, IEEE*, vol. 12, pp. 87–95, 05 2014.

[2.21] Y. Cao and J. Lu, "The startup and shutdown strategies design and verification for hybrid dc grid with renewable power generation," in *2021 IEEE Sustainable Power and Energy Conference (iSPEC)*, 2021, pp. 649–654.

[2.22] C. CENELEC, "En 50549-2:2019/a1:2023 requirements for generating plants to be connected in parallel with distribution networks - part 2: Connection to a mv distribution network - generating plants up to and including type b," *Final Version, November*, 2023.

[2.23] ——, "En 50549-1:2019/a1:2023 requirements for generating plants to be connected in parallel with distribution networks - part 1: Connection to a lv distribution network - generating plants up to and including type b," *Final Version, November*, 2023.

[2.24] *Photovoltaic (PV) systems - Characteristics of the utility interface*, International Electrotechnical Commission Std. IEC 61 727, 2004. [Online]. Available: https://webstore.iec.ch/publication/6102

[2.25] *Test Procedure of Islanding Prevention Measures for Utility-Interconnected Photovoltaic Inverters*, International Electrotechnical Commission Std. IEC 62 116, 2014. [Online]. Available: https://webstore.iec.ch/publication/24311

[2.26] *IEEE Standard for Interconnection and Interoperability of Distributed Energy Resources with Associated Electric Power Systems Interfaces*, Institute of Electrical and Electronics Engineers Std. IEEE 1547-2020, 2020. [Online]. Available: https://standards.ieee.org/standard/1547-2020.html

[2.27] "Grid code for connecting renewable energy sources," Ministry of Economy, Trade and Industry (METI), Japan, 2016, japanese Grid Code for renewable energy integration. [Online]. Available: https://www.meti.go.jp

[2.28] *Norma UNE 206007-1: Sistemas fotovoltaicos conectados a la red. Parte 1: Requisitos técnicos de conexión*, AENOR Std. UNE 206 007-1, 2019. [Online]. Available: https://www.aenor.com/normas-y-libros/buscador-de-normas?codigo=UNE%20206007-1

[2.29] *Norma UNE 206007-2: Sistemas fotovoltaicos conectados a la red. Parte 2: Requisitos técnicos de funcionamiento*, AENOR Std. UNE 206 007-2, 2019. [Online]. Available: https://www.aenor.com/normas-y-libros/buscador-de-normas?codigo=UNE%20206007-2

[2.30] *Electromagnetic Compatibility (EMC)*, International Electrotechnical Commission Std. IEC 61 000, various. [Online]. Available: https://www.iec.ch/standards/iec-61000

[2.31] A. Cerretti, C. Noce, H. Rochereau, and T. Schaupp, "Requirements for generating plants to be connected in parallel with distribution networks-focus on en 50549 series," in *27th International Conference on Electricity Distribution (CIRED 2023)*, vol. 2023. IET, 2023, pp. 681–685.

[2.32] K. De Brabandere, "Voltage and frequency droop control in low voltage grids by distributed generators with inverter front-end," *Katholieke University Leuven, Leuven, Belgie*, 2006.

[2.33] J. Rocabert, A. Luna, F. Blaabjerg, and P. Rodriguez, "Control of power converters in ac microgrids," *IEEE transactions on power electronics*, vol. 27, no. 11, pp. 4734–4749, 2012.

[2.34] Q.-C. Zhong, *Synchronization Mechanism of Droop Control*, 2020, pp. 227–243.

[2.35] E. Espina, J. Llanos, C. Burgos-Mellado, R. Cardenas-Dobson, M. Martinez-Gomez, and D. Saez, "Distributed control strategies for microgrids: An overview," *IEEE Access*, vol. 8, pp. 193 412–193 448, 2020.

[2.36] S. Buso and P. Mattavelli, *Digital control in power electronics.* Morgan & Claypool Publishers, 2015.

[2.37] M. Aredes, A. Aquino, and G. Santos Jr, "Multipulse converters and controls for hvdc and facts systems," *Electrical engineering*, vol. 83, pp. 137–145, 2001.

[2.38] J. Rodriguez, J.-S. Lai, and F. Z. Peng, "Multilevel inverters: a survey of topologies, controls, and applications," *IEEE Transactions on industrial electronics*, vol. 49, no. 4, pp. 724–738, 2002.

[2.39] P. Rodriguez, I. Candela, C. Citro, J. Rocabert, and A. Luna, "Control of grid-connected power converters based on a virtual admittance control loop," in *2013 15th European Conference on Power Electronics and Applications (EPE)*. IEEE, 2013, pp. 1–10.

[2.40] L. Meng, Q. Shafiee, G. F. Trecate, H. Karimi, D. Fulwani, X. Lu, and J. M. Guerrero, "Review on control of dc microgrids and multiple microgrid clusters," *IEEE journal of emerging and selected topics in power electronics*, vol. 5, no. 3, pp. 928–948, 2017.

[2.41] H. Bevrani, A. Ghosh, and G. Ledwich, "Renewable energy sources and frequency regulation: survey and new perspectives," *IET Renewable Power Generation*, vol. 4, no. 5, pp. 438–457, 2010.

[2.42] F. Mandrile, E. Carpaneto, and R. Bojoi, "Grid-tied inverter with simplified virtual synchronous compensator for grid services and grid support," in *2019 IEEE Energy Conversion Congress and Exposition (ECCE)*. IEEE, 2019, pp. 4317–4323.

[2.43] J. W. Simpson-Porco, Q. Shafiee, F. Dörfler, J. C. Vasquez, J. M. Guerrero, and F. Bullo, "Secondary frequency and voltage control of islanded microgrids via distributed averaging," *IEEE Transactions on Industrial Electronics*, vol. 62, no. 11, pp. 7025–7038, 2015.

[2.44] A. Bidram and A. Davoudi, "Hierarchical structure of microgrids control system," *IEEE Transactions on Smart Grid*, vol. 3, no. 4, pp. 1963–1976, 2012.

[2.45] J. M. Guerrero, J. C. Vasquez, J. Matas, L. G. De Vicuña, and M. Castilla, "Hierarchical control of droop-controlled ac and dc microgrids—a general approach toward standardization," *IEEE Transactions on industrial electronics*, vol. 58, no. 1, pp. 158–172, 2010.

[2.46] J. Driesen and K. Visscher, "Virtual synchronous generators," in *2008 IEEE Power and Energy Society General Meeting - Conversion and Delivery of Electrical Energy in the 21st Century*, 2008, pp. 1–3.

[2.47] W.-F. Xu, L.-G. Weng, R. Yu, D.-Q. Lian, H.-H. Ying, and M. Luo, "A robustly real-time economic dispatch strategy of microgrids considering uncertainties," in *2023 International Conference on Power Energy Systems and Applications (ICoPESA)*, 2023, pp. 633–637.

[2.48] R. Teodorescu, M. Liserre, and P. Rodriguez, *Grid converters for photovoltaic and wind power systems*. John Wiley & Sons, 2011.

[2.49] Navarro-Rodríguez, C. Gómez-Aleixandre, P. García, M. Langwasser, and M. Liserre, "Hybrid grid control using smart transformer with multiport grid forming capabilities and interlinked primary control," in *2023 IEEE Energy Conversion Congress and Exposition (ECCE)*, 2023, pp. 837–842.

[2.50] A. Yazdani and R. Iravani, *Voltage-sourced converters in power systems: modeling, control, and applications*. John Wiley & Sons, 2010.

[2.51] H. Bevrani, B. François, and T. Ise, *Microgrid dynamics and control*. John Wiley & Sons, 2017.

[2.52] Q.-C. Zhong and T. Hornik, *Control of power inverters in renewable energy and smart grid integration*. John Wiley & Sons, 2012.

[2.53] I. U. Nutkani, P. C. Loh, and F. Blaabjerg, "Distributed operation of interlinked ac microgrids with dynamic active and reactive power tuning," *IEEE transactions on industry applications*, vol. 49, no. 5, pp. 2188–2196, 2013.

[2.54] J. C. Vasquez, J. M. Guerrero, A. Luna, P. Rodríguez, and R. Teodorescu, "Adaptive droop control applied to voltage-source inverters operating in grid-connected and islanded modes," *IEEE transactions on industrial electronics*, vol. 56, no. 10, pp. 4088–4096, 2009.

[2.55] R. Rosso, X. Wang, M. Liserre, X. Lu, and S. Engelken, "Grid-forming converters: an overview of control approaches and future trends," in *2020 IEEE Energy Conversion Congress and Exposition (ECCE)*, 2020, pp. 4292–4299.

[2.56] B. Fan and X. Wang, "Current-limiting control of grid-forming inverters: State-of-the-art and open issues," *Authorea Preprints*, 2023.

[2.57] C. Liu, J. Xi, Q. Hao, J. Li, J. Wang, H. Dong, and C. Su, "Grid-forming converter overcurrent limiting strategy based on additional current loop," *Electronics*, vol. 12, no. 5, p. 1112, 2023.

[2.58] N. G. E. S. O. (NGESO), "National grid electricity system operator grid code," 2024, available at: https://www.nationalgrideso.com/industry-information/codes/grid-code.

[2.59] S. Golestan, J. M. Guerrero, and J. C. Vasquez, "Three-phase plls: A review of recent advances," *IEEE Transactions on Power Electronics*, vol. 32, no. 3, pp. 1894–1907, 2016.

[2.60] J. Li, "Working principle and application analysis of phase-locked loop," *Applied and Computational Engineering*, vol. 11, pp. 174–180, 09 2023.

[2.61] L. Hadjidemetriou, P. Demetriou, and E. Kyriakides, "Investigation of different fault ride through strategies for renewable energy sources," in *2015 IEEE Eindhoven PowerTech*. IEEE, 2015, pp. 1–6.

[2.62] F. Iov, A. D. Hansen, P. Sørensen, and N. A. Cutululis, "Mapping of grid faults and grid codes," 2007.

[2.63] H. Bevrani, T. Ise, and Y. Miura, "Virtual synchronous generators: A survey and new perspectives," *International Journal of Electrical Power & Energy Systems*, vol. 54, pp. 244–254, 2014.

[2.64] M. Schaefer, "Direct current control for grid connected multilevel inverters," 2017.

[2.65] M. Bozorgmehrian, S. Attarsharghi, and A. Ramezani, "Energy-based controller design for decentralized ac inverter-base micro-grids," in *2023 IEEE International Conference on Control, Electronics and Computer Technology (ICCECT)*, 2023, pp. 225–230.

[2.66] J. Rocabert, G. Azevedo, A. Luna, J. Guerrero, J. Candela, and P. Rodriguez, "Intelligent connection agent for three-phase grid-connected microgrids," *Power Electronics, IEEE Transactions on*, vol. 26, pp. 2993 – 3005, 11 2011.

[2.67] J. Pinto, A. Carvalho, A. Rocha, and A. Araújo, "Comparison of dsogi-based pll for phase estimation in three-phase weak grids," *Electricity*, vol. 2, no. 3, pp. 244–270, 2021. [Online]. Available: https://www.mdpi.com/2673-4826/2/3/15

[2.68] Z. Ali, N. Christofides, L. Hadjidemetriou, E. Kyriakides, Y. Yang, and F. Blaabjerg, "Three-phase phase-locked loop synchronization algorithms for grid-connected renewable energy systems: A review," *Renewable and Sustainable Energy Reviews*, vol. 90, pp. 434–452, 2018.

[2.69] X.-Q. Guo, W.-Y. Wu, and H.-R. Gu, "Phase locked loop and synchronization methods for grid-interfaced converters: a review," *Przeglad Elektrotechniczny*, vol. 87, no. 4, pp. 182–187, 2011.

[2.70] P. Rodríguez, J. Pou, J. Bergas, J. I. Candela, R. P. Burgos, and D. Boroyevich, "Decoupled double synchronous reference frame pll for power converters control," *IEEE Transactions on Power Electronics*, vol. 22, no. 2, pp. 584–592, 2007.

[2.71] P. Rodriguez, A. Lunar, R. Teodorescu, F. Iov, and F. Blaabjerg, "Fault ride-through capability implementation in wind turbine converters using a decoupled double synchronous reference frame pll," in *2007 European Conference on Power Electronics and Applications*. IEEE, 2007, pp. 1–10.

[2.72] P. Tielens and D. Van Hertem, "The relevance of inertia in power systems," *Renewable and sustainable energy reviews*, vol. 55, pp. 999–1009, 2016.

[2.73] D. d. Rivero, P. García, C. Blanco, and Navarro-Rodríguez, "Control of aggregated virtual synchronous generators for pv plants considering communication delays," *IEEE Transactions on Industry Applications*, pp. 1–13, 2024.

[2.74] H.-P. Beck and R. Hesse, "Virtual synchronous machine," in *2007 9th international conference on electrical power quality and utilisation*. IEEE, 2007, pp. 1–6.

[2.75] T. Ise and H. Bevrani, "Virtual synchronous generators and their applications in microgrids," in *Integration of Distributed Energy Resources in Power Systems*. Elsevier, 2016, pp. 282–294.

[2.76] J. García, G. de Donato, J. A. Aguado, C. González-Morán, V. Terzija, R. Azizipanah-Abarghooee, P. Arboleya, P. Siano, M. Sumner, M. Perdigao, C. Mayet, and J. Trovão, Eds., *Encyclopedia of Electrical and Electronic Power Engineering*. Elsevier, 2023. [Online]. Available: https://www.sciencedirect.com/referencework/9780128232118/encyclopedia-of-electrical-and-electronic-power-engineering

[2.77] D. Nourelhouda, Y. Daili, and A. Harrag, "A review of recent control trchniques of virtual synchronous machine for renewable energy," *The Scientific Bulletin of Electrical Engineering Faculty*, vol. 23, no. 2, pp. 20–32.

[2.78] T. Kerdphol, F. S. Rahman, M. Watanabe, and Y. Mitani, *Virtual inertia synthesis and control*. Springer, 2021.

[2.79] C. Sun, *Virtual Synchronous Machine Control for Islanded Power System with Reduced Inertia*, ser. McGill theses. McGill University Libraries, 2021. [Online]. Available: https://books.google.es/books?id=UwSIzgEACAAJ

[2.80] M. A. Islam, *Implementation of virtual synchronous generator methodologies for renewable integration*. Temple University, 2017.

[2.81] K. M. Cheema, "A comprehensive review of virtual synchronous generator," *International journal of electrical power & energy systems*, vol. 120, p. 106006, 2020.

[2.82] Y. Hirase, K. Abe, K. Sugimoto, and Y. Shindo, "A grid-connected inverter with virtual synchronous generator model of algebraic type," *Electrical Engineering in Japan*, vol. 184, no. 4, pp. 10–21, 2013.

[2.83] M. Van Wesenbeeck, S. De Haan, P. Varela, and K. Visscher, "Grid tied converter with virtual kinetic storage," in *2009 IEEE Bucharest PowerTech*. IEEE, 2009, pp. 1–7.

[2.84] V. Karapanos, Z. Yuan, and S. de Haan, "Soc maintenance and coordination of multiple vsg units for grid support and transient stability," in *3rd VSYNC workshop. Cheia, Romania*, 2010.

[2.85] M. Albu, M. Calin, D. Federenciuc, and J. Diaz, "The measurement layer of the virtual synchronous generator operation in the field test," in *2011 IEEE International Workshop on Applied Measurements for Power Systems (AMPS)*. IEEE, 2011, pp. 85–89.

[2.86] K. Sakimoto, Y. Miura, and T. Ise, "Stabilization of a power system with a distributed generator by a virtual synchronous generator function," in *8th International Conference on Power Electronics-ECCE Asia*. IEEE, 2011, pp. 1498–1505.

[2.87] W. Zhang, A. M. Cantarellas, J. Rocabert, A. Luna, and P. Rodriguez, "Synchronous power controller with flexible droop characteristics for renewable power generation systems," *IEEE Transactions on Sustainable Energy*, vol. 7, no. 4, pp. 1572–1582, 2016.

[2.88] P. Rodriguez, I. Candela, J. Rocabert, and R. Teodorescu, "European patent application: Virtual controller of electromechanical characteristics for static power converters," 2014.

[2.89] ——, "United states patent application publication: Synchronous power controller for a generating system based on static power converters," *US*, vol. 49228, p. A1, 2014.

[2.90] C. Verdugo, A. Tarraso, J. I. Candela, J. Rocabert, and P. Rodriguez, "Centralized synchronous controller based on load angle regulation for photovoltaic power plants," *IEEE Journal of Emerging and Selected Topics in Power Electronics*, vol. 9, no. 1, pp. 485–496, 2020.

[2.91] M. Lu, X. Wang, P. C. Loh, F. Blaabjerg, and T. Dragicevic, "Graphical evaluation of time-delay compensation techniques for digitally controlled converters," *IEEE Transactions on Power Electronics*, vol. 33, no. 3, pp. 2601–2614, 2018.

[2.92] S. Bibian and H. Jin, "Time delay compensation of digital control for dc switchmode power supplies using prediction techniques," *IEEE Transactions on Power Electronics*, vol. 15, no. 5, pp. 835–842, 2000.

[2.93] V. Miskovic, V. Blasko, T. Jahns, A. Smith, and C. Romenesko, "Observer based active damping of lcl resonance in grid connected voltage source converters," in *2013 IEEE Energy Conversion Congress and Exposition*, 2013, pp. 4850–4856.

[2.94] R. Kennel, A. Linder, and M. Linke, "Generalized predictive control (gpc)-ready for use in drive applications?" in *2001 IEEE 32nd Annual Power Electronics Specialists Conference (IEEE Cat. No.01CH37230)*, vol. 4, 2001, pp. 1839–1844 vol. 4.

[2.95] T. Matiakis, S. Hirche, and M. Buss, "The scattering transformation for networked control systems," in *Proceedings of 2005 IEEE Conference on Control Applications, 2005. CCA 2005.* IEEE, 2005, pp. 705–710.

[2.96] ——, "Independent-of-delay stability of nonlinear networked control systems by scattering transformation," in *2006 American Control Conference*, 2006, pp. 6 pp.–.

[2.97] A. Ghanaim, G. A. Borges, and G. Frey, "Estimating delays in networked control systems using colored petri nets and markov chain models," in *2009 IEEE Conference on Emerging Technologies & Factory Automation*. IEEE, 2009, pp. 1–6.

[2.98] A. Mirzal, "Delay compensation using the smith predictor: a brief review with numerical examples," *International Journal of Computer-aided Mechanical Design and Implementation*, vol. 3, no. 1, pp. 1–8, 2017.

[2.99] S. H. Zak, "An introduction to model-based predictive control (mpc)," *lecture notes on ECE680, Purdue University*, 2017.

[2.100] Y. Deng, V. Léchappé, E. Moulay, Z. Chen, B. Liang, F. Plestan, and Q.-L. Han, "Predictor-based control of time-delay systems: a survey," *International Journal of Systems Science*, vol. 53, no. 12, pp. 2496–2534, 2022.

[2.101] F. Suzuki and H. Yada, "Delay compensation for servo systems using state prediction control and disturbance observer, and its application to hdd head servo control system," in *The 8th IEEE International Workshop on Advanced Motion Control, 2004. AMC '04.*, 2004, pp. 341–346.

[2.102] L. I. Jianwen, M. A. Xiaotang, W. U. Binyuan, L. I. Rong, and Y. Ruiqing, "Robust control delay compensation method for grid connected inverter based on improved newton interpolation," *CSEE Journal of Power and Energy Systems*, pp. 1–10, 2022.

[2.103] G. I. Song and J. H. Kim, "Time-delay compensation-based robust control of mechanical manipulators: Operator-theoretic analysis and experiment validation," *Mathematical Methods in the Applied Sciences*, vol. 47, no. 1, pp. 318–335, 2024.

[2.104] R. J. Anderson and M. W. Spong, "Bilateral control of teleoperators with time delay," in *Proceedings of the 1988 IEEE International Conference on Systems, Man, and Cybernetics*, vol. 1. IEEE, 1988, pp. 131–138.

[2.105] G. Niemeyer and J.-J. Slotine, "Stable adaptive teleoperation," *IEEE Journal of oceanic engineering*, vol. 16, no. 1, pp. 152–162, 1991.

[2.106] G. Niemeyer and J.-J. E. Slotine, "Telemanipulation with time delays," *The International Journal of Robotics Research*, vol. 23, no. 9, pp. 873–890, 2004.

[2.107] E. Nuño, L. Basañez, and R. Ortega, "Passivity-based control for bilateral teleoperation: A tutorial," *Automatica*, vol. 47, no. 3, pp. 485–495, 2011.

[2.108] A. Loria and H. Nijmeijer, *Passivity based control*, ser. Encyclopedia of life support systems. EOLSS publishers, 2004.

[2.109] T. Matiakis, S. Hirche, and M. Buss, "Independent-of-delay stability of nonlinear networked control systems by scattering transformation," in *2006 American Control Conference*. IEEE, 2006, pp. 6–pp.

[2.110] S. Sang and P. Nie, "Modified smith predictor based on h2 and predictive pi control strategy," *Mathematical Problems in Engineering*, vol. 2021, no. 1, p. 7228637, 2021. [Online]. Available: https://onlinelibrary.wiley.com/doi/abs/10.1155/2021/7228637

[2.111] E. Estremera Toledo, A. Lussón Cervantes, and I. Bausa Ortiz, "Estudio comparativo en sistemas multivariables con retardo: modificaciones del predictor de smith y control predictivo," *Ingeniería Electrónica, Automática y Comunicaciones*, vol. 38, no. 2, pp. 49–64, 2017.

[2.112] C. Süülker and M. T. Emirler, "Comparison of different time delay compensation methods for networked dc motor speed control," in *2019 6th International Conference on Electrical and Electronics Engineering (ICEEE)*, 2019, pp. 225–229.

[2.113] "German grid code," Regulations on Ramp-Rate Control, 2018, applies a 10%/minute ramp-rate limit for PV systems. [Online]. Available: https://www.mdpi.com

[2.114] EirGrid, "Eirgrid grid code version 14.1," 2023, accessed: November 7, 2024. [Online]. Available: https://www.eirgridgroup.com/site-files/library/EirGrid/Grid_Code_Version_14.1.pdf

[2.115] A. Gonzalez-Moreno, J. Marcos, I. de la Parra, and L. Marroyo, "A pv ramp-rate control strategy to extend battery lifespan using forecasting," *Applied Energy*, vol. 323, p. 119546, 2022.

[2.116] J. Marcos, I. De la Parra, M. García, and L. Marroyo, "Control strategies to smooth short-term power fluctuations in large photovoltaic plants using battery storage systems," *Energies*, vol. 7, no. 10, pp. 6593–6619, 2014.

[2.117] J. Marcos, O. Storkël, L. Marroyo, M. Garcia, and E. Lorenzo, "Storage requirements for pv power ramp-rate control," *Solar Energy*, vol. 99, pp. 28–35, 2014.

[2.118] S. Sukumar, M. Marsadek, K. Agileswari, and H. Mokhlis, "Ramp-rate control smoothing methods to control output power fluctuations from solar photovoltaic (pv) sources—a review," *Journal of energy storage*, vol. 20, pp. 218–229, 2018.

[2.119] A. Puri, "Optimally smoothing output of pv farms," in *2014 IEEE PES General Meeting— Conference & Exposition*. IEEE, 2014, pp. 1–5.

[2.120] F. Kourougianni, A. Arsalis, A. V. Olympios, G. Yiasoumas, C. Konstantinou, P. Papanastasiou, and G. E. Georghiou, "A comprehensive review of green hydrogen energy systems," *Renewable Energy*, p. 120911, 2024.

[2.121] F. Birol, "The future of hydrogen: seizing today's opportunities," *IEA Report prepared for the G*, vol. 20, 2019.

[2.122] E. Energy, "Gigastack: bulk supply of renewable hydrogen," *Low carbo n hydrog. Supply Program*, vol. 17, 2020.

[2.123] Z. Abdin, C. Webb, and E. M. Gray, "Modelling and simulation of a proton exchange membrane (pem) electrolyser cell," *International journal of hydrogen energy*, vol. 40, no. 39, pp. 13 243–13 257, 2015.

[2.124] M. Maruf-ul Karim and M. T. Iqbal, "Dynamic modeling and simulation of alkaline type electrolyzers," in *2009 Canadian conference on electrical and computer engineering*. IEEE, 2009, pp. 711–715.

[2.125] A. M. Abomazid, N. A. El-Taweel, and H. E. Farag, "Energy management system for minimizing hydrogen production cost using integrated battery energy storage and photovoltaic systems," in *2021 IEEE Power & Energy Society Innovative Smart Grid Technologies Conference (ISGT)*. IEEE, 2021, pp. 1–5.

[2.126] N. Tlili, B. Neily, and F. B. Salem, "Modeling and simulation of hybrid system coupling a photovoltaic generator, a pem fuel cell and an electrolyzer (part i)," in *2014 IEEE 11th International Multi-Conference on Systems, Signals & Devices (SSD14)*. IEEE, 2014, pp. 1–8.

[2.127] C. Blanco, S. Díaz, I. Peláez, C. Rech, and P. García, "Maximizing green hydrogen production efficiency for hybrid energy storage and solar photovoltaic systems: A design methodology," in *Proceedings of the IEEE Energy Conversion Congress and Exposition (ECCE)*. Gijón, Spain: IEEE, 2024.

[2.128] P. Cardona, R. Costa-Castelló, V. Roda, J. Carroquino, L. Valiño, and M. Serra, "Model predictive control of an on-site green hydrogen production and refuelling station," *international journal of hydrogen energy*, vol. 48, no. 47, pp. 17 995–18 010, 2023.

[2.129] X. Chen, W. Cao, Q. Zhang, S. Hu, and J. Zhang, "Artificial intelligence-aided model predictive control for a grid-tied wind-hydrogen-fuel cell system," *IEEE Access*, vol. 8, pp. 92 418–92 430, 2020.

[2.130] D. del Rivero, A. Navarro-Rodríguez, C. Gomez-Aleixandre, C. Blanco, P. García, and P. Rodríguez, "Control of green hydrogen production on isolated hybrid solar plants considering the effect of communications," in *2024 IEEE Energy Conversion Congress and Exposition (ECCE)*, Phoenix, AZ, USA, 2024, pp. 1122–1128.

[2.131] O. Gomis-Bellmunt, S. D. Tavakoli, V. A. Lacerda, and E. Prieto-Araujo, "Grid-forming loads: Can the loads be in charge of forming the grid in modern power systems?" *IEEE Transactions on Smart Grid*, vol. 14, no. 2, pp. 1042–1055, 2022.

[2.132] S. D. Tavakoli, M. G. Dozein, V. A. Lacerda, M. C. Mañe, E. Prieto-Araujo, P. Mancarella, and O. Gomis-Bellmunt, "Grid-forming services from hydrogen electrolyzers," *IEEE transactions on sustainable energy*, vol. 14, no. 4, pp. 2205–2219, 2023.

[2.133] M. G. Dozein, A. M. De Corato, and P. Mancarella, "Virtual inertia response and frequency control ancillary services from hydrogen electrolyzers," *IEEE Transactions on Power Systems*, vol. 38, no. 3, pp. 2447–2459, 2022.

[2.134] A. M. De Corato, M. G. Dozein, S. Riaz, and P. Mancarella, "Hydrogen electrolyzer load modelling for steady-state power system studies," *IEEE Transactions on Power Delivery*, vol. 38, no. 6, pp. 4312–4323, 2023.

[2.135] M. G. Dozein, A. Jalali, and P. Mancarella, "Fast frequency response from utility-scale hydrogen electrolyzers," *IEEE Transactions on Sustainable Energy*, vol. 12, no. 3, pp. 1707–1717, 2021.

[2.136] A. E. Samani, A. D'Amicis, J. D. De Kooning, D. Bozalakov, P. Silva, and L. Vandevelde, "Grid balancing with a large-scale electrolyser providing primary reserve," *IET Renewable Power Generation*, vol. 14, no. 16, pp. 3070–3078, 2020.

[2.137] N. Veerakumar, Z. Ahmad, M. E. Adabi, J. R. Torres, P. Palensky, M. van der Meijden, and F. Gonzalez-Longatt, "Fast active power-frequency support methods by large scale electrolyzers for multi-energy systems," in *2020 IEEE PES Innovative Smart Grid Technologies Europe (ISGT-Europe)*. IEEE, 2020, pp. 151–155.

Chapter 3

Synchronous Central Angle Controller

3.1 Introduction

This chapter of the thesis presents a comprehensive review of the distributed VSG emulation method, known as Synchronous Central Angle Controller (SCAC). The aim is to provide a comprehensive understanding of its operation, both from a qualitative and quantitative perspective. To this end, a detailed analysis of the different control blocks that make up the system will be carried out, explaining their origin, their purpose and how they interact with each other to emulate the behavior of a real synchronous generator.

This chapter will lay the theoretical and practical foundations necessary for the subsequent testing of the SCAC, providing the technical framework on which the analyses and simulations of the rest of the work will be based.

3.2 Synchronous Central Angle Controller

The inclusion of distributed RES systems is constantly growing, which means that new modifications must be made to the control structures in order to meet the different grid requirements, ensuring the stability and reliability of the power system and complying with the different grid codes established. These VSG systems help to improve the control of distributed systems, improving their behavior when operating connected to the grid, providing frequency and voltage support capacity, or even creating the grid itself to feed other loads.

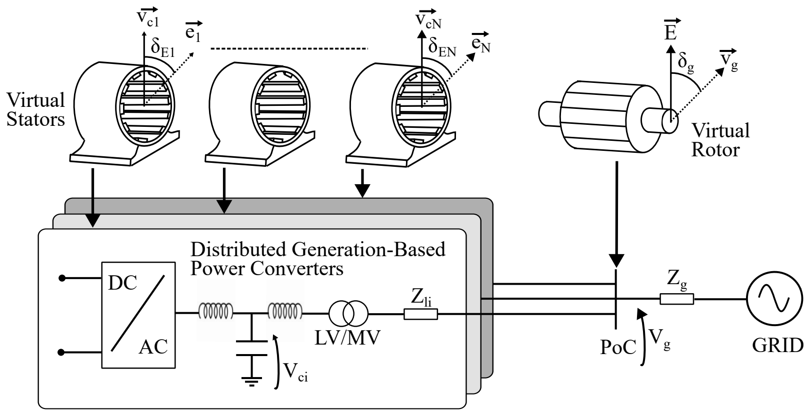

Figure 3.1: Conceptual structure of SCAC [3.1]. As it can be seen, the rotor is emulated at PoC at central controller, and the stators in the converter at local controllers.

Although SPC is one of the most common topologies for the implementation of virtual inertia methods, synthesizing the electromechanical and electrical characteristics of an SG. This system is integrated into the local control of each inverter, delegating control to each distributed unit, providing voltage and frequency support at the point of connection of the converters, and not at the plant's connection to the grid, as required by grid codes. However, in large distributed generation plants, where there may be large distances between inverter and grid, grid support is expected to be performed at the grid, generating a centralized control of the grid, improving control, making it easier to comply with grid codes. This idea is the main motivation for the development of the SCAC.

As mentioned above, the SCAC is based on the SPC, providing voltage and frequency support from the PoC. This system has already been validated in PVPP [3.1]. Therefore, this technique proposes a simultaneous control of several converters, emulating the behavior of a single SG in the PoC. Furthermore, the total power level that this system can handle, in view of system expansions, is simply the addition of the aggregate power of all the generators that compose it.

This technique presents the idea of two-layer control. The first one is known as central controller, where the behavior of a single virtual rotor, emulated in the PoC, is emulated, where the electromechanical model of the SG is considered. The other layer is known as local controller, which emulates the stator or electrical behavior of n synchronous generators, embedded in each of the distributed generation units.

This idea can be seen in Figure 3.1, where in the virtual rotor the central load angle (δ_g), which is the difference of the phase angle between the mains voltage and the voltage emf E, which defines the reference angle of all distributed generators, related to the frequency deviation of the rotor, can be seen. Moreover, in the same figure, one can see the different stators, where each has a force (e_i) and a local load angle δ_{Ei}. The

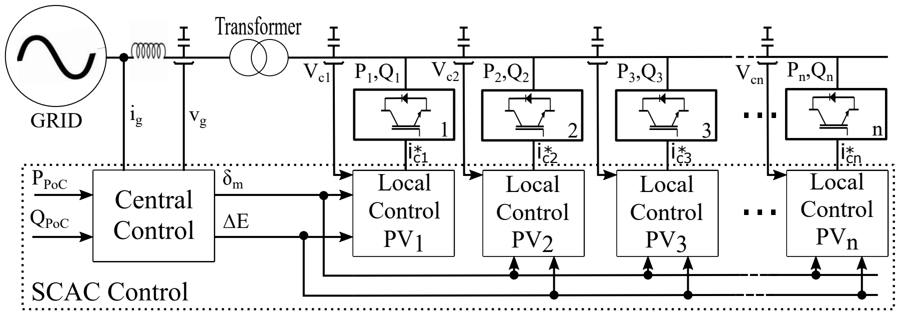

Figure 3.2: SCAC scheme for n-converters. There is a central controller located at PoC with the main grid and a local controller per inverter.

interaction between the local and the global load angle defines the active and reactive power exchanged with the grid.

This idea is further developed in Figure 3.2, where the separation between central and local controller for a group of n-converters is shown in more detail. As can be seen, the central controller, where the electromechanical system is emulated, results in the central load angle (δ_g). In addition, the magnitude emf (E) of the voltage obtained through the reactive power control loop. This central controller is interconnected by communications to the different distributed generation units, all having in common the same electromechanical dynamics. On the other hand, the local controllers embedded in each converter receive these rotor power angle and voltage set-points, transforming the global load angle to local. This is used to calculate the voltage at the virtual stator terminals (e_i), which, after being subtracted from the real voltage at the inverter terminals (V_{ci}), results in the voltage that would fall on the virtual admittance of the SG. With the value of this voltage and knowing the value of the virtual admittances, the welcoming current of each inverter is obtained. In addition, each inverter can generate power at different levels, depending on the power distribution factor K_y, which multiplies the virtual admittance.

However, although it has been mentioned and will be discussed in later chapters in more detail, the fact that this system is based on communications has certain limitations, due to the fact that the remote control of each of the local controllers is subject to communication delays, which would impoverish the stability margins of the system, making it necessary to compensate, as explained above. Despite this, this system is very suitable for future implementation, as communication systems improve year by year, with ever better speeds and latencies, helping to improve the performance of the power system.

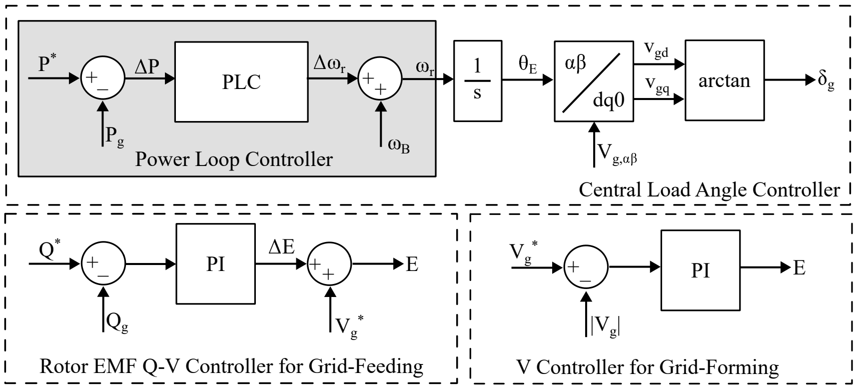

Figure 3.3: SCAC central controller details: central load angle and reactive power controller (left: Grid-Following/Supporting. right: Grid-Forming.

3.3 Central Power Controller

The central controller, as previously mentioned, is the main control layer responsible for emulating the electromechanical behavior of a SG. This controller is the main nerve in the operation of the system, as it not only regulates the active and reactive power exchanged between the converters and the grid, but also has the ability to synchronize the system with an external grid or, in case of stand-alone operation, to create a voltage reference that allows the formation of a grid of its own.

The detailed schematic of the central controller is shown in Figure 3.3, where it can be seen how its different components are implemented and related. The main function of the controller is to maintain the balance between generated and consumed power. Any variation in the load that causes a power mismatch generates a change in the grid frequency. This change is detected and managed by the Power Loop Controller (PLC), which acts by adjusting the virtual rotor frequency (ω_r).

The PLC uses a set of gains that emulate the electromechanical behavior of a real synchronous generator, such as inertia and damping. These gains allow the system to respond appropriately to fluctuations in power by either absorbing or injecting power, depending on the needs of the system or the grid to which it is connected. In subsection 3.3.1, we will go into the different parts of the model of the PLC are going to be described and also how its parameters are tuned to suit the specific requirements of each operating scenario, whether in a stand-alone network or connected to the main grid.

Once a variation in the virtual rotor frequency is obtained, it would be integrated to obtain the phase angle (θ_e), which would be used to rotate the grid voltage by means of the park transformation, obtaining the voltage coordinates in the synchronous reference frame, giving rise to the central load angle (δ_g). As explained above, this angle will be sent to each local embedded controller of each distributed generation unit. In the case of the reactive power controller, as shown in Figure 3.3, through the PI controller, the emf E would be obtained and sent to each of the converters. This would mean that in the event of any change in reactive power, the controller would regulate the voltage level in order to maintain the power set-point.

To get the central load angle (δ_g), as it can be seen in Figure 3.3, the grid voltage, which is in $\alpha\beta$ reference frame is rotated by the rotor angular speed (ω_r) to get the grid voltage in the synchronous reference frame. This can be done because at steady state $\vec{v_g}$ and $\vec{E}$ rotate at same frequency ($\omega_r = \omega_g$) leading to a constant phase difference between them. Hence, the δ_g can be defined by rotating $\vec{v_g}$ into the Virtual Rotor Synchronous Reference Frame (VRSRF). This can be defined by equation (3.1).

$$v_{g.dqE} = |v_g|cos(\delta_g) - j|v_g|sin(\delta_g) = v_{g.dE} - jv_{g.qE} \tag{3.1}$$

where $|v_g|cos(\delta_g)$ and $|v_g|sin(\delta_g)$ are d and q components of the grid voltage $\vec{v_g}$ in VRSRF. After rotating $\vec{v_g}$, the central load angle δ_g can be obtained by equation (3.2).

$$\delta_g = tan^{-1}(\frac{|v_{g.qE}|}{|v_{g.dE}|}) \tag{3.2}$$

3.3.1 Power Loop Controller

The PLC is the control block responsible for establishing the main relationship between the system's active power and frequency, taking into account the electromechanical parameters. This relationship is defined through the well-known swing equation, which allows the emulated system to regulate both power and frequency, as well as adding inertia to the system. In this section, the equation will be developed step by step to obtain the transfer function used in the PLC. To do this, starting with the electromechanical principles of a SG, we can establish the relationship between the moment of inertia, the mechanical torque and the electrical torque through equation (3.3).

$$T_m - Te - D\Delta\omega_r = J\frac{\mathrm{d}\omega_r}{\mathrm{d}t} \tag{3.3}$$

This equation describes how power variations affect the frequency of the system. For small variations in rotor angular frequency (ω_r), equation (3.3) can be reformulated in terms of electrical power, close to the synchronous angular frequency (ω_b), resulting in equation (3.4).

$$\frac{P_m - P_e}{\omega_b} - D\Delta\omega_r = J\frac{\mathrm{d}\omega_r}{\mathrm{d}t} \tag{3.4}$$

In equation (3.3) and equation (3.4, the key parameters are: T_m (mechanical torque), T_e (electrical torque), ω_r (rotor angular frequency), D (damping factor), J

(moment of inertia), P_m (mechanical input power) and P_e (electrical output power). Applying the Laplace transform to equation (3.4) and solving for the rotor angular frequency as a function of the electrical power variation, the PLC transfer function is obtained, described in equation (3.5). This function emulates the main electromechanical characteristics of an SG.

$$G_{PLC}(s) = \frac{\Delta\omega_r}{\Delta P} = \frac{1}{\omega_s(Js + D)} \tag{3.5}$$

According to [3.2], if we consider power converters behaving as a SG, the active and reactive powers exchanged between the SG and the grid can be expressed by equation (3.6a) and equation (3.6b), assuming a purely inductive output impedance. In these equations, E and V_g represent the RMS values of the virtual fem voltage and the grid voltage, respectively, while θ_E and θ_g are their phase angles. The SG reactance is denoted as X, and δ_g is the charging angle, which is the difference between θ_E and θ_g. This load angle (δ_g) has a direct effect on the active power, which implies that its variation will change the power transmitted by the converter to the grid.

$$P_g = \frac{EV_g}{X}\sin(\theta_E - \theta_g) = \frac{EV_g}{X}\sin(\delta_g) \tag{3.6a}$$

$$Q_g = \frac{V_g}{X}\left(E\cos(\theta_E - \theta_g) - V_g\right) = \frac{V_g}{X}\left(E\cos(\delta_g) - V_g\right) \tag{3.6b}$$

The load angle (δ_g) can also be related to the variation of the rotor angular velocity ($\Delta\omega_g$) by means of equation (3.7).

$$\frac{\mathrm{d}\delta_g}{\mathrm{d}t} = \Delta\omega_r \tag{3.7}$$

If the system is assumed as it is synchronized and that any change in the load angle is small, the trigonometric expressions in equation (3.6a) and equation (3.6b) are simplified, resulting in equations (3.8a) and (3.8b).

$$P_g = \frac{EV_g}{X}\delta_g = P_{max}\delta_g \tag{3.8a}$$

$$Q_g = \frac{V_g}{X}(E - V_g) \tag{3.8b}$$

Considering the mathematical model of the Power Loop Controller, using equations (3.5), (3.7) and (3.8a), the block diagram of the active power controller of an SG can be built, as shown in Figure 3.4. From this diagram, the transfer function relating the reference power to the power injected into the grid, expressed in equation (3.9), can be derived.

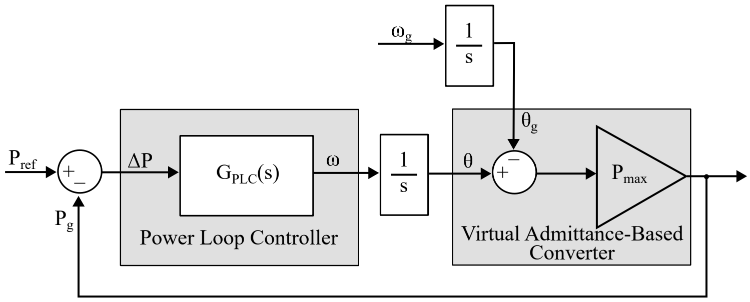

Figure 3.4: Modeling of active power control loop.

$$\frac{P_g}{P_{ref}}(s) = \frac{\frac{P_{max}}{\omega_b J}}{s^2 + \frac{D}{J}s + \frac{P_{max}}{\omega_b J}} \tag{3.9}$$

This second-order transfer function can be associated with the general model of a second-order system, allowing the control system and its parameters to be characterized for correct tuning. From here, the natural frequency (ω_n) and the damping factor (ξ), shown in equation (3.10), can be obtained.

$$\frac{P_g}{P_{ref}}(s) = \frac{\omega_n^2}{s^2 + 2\xi\omega_n s + \omega_n^2} \tag{3.10}$$

By identifying terms, expressions (3.11a) and ξ (3.11b) for ω_n are derived. .

$$\omega_n = \sqrt{\frac{P_{max}}{J\omega_b}} \tag{3.11a}$$

$$\xi = \frac{D}{2}\sqrt{\frac{\omega_b}{JP_{max}}} \tag{3.11b}$$

Although these equations take into account the moment of inertia J, this parameter is less common in practice. Instead, the inertia constant H, shown in equation (3.12), which relates the moment of inertia J to the nominal power (S_N) of the system, is often used.

$$H = \frac{J\omega_b^2}{2S_N} \tag{3.12}$$

By substituting equation (3.12) into equation (3.11a) and equation (3.11b), new expressions for the natural frequency and damping factor are obtained, shown in equations (3.13a) and (3.13b).

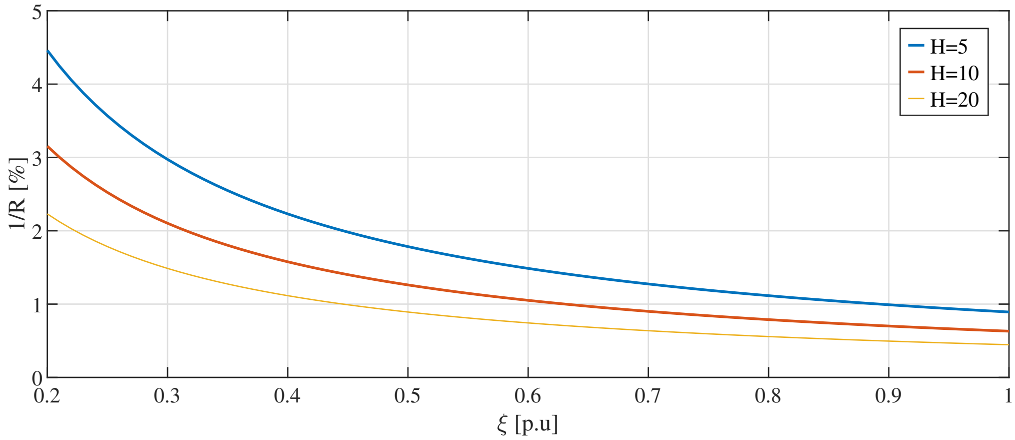

Figure 3.5: The relation between the droop slope $1/R$ and the damping coefficient ξ.

$$\omega_n = \sqrt{\frac{P_{max}\omega_b}{2HS_N}} \tag{3.13a}$$

$$\xi = \frac{D\omega_b}{2}\sqrt{\frac{\omega_b}{2HS_N P_{max}}} \tag{3.13b}$$

To analyze the behavior of the output power as a function of variations in grid frequency, it is necessary to review the transfer function obtained in equation (3.14).

$$\frac{P_g}{\omega_g}(s) = \frac{-P_{max}(s + 2\xi\omega_n)}{s^2 + 2\xi\omega_n s + \omega_n^2} \tag{3.14}$$

This equation shows that the active power controller incorporates a series $P-f$ droop, whose ratio (D_p) describes the steady-state active power variation due to changes in the grid frequency, as illustrated in equation (3.15).

$$D_p = \frac{2\pi}{1000}\left|\frac{\Delta P}{\Delta\omega_g}(s=0)\right| [kW/Hz] \tag{3.15}$$

Combining equations (3.14) and (3.15), the intrinsic droop ratio of the active power controller is obtained in equation (3.16).

$$D_{P(PLC)} = \frac{4\pi\xi P_{max}}{1000\omega_n} \tag{3.16}$$

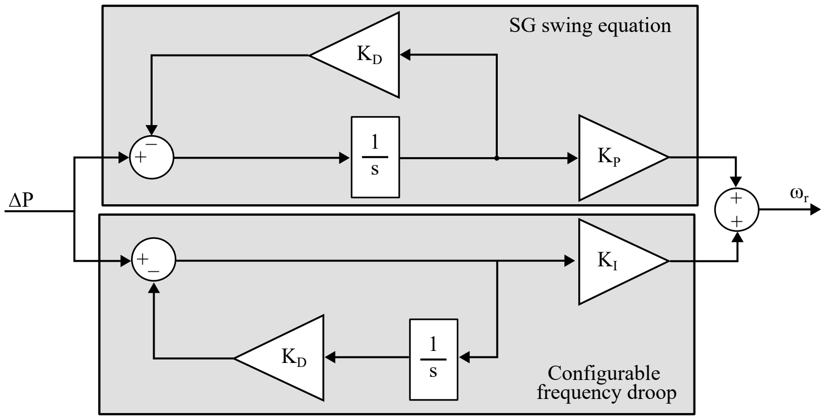

Figure 3.6: Configurable frequency droop controller for the PLC [3.7].

3.3.1.1 Limits of PLC Controller

This droop ratio allows the system to continuously synchronize power to the grid, responding to frequency variations. However, D_p is limited by inertia and damping parameters, which introduces a trade-off in the selection of system parameters.

$$\frac{1}{R} = \frac{2\pi S_N}{D_P \omega_n} \tag{3.17}$$

To show the tuning limits of the controller, the frequency deviation (in percent) required to extract the rated power of the converter is used as an indicator of the droop characteristic, [3.3, 3.4] represented by $1/R$, as shown in equation (3.17). This equation can also be expressed in terms of inertia, damping and droop slope by combining equations (3.12), (3.13a), (3.15) and (3.17), resulting in equation (3.18).

$$\frac{1}{R}(PLC) = \frac{1}{2\xi}\sqrt{\frac{S_N}{P_{max} 2H \omega_n}} \tag{3.18}$$

Since the power and inertia values are fixed in the controller design, the main challenge lies in the relationship between ξ and $1/R$. Knowing that the second-order transfer function parameters require a ξ of 0.707 to obtain an optimal balance between response time and overshoot [3.4–3.6], this sets a finite value for $1/R$, as shown in Figure 3.5.

In summary, although traditional SGs operate with a typical droop range between 4% and 5% [3.6], in RES, $1/R$ can be higher, as it is possible to have technically and economically feasible reserve power to harness.

3.3.1.2 Configurable Droop Controller

As mentioned above, the damping parameter and the slope of the frequency droop are interrelated, which makes it necessary to seek a trade off in their setting. To address this potential challenge, a solution has been developed that consists of incorporating a flexible and configurable droop controller, which improves the response of the converter to the demands of the grid.

This improvement is achieved by adding a parallel branch to the transfer function of the swing equation (3.4), which allows to control the slope of the droop P-f in steady state. By implementing this configuration, both branches share the same denominator of the transfer function, as shown in Figure 3.6, ensuring that the order of the PLC is not altered. This allows the droop setting to be independent of the damping coefficient, improving the tuning feature of the system. The proposed transfer function, which is derived from the scheme shown in Figure 3.6, is specified in equation (3.19).

$$G_{PLC} = \frac{K_P + K_I s}{s + K_D} \tag{3.19}$$

Where K_P, K_I and K_D are the configurable gains of the controller. By substituting the equation (3.19) in the PLC block from Figure 3.4, the close loop transfer function described in equation (3.20a), as well as the new expression for damping coefficient in equation (3.20b) and natural frequency in equation (3.20c).

$$\frac{P}{P_{ref}}(s) = \frac{(2\xi\omega_n - K_D)s + \omega_n^2}{s^2 + 2\xi\omega_n s + \omega_n} \tag{3.20a}$$

$$\xi = \frac{P_{max}K_P + K_D}{2\omega_n} \tag{3.20b}$$

$$\omega_n = \sqrt{P_{max}K_I} \tag{3.20c}$$

Although equation (3.20a) has a difference in its numerator compared to the standard equation equation (3.10), the denominator remains the same. This implies that, in order to ensure that the closed-loop poles are in the left half-plane and thus guarantee the stability of the system, the damping factor must remain greater than zero.

The P-f response with the modified PLC controller is shown in equation (3.21a) with a damping of equation (3.21b).

$$\frac{\Delta P}{\Delta\omega_g}(s) = \frac{-P_{max}(s + K_D)}{s^2 + 2\xi\omega_n s + \omega_n^2} \tag{3.21a}$$

$$D_{PDroop} = \frac{2\pi K_D}{1000K_I} \tag{3.21b}$$

Considering equations (3.20b), (3.20c) and (3.21b), the control parameters K_P, K_I and K_D are specified, taking into account the values of inertia, droop slope and damping. In addition, the frequency droop D_P can be expressed in its equivalent $1/R$, hereafter referred to as R_d. These gains are defined in equations (3.22a), (3.22b) and (3.22c), as [3.1] explains. It is noted that these gains are set by adjusting the inertia constant H, the damping coefficient ξ and the droop slope R_d, since the other parameters are fixed by the nominal values of the system.

$$K_P = \frac{\omega_b}{2HS_N} \tag{3.22a}$$

$$K_D = \frac{1}{2HR_d} \tag{3.22b}$$

$$K_I = \xi\sqrt{\frac{2\omega_b}{HS_N P_{max}}} - \frac{1}{2HR_d P_{max}} \tag{3.22c}$$

This modified system will be used as the active power regulator throughout the thesis, providing a robust and adequate response to the operating conditions.

3.3.2 Rotor EMF Q-V Controller

The Rotor EMF Q-V control block is responsible for regulating the voltage injected by the converter into the grid, managing variations in reactive power through a PI controller. This controller acts when a change in reactive power is detected, either due to fluctuations in grid demand or because it is desired to inject an arbitrary amount of reactive power. The block diagram of this process is depicted in Figure 3.3, where the corresponding control scheme can be observed.

Under normal conditions, when there is no significant variation in reactive power, the controller does not alter its output, allowing the voltage sent by the central controller to be simply the measured grid voltage. However, when there is a variation in reactive power, the PI controller calculates a voltage increase (ΔE) which is added to the mains voltage, thus adjusting the voltage injected by the converter to balance the reactive power demand.

The behavior of the reactive power controller is modeled by a transfer function corresponding to an open-loop PI, as it is shown in equation (3.23).

$$\frac{\Delta E}{\Delta Q}(s) = K_{PQ} + K_{IQ}s \tag{3.23}$$

3.3.3 Voltage Control for Grid-Forming

The system presented in this thesis has been initially designed to operate in grid-feeding/supporting control structures, as demonstrated in previous work [3.8–3.10] and its original design [3.1, 3.7]. However, its application in grid-forming systems is also explored, where the system operates in grids isolated from the main grid, a relevant configuration for certain distributed generation scenarios.

The control structure for grid-forming generators used in this thesis is based on the one developed in [3.11], although with a simplified design. Instead of controlling several system parameters, the focus of this thesis is exclusively on the control of the grid voltage by means of a PI controller, as illustrated in Figure 3.3.

In this configuration, a reference value is set for the grid phase voltage in RMS value, which is then compared to the measured voltage. The difference between these values is processed by a PI controller, which adjusts the modulus of the phase voltage (E) in the created network. Assuming that the voltage generated by the system is the same as the measured voltage (considering a factor $1/\sqrt{2}$ for using RMS values), the closed-loop transfer function can be expressed by the following equation:

$$\frac{E}{V_g^*}(s) = \frac{\sqrt(2)(K_{PV} + K_{IV}s)}{K_{IV}s + \sqrt{2} + K_{PV}} \tag{3.24}$$

This simplified control approach allows the grid-forming system to autonomously generate and regulate voltage in isolated grids, providing stability and efficient control of active and reactive power in such applications.

3.4 Local Controller

The central load angle and voltage emf E calculated by the central controller are sent to the central controllers in order to determine the reference current ac to be injected by the distributed generation units. Figure 3.7 shows the structure of the local controller divided into two main blocks, the local load-angle and electrical emulation.

The load-angle control loop in Figure 3.7, regulates the phase angle θ_{Ei}, according to the sent load-angle center angle reference. This angle is used to rotate and project the output voltage v_{ci} in the local load-angle reference frame.

The error between the local and central load angle is processed through a PI controller, and once integrated, the phase angle required to project the voltage v_{ci} onto the synchronous reference frame is generated, leading to the local load-angle. As discussed the rotor voltage emf E received by the local controller, combined with the phase angle, is used with the Voltage Control Oscillator (VCO) to define the local voltage in the stationary $\alpha\beta$ reference frame, as [3.12] explains. This can be obtained from equation (3.25).

$$e_i = \begin{bmatrix} e_{\alpha i} \\ e_{\beta i} \end{bmatrix} = \sqrt{\frac{3}{2}} E \begin{bmatrix} sin(\theta_{Ei}) \\ -cos(\theta_{Ei}) \end{bmatrix} \tag{3.25}$$

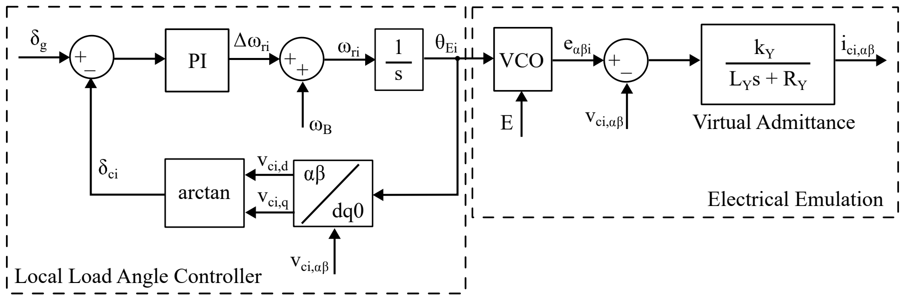

Figure 3.7: SCAC central controller details: central load angle and reactive power controller.

where $e_{\alpha i}$ and $e_{\beta i}$ are the α and β components of local emf e_i. E defines the maximum value of the voltage and θ_{Ei} the phase angle of the local converter.

Then the voltage difference between e_i and v_{ci} is processed through the electrical emulation block to the determinate the reference current which is the one that will be injected into the grid. The main blocks used in the local controller are explained below.

3.4.1 Local Load Angle Controller

The central power angle, received through communications, is transformed into a local power angle, which has the function of regulating the local phase angle (θ_{Ei}). This angle is essential to adjust the local load angle (δ_{ci}), which is used to rotate the converter output voltage in a new reference system, as shown in figure 3.7.

The error between the center power angle and the local angle is processed through a PI controller, whose purpose is to set the local rotor frequency (ω_{ri}). By integrating this frequency, the corresponding phase angle is obtained. This process ensures that the converter remains synchronized with mains or system variations by dynamically adjusting the output voltage.

In addition, in the local load angle controller, a transfer function can be derived that relates the center load angle to the local load angle. This transfer function acts as a reference to properly tune the PI controller, optimizing the dynamic response of the system and ensuring stable and efficient operation. The tuning of this PI is similar to a PLL tuning, by setting ω_n and ξ.

$$\frac{\delta_{ci}}{\delta_g}(s) = \frac{K_{P\delta}s + K_{I\delta}}{s^2 + K_{P\delta}s + K_{I\delta}} = \frac{2\xi\omega_n s + \omega_n^2}{s^2 + 2\xi\omega_n s + \omega_n^2} \tag{3.26a}$$

$$K_I = \omega_n^2 \tag{3.26b}$$

$$K_P = 2\xi\omega_n \tag{3.26c}$$

The natural frequency ω_n can be selected based on the dynamics of the inner current regulator bandwidth to appropriately tune the gains of the local PI controller. By aligning ω_n with the bandwidth of the inner current loop, the PI controller can effectively respond to changes in the system, ensuring stability and dynamic performance. This selection ensures that the outer control loop does not interfere with the faster dynamics of the inner current regulator, thus providing a balanced and well-coordinated control system.

3.4.2 Electrical Emulation

In the electrical emulation block, the virtual admittance is responsible for processing the voltage difference between e_i and v_{ci} to determine the reference current. It should be noted that all distributed generation units receive the same δ_g and voltage, therefore, a value appropriate to the distribution system of the virtual admittance must be found. The power distributed by each of the converters can be calculated using the distribution factor k_{Yi} as shown equation (3.27).

$$k_{Yi} = \frac{P_{ci}}{\sum_{i=1}^{N} P_{ci}} = \frac{P_{ci}}{P_{PoC}} \tag{3.27}$$

P_{ci} is the level of power injected by each converter, P_{PoC} is the total power of the plant, N is the number of distributed generation units. The power distributed by each generator is realized through the distribution factors and the virtual admittance, shown in equation (3.28).

$$Y_i = \frac{k_{Yi}}{L_Y s + R_Y} \tag{3.28}$$

k_{Yi} is the distribution factor, L_Y is the inductive part of the admittance and R_Y is the resistor part.

To select the value of the virtual inductance, a good approximation is to use 30% of the base impedance for the rated power of the converter, which is typically the output inductance of an SG [3.13, 3.14]. Equation (3.29) shows how this would be calculated. In the case of the virtual resistance, it would be selected by considering the cut-off frequency of the LPF characteristic of the virtual admittance.

$$L_Y = \frac{0.3V_b^2}{S_N \omega_b} \tag{3.29}$$

V_b is the base RMS line-to-line voltage, S_N is the rated apparent power and ω_b is the base electrical angular frequency.

Once the reference current is obtained, a current controller will regulate the current to be injected by each generator. This can be done by a simple proportional resonant controller (PR), or by using PLL, passing the current references to SRF and controlling the current through a PI.

3.5 Conclusion

In this chapter, the aggregated VSG system, that is called Synchronous Central Angle Controller which will serve as a basis throughout the thesis, has been comprehensively presented. This system allows the centralized operation of different distributed generation sources, providing the PoC with adequate inertia and damping, which is essential to compensate for disturbances in the main power grid.

First, a detailed theoretical analysis has been presented, explaining each of the system components. Special emphasis has been placed on how these elements interact with each other to achieve optimal behavior in the face of frequency and voltage variations, which are common in power grids with high penetration of renewable energies. In addition, the mechanism by which the SCAC emulates the dynamic characteristics of a conventional synchronous generator has been described, allowing it to provide support to the grid during instability events.

The flexibility of the system to adapt to different grid configurations and distributed generation technologies has also been discussed. This adaptability is a key point, as it allows the SCAC system to be applicable in a wide variety of contexts and use cases, from isolated power grids to large grid-tied systems.

References

[3.1] C. Verdugo, A. Tarraso, J. I. Candela, J. Rocabert, and P. Rodriguez, "Centralized synchronous controller based on load angle regulation for photovoltaic power plants," *IEEE Journal of Emerging and Selected Topics in Power Electronics*, vol. 9, no. 1, pp. 485–496, 2020.

[3.2] W. Zhang, A. M. Cantarellas, J. Rocabert, A. Luna, and P. Rodriguez, "Synchronous power controller with flexible droop characteristics for renewable power generation systems," *IEEE Transactions on Sustainable Energy*, vol. 7, no. 4, pp. 1572–1582, 2016.

[3.3] ——, "Synchronous power controller with flexible droop characteristics for renewable power generation systems," *IEEE Transactions on Sustainable Energy*, vol. 7, no. 4, pp. 1572–1582, 2016.

[3.4] J. D. Glover, T. J. Overbye, and M. S. Sarma, *Power system analysis & design.* Cengage Learning, 2017.

[3.5] L. L. Grigsby, *Power system stability and control.* CRC press, 2007.

[3.6] W. Zhang, A. Luna, I. Candela, J. Rocabert, and P. Rodriguez, "An active power synchronizing controller for grid-connected power converters with configurable natural droop characteristics," in *2015 IEEE 6th International Symposium on Power Electronics for Distributed Generation Systems (PEDG).* IEEE, 2015, pp. 1–7.

[3.7] C. Verdugo, A. Tarraso, J. I. Candela, J. Rocabert, and P. Rodriguez, "Synchronous frequency support of photovoltaic power plants with inertia emulation," in *2019 IEEE Energy Conversion Congress and Exposition (ECCE).* IEEE, 2019, pp. 4305–4310.

[3.8] D. d. Rivero, P. García, C. Blanco, and Navarro-Rodríguez, "Control of aggregated virtual synchronous generators for pv plants considering communication delays," *IEEE Transactions on Industry Applications*, pp. 1–13, 2024.

[3.9] D. Del Rivero, P. G. Fernández, C. Blanco, and Navarro-Rodríguez, "Control of aggregated virtual synchronous generators including communication delay compensation," in *2022 IEEE Energy Conversion Congress and Exposition (ECCE)*, 2022, pp. 1–7.

[3.10] D. Del Rivero, I. Peláez, P. G. Fernández, C. Blanco, and Navarro-Rodríguez, "Integration of ramp-rate compensation in a distributed virtual synchronous generator schema for hybrid pv plants," in *2023 IEEE Energy Conversion Congress and Exposition (ECCE)*, 2023, pp. 1122–1128.

[3.11] H. Bevrani, B. François, and T. Ise, *Microgrid dynamics and control.* John Wiley & Sons, 2017.

[3.12] S. Chatterjee, P. Kumar, and S. Chatterjee, "A techno-commercial review on grid connected photovoltaic system," *Renewable and Sustainable Energy Reviews*, vol. 81, pp. 2371–2397, 2018.

[3.13] T. Z. Getahun, "Decentralized virtual synchronous generator for the integration of energy storage and distributed generation in the electrical grid," Master's Thesis, Universidad de Oviedo, August 2021, submitted to the Department of Electrical Engineering, Electronics, Computers and Systems.

[3.14] P. Rodriguez, I. Candela, C. Citro, J. Rocabert, and A. Luna, "Control of grid-connected power converters based on a virtual admittance control loop," in *2013 15th European Conference on Power Electronics and Applications (EPE).* IEEE, 2013, pp. 1–10.

Chapter 4

System Control Adaptation Considering Delays and Their Compensation

4.1 Introduction

In this chapter, modifications to the SCAC control system will be presented in order to adapt it to operation with commercial converters, taking full advantage of their characteristics through the use of active and reactive power commands. The objective is to optimize the control system, not only by adjusting it to the limitations of commercial converters, but also by taking advantage of its internal capacity to record and monitor critical variables, such as currents, voltages and frequencies. These variables, which are stored in the internal registers of the converters, can be accessed through communication systems. By taking advantage of the internal registers, the data can be read and transmitted via communication protocols, such as MODBUS TCP, facilitating their integration into the control system, being able to reduce the number of external sensors required.

Additionally, since this control system relies on communications between the central controller and the local controllers embedded in the drives, it is very important to consider possible communication delays. These delays, which often occur in MODBUS TCP-based communication systems, can negatively affect the stability and performance of the control system. To address this challenge, a communication delay compensation system, based on Smith Predictor, will be implemented. This method allows anticipating and mitigating the effects of delays, thus ensuring that the system maintains its stability and responsiveness even in the presence of delays. The SP is efficiently adapted to distributed control environments, such as the one being considered in this thesis, where the communication between the central controller and the converters must be accurate and reliable.

Finally, the proposed system will be subjected to different tests, initially at the real-time simulation level. These simulations will allow evaluating the behavior of the system under different operating conditions, verifying the effectiveness of the proposed modifications. Afterwards, the system will be tested in more realistic scenarios using Power Hardware-in-the-Loop (PHIL). It is important to highlight the experimental setup is explained in Appendix A.2, which is the one used for the different real-time simulations. This will allow for more representative results of performance in real applications, facilitating the transition from the simulation environment to practical use in power plants.

This work belongs to a journal (JP1) and a conference contribution (CP1) that can be find in the Appendix B [4.1, 4.2].

4.2 Limitation of Commercial Converters

When developing a power plant, the power converters used to inject energy into the grid are generally not designed from scratch by the plant operator, but are purchased from specialized manufacturers, who supply them based on the plant's specifications and requirements. However, these converters do not usually allow access to internal variables in the time domain, nor to internal control loops (such as current and voltage loops), so they are not adapted to external control systems, such as the system to be implemented, as they usually only allow the adjustment of active and reactive power set-points. In addition, although these devices usually provide records with readings of various variables that could be used in the control system. Due to its wide adoption in power plants, communication protocols such as MODBUS TCP is the system proposed and used as communication system [4.3]. The effective implementation of the control system in this type of converters requires certain modifications to the control system presented in this thesis to ensure optimal operation.

These adaptations are essential to ensure proper operation and could facilitate the implementation of advanced technologies, such as distributed VSG systems as the SCAC, even in existing plants. This opens up the possibility of massively integrating such solutions without compromising the stability and performance of the overall power system. In the next section, the control system modification is going to be described.

4.3 Control System Modification

Most of the current VSG techniques integrate their controllers as add-ons in the firmware of the power converters. However, the SCAC technique used in this thesis requires access to multiple control actions, as well as the reading of signals such as

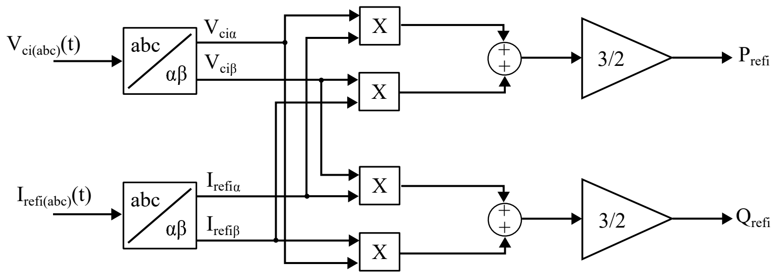

Figure 4.1: Active and reactive reference power calculation [4.1, 4.5].

currents and voltages. This chapter proposes a modification of the control structure that allows SCAC to be applied in new and existing commercial converters that only allow the management of active and reactive power set-points. Besides, by using the MODBUS TCP protocol, which is the coomunitation protocol used for communicating the central to the local controllers, it will be possible to access internal measurements of the converter, as the included in the SunSpec DER specification [4.4].

This section will review how to modify the control system to apply the active and reactive power set-points, as well as explore the converter signal readings and their subsequent reconstruction and modification to integrate them into the proposed control system.

4.3.1 Modification of Power Commands

In commercial converters used in this type of application, generally only active and reactive power commands are accepted as control signals. Through their internal control, these converters generate the necessary signals to inject power into the available grid or, if necessary, to create a grid. For this reason, the control system presented in Chapter 3 has been slightly modified to accommodate this situation. This implies that the reference currents generated by the SCAC must be converted into active and reactive power commands to be compatible with the commercial converters used.

This transformation is detailed in Figure 4.1, where the corresponding block diagrams are shown. The process starts with the reference current generated by the control system, which presents the block diagrams used for the calculation of the power signals in alpha-beta, although other reference frames can be used. This reference current, together with the voltage measured at the output of each converter, also transformed to alpha-beta coordinates to maintain consistency in the representation, is used in the calculation. Through the application of equations (4.1a) and (4.1b), show the calculation of the reference active and reactive powers for each distributed converter. As it will be seen, the output voltage used for the calculation, can be the one reconstructed in the next section.

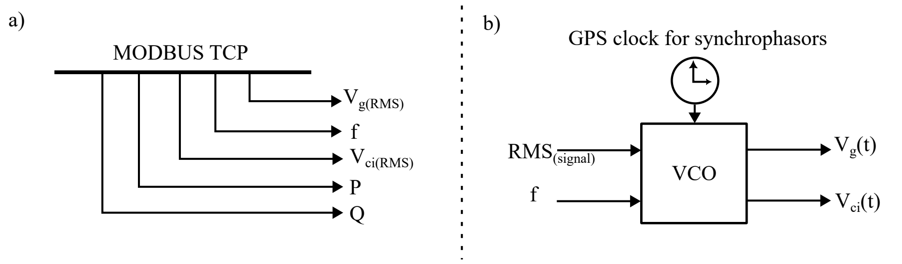

Figure 4.2: a) MODBUS TCP frequency and RMS voltage. b) instantaneous values from the RMS voltage, frequency, and clock signal obtained by a VCO (Voltage Controller Oscillator) [4.6].

$$P_{refi} = \frac{3}{2}(V_{ci\alpha}I_{refi\alpha} + V_{ci\beta}I_{refi\beta}) \tag{4.1a}$$

$$Q_{refi} = \frac{3}{2}(V_{ci\beta}I_{refi\alpha} - V_{ci\alpha}I_{refi\beta}) \tag{4.1b}$$

4.3.2 MODBUS TCP Readings and Reconstruction

Besides of modifying the control system for generating active and reactive power references, the internal registers of the power converters are going to be used in order to obtain some measurements of current, voltage, power and frequency. Thus reducing the need of external sensors, what reduces the cost and complexity of the system. This is based in MODBUS TCP protocol, which is commonly used in industrial applications or commercial converters and also it is used for the communication among the central controller and the others local controllers. Furthermore, the internal registers of the power converter can be based in SunSpec DER Specification [4.4], which also uses MODBUS TCP protocol.

This method relies on measurements of RMS voltage, frequency and active and reactive powers read by communications at each converter (see Figure 4.2a). Therefore, this approach is an attractive solution for the standardization of the SCAC concept for mass implementation in future and existing DEG systems. However, it is important to highlight certain limitations, comparing the use of external sensors with the use of internal readouts, as this implementation only focuses on the fundamental component for signal reconstruction in the time domain. Additionally, achieving a fast response is restricted by communication delays and the time needed for signal reconstruction, which requires at least one fundamental cycle, considering RMS values, which is only possible within the internal control of the power converter.

Nevertheless, the instantaneous voltage signals will be reconstructed from the RMS values, as shown in Figure 4.2b), and used as feedback in the control system, replacing the external sensors. To improve the synchronization accuracy, it is suggested as future work to implement a VCO system synchronized by a GPS clock, as explained in [4.6].

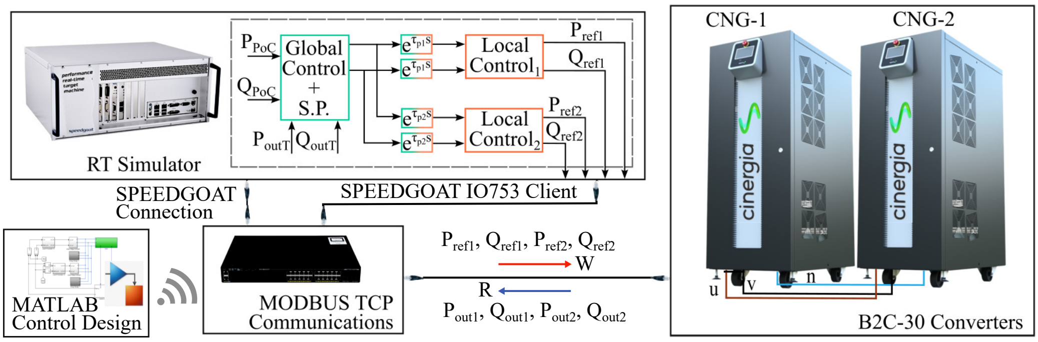

Figure 4.3: Setup for HIL and PHIL experimental tests. The control design is made on Matlab and executed in the real-time Speedgoat target. The converters are controlled by writing/reading published MODBUS TCP variables [4.1, 4.2].

For the application to the SCAC, the main reconstructed used signals are the output voltage of each converter, used in the main control system and also for obtaining the active and reactive power set-points. Also the voltage at the PoC can be computed and used in the control system, as well as the active and reactive power output of each converter.

4.4 Communication Delay and Compensation

As it has being seen and explained, the SCAC control system is a communication-based control system. Communication systems always have some latency, which introduces communication delays into the system. These delays arise mainly due to the fact that the controllers embedded in the converters of the distributed generation units communicate with the central controller of the SCAC through the MODBUS TCP protocol. The magnitude of the delay depends on both the number of signals transmitted over the communication bus and the physical distance between the devices.

This phenomenon can compromise the effectiveness of the closed-loop control system, affecting both the transmission of control signals from the central controller and the reception of feedback information from the drives. Due to the MODBUS TCP is not a real-time protocol, can generate variable delays in the communication between the central controllers and each distributed unit. This adds an additional challenge to the control system design.

Therefore in this section, the communication delays present in this system will be described and modeled, together with the implementation of the SP. Smith predictor will be implemented as an effective strategy to compensate for them, ensuring the stability and performance of the control system.

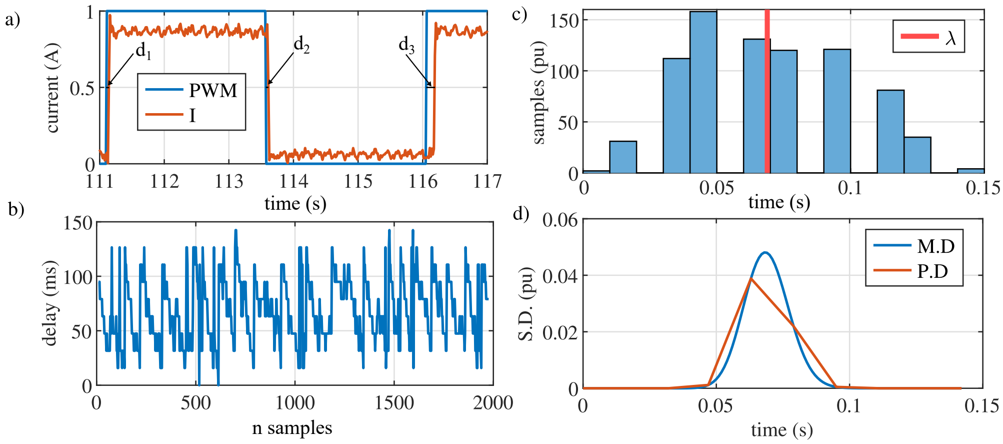

Figure 4.4: a) Instantaneous delay measurement in the lab (PWM is the sent reference signal and I is the actual current the converter develops). b) Time variation of delay. c) Delay histogram from experimental tests. d) Probability density function of the measured communication delay (M.D) in comparison to Poisson distribution (P.D) with λ of 68 ms.

4.4.1 Delay Modeling

This subsection will explain how communication delays in communication systems such as MODBUS TCP have been modeled and estimated. In the literature, there are several proposals to model random delays. One of them uses the Markov chain [4.7, 4.8] as its foundation. A stochastic model called a Markov chain discretely represents certain potential states or events (in this case delays). The probability of those potential outcomes is solely dependent on the outcome of the prior event. For this work, to model the communication latency in the local network where the tests are going to be performed, the communication delays in a link using MODBUS TCP protocol are measured. A 30 kW bidirectional dc/dc from Cinergia SL, as the one shown in Figure 4.3, was employed as the PHIL system. This power supply features different emulation units, including batteries and solar panels, and may work as a voltage, current, and power source. Two of these power sources will be used in the following subsections for the experimental validation. For performing the measurements, a HIL system (Speedgoat target machine) is used to act as a communication gateway between the converters and the control system in a real-time simulation. These components are also displayed in Figure 4.3. A deeper explanation is performed in Appendix A.2, where the different elements are explained as well as the simulation process.

To measure the communication delay, the total time that includes both the sending of data via the MODBUS TCP protocol and the response of the converter operating in current source mode has been considered. This approach allows both components to be treated as an integrated system. The procedure followed is as follows: a digital square reference signal of 0.25 Hz has been supplied simultaneously to the current converter set-point (sent by MODBUS TCP), so it can be used as a trigger signal in an external scope that also captures the output current response. Both signals can be observed in Figure 4.4a). The difference between PWM signal (digital square signal sent by simulator) and the actual current measured (I), will be the communication delay. By applying that difference to all samples the delay distribution from Figure 4.4b) can be obtained. This delay distribution varies between a much wider range, as it can be seen between 0 ms and 150 ms, with a mean value of around 68 ms and a mode of 45 ms. In Figure 4.4c), the time variation of the delay during all the experiments can be easily appreciated. The time variation of the delay throughout the entire experiment is seen in Figure 4.4c). For the delay modeling, a Poisson distribution with the form shown in equation (4.2) is chosen, as proposed in queuing theory delay models for communication networks [4.9, 4.10]. The Poisson distribution is obtained with the delay evolution from Figure 4.4b), with 795 number of events (k) and the mean (λ) value of 68 ms. That distribution is used as delay estimation for compensating the delays in the SP loop. For the real communication delay, the measured data is used.

$$f(k, \lambda) = Pr(X = k)\frac{\lambda^k e^{-\lambda}}{k!}; \lambda > 0; k = 0, 1, 2... \tag{4.2}$$

By using the Poisson distribution, the distribution from Figure 4.4.d) is obtained.

4.4.2 Delay Compensation. The Smith Predictor

For delay compensation, several methods have been evaluated and are described in Chapter 2, where the state of the art is reviewed. However, for the purposes of this thesis, as it was explained, the SP has been chosen due to its simplicity and reliability of operation [4.11].

The SP minimizes or eliminates the delay component of communication in the control loop by incorporating a model of the system that includes an accurate estimate of the delay structure, using a relatively accurate model of the plant [4.12]. In the SCAC system, delay occurs mainly during the sending of control signals from the central controller to the local controllers. The SP compensates for this delay by incorporating a model of the plant ($\widehat{G_p}$) together with an estimated delay term ($\widehat{e^{tps}}$).

The plant model represents the relationship between the control actions (variables such as δ_g and E) and the outputs in terms of active and reactive powers (P_{out}, Q_{out}), as shown in Figure 4.5a. However, obtaining the precise transfer function for a communication-based control system is complex. To overcome this challenge, it is proposed to run a replica of the local controller of each converter in the central controller. In this approach, the central controller has as many replicas as there are converters in the SCAC system. It is important to note that the structure of the local controller is

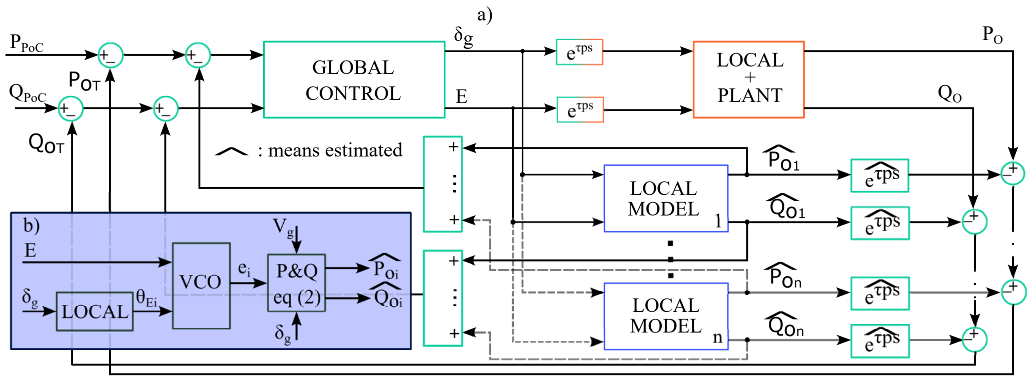

Figure 4.5: a) Global SP architecture for n-converters (light green block for global control and orange for local control) [4.7]. b) Local model for each converter (blue blocks) emulated in the global controller.

the same for all converters; only the instantaneous values of each converter change.

$$P_i = \frac{E_i V_i}{X_i} sin(\delta_g) \tag{4.3a}$$

$$Q_i = \frac{V_i}{X_i}(E_i cos(\delta_g) - V_g) \tag{4.3b}$$

Figure 4.5b shows the model of the plant simulated by the SP, which is the part of the system affected by the delay. The outputs of the emulated system (δ_g and e_i) are used to calculate the output power using the power equations described in equations (4.3a) and (4.3b). Finally, the error between the predicted active and reactive powers and the actual values provided by the local controllers is used to compensate for the delay, as shown in Figure 4.5.

To clarify this point, and showing how SP compensates the delay, Figure 4.6 shows the difference in behavior when using or not the SP under the limit stability delay condition. As it can be seen, by setting the limit delay (75 ms), the response with (d_{LSP}) and without SP (d_{LNSP}) are clearly different, where the additional overshot created by the delay is mostly removed by applying the SP. It is also included a larger delay (d = 80 ms) to illustrate the instability condition above a certain delay level. In this case the unstable case is scaled for representation purposes. Hence, it can be seen that SP really works, and compensate the communication delay, ensuring the stability of the system. In the next subsection, a concise stability analysis is undertaken to complement the explanation and validate the importance of implementing a delay compensation method.

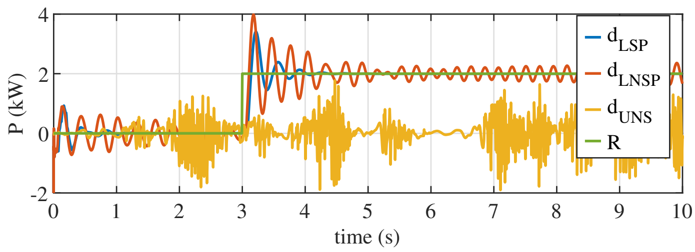

Figure 4.6: System step response with a constant communication delay of $d_3 = 75$ ms (which is the stable limit regarding the delay), with (d_{LSP}) and without delay compensation (d_{LNSP}). Also, the unstable case (d_{UNS}) is represented for a case of $d_2 = 80$ ms. For representation, the unstable power is corrected by a factor of 0.005. R is the reference signal.

Table 4.1: SCAC parameters and set-points for the simulation.

Variable	H (s)	τ	R_p	Sn (VA)	V_g (V)
Value	10	0.98	0.1	6000	400
Variable	f_g (Hz)	R_v (Ω)	X_v (Ω)	P_{set} (W)	Q_{set} (Var)
Value	50	8	0.48	4000	2000

4.4.3 Stability Analysis

Within the framework of the SCAC control system, a stability analysis has been carried out considering the effects of communication delays. Initially, the behavior of the system without communication delays was compared with the system with communication delays, which generate instability. Additionally, the use of the Smith predictor as a compensation technique was evaluated, demonstrating its effectiveness in maintaining system stability. This analysis is presented both in the time domain, in Figure 4.6, and in the frequency domain, in Figure 4.7, where the Bode diagrams corresponding to each case are shown. In these figures, the impact of communication delays on system performance is analyzed, showing the improvements achieved by compensating for these delays. Furthermore a sensitivity analysis is done where the location of the zero and poles are shown, when non delay, delay and delay with SP are used.

The stability response will be compared in two different scenarios: one where the system is operated without communication delays ($d_1 = 0$ ms) and another where communication delay is introduced at the stability boundary ($d_2 = 75$ ms). Those scenarios are introduced in Figure 4.7, where Bode diagrams are depicted. The system parameter, belonging to the base is shown in Table 4.1. Initially, the Bode diagram without communication delays was approximated using the Frequency Response Function (FRF) method, a frequency-based measurement function. It consists of a measurement function based on the frequency sweep of the system, which expresses the frequency domain relationship between an input and an output of a system [4.13]. With this method, it is experimentally proven that the system behaves in a similar way

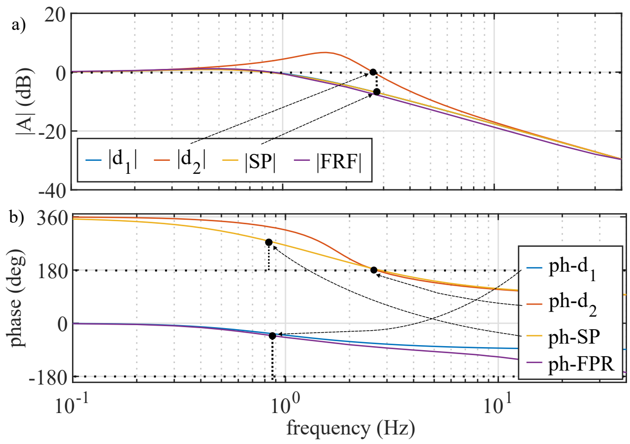

Figure 4.7: Bode diagram of the SCAC system considering no delay ($d_1 = 0$ ms), the limit delay which makes unstable the system ($d_2 = 75$ ms), and the same delay but compensated with the SP method. Furthermore the Bode diagram extracted by FRF method is also presented (just for non delay case). a) The amplitude Bode is presented. b) shows the phase evolution for the different cases, including the PMs. Notice the low-frequency ranges of the system (x-axis) due to the emulated system inertia (10 s). Table 4.2 shows the stability values of these cases.

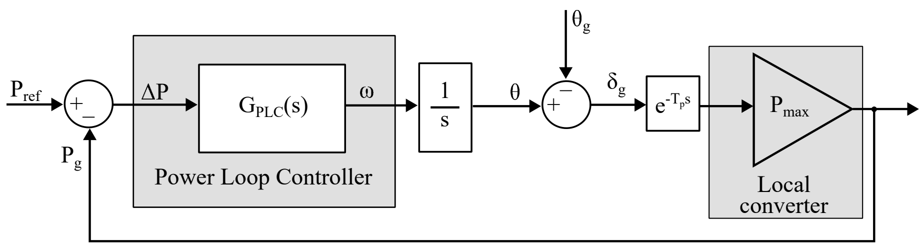

Figure 4.8: Simplified Model of SCAC with one converter.

to the simplified behavior obtained from Figure 4.8. In the Figure 4.7, just the case without delay is included with this method. However, considering that the response at low frequencies closely resembles the transfer function obtained from the system in Figure 4.8 (due to the inertia control system being slow and the rest being fast at low frequencies), the latter has been employed for the subsequent stability tests. The three first cases were analyzed in the Bode by using the system from Figure 4.8.

As observed in the Bode diagram of Figure 4.7 and the data presented in Table 4.2, system stability is evident in the absence of communication delays, with a Phase Margin (PM) of 143.44 and an infinite Gain Margin (GM). When the limiting delay (d_2) is introduced, the system is positioned at the stability boundary, featuring a GM of 1.001 and a PM of 0.0038. Additionally, upon the introduction of the SP, the system regains its stability margin, displaying a GM of 6.86 and a PM of 97.7.

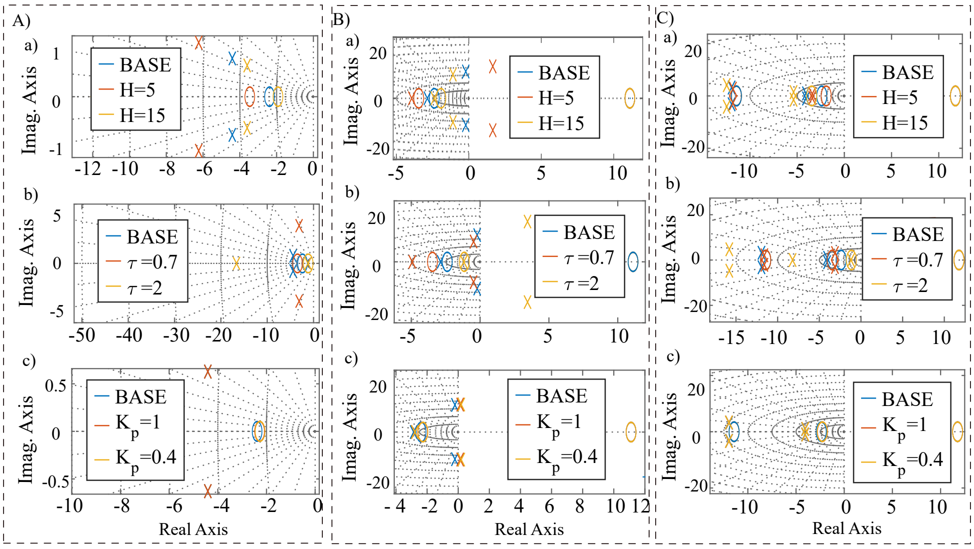

Figure 4.9: Zero-Pole of control system. Base case parameters shown in Table 4.1. A) Z-P map without delay. B) Z-P map with delay. C) Z-P map with SP compensation delay. In the first row of the Figure a), the inertia (H) is varied. In b) the damping (τ), and in c) the droop slope (K_p). In Table 4.2 the improved values are bold.

Taking advantage of the stability analysis conducted in the baseline case, a brief assessment of the system's stability sensitivity has been carried out. Critical parameters such as inertia (H), damping (τ), and droop slope (R_p) were varied across three different scenarios: A) without delay, B) with a limiting delay, and C) limiting delay but employing SP as a compensation method. These variations are reflected in Figure 4.9. Furthermore, the aim of this analysis is to emphasize the significance of certain elements in the control system, demonstrating how they influence the variation of stability margins. Thus, analyzing better the impact of communication delays on the system performance.

Leveraging Figure 4.9 and Table 4.2, it can be observed that, in the case A) without delays, the modification of H values a) causes the system to become more underdamped but faster as its value decreases. Increasing the value of τ b) results in a more overdamped and slower system, while the variation of R_p c) mainly affect to the position of the zeros, moving the root locus to the right, as K_p is increasing. In case B), the system behaves similarly, but with eigenvalues shifted to the right. It is even noticeable that, by increasing H and decreasing τ , the dominant poles can lead the system to the stability margin, as detailed in Table 4.2. In case C), after delay compensation with SP, the significant eigenvalues return to the negative semi-axis, ensuring system stability.

Table 4.2: Stability values for the different cases from Figure 4.9.

Case			GM	PM	ξ
A)	base		inf	144	0.99
	a)	H=15	**inf**	**144**	**0.99**
		H=5	inf	144.5	0.99
	b)	τ=0.7	inf	128.3	0.7
		τ=2	inf	165.7	1
	c)	$R_p = 0.7$	inf	141	0.99
		$R_p = 1$	inf	141	0.99
Case			GM	PM	ξ
B)	base		1	0.04	0.35
	a)	**H=15**	**0.43**	**28.7**	**0.48**
		H=5	inf	-32.9	0.14
	b)	τ=0.7	**1.62**	**23.26**	**0.43**
		τ=2	0.35	-56.8	0.02
	c)	$R_p = 0.7$	0.83	-8.17	0.31
		$R_p = 1$	0.85	-7.03	0.31
Case			GM	PM	ξ
C)	base		6.86	97.7	0.97
	a)	**H=15**	**7.9**	**104**	**0.97**
		H=5	5.15	87.8	0.95
	b)	τ=0.7	7.93	78.9	0.71
		τ=2	4.36	132	0.96
	c)	$R_p = 0.7$	6.4	89.8	0.96
		$R_p = 1$	6.47	91.1	0.96

4.5 Simulations and Tests

In this section, various tests of the VSG control system under study will be carried out. These tests will be performed to evaluate the different control methods, which will be implemented in Cases I to V. First, the main modes of operation, such as active and reactive power injection, frequency compensation and power support, will be tested. These cases will be simulated in real-time, and then they will be validated by using Power-hardware-in-the-Loop (PHIL) simulations using external hardware.

In cases IV and V, the behavior of the system in the event of a phase angle jump and its performance in grid-forming operation will be analyzed in a simulated manner.

4.5.1 Considerations for the Implementation

In this section some results are presented to validate the proposed compensation method, presenting different working modes of the system. Those operations are tested in both local Simulink simulations and real-time experimental proofs through Speedgoat emulator. Real-time tests are based on Figure 4.3, where two 30 kW bidirectional dc/dc converters from Cinergia S.L (CNG) are used. In this case, CNG-2 has three strings working as power sources to emulate the power demand from the control system, which will receive the commands from the simulation (P_{ref1}, Q_{ref1}, P_{ref2}, Q_{ref2}). Those set-points are sent and written in CNG-2 through MODBUS TCP. The energy computed by the control system will be obtained from CNG-1, which works as a battery emulator in each string, which is running in battery emulation mode to replicate the SCAC idea. As it was stated in Section 4.4, a HIL system is used for real-time simulation. As aforementioned, Appendix A.2 explains the every component used for the real-time simulations, as well as their interconnection.

For the case of communication delays between the central controller and the local units, all simulations have considered some delays. For the local Simulink simulations, the Poison distribution calculated and shown in Figure 4.4 (computed in Section 4.4.1). Due to a limitation in Speedgoat, the calculated statistical distribution could not be used in the real-time simulations, and a random distribution with values between 0 and 100 ms had to be used instead, applying to simulated cases I-IV. In case V, a constant delay has been used. However, for experimental simulations with external hardware, due to the CNG converter's internal delay in the processing of the power references and integration windows used for the calculation of the active and reactive power, additional delays are added to the control system (20 ms for active power and 400 ms for reactive power). These delays are also included in the model used by the Smith predictor to achieve better results.

This is a critical step, as the Smith predictor will also tackle the additional delays present in a real implementation.

For these tests, grid, and VSG models are taken from [4.14], where the SCAC idea was first published. In this case, the model includes three DEGs connected to a grid and considers a battery locally connected per converter, which is the element that provides/absorbs energy for frequency support. In this case, feeder impedance is considered, demonstrating that the system could work in a real implementation with real feeders.

4.5.2 Operation Cases

Figure 4.10 shows an overview of the different tests or cases that are going to be evaluated, showing several operation modes to be validated. Going from a simple active and reactive power reference tracking to a power support operation mode, depending on the grid operator requirements modifying the power exchange with the grid. Besides frequency support capability, by injecting/absorbing energy through an ESS, validating the disturbance rejection capability, which is one of the main purposes of the system. Also the phase-jump reaction of the system and the islanding mode operation are analyzed in this work, to show other extra operations of the system. The cases I,

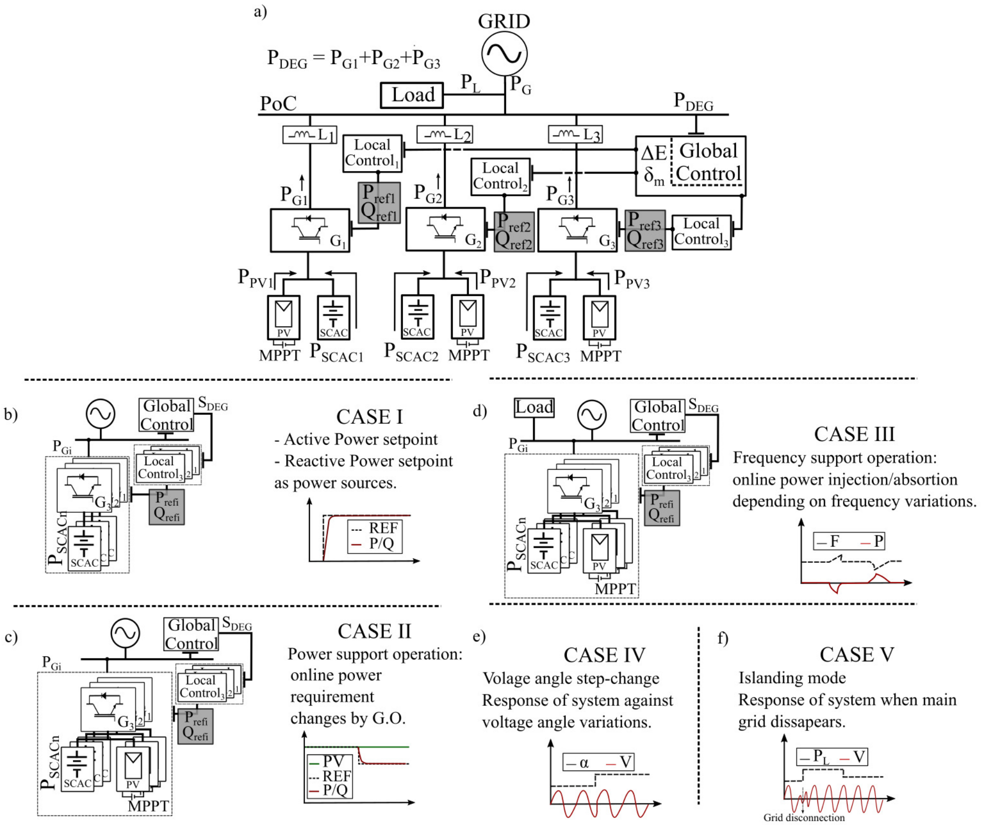

Figure 4.10: a) Power system scheme with three DEGs, showing global and local controllers, ESS-SCAC and PV panels. b) Working mode I: active and reactive power set-points by each DEG, controlled by the SCAC. c) Working mode II: power support operation, taking into account grid operator requests. d) Working mode III: frequency support operation by power management depending on frequency variations. e) Working mode IV: voltage angle step-change. f) Working mode V: islanding mode.

II and III can be seen in Figure 4.11, but in terms of power signals in the form of a complete simulation. Figure 4.11a) shows I, II, and III working modes in terms of active power. Figure 4.11b) depicts the behavior in Case I, injecting the required power by the global controller. Figure 4.11c), depicts Case II, for active power management. Besides, Figures 4.11d) and e) show Case III, which is the injected power when a frequency drop appears in the grid, trying to reduce the frequency variation. These working operations will be explained in more detail in the following subsections. Worth noting that power is oddly shared among the three converters in the next section, providing a distribution shown in Figure 4.12, for each DEG. Simulation parameters are given in Table 4.1.

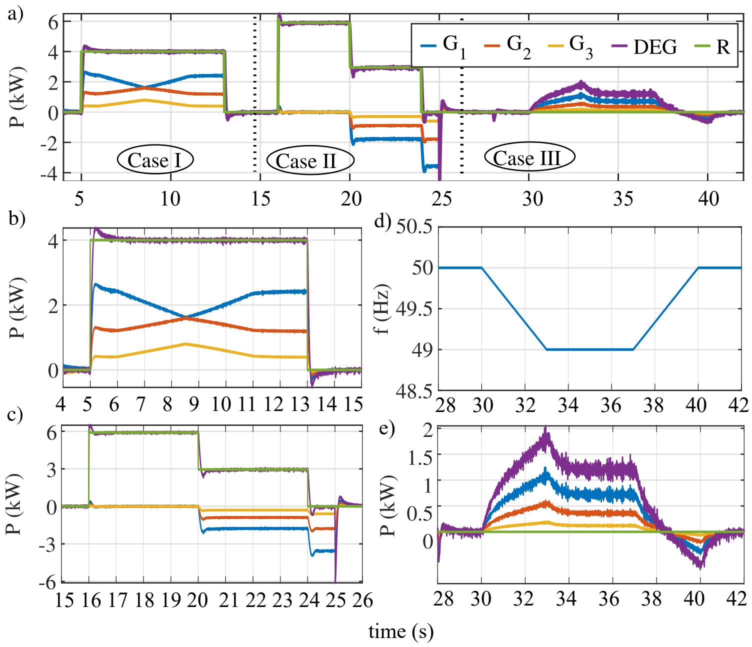

Figure 4.11: a) Active power management for all working modes in each DEG, taking into account the power-sharing between them. Legend G_1 is the first power converter, G_2 is the second power converter, G_3 is the third power converter, DEG is the total power injected by the power plant and R is the power reference. Case I shows the Active and reactive power set-points by each generator, controlled by the SCAC. Case II shows the power support operation. Case III shows the frequency of support operation. b) Zoom of case I for active power injection. c) Zoom of Case II for active power management. d) Grid frequency variation. e) Zoom of Case III for Battery power injection for compensating frequency change

Previous simulation is performed by using an ideal grid. However, in order to validate and demonstrate how the SCAC system works, the following simulations will be performed by using a weak grid formed by a simple synchronous generator (with real frequency variations), with a limited power (300 kW) and inertia (0.116 kgm^2). In these simulations, the five cases from Figure 4.10 are validated: I) active and reactive power injection, II) supporting frequency changes, III) grid operator active power reference tracking, IV) phase angle jump and V) islanding operation.

4.5.3 Real-Time Simulations

In this subsection, the different Cases, from I to V are going to be evaluated by using Speedgoat HIL simulator, without external hardware.

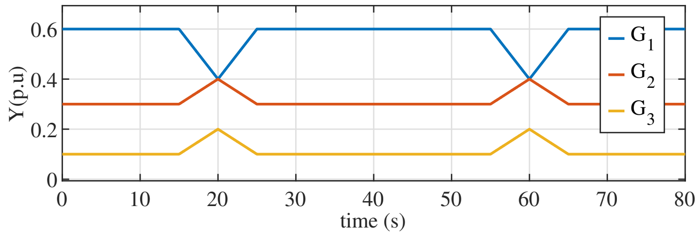

Figure 4.12: Virtual admittance variation for Case I and Case II from this section, in order to modify the output power of each converter. G_1, G_2 and G_3 is the designation of each power converter, as in Figure 4.10.

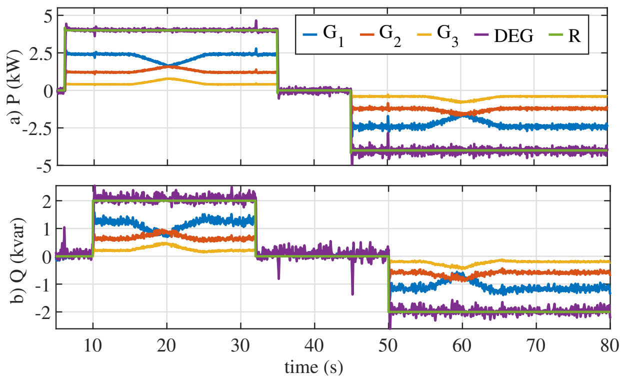

Figure 4.13: Simulation validation: a) active power reference tracking injected to the grid, taking into account the power-sharing between DEGs. b) reactive power reference tracking injected to the grid, taking into account the power-sharing between DEGs. G_1, G_2 and G_3 is the designation of each power converter. *DEG* is the power developed by the power plant, as Figure 4.10 shows. *R* is the reference power.

4.5.3.1 Case I

Considering what is accounted in Figures 4.10b) and 4.11, active and reactive power set-points are established in order to control the power exchange with the grid. This principle is the basis for the other two working modes, showing how the SCAC can manage the required power by the global controller. This operation is tested by a simple local simulation, and also by a real-time simulation. Besides, these power injections are varied by adjusting the virtual admittance in control as Fig. 4.12 shows, where the unit admittance is divided in 3, and it varies during time.

As it can be seen in Figure 4.13 a), the power set-point is reached, sharing the energy among the DEGs, regarding the power distribution between the DEGs shown in Figure 4.12. The same happens with the reactive power in b).

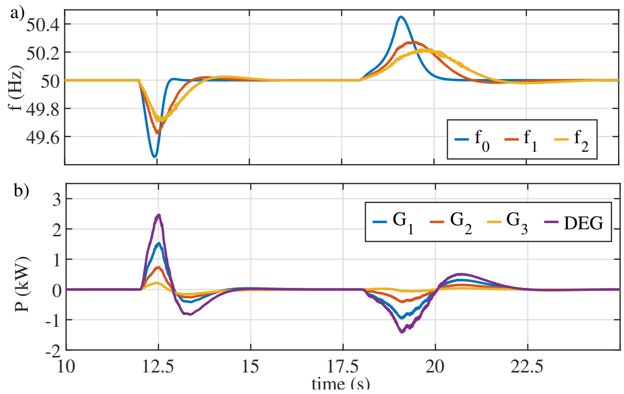

Figure 4.14: Simulation: a) frequency variation of a weak grid due to a power change demand (with and without SCAC), modifying the installed power in the power plant. The higher power the lower frequency variation (f_0 is for the case without SCAC, f_1 is for the case with SCAC and $S_n = 6$ kVA, and f_2 is for the case with SCAC and $S_n = 10$ kVA. b) power injected by each DEG, to mitigate the frequency variation from the case f_1 of b). G_1, G_2 and G_3 are the designations of each power converter and DEG is the power of the total power plant, as Figure 4.10 shows.

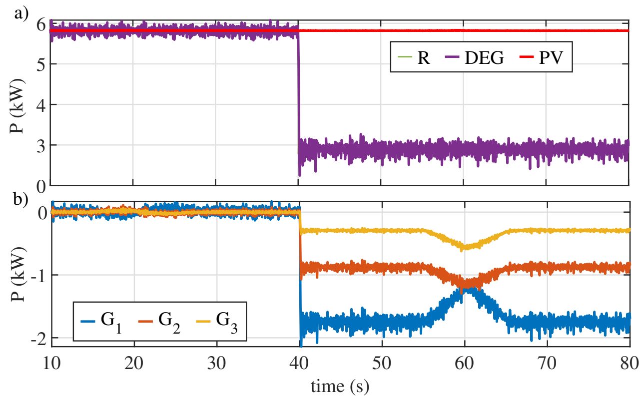

Figure 4.15: Simulation: a) power injected to the grid. At 40 s, the required grid power changes to 2.4 kW. R is the power reference, DEG is the total power injected by the power plant, and PV is the power developed by the PV array. b) ESS-SCAC power absorption to obtain the required 2.4 kW power demand by the PoC. G_1, G_2 and G_3 is the designation of each power converter, as Figure 4.10 shows.

4.5.3.2 Case II

This case aims to demonstrate the main operation mode of the SCAC system. As it was above-mentioned, SCAC system adds virtual inertia capabilities, helping to reduce any frequency disturbance in the grid. Two frequency variations (see Figure 4.14a) are induced by forcing some abrupt load changes (8.5 kW at 12 and -12 kW 18 s) to

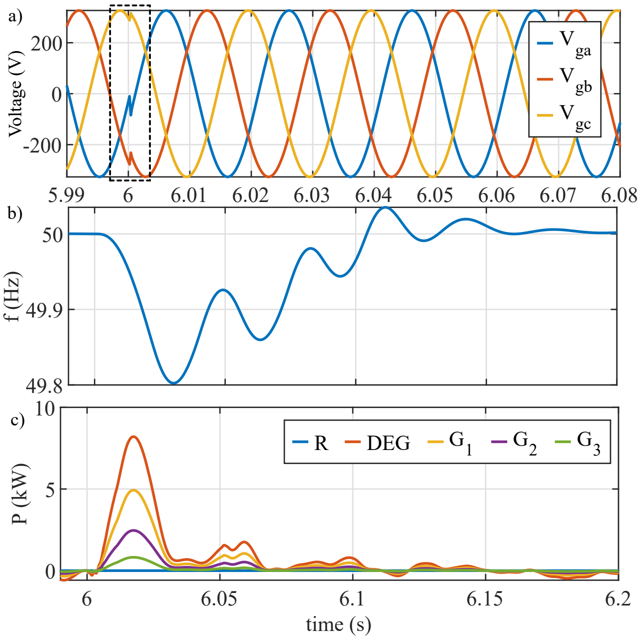

Figure 4.16: a) Grid voltage evolution with angle-step at 6 s. b) Frequency evolution due to the voltage angle-step. c) Power injection caused for the frequency variation.

observe the dynamic behavior of the control system.

In Figure 4.14, the response of the system is demonstrated, when a frequency variation is forced due to a load-step change. Figure 4.14a) shows the frequency variation by using the SCAC system connected to the grid (showing the frequency with and without SCAC system). With SCAC system, the frequencies that appears are for two different rated power of the SCAC system. So frequency is forced to change at 12 s. In case of using the SCAC system, the ESS will inject active power (Figure 4.13a) to the system in order to help the grid to increase its frequency, as it can be seen in b). On the other hand, if a suddenly frequency increase appears, as it can be seen at 18 s, the ESS-SCAC will absorb power from the system to decrease the frequency. Therefore, the power injection/absorption by the SCAC system will depend on the inertia emulated and also the power installed in their ESS. It can be concluded from [4.1], the more power installed in the system, the lower the frequency variation will be.

4.5.3.3 Case III

This operation mode is controlled by the DEG operator (central controller), in order to reduce or increase the power injected by the power plant, depending on the grid requirements, as long as the ratings of the power plant are not exceeded. This

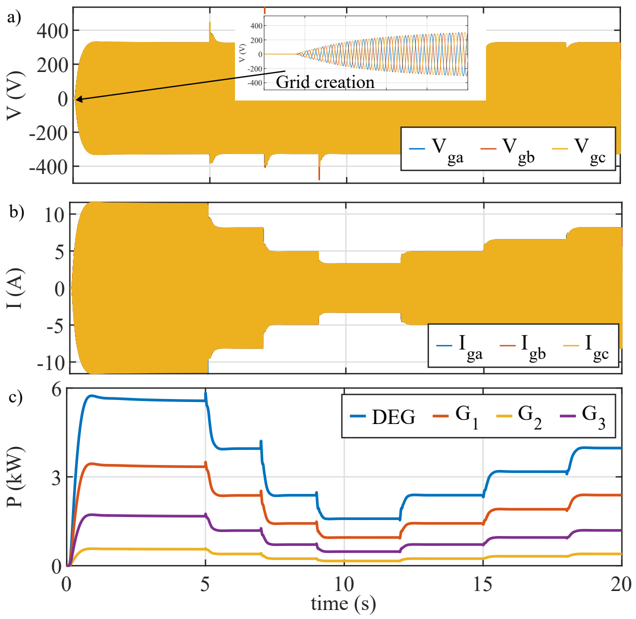

Figure 4.17: a) Grid voltage creation and evolution with different load changes. b) Feeding current by SCAC converter in islanding mode. c) Power injected by SCAC with some load variations.

means that if a power change is requested by the grid operator, the power injected will vary, taking into account that the RES are working normally at their MPP, and the excess or lack of power regarding the new power command will be managed by the ESS-SCAC. Once the grid operator's set-point returns to normal state, the storage system would stop absorbing energy, returning to zero power if there are not frequency changes. Another possible scenario is that the storage system reaches its maximum capacity and it cannot absorb more energy. This would mean that the PV string has to be taken out of its maximum power point to comply with the conditions of the grid operator.

The aforementioned effect can be observed in Figure 4.15, where at t = 40 s, grid operator active power reference varies (P_{DEG}, as shown in Figure 4.14a), forcing to inject less power from the DEG system. In this situation, either an inverter curtailment or a charging of the ESS is required. In this case, the power set-point has been reduced by 2.4 kW, and as the PV system is working at its MPP, the ESS-SCAC will absorb the energy difference. However, in case the ESS-SCAC reach their maximum capacity, the PV arrays will have to be moved out of their maximum power point, in order to comply with TSO requirements.

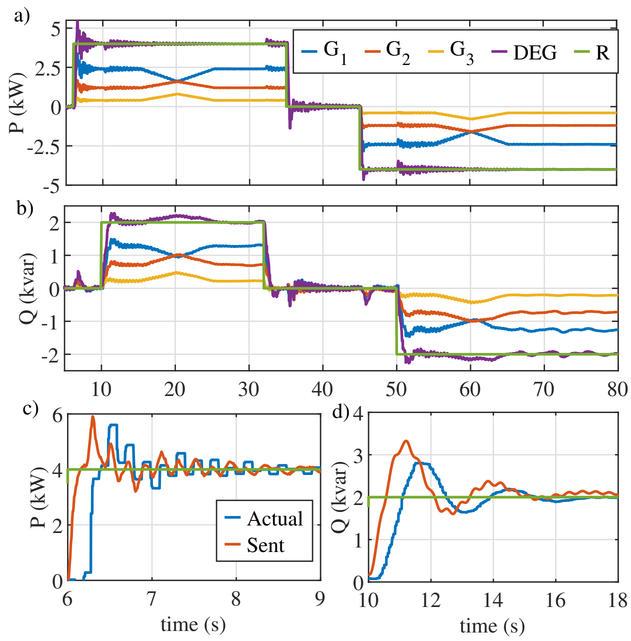

Figure 4.18: Experimental validation: a) Active power command, total power injected to grid and power injected by each converter. b) Reactive power injected to the grid, showing the command and the actual reactive power. The same legends as Figure 4.13 are used in this plot. c) and d) Zoomed active and reactive power values and sent references. *Actual* is the power read by MODBUS TCP. *Sent* is the power sent by MODBUS TCP to the converter.

4.5.3.4 Case IV

The conducted simulation aims to illustrate the operation of the SCAC system in the presence of a phase-jump in the grid voltage. In this specific test, a phase jump of 50 deg. Has been triggered. Variable delay from Figure 4.4 has been considered for this test. Figure 4.16 visually depicts this event. As observed, when the event occurs at 6s (see Figure 4.16.a), there is a decrease in the frequency detected by the converter (see b). In response to this variation, the inertia emulation system takes the task of injecting active power, as it can be seen in c), to actively mitigate the disturbance, working towards reducing the discrepancy until the event completely dissipates. This detailed assessment not only provides a deeper understanding of the SCAC system's behavior under specific conditions but also emphasizes the effectiveness of the implemented strategy in maintaining stability and the continuity of electrical supply in the face of grid disturbances.

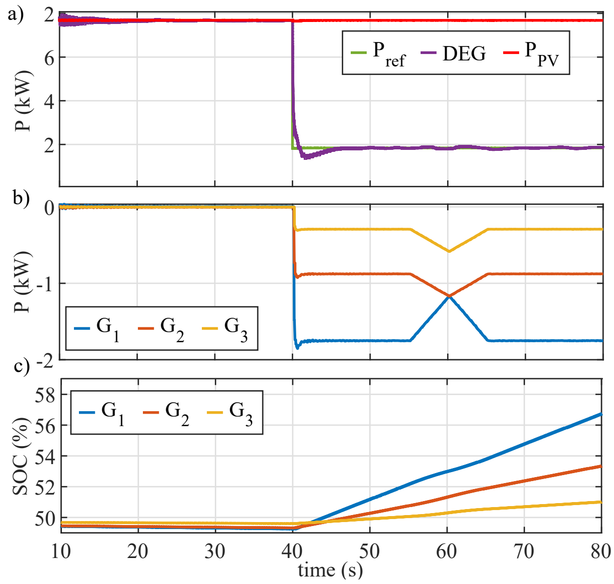

Figure 4.19: Experimental validation: a) power injected to the grid, where at 40 s, the power required by the grid changes to 2.4 kW. b) power absorbed by the ESS-SCAC emulated with CNG to obtain the required power. c) ESS-SCAC state of charge (SOC) increases due to the power absorbed by the SCAC system. The same legends than Figure 4.15 are used in this plot. For SOC information, the colors match with the number of generators from Figure 4.15.

4.5.3.5 Case V

In case V, the objective is to showcase the functionality of the SCAC control system in island mode, demonstrating its ability to create a proper grid, thus providing power to the loads connected to that grid. The converters will power the loads assuming different weights to their power injection (0.6 for G_1, 0.1 for G_2, and 0.3 for G_3). As it can be seen in Fig. 4.17a) the grid is created, starting to feed the connected loads by the VSG converter (see b). The delivered power (see Figure 4.17c) will vary with the load connected to the microgrid. For this case, the reactive power control loop depicted in Figure 2.15c) is employed, in order to add grid forming features to the system. To achieve this, a proportional P gain of 0.05 has been utilized, alongside a PI controller with a P value of 0.27 and an I value of 8. This case has been tested with a constant delay of 75 ms. This scenario underscores the robustness of the SCAC system when operating autonomously, ensuring the stability of the electrical supply even in instances of disconnection from the main grid. The efficient management of loads, considering the distinct characteristics of each converter, highlights the versatility and effectiveness of the system in varied environments.

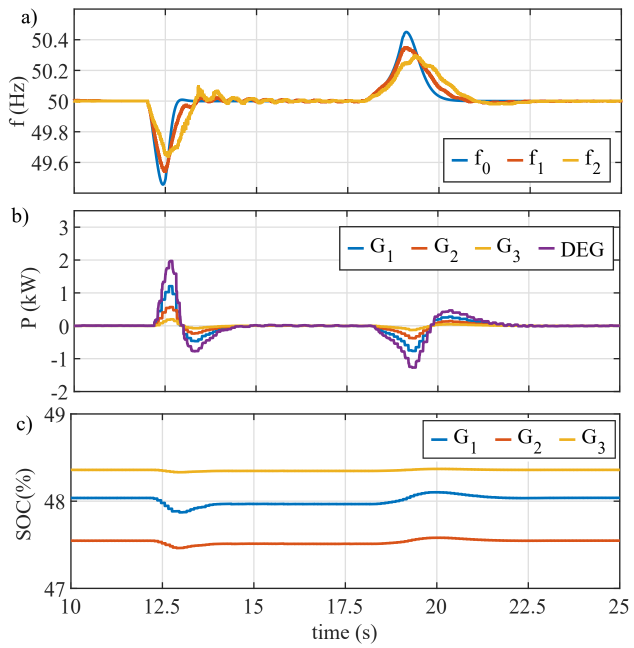

Figure 4.20: Experimental validation: a) frequency variation of a weak grid due to a power change demand (with and without SCAC), modifying the installed power in the power plant. The higher power the lower frequency variation (f_0 is for the case without SCAC, f_1 is for the case with SCAC and S_n = 6 kVA, and f_2 is for the case with SCAC and S_n = 10 kVA. The same legends than Figure 4.14 are used in this plot. b) power injected by each DEG, to mitigate the frequency variation from the case f_1 of a). The same legends as Figure 4.14 are used in this plot. c) SOC of each ESS-SCAC emulated in CNG. The same legends than Figure 4.14 are used in this plot. For SOC information, colors match.

4.5.4 Real-Time Experimental Test

In this subsection Cases I to III are going to be evaluated in real-time but in this cases, by using CNG external hardware, considering what it is explained in Section 4.5.1.

4.5.4.1 Case I

As it was aforementioned, the control system is tested in real-time by using the Speedgoat simulator and CNG converters. The experimental results are presented in Figure 4.18. As it can be seen active and reactive power are tracked perfectly, quite similar to local results. It is important to note that there is a different delay between active and reactive power, which has to do with the integration window from each variable in the power converter used in the HIL system [4.1]. In case of c), the different steps that appear in the read power are directly the delay of the integration window for active power. Nevertheless, those delays are tackled by the Smith predictor making the system controllable and stable. The difference in the ripple between the local simulation and the real-time is because the signals read by MODBUS TCP do not have the ripple data. Although the power with ripple is sent, the converter used for the experimental tests filters the component.

4.5.4.2 Case II

In the case of real-time simulation, the SCAC system has been emulated by using the battery module from CNG. Those results are presented in Figure 4.20. As it can be seen it works as the local simulation, when a frequency dip appears (Figure 4.19a)), DEGs inject power trying to reduce the frequency variation, respecting the power-sharing between converters (Figure 4.19b)). In this case, as a battery emulator is used, the SOC state of each battery is presented in c), showing how the battery is charged or discharged.

4.5.4.3 Case III

The same results are obtained in real-time simulations as can be seen in Figure 4.19. When there is a power set-point requirement by the global controller, the ESS-SCAC absorbs the extra power, charging the batteries as can be seen in c). If the opposite were the case, the batteries would be discharged.

4.6 Conclusion

This chapter proposed a method for the implementation of the aggregated VSG concept in industrial converters by removing access to internal instantaneous variables (current/voltage) and replacing them with a reconstruction technique from RMS values obtained by communications. Considering communications, the effect of a stochastic delay has been addressed, measuring the magnitude of the delay in a MODBUS TCP communication protocol and then employing a delay compensation mechanism to mitigate its effect on the control system performance. Besides, the stability of the system with constant communication delays has been studied, showing that the system remains stable up to 75 ms, although it does not have good dynamics, but the response is significantly improved using the Smith predictor compensation. This study analyses the impact of communication delays, as well as the impact of the SP compensator. This is done in several ways, either by time simulation, frequency analysis and the mapping of zeros and poles. Furthermore, simulation and experimental results show a satisfactory response with the considered constant and variable delay, in which the effect of internal computational delay and integration windows have been also considered. For that, different scenarios were considered, to test different operation modes, such as Case I, II and III, and they were validated in local and in real-time simulations.

In case of Case IV and V, just local simulations. Both reference tracking and disturbance rejection mechanisms have been considered for the system's overall performance evaluation.

References

[4.1] D. Del Rivero, P. G. Fernández, C. Blanco, and Navarro-Rodríguez, "Control of aggregated virtual synchronous generators including communication delay compensation," in *2022 IEEE Energy Conversion Congress and Exposition (ECCE)*, 2022, pp. 1–7.

[4.2] D. d. Rivero, P. García, C. Blanco, and Navarro-Rodríguez, "Control of aggregated virtual synchronous generators for pv plants considering communication delays," *IEEE Transactions on Industry Applications*, pp. 1–13, 2024.

[4.3] I. Modbus, "Modbus application protocol specification v1. 1a," *North Grafton, Massachusetts (www. modbus. org/specs. php)*, 2004.

[4.4] S. Alliance, "Sunspec specification - sunspec der information model specification," https://sunspec.org/, 2019.

[4.5] Y. Hirase, K. Abe, K. Sugimoto, and Y. Shindo, "A grid-connected inverter with virtual synchronous generator model of algebraic type," *Electrical Engineering in Japan*, vol. 184, no. 4, pp. 10–21, 2013.

[4.6] K. E. Martin, "Synchrophasor measurements under the ieee standard c37. 118.1-2011 with amendment c37. 118.1 a," *IEEE Transactions on Power Delivery*, vol. 30, no. 3, pp. 1514–1522, 2015.

[4.7] H. S. Wang and N. Moayeri, "Finite-state markov channel-a useful model for radio communication channels," *IEEE transactions on vehicular technology*, vol. 44, no. 1, pp. 163–171, 1995.

[4.8] Z. Chen, D. Boroyevich, R. Burgos, and F. Wang, "Characterization and modeling of 1.2 kv, 20 a sic mosfets," in *2009 IEEE Energy Conversion Congress and Exposition*. IEEE, 2009, pp. 1480–1487.

[4.9] D. Gross, *Fundamentals of queueing theory*. John Wiley & Sons, 2008.

[4.10] G. Villa Fernández, *Dynamic analysis and development of distributed control systems in power cells and multiport converters for grid integration of distributed resources*. PhD, University of Oviedo, Spain, 2022.

[4.11] A. Ghanaim, G. A. Borges, and G. Frey, "Estimating delays in networked control systems using colored petri nets and markov chain models," in *2009 IEEE Conference on Emerging Technologies & Factory Automation*. IEEE, 2009, pp. 1–6.

[4.12] A. Mirzal, "Delay compensation using the smith predictor: a brief review with numerical examples," *International Journal of Computer-aided Mechanical Design and Implementation*, vol. 3, no. 1, pp. 1–8, 2017.

[4.13] K. C. Konjerla, "Frf based experimental–analytical dynamic substructuring using transmission simulator," 2016.

[4.14] C. Verdugo, A. Tarraso, J. I. Candela, J. Rocabert, and P. Rodriguez, "Centralized synchronous controller based on load angle regulation for photovoltaic power plants," *IEEE Journal of Emerging and Selected Topics in Power Electronics*, vol. 9, no. 1, pp. 485–496, 2020.

Chapter 5

Industrial Applications of the SCAC Concept

5.1 Introduction

In this chapter, two industrial applications where the SCAC concept can be implemented are discussed, both related to hybrid PV systems. The first application focuses on the development of a control algorithm external to the SCAC system, which sends power set-points to the control system to compensate for variations in generation due to solar variability, smoothing power ramps. This part belongs to a conference contribution (CP2) that can be find in the Appendix C [5.1]. In the second application, the SCAC system is used to create an isolated grid to feed an electrolyzer, allowing the generation of green hydrogen in an efficient and stable manner.This part belongs to a conference contribution (CP3) that can be find in the Appendix C [5.2].

5.2 Generation Ramp Mitigation in PV Systems

In this section, one of the most significant challenges facing distributed generation plants is addressed, although in this case focusing on solar plants in terms of generation: generation ramps. These sudden fluctuations in energy production can affect the stability of the electricity grid, leading to inefficiencies and, in some cases, penalties imposed by grid operators. To mitigate this problem, it is proposed to use a distributed VSG system, based on the SCAC, which will be adapted to meet the specific regulations imposed by grid operators. This modified system will not only enable compliance with regulatory requirements, but will also optimize the operational efficiency and stability of the electricity system to which the solar plants are connected. Furthermore, as the inclusion of this strategy is an economical decision, a LCOE study is carried

Table 5.1: RR restrictions for relevant countries and regions. Ordered from more to less restrictive.

Mexico	Atlanta (USA)	Puerto Rico (USA)	Germany
$1\%/min$	$3.3\%/min$	$10\%/min$	$10\%/min$

out in order to determine the suitability of this method, and how worth it is. In the following sections, the problem will be explained in more detail, the proposed system will be shown, certain simulation results will be shown as well as certain economic calculations to demonstrate the need for its implementation, especially in the grids that contemplate it.

5.2.1 Problem Description

It is well known that the generation of energy from renewable sources, such as solar energy, is characterized by being intermittent and strongly dependent on climatic conditions. In the particular case of solar panels, which is the focus of this thesis and this chapter, their energy production is directly influenced by solar irradiance and temperature, factors that can change abruptly, causing significant variations in the power delivered to the grid. These fluctuations, especially when rapid and pronounced, can seriously compromise the quality of power in electricity systems.

Rapid power variations present a considerable challenge to TSOs, as their ability to respond to these fluctuations is limited and can exceed established limits. This behavior can lead to frequency and voltage stability problems in the power grid, affecting its stability and security.

To mitigate these problems, many TSOs have implemented specific regulations in their grid codes, limiting the maximum rate of power change allowed in solar plants, known as RR. However, there is no globally standardized regulation, and requirements vary considerably between different countries and regions. In fact, in some places, this issue is still not covered by grid codes.

An example of strict regulation is found in Mexico [5.3], where the ramp-rate is limited to 1% per minute, which means that the power of a PV plant can only vary by 1% of its nominal power from one minute to the next. Other countries, such as Germany [5.4, 5.5] or regions such as Puerto Rico [5.6] also have limitations, although they are somewhat less restrictive. In Table 5.1, a summary of the most relevant international regulations is shown. Other TSOs are adopting more stringent limits as awareness of the impact of these fluctuations grows [5.7].

For the purposes of this thesis, a standard 10%/min has been adopted as the ramp-rate limit. To meet these constraints, solar plants must have an additional power reserve that allows them to absorb or inject energy according to variations in generation. A common solution to achieve this is through the use of ESS, with lithium-ion battery technology being the most widely used due to its high technical development, high efficiency and significant cost reduction [5.8]. These storage systems allow rapid

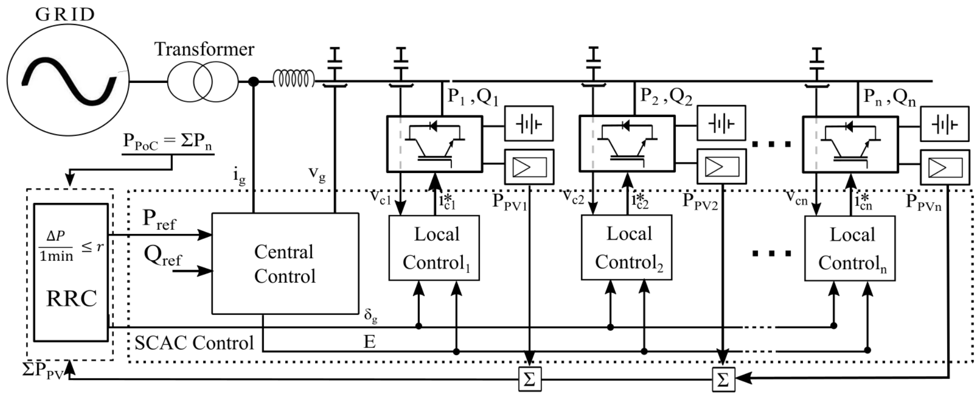

Figure 5.1: Virtual synchronous generator scheme with n-PV plants and batteries, working with a ramp-rate compensation method.

management of fluctuations in generation, compensating for any violation of the RR limits.

As reviewed in the state of the art (Chapter 2), there are mainly two common strategies for ramp compensation in solar power plants: the classical ramp-rate control [5.9] and the moving average filter [5.10], although other techniques are currently being investigated and developed. In the context of this work, the classical ramp-rate control method has been chosen to mitigate these power fluctuations.

It is important to note that the design of these compensation strategies not only responds to technical criteria, but also involves economic decisions. The design and sizing of the ESS must be carried out in the planning phase of the solar plant, ensuring that it complies with the RR requirements set by the relevant grid code. In addition, non-compliance with these regulations can lead to penalties that would apply directly to the PV plant operator.

Taking these aspects into account, it is also key to carry out an economic analysis to evaluate the effectiveness of the compensation system not only in reducing penalties, but also in optimizing the plant's operation.

This ramp compensation system will be integrated into the SCAC system studied in this thesis. The proposed methodology includes an adaptive technique for weight distribution, based on a variable virtual admittance. The integration of this system in the SCAC will be detailed in the next section of this chapter.

5.2.2 SCAC System Used for Ramp Mitigation

As previously mentioned, power ramp compensation will be included in the distributed VSG system studied in this thesis. The SCAC system, which emulates the inertia of a synchronous generator, has the ability to control the power injected to the grid and compensate for frequency variations. This functionality is fundamental for implementing effective RR control, since, by adjusting a simple power set-point (calculated using the RR method) it is possible to smooth power ramps without losing frequency compensation capacity.

The integration of both control systems is illustrated in Figure 5.1, where the RR limiter block is connected to the SCAC controller. This approach allows power fluctuations to be managed efficiently while maintaining system stability. In addition, it takes advantage of the virtual admittance concept used in this control system [5.11], which allows determining the proportion of power that each converter can deliver, facilitating local and adaptive compensation in each of the PV collectors.

This mechanism is implemented by modifying the virtual admittance value according to the local RR violations. Figure 5.2.c) shows a flowchart for the calculation of the virtual admittance in a system considering two converters. In this way, the distribution of the generated power between the converters is optimized, ensuring a dynamic and efficient response to generation fluctuations and avoiding local overloads. It can be described as:

- If the slope for one PV panel exceeds the limit (r_{max}), and the other not, during this event, the total amount of power is delivered by the local converter. The local converter is the converter which is close to the PV generation where the ramp is violated.
- If none PV panel surplus the limit, the admittances are set fairly ($k_n = 1$).
- Otherwise, if both converters exceed the limits, the calculation is done by weighting the slopes ($k_n = |m_n|$).
- In case of having more than two converters, the algorithm can be calculated using a small truth table (1-0) to select the cases in a simple way.

This variable virtual admittance concept is following evaluated in the simulation results section. Furthermore it is going to be used for calculating the cost-effectiveness of this method, comparing with other, in order to evaluate its suitability in economical terms. In this way, the distribution of the generated power between the converters is optimized, ensuring a dynamic and efficient response to generation fluctuations and avoiding local overloads

5.2.2.1 Ramp-Rate Method

Although the SCAC system will be used as the basis for the implementation of the RR monitoring method, it is crucial to define the specific approach to be used and how it will work. Currently, there is no unified consensus on the calculation methods for

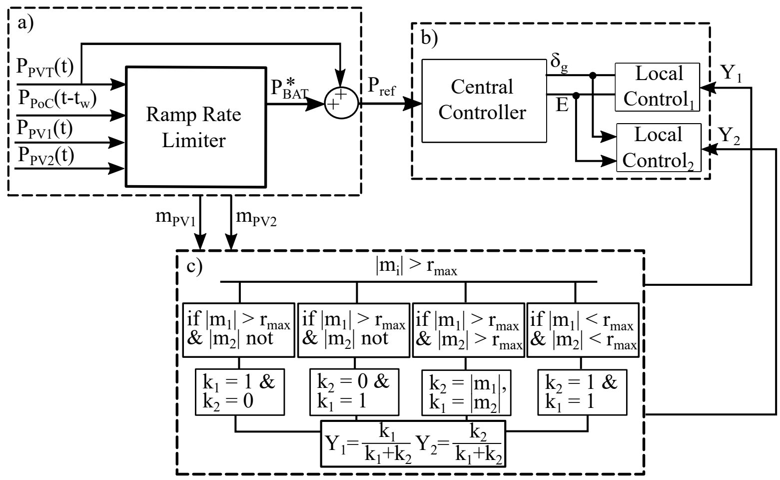

Figure 5.2: a) Ramp-rate limiter algorithm explained in Section 5.2.2.2. b) SCAC controller. c) Virtual admittance calculator.

determining RR violations from the perspective of TSOs. As a result, several methods for calculating the ramp-rate have been reported in the literature.

Among the most common approaches are the moving average (MA) method, which is the most commonly used; the exponential moving average (EMA); and methods based on low-pass filters (LPF) [5.5]. The choice of method may vary depending on the grid code requirements of the country where the power plant is installed.

$$RR(t) = \frac{P_{PoC}(t) - P_{PoC}(t-60)}{t(t) - t(t-60)} \tag{5.1}$$

$P_{PoC}(t)$ and $t(t)$ are the grid power and time at the current instant and the index $(t-60)$ represents the time interval 60 seconds ago.

The calculation of the RR violation can be done using instantaneous values or averages calculated by time intervals. However, for the development of this work it has been decided to use an approach similar to that used in the grid codes of Puerto Rico and Germany, which allow a maximum power variation of 10% per minute. In these cases, RR violations are calculated using a time window of 60 seconds, as expressed in equation 5.1. It is important to note that this 10% variation is calculated in relation to the total installed power of the PV collectors.

The proposed strategy attenuates the fluctuations of the power injected into the grid (P_{PoC}) during a predefined time window (normally 1 minute), evaluating the PV power variation in order to inject or absorb power when the predefined RR limit (r_{max}) is exceed. This strategy allows direct control of the ramp rate in contrast to other techniques. This will allow injecting or absorbing power from the ESS when it is strictly necessary, resulting in a lower cycling of the batteries [5.9].

Table 5.2: SCAC parameters and set-points for the simulation.

Variable	Value	Variable	Value
$H(s)$	10	τ	1
$S_n\ (kVA)$	20	Z_v	$8.014\angle 3.4$
$Pn_{PV}/PV\ (kW$	28	$r_{max}\ (\%/min)$	10

5.2.2.2 Description of the Method

As it was aforementioned, TSOs normally impose the time window (t_w) for deciding if there is a violation or not. However, a quicker RR evaluation is in here considered by using a lower time window ($t_w = 12$ s). The algorithm is executed at half the window size ($t_s = 6$ s), thus allowing to obtain the values of $P_{PV}(t)$ and $P_{PoC}(t - t_w)$ to be compared against the ramp rate limit [5.12, 5.13].

The method can be summarized in the following statements:

- If P_{PV} increases too fast, the ESS will absorb the excess of power ($P_{bat} < 0$), so P_{PoC} will comply to the maximum ramp rate.
- Otherwise, if P_{PV} decreases too fast, in this case the battery will deliver the lack of power ($P_{bat} > 0$) so P_{PoC} will comply to the minimum ramp rate.
- If $P_{PV}(t) - P_{PoC}(t - t_w)$is within the ramp rate limitation, the battery will not inject power ($P_{bat} = 0$).

5.2.3 Results

Simulation results are presented in this section. Grid and VSG models are taken from [5.11], where the SCAC idea was first published. In this case the model includes two PV DEGs connected to a grid, considering a battery locally connected to each one. This element will provide/absorb energy for RR compensation and for frequency support. The simulated system is similar to the one shown in Figure 5.1, but considering two PV collectors and their respective ESS.

5.2.3.1 Ramp-Rate Simulation

In this subsection the classical ramp rate strategy is applied in order to smooth the ramps of the PV collector. A small zoom of the PV profiles for each PV collector are presented in Fig. 5.3 a). In Figure 5.3 b), the power injected at the PoC is depicted. The resulting power without the RR compensation method is labeled as P_{Gr}, while the corrected one is P_{Gc}. As it was explained in Section 5.2.2, the algorithm compensates the ramps when they exceed the ramp limitation. In Figure 5.3 c) the limits (yellow and purple discontinue lines) , the ramp for total PV power r_{pv} and the ramp for PoC

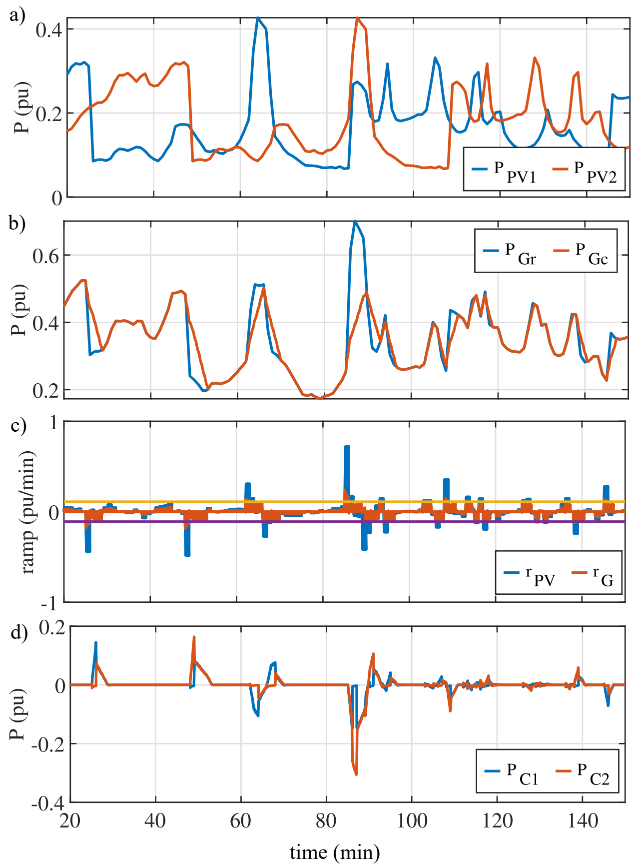

Figure 5.3: a) Active power injected by each PV collector. b) P_{PoC} injected to grid. P_{Gc} is by applying the ramp rate compensation (ΣP_{PVn}) and P_{Gr} without. c) power ramp for PV power (r_{PV}), and ramp for P_{PoC} (r_G) and the limits. d) Injected power for each battery (P_{C1} and P_{C2}).

power r_G are depicted. It can be seen r_G is within the limits. Figure 5.3 d) shows the power injection by each battery. As it has been told, these batteries will inject more or less power depending on the PV collector that violates the ramp conditions represented in Figure 5.4 a), that considers the $10\%/min$ limit with respect to the nominal power of each of them. So, the virtual admittance values will vary (see Figure 5.4 b).

5.2.3.2 Frequency compensation by VSG

In this subsection, a grid frequency variation is forced, in order to see the simultaneous operation with the ramp controller. As it can be seen in Figure 5.5, even when a frequency variation appears (see a)), the power ramps are compensated by the ramp-rate violation. Figure 5.5b) shows the ramp evolution that during the frequency

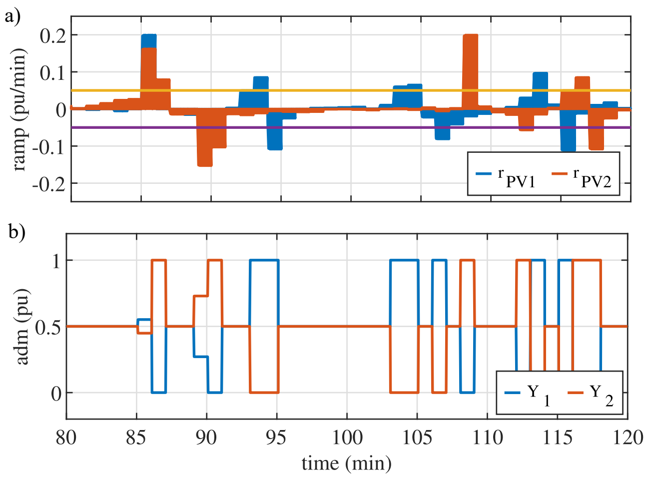

Figure 5.4: a) Power ramps for each PV collector and the limits. b) Virtual admittance calculation for each converter. Y_1 is the admittance calculated for P_{C1}. Y_2 is the admittance calculated for P_{C2}. a) and b) have a small to better see the variation of ramp and admittance.

event violates the restriction. Figure 5.5c) depicts the power evolution of each ESS. However, the SCAC prioritizes the frequency compensation. In Figure 5.5 d), the ramp rate variation are shown in Figure 5.2. Those PV ramp power variations are used for computing the admittance weights which manage the injected power by the ESS.

5.2.4 Economical Analysis

The inclusion of a RR mitigation strategy is mainly an economical decision that must be taken during the design stage of the PV plant. So, it is critical to determine the size of the ESS in order to meet the requirements for RR compensation, keeping the cost as low as possible.

The LCOE index will be determined for this application, considering the incorporation of the RR method described in Section 5.2.2 by means of using a variable admittance compensating the RR violation locally. Also, same index will be obtained with the incorporation of the RR method but maintaining a constant admittance and delivering the same energy of all ESS. Finally, the LCOE is obtained considering the non-inclusion of any compensation method. With these indexes, in summary, the proposed metric looks for a trade off between ESS operation, installation costs and the penalization costs because of RR violations. With the aim to obtain the LCOE index, some parameters must be computed, considering the characteristics of the system.

In order to analyze the minimum required ESS, the associated PV plant costs, C_{PV},(5.2a), and the ESS, C_{ESS} (5.2b), are considered in the LCOE (5.2c) [5.14]. CP_V includes the annual investment cost (I_{PV}) considering the PV plant investing stage,

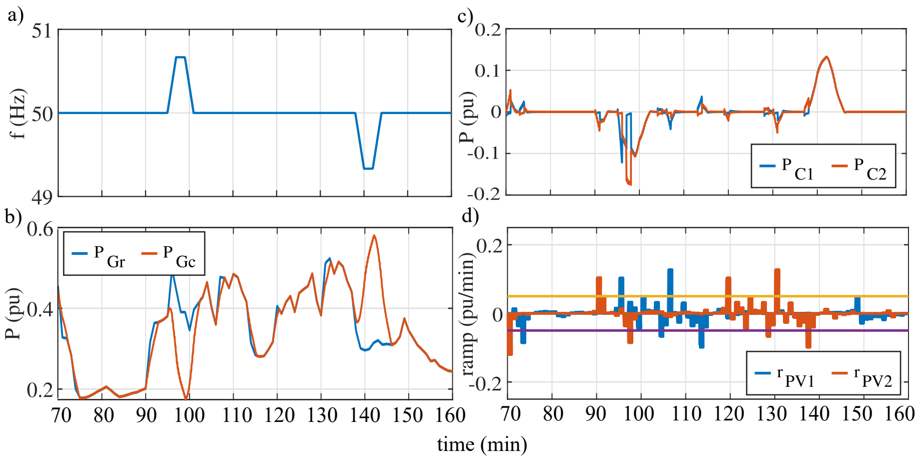

Figure 5.5: a) Positive grid frequency variation at 94 min and negative grid frequency variation at 138 min. b) P_{PoC} injected to grid. P_{Gc} is the PoC injected power by applying the ramp rate compensation and P_{Gr} without, trying to compensate the frequency variation. c) Injected power for each battery (P_{c1} and P_{c2}). d) RR variation at each PV collector to calculate the Y admittance.

Table 5.3: LCoE terms.

Type	I [€/kW]	$O\&M$ [€/kW/year]	N [year]	C_{dis} C_{ch}	η [%]
$PV_{utility}$	800	11.5	25	-	[5.16]
LFP	400	8.2	12	$1.2 - 1$	92

the fixed operation and maintenance costs ($O\&M$) and the annual charge due to RR violations (RR_c). The charge associated with the violation of the RR is estimated to be $10 cents/s/MWp$, where MWp is the installed power of the plant [5.15]. So taking into account the maximum power of this plant, it corresponds to 5 €/s [5.15].

C_{ESS} considers the energy storage installation cost (I_{ESS}) which includes the associated cost of the ESS power conversion stage, considering a dc-link coupling mechanism, common cost for grid connection among others [5.17, 5.18], and its $O\&M$ annual costs. In the present case I_{ESS} investments are assumed to be during the first year of operation. However, $O\&M$ are paid with some interests.

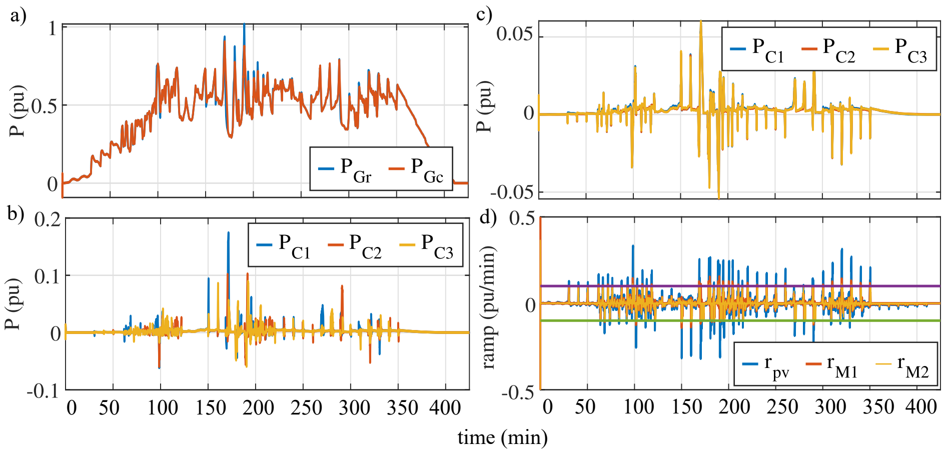

Figure 5.6: a) Power profile with and without ramps. P_{Gr} is the power with RR correction, and P_{Gc} is the power without RR correction. Data in pu. For analysis lets assume a 50 MW base power. b) Power demand of batteries for case with varying admittance. P_{C1}, P_{C2}, P_{C3} is the power injected for each converter respectively. c) Power demand of batteries for case with constant admittance. P_{C1}, P_{C2}, P_{C3} is the power injected for each converter respectively. Same power for all of them. d) Ramp violations for the PV power injection without RR (r_{pv}), with RR at constant admittance (r_{G1}), and varying admittance (r_{G2}).

Table 5.4: Efficiency results for variable (Y_v) and constant (Y_c) admittance methods.

Y_v			Y_c		
η_{v1}	η_{v2}	η_{v3}	η_{c1}	η_{c2}	η_{c3}
87.48	87.42	87.39	87.34	87.37	87.36

$$C_{PV} = \sum_{k=1}^{k=N_{PV}} \frac{I_{PV} + O\&M_{PV} + RR_c}{(1+r)^k} \tag{5.2a}$$

$$C_{ESS} = \sum_{k=1}^{k=N_{PV}} \frac{I_{ESS} + O\&M_{ESS} + Ch_{ESS}}{(1+r)^k} \tag{5.2b}$$

$$LCoE = \frac{C_{PV} + C_{ESS}}{\sum_{k=1}^{k=N_{PV}} \frac{E_{grid}(1-d)^k}{(1+r)^i}} \tag{5.2c}$$

The discount rate r considered in equation (5.2c) is 4% [5.19], N is the technology lifespan and E_{grid} is the grid energy injected in the year base-case presented. Furthermore, the PV system is expected to degrade each year at a rate d equal to 0.8% [5.20]. Regarding battery technology, a LFP cathode battery is assume for the application, because it has a cheaper price in terms of energy. Table 5.3 shows the LCOE parameters for the PV and the battery.

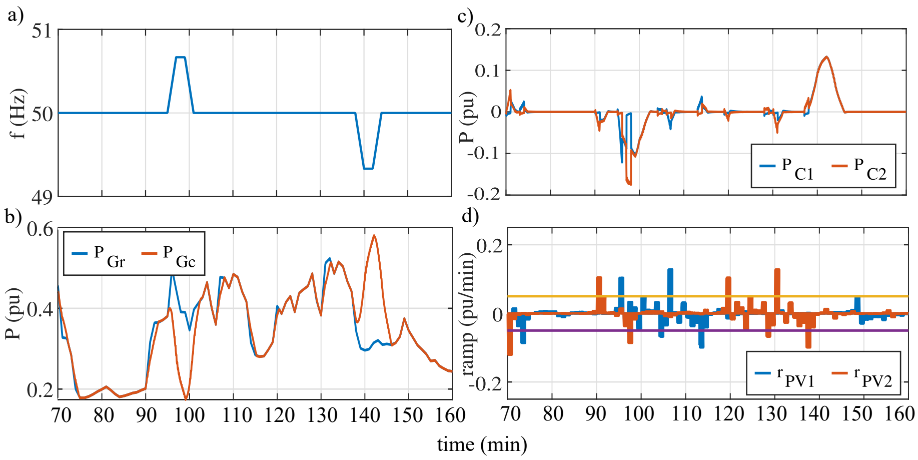

Figure 5.7: Computed efficiency taking into account the efficiency curve of the power converter used for each PV string and ESS. η_{v1}, η_{v2}, η_{v3} are the efficiency for P_{C1}, P_{C2} and P_{C2} taking into account variable admittance. Average efficiencies are 87.2885%, 87.2871% and 87.2815% respectively. η_{c1}, η_{c2}, η_{c3} are the efficiency for P_{C1}, P_{C2} and P_{C2} taking into account constant admittance. Average efficiencies are 87.2471%, 87.2195% and 87.2533% respectively.

To calculate the LCOE, a daily the profile shown in Figure 5.6 a) will be assumed and repeated along the years used for the economic study. This power profile is the same than the one in Section 5.2.3, but extended for a complete day, with a total energy production of around 7 hours. The data is calculated in pu, but for the analysis, a base power of 50 MW will be assumed, for the entire power plant. In this case, the simulated system replicates the one in Section 5.2.2, but using three PV strings, converters and their respective ESS. In addition, in order to observe the behavior of the system operating at constant admittance and at variable admittance, the results of power injection by each one of the converters are presented in Figure 5.6 b) and c). It can be seen in b) that the power at variable admittance changes as needed, and in c) it is the same for all converters. In addition, it can be seen in Figure 5.6 d) how the ramps of the PV collectors vary, violating the 10% norm, and by introducing the compensation method, these violations drop drastically.

The data from Figures 5.6 b) and c), beside the power injected by each PV string is used for calculating the power injected to the grid. However that power is ideal without considering power converters. So the total amount of power generated by the PV system beside the efficiency of both methods (variable and constant admittances) will be computed taking into account the efficiency curve of the power converter from [5.16], assuming that the efficiency (η) curve belongs to the power inverter and DC/DC converter. Then, η is calculated in Fig. 5.7, for each PV string and battery. Table 5.4 show the average η values, showing a best performance in the variable admittance case. Note that in this case feeder impedance is considered.

It must be accounted this example is only for demonstration purposes, so the bat-

Table 5.5: Economical results for the application without RR compensation, with RR and constant admittance (Y_c), and RR with varying admittance (Y_v).

Cases	ESS [MW]	$LCOE$ [€/MWh]	t_{RR} [s]	RR_c [M€]
PV		74.22	841	30711
PV+ESS+Y_c	4.95	57.61	161.5	5897
PV+ESS+Y_v	5.61	56.44	89.23	3257

teries are sized taking into account the energy demand of each day. Taking into account these data, and by using the aforementioned formulas the LCOE can be computed approximately. Table 5.5 shows the calculation results of the LCOE, taking into account the data from Figure 5.6. As can be seen in the Table 5.4, the ramp-rate violations (RR_c) are reduced by 90% and 80% using a variable RR and constant RR admittance method respectively, with respect to no use none. Having a lower expense for ramp violations, as well as less time breaking the rule. The variable admittance method is more economical by calculating the LCOE index. Also, as explained, Y_v is more efficient. From here it arises an interesting optimization problem for the calculation of the Y_v value. Depending on the line impedances connecting each collector to the PoC and the ramp violation location, the Y_v should be optimally calculated. This is concern of future research.

5.3 Green Hydrogen Production

The use of solar energy for the generation of green hydrogen is presented as an essential solution on the path towards a cleaner and more sustainable energy matrix. This innovative approach uses off-grid solar plants to power water electrolysis processes, producing green hydrogen without generating carbon emissions, which contributes significantly to greenhouse gas mitigation [5.21, 5.22].

Green hydrogen offers a wide range of applications in various energy sectors, positioning it as a versatile and crucial resource in the transition to a decarbonized energy future. In the transport sector, for example, it can be used in fuel cell-powered vehicles, providing an emission-free alternative to conventional fossil fuels. In the industrial sector, green hydrogen is capable of replacing high carbon footprint energy sources in various chemical and manufacturing processes, helping to reduce the emissions associated with these activities. Furthermore, in the power generation sector, it can be used both in fuel cells and blended with natural gas, thus increasing the sustainability of the energy mix [5.23, 5.24].

The green hydrogen production process harnesses not only solar energy, a renewable and abundant source, but also water resources, ensuring greater long-term energy security and diversification [5.25]. This is particularly relevant in the current context of

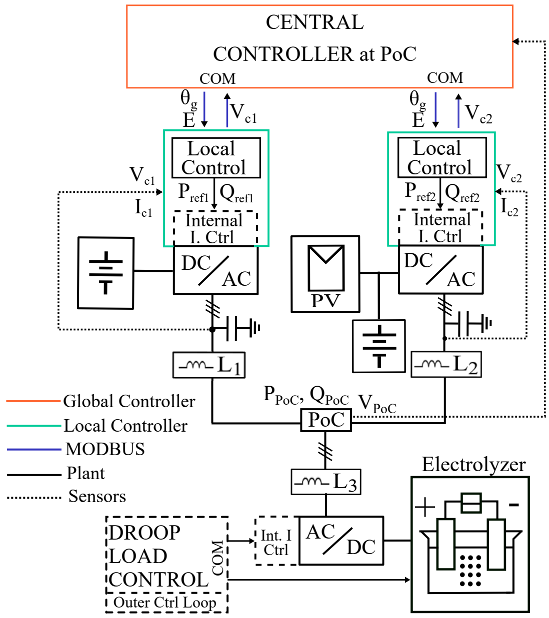

Figure 5.8: Topology of the proposed green hydrogen generation system (GHGS), with PV generation and dc-coupled ESS operating in grid-forming to create the grid that feeds the electrolyzer.

dwindling fossil fuel reserves and the growing need for energy systems that are resilient in the face of geopolitical uncertainties and global environmental challenges.

As for the operation and control of these green generation plants, as a conclusion of this thesis, the use of the SCAC control system is proposed, with certain adaptations, to efficiently manage an isolated control structure that will feed the electrolyzer. This grid will be composed of PV generation and an energy storage system, guaranteeing a stable and efficient supply for the production of green hydrogen. This system will manage the intermittency inherent in renewable energy sources, ensuring optimized operation and maximum efficiency in the electrolysis process.

5.3.1 System Description

In this section, a description of the different components of the ADN system is provided, considering PV generation system, ESS and the electrolyzer system. Those elements are depicted in Figure 5.8.

Figure 5.8 shows the different control layers of the ADN, differentiating between external and internal control. As mentioned above, and following the topic developed in this thesis, the main control of the plant is based on the SCAC controller, although in this case operating in grid-forming mode. In the external control layer is the central controller, located at PoC between the two distributed generators and the electrolyzer.

While this control system has been described previously, it will be redefined in more detail in the next section [5.26, 5.27].

The central controller is responsible for calculating the polar components of the voltage, which will be transmitted to the local controllers of each converter via MODBUS TCP [5.28].

In the local controllers, voltage commands are received, which are used to feed a virtual impedance model, already explained in previous chapters, which is responsible for calculating the reference currents to be injected by each of the converters.

As detailed in Chapter 4, this control system has been modified to adapt to commercial converters, which only accept active and reactive power commands instead of current signals. Therefore, the reference currents calculated by the virtual impedance model are transformed into active and reactive power set points, which are used by the internal control loops of each converter to inject the necessary power into the grid.

This modification allows the SCAC system to be efficiently integrated with commercial converters, respecting their limitations, while maintaining the ability to control power injection and grid stability.

The active and reactive power commands are obtained by applying equations (5.3a) and (5.3b), which allow the power set points to be calculated. For that, normally currents and voltages are passed to the stationary reference frame or $\alpha - \beta$. These calculations are made under the premise of using commercial inverters, taking as a basis the reference current generated by the control system and the voltage measured at the terminals of each converter.

$$P_{refi} = \frac{3}{2}(V_{ci\alpha}I_{ref\alpha} + V_{ci\beta}I_{ref\beta}) \tag{5.3a}$$

$$Q_{refi} = \frac{3}{2}(V_{ci\beta}I_{ref\alpha} - V_{ci\alpha}I_{ref\beta}) \tag{5.3b}$$

Furthermore, these converters are strategically distributed at different distances from the PoC, which contributes to the formation of a resilient and adaptable network.

The power plant considered in this scenario is a hybrid PV plant, combining solar generation with ESS. These storage systems include both a dc coupled ESS and an inverter-based ESS. An important aspect of this configuration is that an ac grid is used to interconnect the electrolyzer with the energy resources. Although an interconnection via a dc grid could offer clear advantages for this application, there are currently no suitable commercial solutions that allow such an implementation.

In the case of the load, which has been explained to be an electrolyzer used for the generation of green hydrogen, it is noted to have relatively slow dynamics and its behavior can be varied depending on the energy available in the system. The operating dynamics of the HE is characterized by a time constant of 2.85 s. This value has been derived from the dynamic model of an electrolyzer, as detailed in [5.29, 5.30]. This dynamic model is based on the Randles-Warburg electrical equivalent circuit, which is widely used to represent the electrochemical behavior of the electrolyzer.

Furthermore, the inclusion of a VSG method not only assists in establishing a grid with a certain level of inertia, thereby enhancing system stability, but also enables automatic adjustment of the energy consumed by the HE based on voltage and frequency readings, through the incorporation of a dual droop system. These considerations will be further expanded upon in the next section.

5.3.2 Control System

The ADN control system presented in this chapter is based on the distributed VSG concept that has been discussed throughout this thesis, specifically the SCAC controller. This controller manages both the PV converters and the ESS, creating an isolated grid with a certain level of virtual inertia.

The design of the control system takes into account the possible communication delays that may arise, guaranteeing its stability by means of appropriate compensation techniques. At the electrolyzer level, a dual droop control is implemented to regulate the frequency as a function of power and voltage, allowing greater flexibility in operation.

The main objective of this chapter is to develop an efficient grid-forming control system in the generation units and a flexible controller in the load units. In this way, hydrogen production can be adjusted according to power generation levels, contributing to the stability of the electricity system and optimizing the use of available energy resources.

5.3.2.1 VSG control system

As explained in previous chapters, the SCAC control system is structured on two levels: central control and local control. The central control acts as the nerve center of the system, dynamically adjusting the frequency and voltage references, which are then sent to the local controllers. These local controllers, in turn, use these references to calculate reference powers based on real-time generation levels. In this way, the SCAC system allows multiple converters to be controlled in a coordinated manner, emulating a single SG in the PoC, creating an aggregated VSG system operating in an isolated grid [5.11, 5.27]. Figure 5.9 shows the control system used to manage the entire power plant. This virtual rotor concept emulated in the PoC integrates an electromechanical model that provides the system with inertia and damping characteristics similar to those of an SG. Although the presented structure is based on two aggregated power converters, it is scalable and can be applied to any number of converters.

Until now, the SCAC system has mainly been used for feeding or supporting connected grids, but in this chapter the control loop has been adapted to become a grid-forming control structure. This modification replaces the reactive power drop control

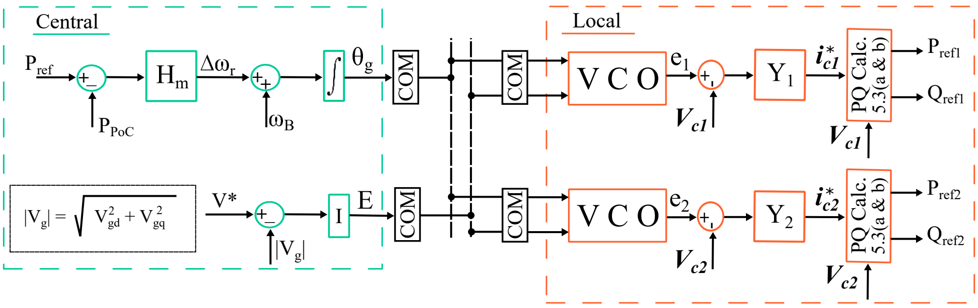

Figure 5.9: SCAC control structure for grid-forming converters. Light Blue: Global controller. Light Orange: Local controllers.

loop with the direct calculation of the voltage modulus. With this new configuration, the voltage magnitude in the PoC can be adjusted through a simple integral controller (I) [5.27, 5.31].

Figure 5.9 also shows how the stator voltage is sent in polar coordinates (phase angle θ_g and magnitude E) to the local controllers of each converter via MODBUS TCP communications. These voltage components are derived from the voltage control loop and the dynamic model of the VSG. The voltage angle and magnitude are used to drive the VCO, which calculates the local stator voltage. Subtracting this voltage from the converter terminal voltage gives the voltage drop across the virtual impedance of the SG. The concept of virtual admittance, explained in Chapter 3, is used to calculate the reference current required to drive the converter. The virtual admittances (Y_i) allow the weight or contribution of each converter within the aggregated system to be adjusted. In the converter's local controller, these values are transformed into active and reactive power set-points, as detailed in Figure 5.9, using equations (5.3a) and (5.3b). Finally, these set-points are sent to the converter's internal control, which is responsible for tracking the references through a closed loop, thus ensuring the stability and operation of the system.

The SCAC system used in this application, operating under GFM structure, faces technical challenges characteristic of this type of control, such as maintaining stable grid voltage and frequency. In addition, it requires precise control of virtual inertia to respond effectively to disturbances, which is key in weak grids like the one created for green hydrogen production. These challenges are compounded by communications issues, including communication delays, and the need to adapt the system to mitigate variations in generation ramps, thus ensuring reliable grid operation.

5.3.2.2 Communication Delay Compensation

Since the system is based on communications, it will be subject to communication delays that may cause the control system to become unstable, thus necessitating compensation. Therefore, the SP compensation method [5.32] has been chosen, as depicted

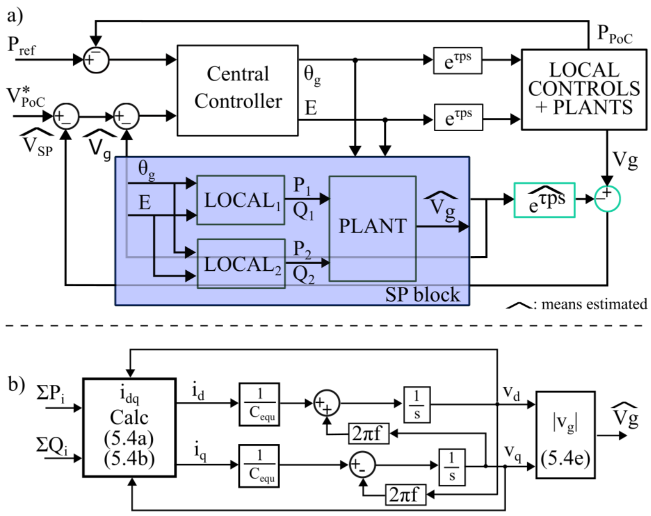

Figure 5.10: a) Central controller with SP architecture for 2-converters with voltage delay compensation [5.27]. b) Voltage at PoC estimation for SP.

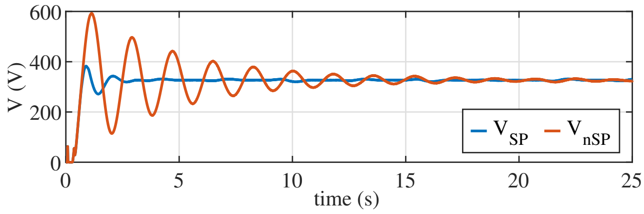

Figure 5.11: Grid voltage envelope created by ADN at PoC with and without SP, by using a delay of 300 ms.

in Figure 5.10 a). It illustrates that the angle and voltage computed by the central controller are subject to delays, and by employing a model of the local control and plants, these delays can be compensated for. The delay compensation will be carried out only for the voltage control loop, and not at the active power control loop. This is because although it is a variable load, which will depend on the existing generation level, this variation is very slow and does not have much effect on the control system. In order to do so, as it can be seen in equation 5.10, two replicas of the local controllers are used in the SP, using the scheme from Figure 5.10 b), in order to estimate the voltage at the PoC. Those replicas are used to calculate the active an reactive set-points of each converter. The references are transformed into currents by using equations (5.4a) and (5.4b). However, the voltage value that will be used for the calculation is the estimated voltage at PoC that comes from equations (5.4c) and (5.4d). Once this is done, equation (5.4e) is used to calculate the voltage module to be used in the SP compensation.

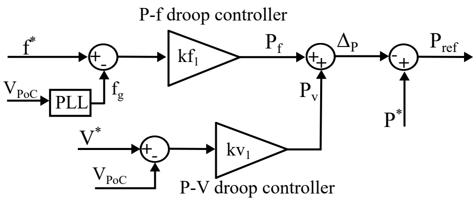

Figure 5.12: Proposed dual-droop controller.

Although the system stability withstands relatively high values of the communication delay without compensation, increased delay values have been used to test the system behavior under certain conditions that can show-up in a real application. Figure 5.11 shows the evolution of the voltage envelope by using a delay of 300 ms, by applying SP or without. As it can be seen, a noticeable compensation effect clearly improves the transient response when the SP is considered.

$$i_d = \frac{2(Pv_d + Qv_q)}{3(v_d^2 + v_q^2)} \tag{5.4a}$$

$$i_q = \frac{2(Pv_q - Qv_d)}{3(v_d^2 + v_q^2)} \tag{5.4b}$$

$$\frac{dv_d}{dt} = \frac{id}{C_{equ}} + \omega v_q \tag{5.4c}$$

$$\frac{dv_q}{dt} = \frac{iq}{C_{equ}} - \omega v_d \tag{5.4d}$$

$$|V_g| = \sqrt{v_d^2 + v_q^2} \tag{5.4e}$$

5.3.2.3 Droop Control of Electrolyzer

As mentioned above, a minor adaptation is implemented in the control system of the electrolyzer to obtain a better adaptability of the energy to the power available in the grid. It is known that this type of load is mainly constant, in order to get the greater amount of hydrogen, but it is expected to vary according to the demand and the power available in the grid. There are different kind of controllers to make the electrolyzer behaving as a flexible load as in [5.33] or responsive load as explained in Chapter 2. However in this case, a dual frequency and power voltage droop is implemented [5.34], as shown in Figure 5.12. A dual droop has been selected to make the system more flexible to any variation in generation, allowing operation, although more variable, also more stable. These droops come into effect when the frequency or voltage of the grid changes due to a mismatch between the power generated and consumed, resulting from a decrease in the power generated by any of the converters. In normal situations, when

Table 5.6: System parameters

Variable	Value	Variable	Value	Variable	Value
V_g	400 V	C_{filter}	200 μF	H	10 s
S	8 kVA	R_p	0.01	τ	1
f	50 Hz	R_v	2.2918Ω	L_v	0.0218 H
y_1	0.6	y_2	0.4	I_v	$2\pi 2$
L_1	$10\mu H$	L_2	$10\mu H$	L_3	$10\mu H$
R_1	$10\mu\Omega$	R_2	$10\mu\Omega$	R_3	$10\mu\Omega$

there is no significant frequency or voltage variation, the implemented scheme remains inactive. However, when the available power decreases, both frequency and voltage drop, leading to a reduction in the HE's power consumption.

This adjustment is critical to ensure grid stability while sustaining hydrogen production, allowing the electrolyzer to operate as a flexible load. The droop control parameters in this system are $kf_1 = 100$ W/V and $kv_1 = 600$ W/Hz. These parameters have been selected to enable proper system operation. In future research, more realistic and studied droop values will be explored to optimize the performance of the system.

The principle of operation of this dual droop controller will be demonstrated in Section 5.3.3, where detailed results and analysis will be presented. This adaptation allows a dynamic response to power variations, ensuring that the electrolyzer effectively contributes to the stability of the power system. By adjusting consumption according to power availability, the system increases resilience to unforeseen fluctuations in power generation.

5.3.3 Simulation Results

This section presents the simulation results that aim to evaluate the performance of the proposed control system. For this analysis, we start from a base scenario in which the generation capacity is sufficient to cover the load demand without difficulties. From this initial configuration, constraints on the generation capacity are introduced in order to study the impact of the dual voltage-frequency (V-f) droop based control strategy on the system stability.

The dual V-f droop approach seeks to improve system stability by more efficiently managing variations in generation and load, allowing the system to maintain supply-demand balance under adverse conditions. The results obtained are key to demonstrating how this control allows the system to avoid stability problems that could arise from imbalances between available generation and connected load.

All simulations performed include a communication delay of 160 ms between the central controller and the local controllers. This delay has been selected because it is

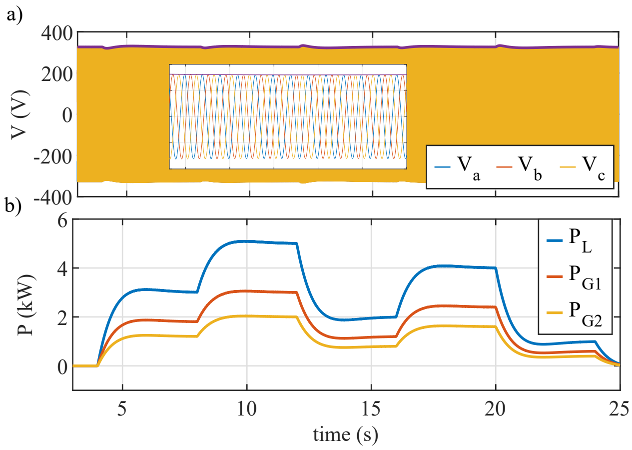

Figure 5.13: Nominal operation: a) PoC voltage. b) Injected power by converters with weights between both of 0.6 and 0.4, converter 1 and converter 2 respectively.

within the typical range observed in industrial applications, which adds realism to the simulations and ensures that the results are representative of practical scenarios.

Table 5.6 provides the key parameters used in the simulations, which include the characteristics of the power plant, controller and lines. These parameters form the basis for the evaluation of the system's performance in different scenarios, allowing analysis of its behavior to variations in operating conditions and the effect of communication delay.

5.3.3.1 Base Case. Normal Operation

The simulation results of the nominal operation of the system are depicted in Figure 5.13. In this simulation, the hybrid PV is used for creating the ac grid to feed the HE. Figure 5.13 a) shows the three-phase grid voltage established by the two converters. In this simulation, these two converters share the power delivered to the load by using different weights in their control, with 0.6 pu for converter 1 and 0.4 pu for converter 2. The virtual admittance values are updated based on the selected sharing weights, as explained in Chapters 3 and 4. As it can be seen in Figure 5.13 b), the electrolyzer starts to demand power, so the power converters start to inject the shared power to feed the load.

5.3.3.2 Limited Generation Case

This simulation presents the common case where the power of one of the converters is limited for various reasons. In this particular case, a drop in the generation

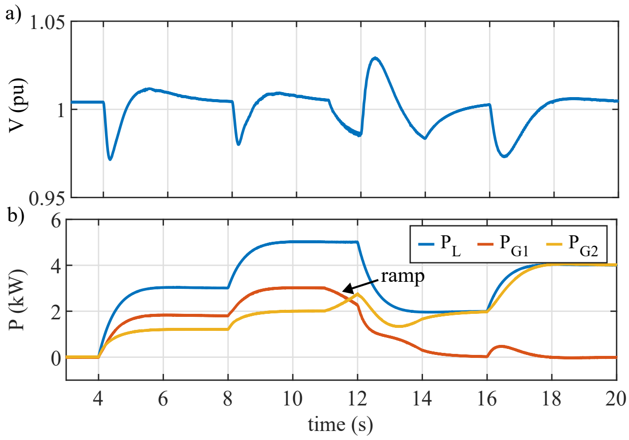

Figure 5.14: Limitation case: a) PoC voltage magnitude. b) Load power and power supplied with a weight distribution of 0.6 and 0.4. When a PV ramp appears, the ESS compensates the lack of PV power.

of converter 1, which corresponds to the PV-hybrid converter, is considered. This generation drop occurs due to a ramp-down event, which can be triggered by varying environmental conditions, such as passing clouds or a sudden drop in temperature.

As depicted in Figure 5.14 a) shows the voltage created by the ADN, which barely varies in this case and in b), when the ramp-down event in generator 1 appears at 11 s. Under those circumstances, the ESS plays an important role, compensating the generation decrease of the PV-hybrid converter by increasing its energy injection to maintain supply to the load. This dynamic response of the batteries is essential to ensure stability and continuity of power supply in situations where primary generation is intermittent or undergoes significant fluctuations.

5.3.3.3 Unstable Case

In this case, shown in Figure 5.15, the main reason for the implementation of the dual droop concept in the electrolyzer is demonstrated. This idea becomes essential in scenarios where there is a very abrupt ramp in the solar generation, or when the battery cannot deliver the necessary balancing power to the system due to its own limitations, such as being partially discharged.

In such circumstances, the system cannot meet the power demand, leading to instability. This situation can be clearly seen in Figure 5.15. In a), the system voltage up to the point of instability is shown, illustrating how abrupt fluctuations can affect system stability. In b), the power injected or absorbed by each of the power converters is shown, providing a detailed view of how each component of the system responds to variations in generation and demand.

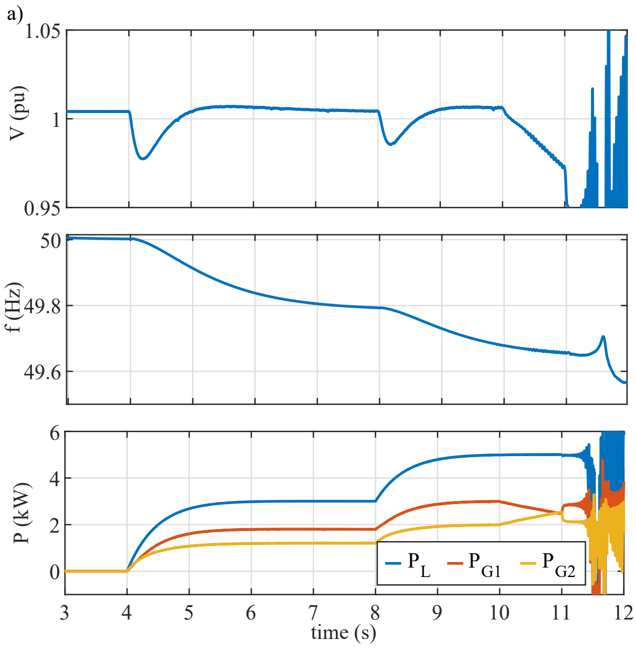

Figure 5.15: Unstable case: a) Module of voltage, which is unstable when the generators have a lack of power to feed the load. b) Load and converter powers with a ramp in PV generation, which is too big, making the system unstable.

The implementation of the dual droop concept in the electrolyzer mitigates these instability issues. By dynamically adjusting the operation of the electrolyzer in response to sudden changes in solar generation or battery capacity, the system can maintain a more stable and reliable power supply, as will be demonstrated in the next subsection.

5.3.3.4 Ramp Limitation with Droop Controller

To mitigate the unstable operating region, the proposed dual droop control is introduced. The results of this implementation are shown in Figure 5.16, where the effect of the dual frequency and voltage droop can be observed.

As mentioned before, the inclusion of this droop is used to safeguard the grid stability by adjusting the load consumption as a flexible load when one or more converters cannot deliver the required power to the load. In Figure 5.16, several key aspects of this process are presented.

In a), the system voltage variation is observed. This variation is critical to understanding how fluctuations in generation or consumption affect voltage stability. In b), the frequency variation of the grid is depicted. Frequency fluctuations are equally important, as they can indicate instabilities in generation or power demand. These voltage

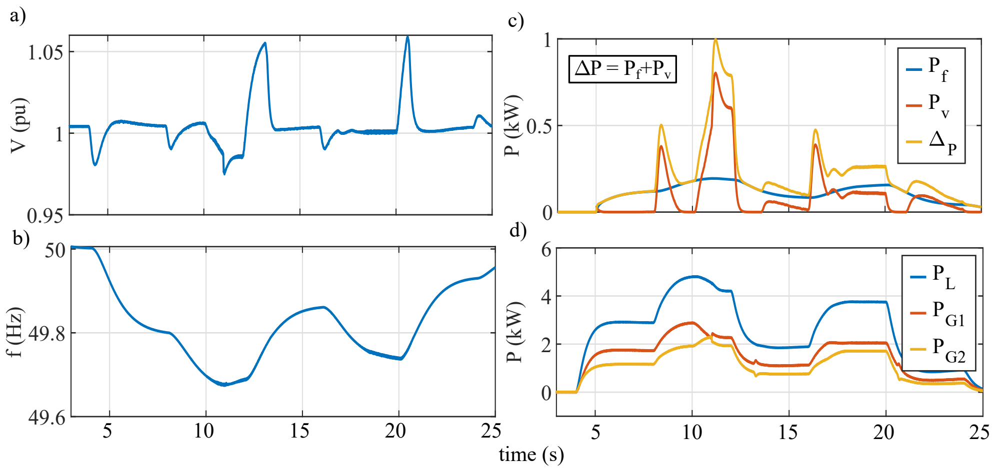

Figure 5.16: Ramp limitation with electrolyzer droop controller: a) Module of voltage at load level used for droop control. b) PV panel ramp generation in converter 1, compensating the power for the battery and reducing the load power as a flexible load. c) frequency variation used for droop control. d) Δ_P which is subtracted to the load set-point, in order to keep the stability of the system.

and frequency variations are read by the electrolyzer, which feeds them into the droop controller to modify the load consumption. This mechanism allows the electrolyzer to act adaptively, responding to changing system conditions to maintain stability. In c), the powers calculated by the system can be seen. These powers are subtracted from the power limit of the HE, which allows the consumption to be adjusted precisely according to the current operating conditions.

Finally, in Figure 5.16 d), the effect of a ramp on the PV generation is depicted. This ramp alters both the grid voltage and frequency, which in turn modifies the power command of the electrolyzer. This adaptive behavior is crucial to maintain grid stability in the face of rapid and unexpected fluctuations in renewable energy generation.

The implementation of dual droop control proves to be an effective strategy for managing system stability in the presence of significant variations in generation and consumption. By allowing dynamic adjustments in load consumption, it ensures that the system can operate stably and efficiently, even under challenging conditions.

5.3.3.5 Additional Considerations

One of the critical points for the correct operation of the system was the selection of the references sent from the central controller to the local controllers. Two alternative approaches can be used, as shown in Figure 5.17: 1) polar coordinates (E and θ_g) or, 2) rectangular coordinates (P_{ref}, Q_{ref}). A preliminary numerical evaluation under the simulation environment has been carried out for the two options. The results obtained are shown, respectively, in Figure 5.17 a) and b). As can be seen, the use of polar

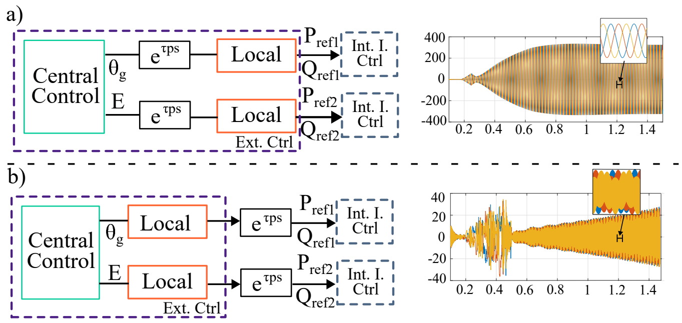

Figure 5.17: a) Control structure sending θ_g and E, computing power set-points in local controllers at converter level. b) Control structure sending active and reactive power from global controller.

coordinates leads to stable operation, while rectangular ones cannot guarantee it. In the control system used in this work, the strategy that guarantees stability (sending polar coordinates) is used. However, it will be necessary to study the limitations of sending active and reactive power references for future work, due to their relevance in industrial applications. It is important to note that this problem appears only with the application of communication delays in the communication channel, since when working with ideal delays (without delay) the behavior is identical.

5.4 Conclusions

In this chapter, the SCAC system has been implemented in two industrial applications. It highlights the integration of two control methods applied in renewable energy systems, specifically in PV generation: ramp-rate compensation within an aggregated VSG technique and the use of the same VSG system for green hydrogen production.

In the first part of the chapter, a ramp-rate compensation method within the SCAC framework was presented, successfully addressing both power fluctuations and efficiency concerns while meeting the 10%/min constraints. Simulation results demonstrated that the proposed method, based on variable admittance, outperforms classical constant admittance approaches, offering significant economic benefits, especially when managing large amounts of power. A LCOE study further confirmed that this technique generates real savings, demonstrating higher efficiency for converters with variable admittance.

The second part proposed the application of the SCAC system for multiple converters, forming a stable network for green hydrogen production. This system incorporates SCAC, with its central controller, using communications to integrate the local control system of the converters, introducing challenges related to communication delays. These delays were mitigated using compensation techniques, specifically the Smith predictor. In addition, a local double droop control was introduced on the electrolyzer side to manage power mismatches by adjusting the electrolyzer consumption according to voltage and frequency variations, acting as a flexible load.

Taken together, these methods demonstrate promising approaches to improve the stability and efficiency of power systems using the SCAC system, especially in the integration of renewable energies in a grid-tied or grid-off modes.

References

[5.1] D. Del Rivero, I. Peláez, P. G. Fernández, C. Blanco, and Navarro-Rodríguez, "Integration of ramp-rate compensation in a distributed virtual synchronous generator schema for hybrid pv plants," in *2023 IEEE Energy Conversion Congress and Exposition (ECCE)*, 2023, pp. 1122–1128.

[5.2] D. del Rivero, A. Navarro-Rodríguez, C. Gomez-Aleixandre, C. Blanco, P. García, and P. Rodríguez, "Control of green hydrogen production on isolated hybrid solar plants considering the effect of communications," in *2024 IEEE Energy Conversion Congress and Exposition (ECCE)*, Phoenix, AZ, USA, 2024, pp. 1122–1128.

[5.3] D.-D. O. de la Federación, "Resolución por la que la comisión reguladora de energía expide las reglas generales de interconexión al sistema eléctrico nacional para generadores o permisionarios con fuentes de energías renovables o cogeneración eficiente. consultado el 20 de marzo de 2018," 2012.

[5.4] "German grid code," Regulations on Ramp-Rate Control, 2018, applies a 10%/minute ramp-rate limit for PV systems. [Online]. Available: https://www.mdpi.com

[5.5] J. Martins, S. Spataru, D. Sera, D.-I. Stroe, and A. Lashab, "Comparative study of ramp-rate control algorithms for pv with energy storage systems," *Energies*, vol. 12, no. 7, p. 1342, 2019.

[5.6] V. Gevorgian and S. Booth, "Review of prepa technical requirements for interconnecting wind and solar generation," National Renewable Energy Lab.(NREL), Golden, CO (United States), Tech. Rep., 2013.

[5.7] R. Piwko *et al.*, "Interconnection requirements for variable generation," *North American Electric Reliability Corporation (NERC), Atlanta, GA, USA, Tech. Rep*, vol. 19, 2012.

[5.8] D. Cormode, A. Lorenzo, W. Holmgren, S. Chen, and A. Cronin, "The economic value of forecasts for optimal curtailment strategies to comply with ramp rate rules," in *2014 IEEE 40th Photovoltaic Specialist Conference (PVSC)*. IEEE, 2014, pp. 2070–2075.

[5.9] A. Gonzalez-Moreno, J. Marcos, I. de la Parra, and L. Marroyo, "A pv ramp-rate control strategy to extend battery lifespan using forecasting," *Applied Energy*, vol. 323, p. 119546, 2022.

[5.10] J. Marcos, I. De la Parra, M. García, and L. Marroyo, "Control strategies to smooth short-term power fluctuations in large photovoltaic plants using battery storage systems," *Energies*, vol. 7, no. 10, pp. 6593–6619, 2014.

[5.11] C. Verdugo, A. Tarraso, J. I. Candela, J. Rocabert, and P. Rodriguez, "Centralized synchronous controller based on load angle regulation for photovoltaic power plants," *IEEE Journal of Emerging and Selected Topics in Power Electronics*, vol. 9, no. 1, pp. 485–496, 2020.

[5.12] E. Bullich-Massagué, M. Aragüés-Peñalba, A. Sumper, and O. Boix-Aragones, "Active power control in a hybrid pv-storage power plant for frequency support," *Solar Energy*, vol. 144, pp. 49–62, 2017.

[5.13] D. Lin, X. Li, S. Ding, and Y. Du, "Strategy comparison of power ramp rate control for photovoltaic systems," *CPSS Transactions on Power Electronics and Applications*, vol. 5, no. 4, pp. 329–341, 2020.

[5.14] C. S. Lai and M. D. McCulloch, "Sizing of stand-alone solar pv and storage system with anaerobic digestion biogas power plants," *IEEE Transactions on Industrial Electronics*, vol. 64, no. 3, pp. 2112–2121, 2017.

[5.15] D. Cormode, A. Lorenzo, W. Holmgren, S. Chen, and A. Cronin, "The economic value of forecasts for optimal curtailment strategies to comply with ramp rate rules," in *2014 IEEE 40th Photovoltaic Specialist Conference (PVSC)*, 2014, pp. 2070–2075.

[5.16] W. E. Boyson, G. M. Galbraith, D. L. King, and S. Gonzalez, "Performance model for grid-connected photovoltaic inverters." Sandia National Laboratories (SNL), Albuquerque, NM, and Livermore, CA . . . , Tech. Rep., 2007.

[5.17] F. Durakovic, "Levelized cost of electricity of renewable energy technologies as a criterion for project prioritization," 2021.

[5.18] I. Peláez Acedo, C. Blanco Charro, A. Suárez González, Á. Navarro Rodríguez, P. García Fernández *et al.*, "Levelized cost of energy optimization in hybrid pv plants by energy storage for ramp-rate control operation," in *2021 IEEE energy conversion congress and exposition, ecce 2021-proceedings*, 2021.

[5.19] D. Lin, X. Li, S. Ding, and Y. Du, "Strategy comparison of power ramp rate control for photovoltaic systems," *CPSS Transactions on Power Electronics and Applications*, vol. 5, no. 4, pp. 329–341, 2020.

[5.20] D. C. Jordan, S. R. Kurtz, K. VanSant, and J. Newmiller, "Compendium of photovoltaic degradation rates," *Progress in Photovoltaics: Research and Applications*, vol. 24, no. 7, pp. 978–989, 2016.

[5.21] S. E. Hosseini and M. A. Wahid, "Hydrogen from solar energy, a clean energy carrier from a sustainable source of energy," *International Journal of Energy Research*, vol. 44, no. 6, pp. 4110–4131, 2020.

[5.22] L. Palma, B. Molina, and A. Díaz, "Design and sizing of power conversion system with energy storage for improved pv-electrolyzer energy coupling," in *2023 International Conference on Clean Electrical Power (ICCEP)*, 2023, pp. 784–788.

[5.23] D. Guilbert, M. Zasadzinski, H. Rafaralahy, and L. Boutat-Baddas, "Modeling of the dynamic behavior of a pem electrolyzer," in *2022 10th International Conference on Systems and Control (ICSC)*, 2022, pp. 78–84.

[5.24] C. Wang, Y. Hao, G. Han, C. Zhou, and C. Wang, "Coordinated scheduling of integrated energy systems with hydrogen electrolyzer units," in *2022 IEEE/IAS Industrial and Commercial Power System Asia (ICPS Asia)*, 2022, pp. 546–550.

[5.25] X. Yan, X. Zhang, C. Gu, and F. Li, "Power to gas: addressing renewable curtailment by converting to hydrogen," *Frontiers in Energy*, vol. 12, pp. 560–568, 2018.

[5.26] W. Zhang, A. M. Cantarellas, J. Rocabert, A. Luna, and P. Rodriguez, "Synchronous power controller with flexible droop characteristics for renewable power generation systems," *IEEE Transactions on Sustainable Energy*, vol. 7, no. 4, pp. 1572–1582, 2016.

[5.27] D. d. Rivero, P. García, C. Blanco, and Navarro-Rodríguez, “Control of aggregated virtual synchronous generators for pv plants considering communication delays,” *IEEE Transactions on Industry Applications*, pp. 1–13, 2024.

[5.28] I. Modbus, “Modbus application protocol specification v1. 1a,” *North Grafton, Massachusetts (www. modbus. org/specs. php)*, 2004.

[5.29] M. Rubio, A. Urquia, and S. Dormido, “Diagnosis of pem fuel cells through current interruption,” *Journal of Power Sources*, vol. 171, no. 2, pp. 670–677, 2007.

[5.30] C. A. Martinson, G. Van Schoor, K. Uren, and D. Bessarabov, “Characterisation of a pem electrolyser using the current interrupt method,” *International journal of hydrogen energy*, vol. 39, no. 36, pp. 20 865–20 878, 2014.

[5.31] H. Bevrani, B. François, and T. Ise, *Microgrid dynamics and control*. John Wiley & Sons, 2017.

[5.32] A. Mirzal, “Delay compensation using the smith predictor: a brief review with numerical examples,” *International Journal of Computer-aided Mechanical Design and Implementation*, vol. 3, no. 1, pp. 1–8, 2017.

[5.33] B. Guha, R. Jain, and S. Veda, “Bulk grid frequency support using electrolyzers,” in *2020 IEEE Industry Applications Society Annual Meeting*. IEEE, 2020, pp. 1–5.

[5.34] S. Akkari, J. Dai, M. Petit, and X. Guillaud, “Interaction between the voltage-droop and the frequency-droop control for multi-terminal hvdc systems,” *IET Generation, Transmission & Distribution*, vol. 10, no. 6, pp. 1345–1352, 2016.

Chapter 6

Real-Time Co-Simulation of Power Systems

6.1 Introduction

When simulating complex control systems, such as the one used in this thesis work, on a large scale and in traditional power grids, certain limitations in terms of numerical computation may arise, such as long run times and convergence errors, especially if the models used are very detailed. To overcome these barriers and improve the accuracy of the results, real-time simulations are used on powerful platforms such as those offered by OPAL-RT. These simulators allow the integration of real hardware, which not only improves the accuracy of the system, but also facilitates rapid control prototyping and research on large-scale power grids.

In this chapter, OPAL-RT real-time simulators will be used to carry out power converter simulations, using the SCAC system in conjunction with a simulated power system. As the number of converters and the size of the network increases, the calculation time may eventually reach the limit of real-time operation. To speed up the calculations, two main approaches are proposed: the parallelization of the calculations by splitting the main control system into subsystems, and the use of acceleration tools such as OPAL-RT's ARTEMIS toolbox.

In addition, two advanced methods are introduced to increase the speed of simulations. The first is co-simulation, which allows the simultaneous simulation of several systems, including detailed models (DEM), or combinations of domains such as average models (AVM) and phasor models (PhM) [6.1, 6.2]. The OPAL-RT simulator has modules such as eMEGASIM and ePHASORSIM, which allow the simulation of large-scale networks and detailed power converters, respectively, allowing their interaction.

Phasor simulation, unlike time-domain simulation, simplifies mathematical models

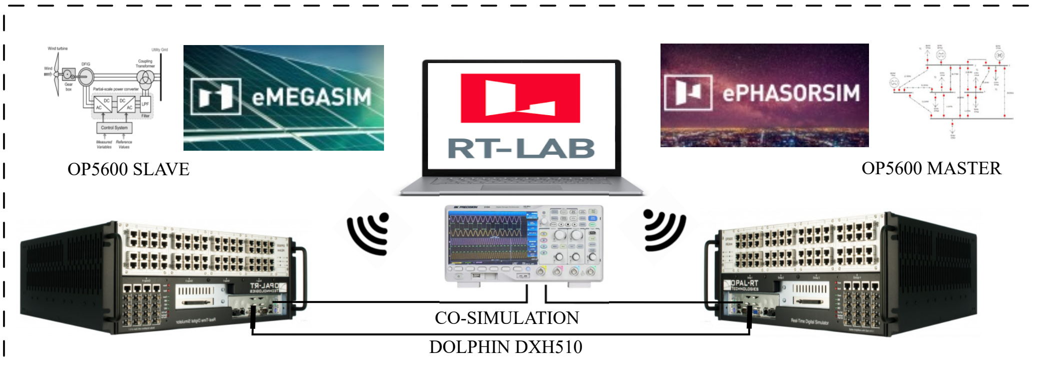

Figure 6.1: Co-simulation structure with both simulators. Each of them will simulate one part of the system. The Master will simulate the ePHASORSIM simulation, and the slave will simulate the eMEGASIM simulation [6.4].

by assuming linear behavior, allowing large systems to be solved quickly and steady-state results to be obtained, although without capturing fast dynamics. For this reason, it is used to model the network in this chapter. On the other hand, time domain simulation allows modeling system dynamics, such as converter behavior, although at the cost of higher computational resource consumption [6.3]. By combining and interfacing the simulation of the converters in the time domain with the distribution network modeled in the phasor domain through co-simulation, it is possible to analyze the interaction between the converters and the control system, as well as their dynamics in the context of the distribution network, achieving a detailed view that integrates both perspectives.

Taking all the above into account, the test setup described in Appendix A.3 will be used. This annex provides a detailed explanation on how to carry out such simulations using two OP5600 simulators from OPAL-RT, together with a DOLPHIN synchronization cable for co-simulation. The explanation covers both the hardware connections and the simulation processes in the software, providing a complete understanding of how the system operates and interacts during testing. Although in Appendix A.3 is explained, in Figure 6.1 the setup connection for the co-simulation between both OPAL-RT simulators is shown for a better understanding of the concept. This work belongs to a conference contribution (CP4) that can be find in the Appendix C [6.4].

6.2 Simulation Models

This section describes the systems used for the real-time simulations: the VSG system, controlled by the SCAC system (see Figure 6.2), and the 2-area KUNDUR system (see Figure 6.3), which represents an interconnected power grid. Their most important parameters will be explained to facilitate the understanding of their behavior

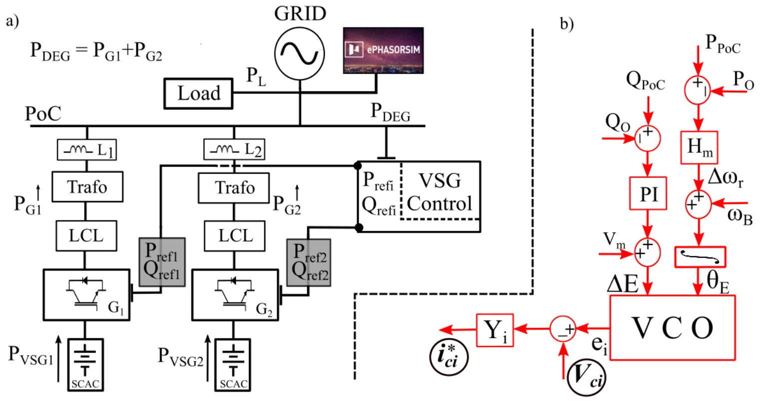

Figure 6.2: a) Power converter distribution scheme connected to grid simulated by ePHASORSIM. b) SCAC control system [6.5].

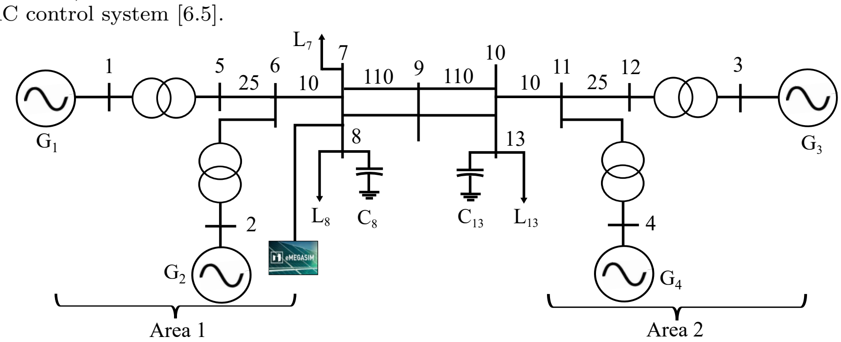

Figure 6.3: Kundur's two-area system used for simulating the power grid with ePHASORSIM. Example 12.6 in [6.6]. The distances between buses are in km.

and the interaction between both systems during the simulations.

6.2.1 VSG Converter

The simulation model of the power converter control used in this chapter of the thesis is the VSG system, based on the SCAC [6.5, 6.7]. This system will control from a central controller two battery converters distributed within a DER, connected to a Kundur-type grid. Both converters have the same nominal power capacity, as well as identical filters and transformers, but are located at different distances from the connection point, which introduces variations in the impedances of the feeders, thus simulating real grid conditions. As explained above, the SCAC emulates the inertia of a conventional synchronous generator from a central controller, sending angle and voltage modulus references to each of the local converters, providing both frequency and voltage stability to the power system [6.4, 6.5]. One of the key features of this control system is the incorporation of a virtual admittance (Y_i), which allows the

Table 6.1: Power converter and VSG parameters.

POWER CONVERTER				VSG	
Variable	Value	Variable	Value	Variable	Value
Converter				Control system	
$Power$	100 kVA	V_{DC}	750 V	H	10 s
f_{sw}	3.150 kHz	V_{AC}	400	S_n	200 kVA
Filter				K_p	0.1
L_{f1}	777 μH	R_d	0.5 Ω	τ	1
L_{f2}	200 μH	C	66 μF	f	50 Hz
Transformer				R_v	1.5 Ω
V_1	400 V	V_2	20 kV	X_v	0.7709 Ω
Lines				Y_1	0.4
L	0.76 H/km	R	0.61 Ω/km	Y_2	0.6
$Line_1$	0.6 km	$Line_2$	1 km	V_g	400 V

injected power generation to be distributed among the different converters according to their nominal capacity. This distribution is achieved by applying different weights on the admittance according to the nominal power of each converter. In this way, the converters respond optimally to variations in demand or disturbances in the grid, adapting their power injection.

Figure 6.2 shows a schematic of the system in terms of the distribution of the converters (a) and the control implemented within it (b) according to the model described in [6.5]. In Table 6.1, the specific parameters of the converters used in the simulation are detailed, including the values of the virtual admittances and the relevant electrical parameters for the correct representation of their behavior. This model provides a realistic view of how the stability of an electrical grid with multiple renewable energy converters can be managed through inertia emulation and efficient power distribution.

6.2.2 Kundur 2 Areas Model

The power grid used for phasor simulation is known as the 2-area Kundur system. This system represents an electrical grid composed of two distinct areas, each emulating real electrical systems. The areas are interconnected by a weak link, which simulates the usual connections found in real transmission networks, where geographically separated areas communicate through high impedance transmission lines. In each of the areas there are two generating units, each with a nominal capacity of 900 MVA and operating at 20 kV. The transmission lines between the areas are operating at 230 kV, reflecting a typical configuration of large-scale power grids, where power generation is transported over long distances at high voltages. This configuration allows the analysis of stability dynamics and disturbance behavior similar to real power grids.

In this model, the converters simulated in eMEGASIM are integrated into the system through bus 8, as illustrated in Figure 6.3. Table 6.2 details the main parameters

Table 6.2: Kundur 2 Areas parameters

Generator Parameters			
X_d=1.8	X_q=1.7	X_l=0.2	X'_d=0.3
X'_q=0.55	X''_d=0.25	X''_q=0.25	R_a=0.0025
T'_{d0}=8.0 s	T'_{q0}=0.4 s	T''_d=0.03 s	T''_{q0}=0.05 s
A_{Sat}=0.015	B_{Sat}=9.6	Ψ_{T1}=0.9	$k_D = 0$
H=6.5 (for G_1 and G_2)		H=6.174 (for G_3 and G_4)	
Line Parameters			
Impedances	r=0.0001pu/km	x_L=0.001pu/km	b_C=0.00175pu/km
Powers and voltages			
G_1	P=8 pu	Q=2.86 pu	E_t=1.03∠20.2°
G_2	P=8 pu	Q=4.28 pu	E_t=1.01∠10.5°
G_3	P=7.16 pu	Q=2.48 pu	$E_t = 1.03\angle -6.8°$
G_4	P=7 pu	Q=3.49 pu	$E_t = 1.01\angle -17°$
Bus 7	P_L=8.56 pu	Q_L=0.59 pu	Q_c=0 pu
Bus 8	P_L=2.99 pu	Q_L=0.59 pu	Q_c=0 pu
Bus 13	P_L=22.73 pu	Q_L=1.15 pu	Q_c=0 pu
BASE			
S	100 MVA	V	20 kV

of the network, providing a framework for understanding the interaction between the generating units and the controlled converters. For more information on the characteristics and specifications of this system, please refer to the reference provided [6.6]. This two-area Kundur grid model is widely used for power system stability studies and testing of advanced controllers in interconnected grids.

6.3 Simulation Results

This section presents some of the results obtained from the co-simulation between the two simulators, showing three scenarios: scenario 6.3.1) Power support, scenario 6.3.2) Frequency support and scenario 6.3.3) Voltage support. In each of these scenarios, the power converter is connected to the 8 bus of the system. The power support scenario 6.3.1) analyses the converter's ability to inject active power in response to system demands, adjusting its operation according to fluctuating load or generation. In frequency support scenario 6.3.2), it is studied how the converter contributes to stabilize frequency variations in the grid, emulating virtual inertia by means of VSG control. Finally, voltage support scenario 6.3.3) evaluates the converter's ability to inject or absorb reactive power, in order to maintain adequate voltage levels at the connection point (bus 8), depending on the system operating conditions.

Table 6.3: Phasor voltages with phasor simulation and with cosimulation, adding converter dynamics for cases A and B.

Voltages			V_1	V_2	V_3	V_4	V_5	V_6
6.3.1	Phasor	1)	1.03	1.01	1.03	1.01	0.9921	0.9484
		2)	1.0444	1.0243	1.0444	1.0243	1.0067	0.9618
		3)	1.0381	1.0183	1.038	1.0179	1.0029	0.9621
	Cosim	1)	1.03	1.01	1.03	1.01	0.9921	0.9484
		2)	1.0443	1.0242	1.0442	1.0242	1.0065	0.9615
		3)	1.0379	1.0181	1.0377	1.0177	1.0027	0.962
6.3.2	Phasor	1)	1.0303	1.0103	1.0304	1.0104	0.9924	0.9488
		2)	1.0141	0.994	1.0141	0.9942	0.9741	0.9292
		3)	1.0307	1.0107	1.0307	1.0107	0.9927	0.9491
	Cosim	1)	1.0303	1.0103	1.0304	1.0104	0.9924	0.9487
		2)	1.014	0.994	1.014	0.994	0.974	0.929
		3)	1.0306	1.0106	1.0306	1.0106	0.9926	0.9490
Voltages			V_7	V_8	V_9	V_{10}	V_{11}	V_{12}
6.3.1	Phasor	1)	0.9138	0.9146	0.93	0.9593	0.9975	0.8785
		2)	0.9246	0.9255	0.9388	0.9714	1.0114	0.8775
		3)	0.9304	0.9313	0.9364	0.9669	1.0057	0.8829
	Cosim	1)	0.9137	0.9145	0.93	0.9594	0.9976	0.8783
		2)	0.9245	0.9253	0.9387	0.9712	1.0112	0.8776
		3)	0.9302	0.9311	0.9362	0.9667	1.0055	0.8830
6.3.2	Phasor	1)	0.9142	0.915	0.9304	0.9597	0.9978	0.8788
		2)	0.8938	0.8959	0.9183	0.9449	0.9816	0.8738
		3)	0.9145	0.9153	0.9307	0.96	0.9961	0.8792
	Cosim	1)	0.914	0.914	0.9302	0.9596	0.9977	0.8786
		2)	0.8937	0.8957	0.9182	0.9448	0.9814	0.8736
		3)	0.9144	0.9151	0.9306	0.959	0.996	0.879

6.3.1 Power Support

In this first scenario, the active and reactive power set-points are set to control the power injected into the grid. To demonstrate one of the main features of the co-simulation, a phasor simulation was performed where only the bus voltages are shown. In ePHASORSIM, the load is modified without including dynamics, achieving practically the same steady-state results as when dynamics are introduced, as seen in Figure 6.4 a) and b).

Additionally, Table 6.3, which is at the end of the chapter, presents a summary of the steady-state results for the bus voltages in per-unit (p.u.) for three specific cases, both with phasor simulation and co-simulation: 1) when no power is injected, 2) when 100 kW of active power is injected, and 3) when 50 kVar of reactive power is injected. These results are assumed to be representative for the other scenarios.

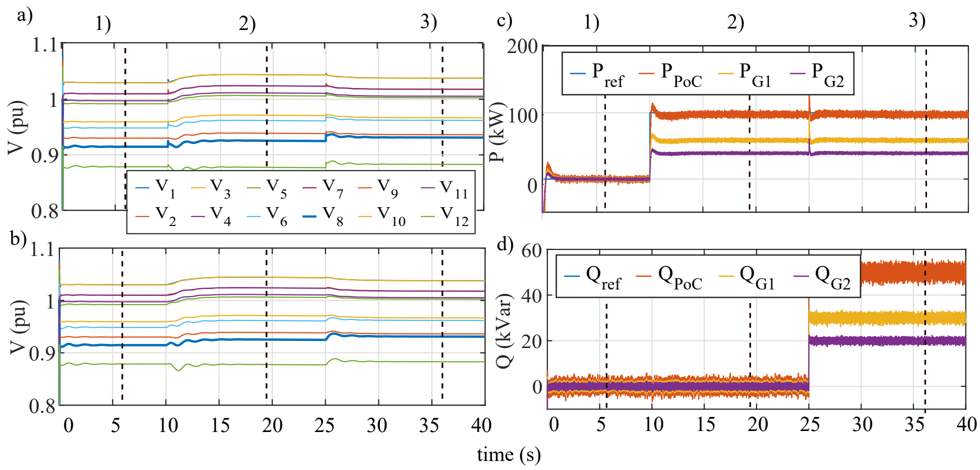

Figure 6.4: a) Voltages in p.u. of all buses of KUNDUR2AREA model without co-simulation, just phasor simulation. b) Voltages in p.u. of all buses of KUNDUR2AREA model with co-simulation, introducing the dynamics of c) and d). c) Active power injection of VSG system. d) Reactive power injection of VSG system.

Figure 6.4 a) and b) show the different bus voltages in p.u., with particular attention to V_8, which is the voltage at the connection point of the power converter and is used to construct the local three-phase voltage in eMEGASIM. As can be seen in Fig. b) and c), the injection of 100 kW of active power at 10 s and 50 kVar of reactive power at 25 s into the grid increases the voltage. As mentioned earlier, the power is unevenly distributed between the two converters, with the first converter supplying 60% and the second one the remaining 40%, by means of the virtual admittance weights.

6.3.2 Frequency Support

In this scenario, a frequency variation is induced by a load change in the grid. Similar to case 6.3.1, to demonstrate one of the main features of co-simulation, a phasor simulation has been performed in which only the bus voltages are shown. In Fig. 6.5 a), the voltage at each bus during the phasor simulation is observed, while in Figure 6.5 b), the result of the co-simulation is presented, with a special focus on bus V_8, which is the connection point of the power converter.

However, in this case, the system's dynamics do not change significantly because the power injected by the converter is small compared to the total grid power. In Table 6.3, which is at the end of the chapter, presents a summary of the steady-state voltage at different points, and the final results are seen to be equivalent in both the phasor simulation and the co-simulation.

As the load increases, a general voltage drop occurs across the grid, which also leads to a frequency reduction, as seen in Figure 6.5 c), where a negative frequency variation

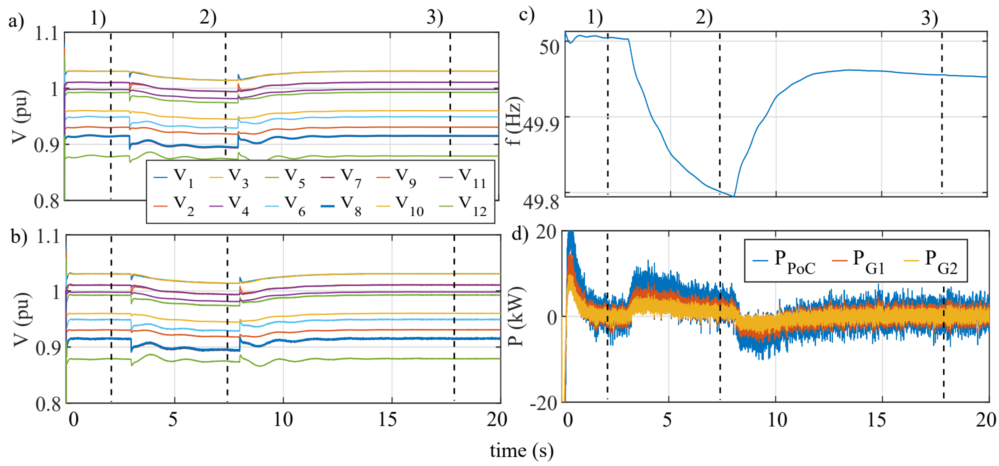

Figure 6.5: a) Voltages in p.u. of all buses of KUNDUR2AREA model without co-simulation, just phasor simulation. b) Voltage in p.u. of all buses of KUNDUR2AREA model. c) Frequency variation provoked by a load change. d) Active power injection of VSG system.

appears. This frequency drop triggers the VSG system, which injects active power into the grid in an attempt to compensate for the frequency variation, as shown in Figure 6.5 d). This behavior reflects the ability of the VSG system to provide frequency support, helping to stabilize the grid during disturbances.

6.3.3 Voltage Support

In this scenario, a voltage sag is induced in the power grid at 3 s, with a duration of 0.5 s, in order to assess the performance of the VSG control system. Until this point, the control system had been operating like a grid-feeding converter, meaning it simply injected the generated power into the grid without compensating for voltage variations. However, to mitigate the observed voltage sag, a Q-V droop controller must be included in the reactive power loop so the system can inject reactive power to compensate for the voltage drop, thus behaving like a grid-supporting controller.

The Q-V droop used in this implementation follows equation (6.1), which establishes the relationship between the voltage and the reactive power injected into the system:

$$V = (0.95 - \frac{0.95 - 0.85}{20 \cdot 10^4}(Q + 20 \cdot 10^4)) \cdot 400 \tag{6.1}$$

Figure 6.6 a) shows the voltage evolution at the main buses of the system, with special attention to bus V_8, which is directly connected to the power converter. After implementing the Q-V droop controller, the system begins to follow the relationship defined in equation (6.1), injecting reactive power into the system to counteract the

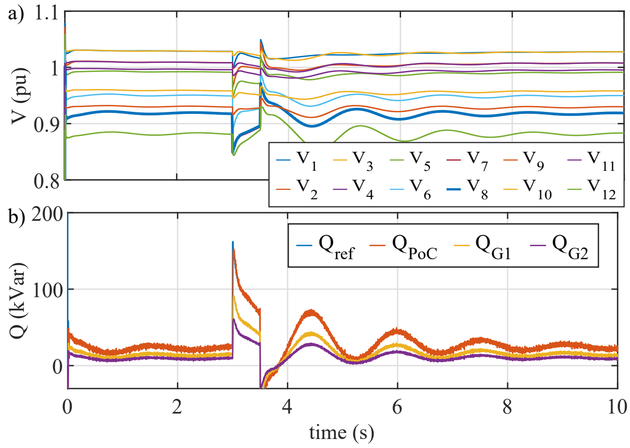

Figure 6.6: a) Voltage in p.u. of all buses of KUNDUR2AREA model, where a 0.85 p.u. voltage sag appears. b) Reactive power injection due to the voltage variation.

voltage sag. This behavior can be clearly seen in Figure 6.6b), where the reactive power injection is evident, and the voltage drop is compensated, helping to stabilize the system.

6.4 Conclusion

In this chapter, the procedure for conducting a co-simulation between two OPAL-RT simulators is thoroughly explained. The simulators used in this process are eMEGASIM, which facilitates detailed time-domain system simulation, and ePHASORSIM, which operates in the phasor domain. By combining both simulators, it becomes possible to simulate large and complex systems that would otherwise demand a significant amount of real-time computational resources. This approach also allows the incorporation of dynamic effects into the phasor-domain simulation, providing more accurate and realistic results in scenarios where system behaviors are time-dependent.

To illustrate the effectiveness of the co-simulation approach, a comparison between phasor-domain simulation and co-simulation is conducted, specifically focusing on cases A and B. The comparison highlights the differences in system performance, showing how the dynamics of the system are captured more precisely in co-simulation, even when phasor simulation is used for steady-state analysis. Three fundamental scenarios have been simulated to evaluate the behavior of the system under different conditions: 6.3.1) injecting arbitrary power into the grid to observe power flow and stability, 6.3.2) injecting active power for frequency compensation to support grid stability during fluctuations, and 6.3.3) injecting reactive power for voltage compensation to stabilize voltage levels in the grid. These simulations showcase how the co-simulation approach can effectively model the performance of power systems and the interactions between different grid-supporting functions.

References

[6.1] N. Mohan, W. Robbins, T. Undeland, R. Nilssen, and O. Mo, "Simulation of power electronic and motion control systems-an overview," *Proceedings of the IEEE*, vol. 82, no. 8, pp. 1287–1302, 1994.

[6.2] T. Demiray, "Simulation of power system dynamics using dynamic phasor models," Ph.D. dissertation, ETH Zurich, 2008.

[6.3] P. W. Sauer, M. A. Pai, and J. H. Chow, *Power system dynamics and stability: with synchrophasor measurement and power system toolbox.* John Wiley & Sons, 2017.

[6.4] D. del Rivero, S. Singh, P. García, and P. Rodríguez, "Real-time cosimulation of power systems: Integration of emegasim and ephasorsim using opal-rt simulators," in *2024 IEEE 15th International Symposium on Power Electronics for Distributed Generation Systems (PEDG)*, 2024, pp. 1–6.

[6.5] D. d. Rivero, P. García, C. Blanco, and Navarro-Rodríguez, "Control of aggregated virtual synchronous generators for pv plants considering communication delays," *IEEE Transactions on Industry Applications*, pp. 1–13, 2024.

[6.6] P. Kundur, "Power system stability," *Power system stability and control*, vol. 10, pp. 7–1, 2007.

[6.7] C. Verdugo, A. Tarraso, J. I. Candela, J. Rocabert, and P. Rodriguez, "Centralized synchronous controller based on load angle regulation for photovoltaic power plants," *IEEE Journal of Emerging and Selected Topics in Power Electronics*, vol. 9, no. 1, pp. 485–496, 2020.

Chapter 7

Conclusion and Future Works

7.1 Conclusiones

Las conclusiones de esta tesis sintetizan los aportes realizados en el análisis, desarrollo e implementación de sistemas DER y su integración eficiente en redes eléctricas modernas. Además, reflejan el avance significativo logrado en el análisis, desarrollo e implementación de sistemas de Generadores Sincrónicos Virtuales (VSG) basados en el Sistema de Control de Ángulo Central Sincrónico (SCAC). Estos sistemas han sido diseñados con el objetivo de mejorar la estabilidad y eficiencia en DER, integrando de manera efectiva fuentes de energía renovable, como la solar y eólica, con la capacidad de adaptación a las fluctuaciones de la red. Dichos sistemas se implementarían a través de sistemas PMS, o para ser más precisos, de cara a su implementación industrial, a través de PPC, que permitan cumplir con las normativas actuales, como la norma EN.50459 en Europa. A través de este trabajo, se ha demostrado que el SCAC puede ser una solución viable para garantizar la estabilidad y optimización en redes eléctricas modernas. Las principales contribuciones de esta tesis, como se presentan posteriormente en el documento, se enumeran a continuación.

- **Capítulo 2:** el estado del arte desarrollado en esta tesis doctoral resalta la importancia de los DER y la necesidad de una gestión eficiente de la energía a través de los PMS, integrados en PPCs. Se ha hecho una revision de las principales caracteristicas de estos, así como la normativa vigente que estos deben cumplir. A lo largo del análisis de los modos de interfaz entre convertidores y la red, y de los VSG, se discuten los componentes clave para una integración adecuada de las plantas distribuidas en el sistema eléctrico, con especial énfasis en el sistema SCAC, que constituye el pilar central de esta tesis. Asimismo, se abordan los desafíos que presentan las comunicaciones en el sistema SCAC, proponiendo soluciones para compensar los retrasos de comunicación, un aspecto crucial para la estabilidad y eficiencia del control. Además, se examina el estado del arte en la compensación de variaciones de rampas, detallando los sistemas más utilizados. En este contexto, también se analizan los sistemas aplicados a la generación de hidrógeno verde, tanto desde la perspectiva de la generación como del control del electrolizador, subrayando su relevancia en el actual proceso de transición energética y sostenibilidad. Con este analisis se obtiene una base sólida para la comprensión del trabajo presentado.

- **Capítulo 3:** el sistema SCAC se presenta como una solución para la operación centralizada de diferentes sistemas de generación distribuida, siendo capaz de emular las características dinámicas de los generadores síncronos convencionales, proporcionando soporte a la red, en condiciones de inestabilidad. Para ello se ha detallado su modelo dinámico asi como el desarrollo de una modelización matemática detallada del mismo. Dichos modelos permiten una evaluación precisa de su comportamiento dinámico bajo distintos escenarios operativos. Este modelado ha sido clave para adaptar el SCAC a diversas configuraciones de red y ha permitido que los sistemas de generación distribuidos gestionados por el controlador central puedan operar de manera coordinada, proporcionando soporte tanto en la regulación de frecuencia como de tensión. Asimismo, el uso de esta modelización permitió identificar las fortalezas del SCAC en términos de flexibilidad, tanto en redes conectadas como en microrredes aisladas.

- **Capítulo 4:** en el ámbito industrial, la tesis abordó con éxito la implementación del SCAC en convertidores comerciales, superando desafíos significativos, como los asociados a la falta de acceso a las variables internas de estos dispositivos y los retrasos en la comunicación. La capacidad de mitigar estos retrasos mediante el uso de métodos avanzados como el predictor de Smith fue uno de los principales avances. Se realizaron pruebas experimentales y simulaciones que mostraron que el sistema SCAC puede compensar eficazmente los retrasos de comunicación de hasta 75 ms, asegurando la estabilidad operativa incluso en redes complejas. Además, se realizó un estudio de estabilidad, para comprender mejor el sistema de compensación de retrasos, mostrando como su implementación, desplaza los polos y ceros a la izquierda, mejorando la respuesta y estabilizando el sistema. Este resultado es de gran relevancia, ya que permite que los convertidores comerciales, que son esenciales en aplicaciones industriales, operen bajo el control centralizado del SCAC sin comprometer la estabilidad de la red.

- **Capítulo 5:** otra contribución importante de este trabajo fue la implementación del SCAC en la gestión de sistemas de generación fotovoltaica, donde se destacó el uso de técnicas avanzadas para la compensación de rampas de generación. En sistemas solares, la variabilidad en la generación es un reto constante, y la capacidad del SCAC para ajustar de manera dinámica la potencia activa y reactiva, así como para mitigar los cambios abruptos en la producción, resulta clave para evitar inestabilidades en la red. Para ello, además se tomó como ventaja en la implementación los pesos de distribución que disponen las admitancias virtuales de cada uno de los controladores locales, para desarrollar un algoritmo que ayude a compensar la rampa de generación solar de manera local. Este enfoque permitió mejorar el rendimiento de las plantas fotovoltaicas, maximizando su integración en el sistema eléctrico y reduciendo la necesidad de recurrir a fuentes de respaldo no renovables.

En cuanto a la producción de hidrógeno verde, la tesis también logró avances significativos. Se utilizó el sistema SCAC para crear una red aislada, con un control centralizado para controlar los sistemas DEG, teniendo en cuenta los posibles retrasos de comunicación en su control, asi como su compensación. Además, se ha utilizado un controlador droop dual que permite una mejor gestión de la demanda de energía por parte de estos equipos en función de la disponibilidad de energía renovable, optimizando la operación de los electrolizadores. Este enfoque no solo mejora la eficiencia del proceso de electrólisis, ya que ayuda a que no se detenga la producción de hidrógeno, adaptándose su consumo a la energía disponible, actuando como una carga flexible, sino que también abrió nuevas posibilidades para la producción de hidrógeno verde en microrredes y sistemas aislados, lo cual es esencial para la transición hacia un sistema energético más sostenible. Los resultados mostraron que el SCAC puede mantener la estabilidad operativa incluso en condiciones de variabilidad extrema en la generación renovable, lo que refuerza su aplicabilidad en el sector del hidrógeno verde.

- **Capítulo 6:** además de las contribuciones en control y optimización, este trabajo también propuso una novedosa metodología de cosimulación que combina simulaciones en dominios temporales y fasoriales. Esta metodología permitió evaluar de manera precisa el rendimiento del sistema bajo condiciones operativas relativamente realistas, lo que facilita el análisis de la interacción entre el SCAC y los convertidores distribuidos en escenarios de generación renovable. La cosimulación puede destacarse como una herramienta clave para validar el diseño, no solo del SCAC, sino de cualquier sistema que quiera implementarse en una red real, debido al procedimiento explicado, siendo un buen aporte metodológico a la literatura científica.

Los experimentos y simulaciones presentados en esta tesis validaron la eficacia del SCAC para gestionar redes eléctricas distribuidas, proporcionando resultados satisfactorios incluso con la inclusión de retrasos de comunicación. El éxito de su implementación en escenarios experimentales refuerza su viabilidad para aplicaciones a gran escala, tanto en plantas solares como en sistemas de generación de hidrógeno verde.

En resumen, las conclusiones de esta tesis demuestran que el SCAC representa una solución robusta y flexible para la gestión de redes eléctricas modernas con alta penetración de energías renovables. Su capacidad para coordinar múltiples sistemas de generación distribuida, optimizar el uso de recursos energéticos y garantizar la estabilidad de la red abre nuevas oportunidades de investigación y desarrollo en el campo de los sistemas energéticos.

7.2 Conclusions

The conclusions of this thesis synthesize the contributions made in the analysis, development and implementation of DER systems and their efficient integration in modern power grids. Furthermore, they reflect the significant progress achieved in the analysis, development and implementation of Virtual Synchronous Generator (VSG) systems based on the Synchronous Central Angle Control (SCAC) system. These systems have been designed with the objective of improving stability and efficiency in DER, effectively integrating renewable energy sources, such as solar and wind, with the ability to adapt to grid fluctuations. Such systems would be implemented through PMS systems, or to be more precise, in view of their industrial implementation, through PPC, which would allow compliance with current regulations, such as the EN-50459 standard in Europe. Through this work, it has been demonstrated that SCAC can be a viable solution to guarantee stability and optimization in modern electricity grids. The main contributions of this thesis, as presented later in the paper, are listed below.

- **Chapter 2:** the state of the art developed in this doctoral thesis highlights the importance of the DER and the need for an efficient energy management through the PMS, integrated in the PPCs. A review has been made of the main characteristics of these, as well as the current regulations that they must comply with. Throughout the analysis of the interface modes between converters and the grid, and of the VSGs, the key components for an adequate integration of distributed plants in the electrical system are discussed, with special emphasis on the SCAC system, which constitutes the central pillar of this thesis. It also addresses the challenges presented by communications in the SCAC system, proposing solutions to compensate for communication delays, a crucial aspect for control stability and efficiency. In addition, the state of the art in ramp variation compensation is examined, detailing the most widely used systems. In this context, the systems applied to green hydrogen generation are also analyzed, both from the perspective of generation and control of the HE, highlighting their relevance in the current process of energy transition and sustainability. This analysis provides a solid basis for the understanding of the work presented.

- **Chapter 3:** the SCAC system is presented as a solution for the centralized operation of different distributed generation systems, being able to emulate the dynamic characteristics of conventional synchronous generators, providing support to the grid under unstable conditions. For this purpose, its dynamic model has been detailed, as well as the development of a detailed mathematical modeling of the same. These models allow an accurate assessment of their dynamic behavior under different operating scenarios. This modeling has been key to adapting the SCAC to different network configurations and has allowed the distributed generation systems managed by the central controller to operate in a coordinated manner, providing support in both frequency and voltage regulation. Furthermore, the use of this modeling allowed the strengths of the SCAC in terms of flexibility to be identified, both in connected grids and in isolated ADNs.

- **Chapter 4:** at the industrial level, the thesis successfully addressed the implementation of SCAC in commercial converters, overcoming significant challenges, such as those associated with the lack of access to the internal variables of these devices and communication delays. The ability to mitigate these delays through the use of advanced methods such as the Smith predictor was a major breakthrough. Experimental tests and simulations showed that the SCAC system can effectively compensate for communication delays of up to 75 ms, ensuring operational stability even in complex networks. In addition, a stability study was performed to better understand the delay compensation system, showing how its implementation shifts the poles and zeros to the left, improving the response and stabilizing the system. This result is of great relevance, as it allows commercial converters, which are essential in industrial applications, to operate under the centralized control of the SCAC without compromising the stability of the grid.

- **Chapter 5:** another important contribution of this work was the implementation of SCAC in the management of PV generation systems, where the use of advanced techniques for generation ramp compensation was highlighted. In solar systems, generation variability is a constant challenge, and the ability of SCAC to dynamically adjust active and reactive power, as well as to mitigate abrupt changes in production, is key to avoid grid instabilities. To this end, the distribution weights provided by the virtual admittances of each of the local controllers were also taken as an advantage in the implementation, to develop an algorithm that helps to compensate the solar generation ramp locally. This approach improved the performance of the photovoltaic plants, maximizing their integration into the electricity system and reducing the need to resort to non-renewable backup sources.

  In terms of green hydrogen production, the thesis also made significant progress. The SCAC system was used to create an isolated grid, with centralized control to control the DEG systems, taking into account possible communication delays in their control, as well as their compensation. In addition, a dual droop controller has been used to better manage the energy demand of this equipment according to the availability of renewable energy, optimizing the operation of the HEs. This approach not only improves the efficiency of the electrolysis process, as it helps to ensure that hydrogen production does not stop, adapting its consumption to the available energy, acting as a flexible load, but also opened new possibilities for the production of green hydrogen in ADNs and isolated systems, which is essential for the transition towards a more sustainable energy system. The results showed that SCAC can maintain operational stability even under conditions of extreme variability in renewable generation, which reinforces its applicability in the green hydrogen sector.

- **Chapter 6:** furthermore, to the contributions in control and optimization, this work also proposed a novel co-simulation methodology combining time-domain and phasor domain simulations. This methodology allowed accurate assessment of system performance under relatively realistic operating conditions, which facilitates the analysis of the interaction between SCAC and distributed converters in renewable generation scenarios. Co-simulation can be highlighted as a key tool to validate the design, not only of the SCAC, but of any system to be implemented in a real grid, due to the procedure explained, being a good methodological contribution to the scientific literature.

The experiments and simulations presented in this thesis validated the effectiveness of SCAC for managing distributed power grids, providing satisfactory results even with the inclusion of communication delays. The success of its implementation in experimental scenarios reinforces its viability for large-scale applications, both in solar plants and in green hydrogen generation systems.

In summary, the conclusions of this thesis demonstrate that SCAC represents a robust and flexible solution for the management of modern power grids with high renewable energy penetration. Its ability to coordinate multiple distributed generation systems, optimize the use of energy resources and guarantee grid stability opens up new opportunities for research and development in the field of energy systems. The future of SCAC, especially in green hydrogen production and integration with energy storage technologies, promises to continue to deliver innovative solutions for a cleaner and more efficient energy system.

7.3 Future Work

This thesis work has addressed the key aspects of the SCAC control system and its application to hybrid PV plants. However, not all the work is done, as several opportunities for future research remain. This chapter describes possible future directions and areas for improvement, considering current trends and technological advances.

1. **SCAC System Optimization Using Synchrophasors and GPS Clock**: in line with what was raised in Chapter 4, a logical extension would be to go deeper into reducing the use of physical sensors by reconstructing signals, taking advantage of technologies such as Synchrophasors. The use of a synchronized GPS clock would allow more accurate measurements to be obtained in distributed systems, improving the fidelity of MODBUS TCP signals and allowing effective synchronization of converters. The practical implementation of this system, both in simulated scenarios and in real environments, would be a significant contribution to the control and monitoring of SCAC systems with minimal sensors.

2. **Adaptation to network codes**: currently the SCAC system has been analyzed in terms of its operation, for a possible integration in a PMS system. However, for integration in real systems connected to the grid, through PPCs, it must be taken into account and a suitable parametrization must be carried out to comply with the different grid code conditions, as shown in Sections 1 and 2.

3. **Implementation of Distributed Controllers in Real Systems**: the integration of the SCAC system in real converters, either in off-grid or grid-connected configurations, could provide key experimental data on system performance. This would allow experimental validation of the theory and simulations presented in the thesis, identifying the advantages and limitations of the implementation in real operating conditions. Furthermore, the interaction between central and local controllers could be explored, optimizing multilevel control for different distributed generation scenarios.

4. **Improved Delay Compensation Systems**: considering the challenges related to communication delays, an interesting line of research would be to explore new compensation techniques, such as the Scattering Transform. This method is less dependent on accurate plant modeling and could offer a more robust solution in distributed systems where communication delays vary unpredictably. Implementing and experimentally testing this type of compensation would improve the stability and responsiveness of the SCAC system.

5. **Adaptation of the Communication Delay Ramp Compensation System**: although a ramp-rate compensation system has been developed, the effects of communication delays on its performance have yet to be considered. Experimental tests integrating these conditions would allow optimization of the system.

In addition, further study of the optimal distribution of weights between converters could improve efficiency and reduce operating costs, making the system even more competitive and viable on a large scale.

6. **Experimental Testing for Green Hydrogen Generation**: the green hydrogen generation system described in Chapter 4 could be evaluated under different communication scenarios, including variable delays. Experimental testing would allow analyzing the performance under real conditions, optimizing both centralized and local control. An interesting alternative would be to eliminate local controllers, sending commands directly from the central controller, which would simplify the system architecture, but would also require robust solutions for delays.

7. **Extension of the Co-Simulation Setup for Contingency Studies**: taking advantage of the co-simulation setup described in Chapter 6, the model could be extended to simulate various contingencies, such as those described in European grid codes, in both grid-connected and grid-forming operating scenarios under isolated bus conditions. This extension would allow validation of system behavior in failure situations, ensuring robustness and regulatory compliance in different operational contexts.

These future research directions would not only complement the work developed in this thesis, but would also broaden the scope of applications of SCAC and VSG systems in real environments, helping to optimize their integration in electricity grids with high levels of renewable energy penetration.

Appendix A

Laboratory Setup

A.1 Introduction

This appendix describes the different setups used for the tests carried out in the context of this thesis. First, the setups used in the experimental tests carried out at the University of Oviedo will be detailed. With this setup, significant contributions JP1 and CP1 were obtained [A.1, A.2]. Subsequently, the setup used in the facilities of the Luxembourg Institute of Science and Technology (LIST) during the three-month stay, which took place from September to December 2023, will be presented. A contribution [A.3] was obtained from this stay (CP4).

A.2 University of Oviedo Setup

The experimental setup used in some of the tests carried out during this thesis work at University of Oviedo headquarters will be detailed. These tests have focused on the evaluation of control systems by means of HIL and PHIL simulation techniques, using a real-time simulator. For this purpose, a Speedgoat Performance Real-Time Target Machine has been used, which acts as the control and simulation core. The simulator is connected via the MODBUS TCP communications protocol to a communications switch, which in turn is connected to two dc bi-directional CNG converters (BDC), which allow real-time power exchange. This configuration not only facilitates the dynamic interaction between the simulated model and the real hardware, but also allows the accurate validation of the control algorithms and the evaluation of the converters' behavior under different operating conditions. Before dealing in detail with the interconnection and communication between these elements, a brief but comprehensive description of each of the components used in the experimental setup will be

Figure A.1: Speedgoat Performance Real-Time Target Machine.

presented. This includes the Speedgoat simulator, the CNG converters, the communication interfaces, and other auxiliary equipment used for testing. Subsection 3 will shown the configuration setup used for estimating the communication delay due to communications and also, the setup for the experimental tests is going to be shown and explained.

A.2.1 Experimental Elements

This subsection will review the different elements used in the experimental setup, with the objective of understanding the nature and function of each one, as well as their integration in the overall system. This will allow to understand how each component contributes to the correct functioning of the system and its role within the real-time control and simulation scheme.

A.2.1.1 Speedgoat

The simulator used in the test setup of this thesis is a Speedgoat Performance Real-Time Target Machine [A.4], which is a real-time platform designed to run complex control models in industrial applications, such as power converter control. This system is used in this thesis to perform PHIL simulations, allowing real-time interaction between the physical hardware and the simulation models. This simulator is shown in Figure A.1.

In this case, the simulator remotely controls two CNG converters in real time, using the MODBUS TCP communications protocol, through an IO753 MODBUS client module (see Figure A.2) [A.5]. This integration facilitates the simulation and control of the converters under various operating conditions, the control system in a safe and flexible environment prior to field deployment. The simulator's ability to operate in real time allows the validation of the SCAC control algorithm and its stability verification, including the addition of communication delays and their compensation.

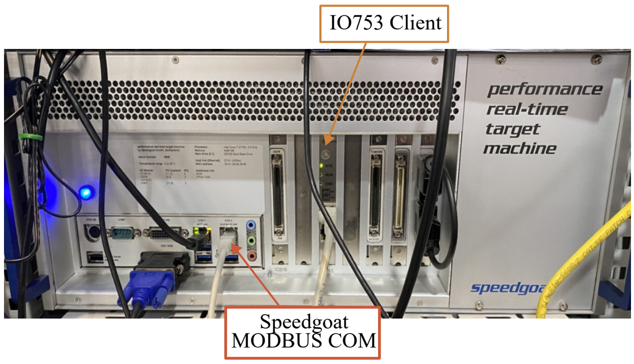

Figure A.2: Speedgoat MODBUS TCP Connections.

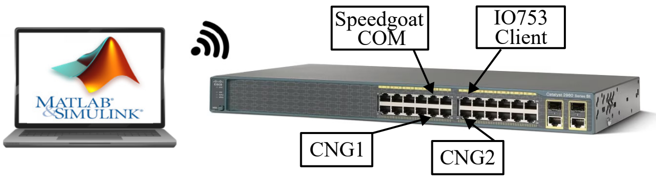

Figure A.3: Communication switch interconnecting Speedgoat, IO753, CNG1 and CNG2 with control system on computer [A.6].

A.2.1.2 Communication Switch

The Catalyst 2960 Plus Series SI is a communications switch used for the experimental tests of this thesis work, which functions as a gateway for the interconnection of multiple Ethernet devices within a unified network [A.6]. This switch allows all devices to be efficiently integrated, enabling fast and reliable communication between them. Its main function is to manage and distribute the data traffic between the connected devices, ensuring continuous and stable communication.

In the experimental setup, this switch connects the Speedgoat simulator, in charge of performing the real-time simulations, the IO753 module, which is used to manage the MODBUS TCP communications, and the BDC. In addition, it is also linked to the computer, which connects to the system via WiFi, allowing remote access for monitoring and control of the tests. This can be seen in Figure A.3. By centralizing connections, the switch ensures that all devices can interact on a shared network, facilitating data flow and ensuring efficient management of the control system.

Thanks to the switch 's ability to handle multiple connections simultaneously, it is possible to work with multiple devices in a coordinated manner, which optimizes overall system performance. This is essential for HIL and PHIL testing, where accuracy and synchronization in data transmission are so important for proper validation of controlled models and devices.

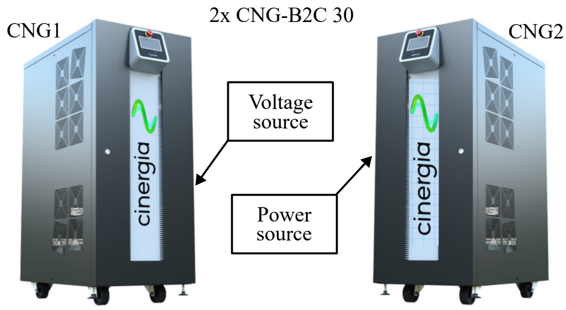

Figure A.4: Cinergia B2C-30 used for experimental setup.

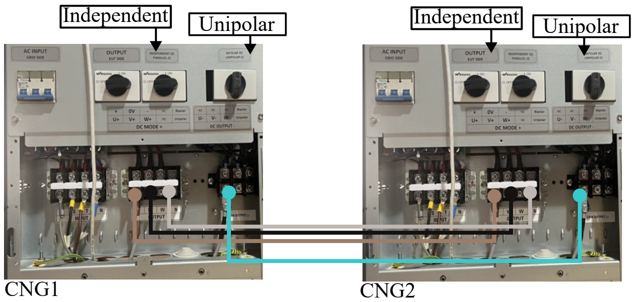

Figure A.5: 2x BDC interconnected. $CNG1$ working as voltage source and $CNG2$ as power source.

A.2.1.3 Cinergia Converters

The Cinergia B2C-30 bidirectional power supply is a highly versatile 30 kW DC power converter, which offers various control functionalities, such as voltage, current, power and resistance control (see Figure A.4). This equipment is ideal for multiple applications, being able to be used as a battery charger, battery emulator, and even as a solar panel emulator. Its flexibility makes it a key tool for the emulation and testing of energy storage and distributed generation systems.

The converter has several control options. It offers three independently controllable phases, which can be integrated in parallel to achieve maximum source power, or in a independent way, being able to use each phase independently. In addition, it can be operated in unipolar or bipolar mode. In unipolar mode, each phase has its own independent neutral, while in bipolar mode, two phases share a neutral at the midpoint. Figure A.5 shows a schematic of the hardware used for the experimental tests, where it can be seen that $CNG1$ operates independently and unipolar mode, while $CNG2$ operates independently and unipolar, although these mode can be changed as desired. To emulate the behavior of three converters, the three phases of $CNG2$ are configured as power sources and $CNG1$ emulated each of them a battery, simulating the behavior of the SCAC system.

In terms of software control modes, each of the phases of $CNG1$ is configured as a battery emulator, in charge of accepting or ceding the active power demanded by the control system, which comes from each of the $CNG2$ phases. The reactive power control is managed by injecting or absorbing reactive power in the power supply network of each of the converters, although this function is limited by the use of only two converters in this configuration.

This converter also allows remote control through a client program provided with the equipment, which facilitates the configuration and adjustment of the different operating modes. In addition, it can be operated by digital or analogue signals, functioning as a power amplifier. In this thesis work, the control is carried out mainly by MODBUS TCP, configuring the read and write registers in the Speedgoat simulator. Although the primary control is carried out by external software, the initial conditioning of the equipment is carried out using the CNG client for convenience, although it would also be possible to implement an initial configuration from Matlab for greater automation.

A.2.2 Experimental Setup

This section explains how the different elements used in the real-time experimental tests are interconnected. Two different configurations or setups will be described. The first one is focused on measuring communication delays. The idea is to capture these delays, model them and then integrate them into the control system in order to compensate for them. For this test, the same components are used as in the second setup, with one important difference: here only one converter is used instead of two. This allows us to better isolate the response times and to understand more clearly how the communication between the Speedgoat simulator and the converter is affected.

The second setup is for PHIL testing, where both CNG converters are used. In this case, the complete system, which also includes the switch and the Speedgoat simulator, is tested to validate how the hardware and the simulated model interact in real time. This setup allows us to observe the behavior of the system in more complex situations, similar to real power grid conditions.

A.2.2.1 Delay Measurement

To measure the communication delay between the control system and the converters, the scheme shown in Figure A.6 is used. During the real-time simulation run, two signals are sent: a digital square reference signal of 0.25 Hz has been supplied simultaneously to the current converter set-point, so it can be used as a trigger signal in an external scope that also captures the output current response. The digital signal is taken as a reference for the exact time of sending, while the MODBUS signal corresponds to the current command that activates the converter.

The communication delay is measured using an oscilloscope. This instrument will capture both the digital signal and the current signal measured at the converter termi-

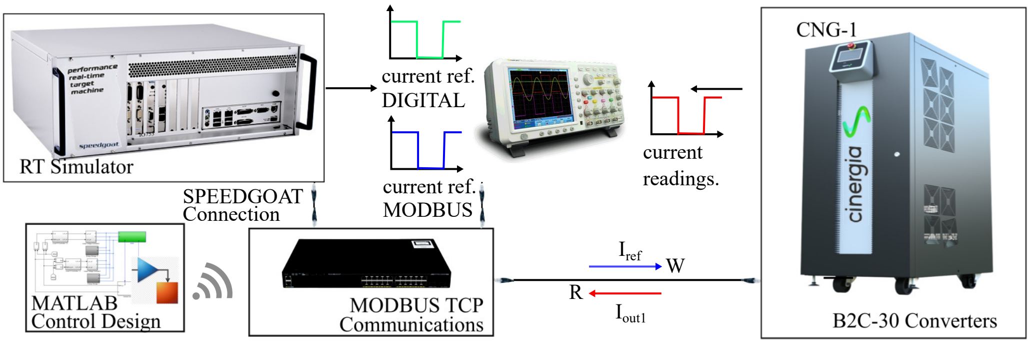

Figure A.6: Setup for delay measurement [A.2, A.1].

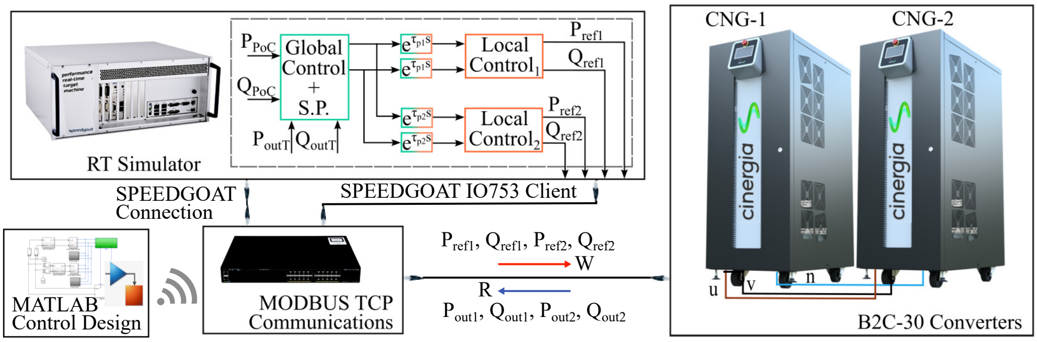

Figure A.7: Setup for HIL and PHIL experimental tests. The control design is made on Matlab and executed in the real-time Speedgoat target. The converters are controlled by writing/reading published MODBUS/TCP variables [A.2, A.1].

nals. Assuming that the internal control of the drive is sufficiently fast, the difference between the reference signal and the reading at the drive terminals will be interpreted as the communication delay time, i.e. the time from sending the signal to its reception and execution by the drive.

A.2.2.2 HIL Setup

The real-time tests were carried out following the scheme presented in Figure A.7, where the interconnection between the two BDC, the Gateway and the real-time simulator can be observed. The simulation is loaded into the Speedgoat system through Matlab/Simulink, using MODBUS TCP communications to send and receive signals between the different components of the system.

The simulator, through the IO753 module, is responsible for transmitting read and write signals to each of the drives via the MODBUS TCP protocol. These signals allow the converters to receive the power control commands generated by the simulation (val-

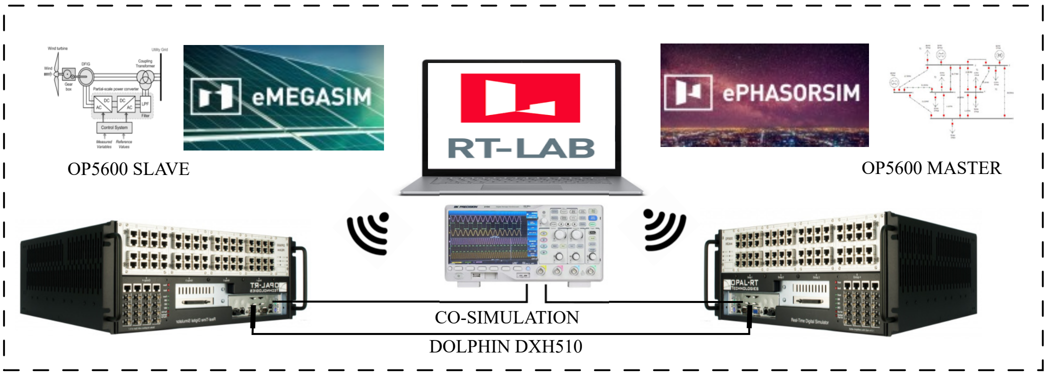

Figure A.8: Co-simulation structure with both simulators. Each of them will simulate one part of the system. The Master will simulate the ePHASORSIM simulation, and the slave will simulate the eMEGASIM simulation [A.3].

ues of P_{ref1}, Q_{ref1}, P_{ref2}, Q_{ref2}), which correspond to the active and reactive power references for each phase. As explained above and as can be seen in the schematic, the $CNG2$ system operates with the three phases acting as power sources. This allows emulating the power demanded by the control system, where the converters respond to the orders received from the simulation. In this configuration, $CNG1$ operates as a battery on each phase, operating in battery emulation mode to simulate the delivery and storage of energy, which facilitates the evaluation of the behavior of the control system under different load and demand conditions.

A.3 LIST Setup

The experimental setup used at the Luxembourg Institute of Science and Technology (LIST) will be presented in detail. The tests mainly focused on the real-time co-simulation procedure of the system underlying this thesis, in conjunction with a real power grid. This co-simulation [A.7] has the particularity of operating in different domains, simulating the SCAC control system in the time domain and the real grid in the phasor domain. To carry out this process, two OPAL RT simulators will be used: one in the time domain, based on eMEGASIM, and the other in the phasor domain, using ePHASORSIM. The synchronization between the two simulators will be done by means of a DOLPHIN cable. Therefore, a brief explanation of each of the simulators and the cable, as well as the simulation execution procedure, will be given. Figure A.8 shows the main scheme used for the simulations.

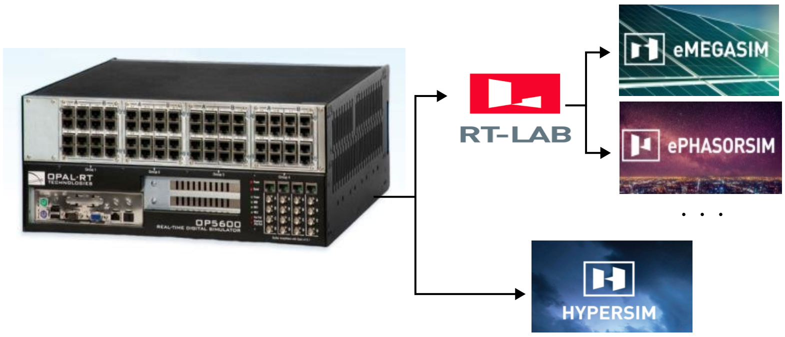

Figure A.9: OP5600 simulator from OPAL RT.

A.3.1 Simulation Elements

This subsection will review the different elements used in the co-simulation setup, with the objective of understanding the nature and function of each one, as well as their integration in the overall system. Also, the software elements and configuration for the co-simulation is reviewed .

A.3.1.1 OPAL RT OP5600

OP5600 simulators from OPAL-RT are advanced tools designed to perform real-time simulations of complex systems, such as electrical power systems and control systems, which makes them essential for laboratory tests such as those used in this thesis. Thanks to their ability to emulate in real-time, they allow studying the behavior of systems under realistic conditions, being especially useful for validating controllers and performing HIL tests (see Figure A.9). The OP5600 combines multi-core processors and Field Programmable Gate Arrays (FPGA) technology, allowing it to handle detailed models with high temporal accuracy. In addition, its ability to connect to other laboratory equipment via various interfaces (such as Ethernet or PCI Express) makes it very flexible and adaptable to different test scenarios. These simulators are compatible with specialized software based in RT-LAB, such as eMEGASIM ePHASORSIM, which facilitates the joint simulation of electrical and control systems in different domains, or even HYPERSIM, a new powerful simulation tool. Therefore, this simulator is a versatile tool that allows accurate and detailed simulations.

A.3.1.2 Dolphin Interface

Dolphin interface (DXH510) is a technology used for real-time simulations, as the OPAL-RT simulators, in order to facilitate the co-simulation of complex systems. This interface builds a bridge between different simulators, allowing the synchronization of data between them. In OPAL-RT context, DXH510 is used for integrating real-time

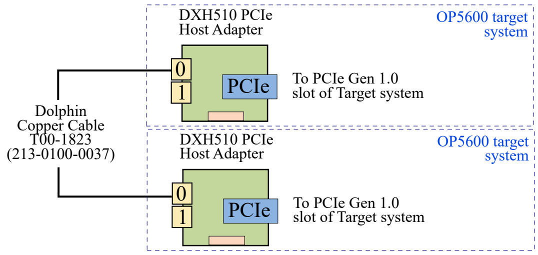

Figure A.10: Connection between the two OP5600 real-time simulator.

control systems with models of electrical power systems. To configure Dolphin, it is important to make the physical connection between both simulators correctly, following the instructions provided in the OPAL-RT manuals. A small scheme of the connection is depicted in Fig. A.10.

A.3.2 Simulation Process

Two OP5600 simulators have been used for simulations, as shown in Figure A.11, controlled by Matlab version 2017a and OPAL RT-LAB version 2019.2.3.176. Each simulator will run a different type of simulation. In the case of the OP5600 slave, the simulation will run on eMEGASIM, and in the case of the master, the simulation will run on ePHASORSIM. Both simulations will be synchronized using the DOLPHIN DXH510 communication cable. As is depicted in Figure A.11 a), to perform any simulation on any of the simulators, it is needed to follow the model structure. The model in each simulator, must include a subsystem called “SM NAME”, where M, besides S indicates that it is the master model, and slave model respectively. From here, the monitoring signals will go to “SC NAME”, where the real-time signals can be monitored. Furthermore, this same system can also be used as a simulation control, sending different set-points to the simulated model, changing parameters in real time. Considering this, a brief explanation of each simulator as well as the interface is performed in this section, to merge both in an unique model of co-simulation, explaining the procedure.

A.3.2.1 eMEGASIM

EMEGASIM is a real time simulator from OPAL-RT Technologies. This simulator is a tool specifically designed for the analysis and simulation of power systems in real time.With the ability to simulate complex electric power systems, including distribution grids, transmission systems and renewable energy generation, eMEGASIM is widely used in research, development and validation of electric power technologies [A.8]. It is important to highlight, that for performing a real-time simulation its mandatory to use a discrete simulation with the POWERGUI block.

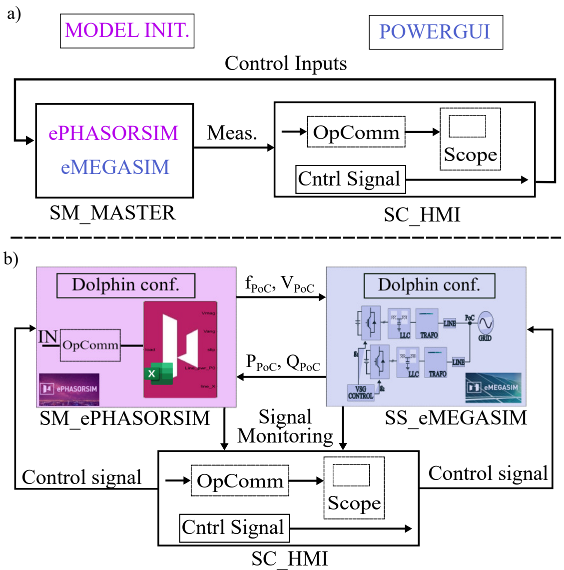

Figure A.11: a) Real-time simulation structure for eMEGASIM or ePHASORSIM, using POWERGUI and Model Initialization blocks respectively. b) Co-simulation structure with a Master subsystem based in ePHASORSIM and a Slave subsystem based in eMEGASIM. Both subsystem will share data through the Dolphin interface. Furthermore, the SC HMI block will monitor some signals, and also it will send some set-points to the simulators.

A.3.2.2 ePHASORSIM

EPHASORSIM is a real-time simulator also developed for OPAL-RT Technologies. This simulator is used for carrying out real-time simulation of electrical power systems based on phasors [A.9]. It allows to model and analyze those system in large-scale, including transmission and distribution lines, as well as including different generation elements. This tool can be crucial in the research and development of different technologies. To perform a simulation in ePHASORSIM, the model of the grid must be included in the ".xls" template with the input and outputs of the system, and a ".raw" file with all the characteristics of the system, and it must be included in the solver RT-LAB block to work (this configuration will depend on the simulator version). The model initialization block is important to include all the simulation characteristics and parameters of both simulations. In Figure A.11 a), a scheme example is shown.

A.3.2.3 Co-Simulation

In order to carry out the co-simulation between the two simulators, specific steps must be followed. First, for the system addressed in this article, the structure depicted in Figure A.11 b) will be followed. In this environment, the master simulator is implemented in ePHASORSIM, which exchanges data with the slave simulator in eMEGASIM through the Dolphin interface, as previously mentioned. Due to both systems are set in parallel, a memory block it is needed at the output of each subsystem to allow a proper simulation. The signals from both systems are monitored by the HMI subsystem, which sends the set-points to both simulators. In order to be able to run the simulation in real time, in addition to the configurations made so far, it is important to transfer the corresponding cluster information file, known as "dishosts.conf", to each of the "etc/dis/" directories of both simulators. This configuration file is used to set some global interconnection properties and the position of each node within the interconnection topology used. It is crucial to use the same file on both simulators and to make sure that the IP addresses used in the file match the IP addresses of the simulators. Once this is done, the simulation can be run following the next steps:

1. Lunch RT-LAB 2019.2.3.176 in admin mode.
2. Check the Target number: PFXXXXXXS01 (OPAL2) and PFXXXXXXS02 (OPAL1) for both simulators.
3. Check the RT-LAB Version 2019.2.3.176 is installed in both targets.
4. Set the Real-time simulation mode to Hardware synchronized and Real-time communication link type to Dolphin under Execution Properties tab.
5. Assign the subsystems SM ePHASORSIM to OPAL2 and SS eMEGASIM to OPAL1. Make sure that XHP mode is enable for both nodes.
6. Load the model in RT-LAB and check the display tab for compilation.
7. Once the model is successfully loaded with no errors, execute the model.

References

[A.1] D. d. Rivero, P. García, C. Blanco, and Navarro-Rodríguez, "Control of aggregated virtual synchronous generators for pv plants considering communication delays," *IEEE Transactions on Industry Applications*, pp. 1–13, 2024.

[A.2] D. Del Rivero, P. G. Fernández, C. Blanco, and Navarro-Rodríguez, "Control of aggregated virtual synchronous generators including communication delay compensation," in *2022 IEEE Energy Conversion Congress and Exposition (ECCE)*, 2022, pp. 1–7.

[A.3] D. del Rivero, S. Singh, P. García, and P. Rodríguez, "Real-time cosimulation of power systems: Integration of emegasim and ephasorsim using opal-rt simulators," in *2024 IEEE 15th International Symposium on Power Electronics for Distributed Generation Systems (PEDG)*, 2024, pp. 1–6.

[A.4] Speedgoat GmbH, *SN3808 Technical Reference Information and Full System Test*, Liebefeld, Switzerland, 2017, prepared for the University of Oviedo.

[A.5] ——, *IO753 Configuration and Testing Information*, Liebefeld, Switzerland, 2021, available on Speedgoat Customer Portal: https://www.speedgoat.com/login.

[A.6] Cisco Systems, Inc., *Cisco Catalyst 2960-Plus Series Switches - Configuration and Installation Guide*, San Jose, CA, USA, 2017.

[A.7] F. Plumier, C. Geuzaine, and T. Van Cutsem, "A multirate approach to combine electromagnetic transients and fundamental-frequency simulations," 07 2013.

[A.8] O.-R. Technologies, "eMEGASIM," Recovered from: https://www.opal-rt.com/products/emegasim/, s.f.

[A.9] ——, "ePHASORsim," Recovered from: https://www.opal-rt.com/products/ephasorsim/, s.f.

Appendix B

Journal Publications

B.1 Control of Aggregated Virtual Synchronous Generators for PV Plants Considering Communication Delays.

6512 IEEE TRANSACTIONS ON INDUSTRY APPLICATIONS, VOL. 60, NO. 4, JULY/AUGUST 2024

Control of Aggregated Virtual Synchronous Generators for PV Plants Considering Communication Delays

Daniel del Rivero, *Graduate Student Member, IEEE*, Pablo García, *Senior Member, IEEE*, Cristian Blanco, *Senior Member, IEEE*, and Ángel Navarro-Rodríguez, *Member, IEEE*

***Abstract*—In this paper, a new method for the delay compensation when using an aggregation of virtual synchronous generators is proposed. Lack of inertia in power converters can potentially provoke stability issues that can be mitigated by the use of virtual inertia techniques. Among those, the Virtual Synchronous Generator (VSG) concept has received strong impulse in the last years. This paper is focused on the idea of using the distributed VSG concept in a renewable power plant, in which a single Synchronous Central Angle Controller (SCAC) is used for the power control exchange at the Point of Connection (PoC), while distribution control units are employed for the local inverter control. This idea, already discussed in the literature, is in here extended to consider the implementation on industrial string-level commercial power converters, recalling the importance of accessible measurements and communication delays. In order to validate the proposal, firstly communication delays are measured and modelled. Following, simulations with different SCAC operating modes are conducted, and finally experimental results validation of different operation modes with commercial converters are presented.**

***Index Terms*—Communication delay, real-time simulation, smith predictor, virtual synchronous generator.**

I. Introduction

THE world's power generation is currently moving toward a more sustainable and environmentally friendly approach. This is due to the usage of Distributed Energy Generation (DEG) facilities based on Renewable Energy Sources (RES) has replaced fossil fuels because of their significant environmental cost (greenhouse emissions, lack of source material, etc.). Additionally, the most widely used RES, like photovoltaic (PV) and wind power, are becoming more affordable, offering improved Levelized Cost of Electricity (LCOE) indices [1].

However, the inclusion of this kind of generation systems provokes a weaker power system due to the inertia reduction currently provided by synchronous generators with rotating mass, to a power converter-based system with little to no inertia [1], [2], [3].

Since power converters lack both inertia and damping, this problem could affect the power grid's stability. It is currently understood that grid-forming and grid-supporting services must be taken into account in the design when significant penetration of DEG, with aggregated sizes comparable to traditional power plants [4], [5], [6]. This is where the Virtual Synchronous Generator (VSG) approach arises. For the power electronics-based DEG/RES units, this control method enables the emulation of the dynamic characteristics of a real or arbitrary Synchronous Generator (SG) [2], [3].

Using Energy Storage Systems (ESS), power converters, and an appropriate control mechanism, the virtual inertia concept is applied to provide a specific amount of inertia for supplied (usually in the range of ms to a few dozen seconds). In this way, VSG establishes the framework for later widespread application in RES systems without jeopardizing system stability. Several VSG approaches have been explored and implemented [1], [2], [3], [4], [5], [6], [7], [8], [9], [10], [11]. Two alternative implementations exist. A first approach refers to those methods rooted in mathematical equations (e.g., synchronverters [8], [9], Kawasaki Heavy Industries [10], VISMA and IEPE topologies [9]). A second group relies on swing equations (e.g., Ise Lab's topology [11], the Synchronous Power Controller [5], [12], Virtual Oscillator Control [9]). The Synchronous Power Controller (SPC) is a prevalent topology for virtual inertia implementation, synthesizing the electromechanical and electrical characteristics of a SG. This approach regulates inverter frequency by employing virtual inertia and damping factors to counteract grid frequency disturbances.

SPC operates with inner current and outer voltage control loops, using a virtual admittance to establish a cascaded control loop. SPC is typically integrated into the local control of each inverter, offering frequency and voltage support at local PV collector connection points [5]. However, for PV plants,

Manuscript received 12 September 2023; revised 25 January 2024; accepted 26 February 2024. Date of publication 13 March 2024; date of current version 22 July 2024. Paper 2023-SECSC-1316.R1, presented at the 2022 IEEE Energy Conversion Congress and Exposition, Detroit, MI, USA, Oct. 09–13, and approved for publication in the IEEE Transactions on Industry Applications by the Renewable and Sustainable Energy Conversion Systems Committee of the IEEE Industry Applications Society [DOI:10.1109/ECCE50734.2022.9947466]. This work was supported in part by European Union's H2020 Research and Innovation Program under Grant 864459 (UE-19- TALENT-864459), in part by the Spanish Ministry of Innovation and Science under Grant CI-MCINN-23-PID2022-139479OB-C22 and Grant MCINN-22- TED2021-129796B-C21, and in part by the Principality of Asturias, FICYT, FEDER Funds under Grant SV-PA-21-AYUD/2021/57546. *(Corresponding author: Daniel del Rivero.)*

The authors are with the Department Electrical Engineering, University of Oviedo, 33203 Gijón, Spain (e-mail: riverodaniel@uniovi.es; garciafpablo@uniovi.es; blancocristian@uniovi.es; navarroangel@uniovi.es).

Color versions of one or more figures in this article are available at https://doi.org/10.1109/TIA.2024.3377169.

Digital Object Identifier 10.1109/TIA.2024.3377169

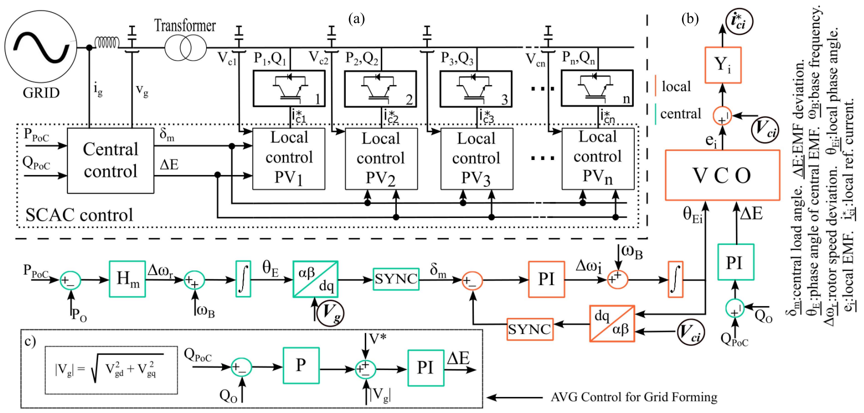

Fig. 1. (a) SCAC scheme for n-converters. (b) Simplified Local control scheme. The light green control loop is implemented in the central controller. The orange control loop is implemented in the local controller [13]. (c) Added AVG Control for grid forming capabilities [2].

grid support is ideally expected at the Point of Connection (PoC). With that motivation, a modification of the SPC designed to provide grid support at the PoC has been proposed, the Synchronous Central Angle Controller (SCAC) [4].

The SCAC technique suggests simultaneously driving several converters, emulating a unique SG in the PoC, giving rise to an aggregated VSG. This concept presents the idea of a single virtual rotor, emulated at the PoC, where the electromechanical model of the SG is considered (central control architecture). Hence, the SG inertia and damping response are emulated at the PoC. Regardless of the distances between the local converters, this control structure enables the system operator at the PoC to control the exchange of power (both active and reactive), allowing each converter to distribute the energy to be delivered under different operating modes (power and frequency support) on their own. A more detailed explanation can be found in the literature, where both, central and local control systems are detailed [7].

A concept for a structure with N converters is shown in Fig. 1, where a central controller handles the local controller references of each converter. In this system, it is possible to independently control the exchanged active and reactive power, as indicated in the dynamic model and control loops. In Fig. 1(a), a comprehensive connection diagram illustrates the interconnection of various converters. In Fig. 1(b), the control block diagram is depicted, with the global controller in green and the local controller for each power converter in orange. Each power converter requires a replicated local controller tailored to its specific characteristics. Further explanations for these blocks are provided below. The key control system is implemented in the central controller, where the inertia is emulated by the swing equation of a virtual synchronous generator (see (1) and (2)).

$$\frac{\mathrm{d}\delta_{sm}}{\mathrm{d}t} = \Delta\omega_r \tag{1}$$

$$J\frac{\mathrm{d}\Delta\omega_r}{\mathrm{d}t} = \frac{P_m - P_e}{\omega_B|} - D\Delta\omega_r = \frac{\Delta P}{\omega_B} - D\Delta\omega_r \tag{2}$$

where δ_{sm} is the power angle, $\Delta\omega_r$ is the angular speed deviation of the rotor, J is the SG inertia, P_m is the mechanical power, P_e is the electrical power, D is the damping constant and ω_B is the base frequency. In [5], the electromechanical control has been studied, and a frequency analysis has been taken into account to obtain the power loop control H_M (3). k_p, k_i, and K_D have been designed, according to the required inertia constant and frequency droop slope, respectively.

$$H_M = \frac{\Delta\omega_r}{\Delta_P} = \frac{k_p + k_i s}{s + k_D}\begin{cases} k_p = \frac{\omega_n^2}{P_{\max}} \\ k_D = \frac{\omega_n^2 D}{P_{\max}} \\ k_i = \frac{2P_{\max}\xi\omega_n - \omega_n^2 D}{P_{\max}^2} \\ w_n = \sqrt{\frac{P_{\max}\omega_B}{2HS_N}} \\ H = \frac{J\omega_B^2}{2S_N} \end{cases} \tag{3}$$

In (3), H is the inertia constant, $P_{\max}$ is the maximum active power of the converter, S_N is the nominal power, ω_n is the natural frequency and ξ is the damping factor. In this control system, the dynamic response is mainly supported by the inertia, while the frequency droop supports the steady state behavior. Based on the analysis presented in [4], [5], (4) shows the relationship between ΔP_o and the frequency change $\Delta\omega_g$.

$$\frac{\Delta P_o}{\Delta\omega_g} = \frac{S_N}{\omega_B D_P} \tag{4}$$

The internal time-domain variables and control loops (current/voltage) of the converter are presumed to be accessible by this control system, though. However only active and reactive power set-points are normally externally accessible for commercial converters that have already been installed, typically via a communications link. So, a modification of this control is required for a wider applicability. Due to its wide adoption as the go-to solution in power plants, MODBUS TCP is proposed as the communication system [14].

In the following sections, the control system architecture is modified in accordance with the prior motivation using a communication-based implementation. In order to perform that implementation, the system communication delay is measured, the integration of the Smith predictor (SP) in the system is explained, and also a small stability analysis is performed. For validating the model, several working operations will be tested in local simulation and in real-time operation with commercial converters. Those working modes are: I) Active and reactive injection. II) Power support operation, taking into account grid operator requests. III) Frequency support operation by power management depending on frequency variations. IV) Phase-jump in the grid voltage performance. V) Island operation. First, a local simulation is used to evaluate the control system, and following a real-time hardware controller with commercial converters is employed for the first three cases. The main article contribution is the proposal of using a distributed virtual synchronous generator in an industrial environment considering communication delays and their compensation.

This paper is based on the paper in [13] by the same authors, with extended analysis and results. The added content includes a stability analysis of the system considering the delay impact. Regarding the results, a variety of different operating conditions is included, considering Hardware-In-the-Loop (HIL) and Power-Hardware-In-the-Loop (PHIL) validation schemes.

II. Proposed Control System

Most of the VSG techniques integrate their controllers into each converter's firmware as an add-on. However, as it was already indicated, the SCAC technique requires having access to different control actions and sensor readings (current, voltages). This paper proposes a new control structure that can be applied to already-existing commercial converters, that only requires access to active and reactive powers set-points and measurements obtained by MODBUS TCP communications and the dictionary variables included in the SunSpec DER specification [15]. The method does not require any additional measuring elements, such as extra voltage and current sensors, which would make implementation more complicated and expensive. Instead, it relies on the RMS voltage, frequency, and active and reactive power communication-based readings from each converter. Therefore, this approach is an appealing solution for the standardization of the VSG concept for a massive implementation in future and existing DEG's. However, it is important to acknowledge certain limitations when comparing the external implementation of the VSG concept in power converters to its internal counterpart. The external implementation focuses solely on the fundamental component for signal reconstruction in the time domain. Additionally, achieving a rapid response is constrained by communication delays and the necessary time for reconstruction, which

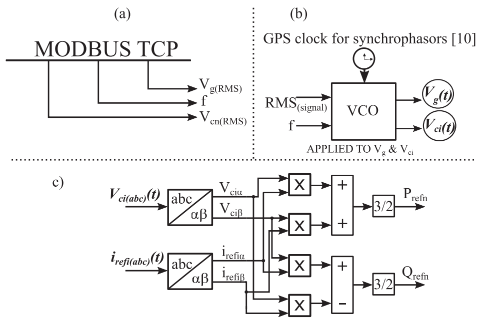

Fig. 2. (a) MODBUS TCP frequency and RMS voltage. (b) Instantaneous values from the RMS voltage, frequency, and clock signal obtained by a VCO (Voltage Controller Oscillator) [16]. (c) Active and reactive reference power calculation [13].

entails one fundamental cycle, taking into account RMS values, and it is feasible only within the internal control of the power converter.

For the application of this concept, instantaneous voltage signals for each converter and PoC are built from the RMS values as shown in Fig. 2(a) and (b). These signals are employed in the control system's feedback variables (as a replacement of bold and circled variables in the original scheme shown in Fig. 1(b). At the same time, as it was already indicated, commercial converters typically accept power (active/reactive) setpoints. However, for the implementation of the VSG concept, current commands computed from the control system are needed instead. This proposal derives the power references from the current references and the reconstructed voltage signals, as shown in Fig. 2 in the $\alpha - \beta$ reference frame.

III. Delay Compensation

Each converter control unit communicates with the central controller in the proposed renewable energy plant application using MODBUS TCP. The communication between the central controller and each of the distributed units may experience some delay since MODBUS TCP is not a real-time protocol, the delay depending on the number of components in the bus and the distance. The effectiveness of the closed-loop system is compromised by these delays, which have a direct impact on the control instructions transmitted from the central controller and the provided feedback information.

Considering that MODBUS TCP is not a real-time protocol, it is expected a variable delay distribution. Accordingly, the delay statistical distribution is modeled in this section and a compensating mechanism is discussed.

A. Delay Modelling

In the literature, there are several proposals to model random delays. One of them uses the Markov chain [17], [18] as its foundation. A stochastic model called a Markov chain discretely represents certain potential states or events (in this case delays).

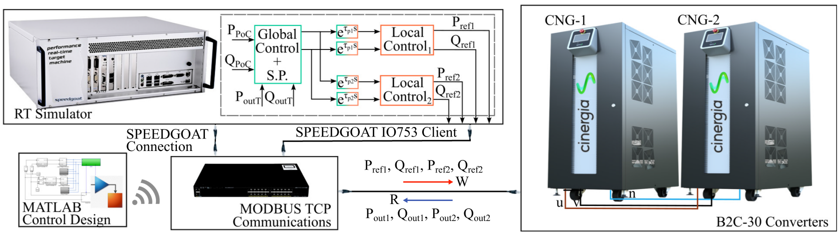

Fig. 3. Setup for HIL and PIL experimental tests. The control design is made on Matlab and executed in the real-time Speedgoat target. The converters are controlled by writing/reading published MODBUS/TCP variables [13].

The probability of those potential outcomes is solely dependent on the outcome of the prior event. For this paper, to model the communication latency in the local network where the tests are going to be performed, the communication delays in a link using MODBUS TCP protocol are measured. A 30 kW bidirectional dc/dc converter (CNG) from Cinergia SL, similar to the one in Fig. 3, was employed as the PHIL system. This power supply features different emulation units, including batteries and solar panels, and may work as a voltage, current, and power source. Two of these power sources will be used in Section IV for the experimental validation. For performing the measurements, a HIL system (Speedgoat target machine) is used to act as a communication gateway between the converters and the control system in a real-time simulation. These components are also displayed in Fig. 3.

The delay measurement procedure is as follows: a digital square reference signal of 0.25 Hz has been supplied simultaneously to the current converter set-point, so it can be used as a trigger signal in an external scope that also captures the output current response. Both signals can be observed in Fig. 4(a). The delay distribution varies between a much wider range, as it can be seen in Fig. 4(b), with a mean value of around 68 ms and a mode of 45 ms. In Fig. 4(c), the time variation of the delay during all the experiments can be easily appreciated. The time variation of the delay throughout the entire experiment is seen in Fig. 4(c). For the delay modelling, a Poisson distribution with the form (5) is chosen, as proposed in queuing theory delay models for communication networks [19], [20]. The Poisson distribution is obtained with the delay evolution from Fig. 4(b), with 795 number of events (k) and the mean (λ) value of 68 ms. That distribution is used as delay estimation for compensating the delays in the SP loop. For the real communication delay, the measured data is used.

$$f(k,\lambda) = Pr(X = k) = \frac{\lambda^k e^{-\lambda}}{k!}; \lambda > 0; k = 0, 1, 2 \ldots \quad (5)$$

By using the Poisson distribution, the distribution from Fig. 4(d) is obtained.

B. Delay Compensation. The Smith Predictor

Various methods for delay compensation have been explored, including the study of the Smith predictor (SP) and its modifications [21], [22], the investigation of the Scattering transformation [23], [24], the examination of the linear predictor [25], [26], and the consideration of predictive control [27], [28], among other strategies. The Scattering transformation serves as a method to passivate the control system, mitigating delay effects and contributing to stabilization. Similarly, the linear predictor, a commonly used model-free scheme, employs the linear extrapolation concept to predict future control variables. However, for the purposes of this paper, the SP has been chosen due to its simplicity and reliable operation [21]. Ongoing research in this field aims to identify alternative delay compensation methods more suitable for the stochastic nature of communication-based delays. The SP achieves the removal of the delay component from the system's control loop by incorporating a model of the

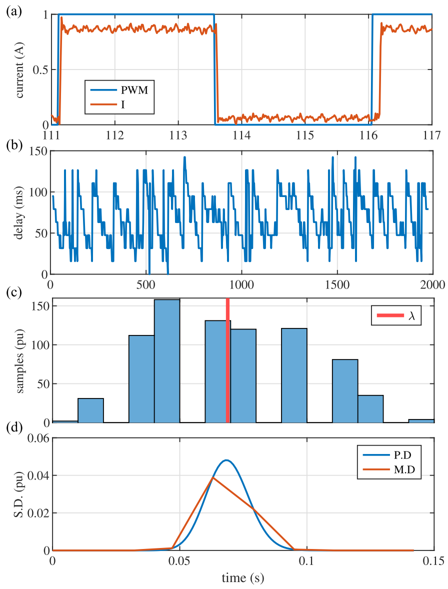

Fig. 4. (a) Instantaneous delay measurement in the lab (PWM is the sent reference signal and I is the actual current the converter develops). (b) Time variation of delay. (c) Delay histogram from experimental tests. (d) Probability density function of the measured communication delay (M.D) in comparison to Poisson distribution (P.D) with λ of 68 ms.

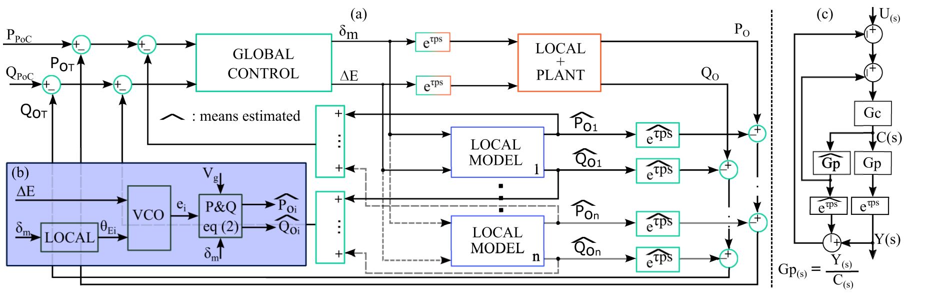

Fig. 5. (a) Global SP architecture for n-converters (light green block for global control and orange for local control) [17]. (b) Local model for each converter (blue blocks) emulated in the global controller. (c) Basic Smith predictor structure.

delay structure, along with a relatively precise modeling of the system plant [22].

In the SCAC system, the delay is presented in the control actions sent to the local converters. The SP compensates for the plant delay, through a plant model ($\widehat{G_p}$) and an estimated delay ($\widehat{e^{tps}}$). The plant model shall be the one between the control actions (δ_m, ΔE) and the output (P_{out}, Q_{out}) (see Fig. 5(a). Unfortunately, finding the transfer model for the proposed communications-based control system is not an easy task. The suggested approach is to run a replica of the local control for each converter in the central controller. As many replicas of the local control will be used as there are SCAC converters. It should also be clarified that the local control structure of each of the converters is the same in all of them, simply changing the value of the instantaneous values of each converter. Fig. 5(c) shows the simulated plant for SP which is considered as the affected plant by the delay. Besides, δ_m and e_i outputs of the emulated local model are used for computing the output power using the power (6). Finally, the error between the predicted active and reactive power and the values given by the local control units is used to compensate for the delay (see Fig. 5).

$$P_i = \frac{E_i V_i}{X_i}\sin(\delta_m);\; Q_i = \frac{V_i}{X_i}(E\cos(\delta_m) - V_g) \quad (6)$$

In order to demonstrate and validate the operation of the SP, the limit stability constant delay is firstly considered while the compensation method is applied. The system used for applying the delay with SP is the one shown in Fig. 5, and without compensation the one shown in Fig. 1.

To clarify this point, Fig. 6 shows the difference in behavior when using or not the SP under the limit stability delay condition. As it can be seen, by setting the limit delay (75 ms), the response with (d_{LSP}) and without SP (d_{LNSP}) are clearly different, where the additional overshot created by the delay is mostly removed by applying the SP.

It is also included a larger delay ($d = 80$ ms) to illustrate the instability condition above a certain delay level. In this case the unstable case is scaled for representation purposes. In the next subsection, a concise stability analysis is undertaken

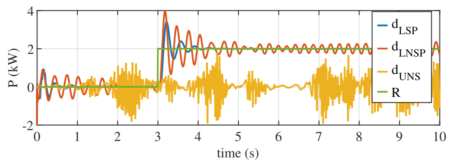

Fig. 6. System step response with a constant communication delay of $d_3 = 75$ ms (which is the stable limit regarding the delay), with (d_{LSP}) and without delay compensation (d_{LNSP}). Also, the unstable case (d_{UNS}) is represented for a case of $d_2 = 80$ ms. For representation, the unstable power is corrected by a factor of 0.005. R is the reference signal.

to complement the explanation and validate the importance of implementing a delay compensation method.

C. Stability Analysis

In this section, a comparative stability study is conducted, considering both the system without considering communication delays and those that include them, leading to the system instability. This analysis is visually presented in Fig. 7, illustrating Bode diagrams for the different enumerated cases.

The stability response will be compared in two different scenarios: one where the system is operated without communication delays ($d_1 = 0$ ms) and another where communication delay is introduced at the stability boundary ($d_2 = 75$ ms). Those scenarios are introduced in Fig. 7, where Bode diagrams are depicted. Initially, the Bode diagram without communication delays was approximated using the Frequency Response Function (FRF) method, a frequency-based measurement function. It consists in a frequency-based measurement function that expresses the frequency domain relationship between an input and output of a system [29]. In the Fig. 7, just the case without delay is included with this method. However, considering that the response at low frequencies closely resembles the transfer function obtained from the system in Fig. 8 (due to the inertia control system being slow and the rest being fast at low frequencies), the latter has been employed for the subsequent stability tests. The three first cases were analysed in the Bode by using the system from Fig. 8.

TABLE I
STABILITY VALUES FOR THE DIFFERENT CASES FROM FIG. 9

Case			GM	PM	ξ	Case			GM	PM	ξ	Case			GM	PM	ξ
A)		$base$	inf	144	0.99	B)		$base_d$	1	0.04	0.35	C)		$base_{SP}$	6.86	97.7	0.97
	a)	H=15	inf	144	0.99		a)	**H=15**	**0.43**	**28.7**	**0,48**		a)	**H=15**	**7.9**	**104**	**0.97**
		H=5	**inf**	**144.5**	**0.99**			H=5	inf	-32.9	0.14			H=5	5.15	87.8	0.95
	b)	τ=0.7	inf	128.3	0.7		b)	**τ=0.7**	**1.62**	**23.26**	**0.43**		b)	τ=0.7	7.93	78.9	0.71
		τ=2	inf	165.7	1			τ=2	0.35	-56.8	0.02			τ=2	4.36	132	0.96
	c)	K_p = 0.7	inf	141	0.99		c)	K_p = 0.7	0.83	-8.17	0.31		c)	K_p = 0.7	6.4	89.8	0.96
		K_p = 1	inf	141	0.99			K_p = 1	0.85	-7.03	0.31			K_p = 1	6.47	91.1	0.96

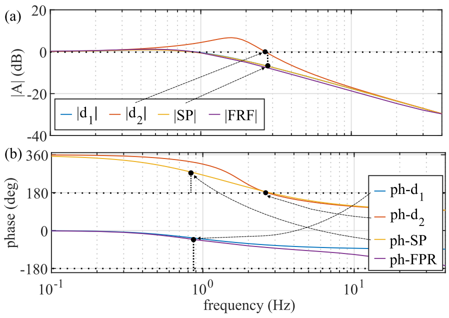

Fig. 7. Bode diagram of the SCAC system considering no delay ($d_1 = 0$ ms), the limit delay which makes unstable the system ($d_2 = 75$ ms), and the same delay but compensated with the SP method (SP). Furthermore the Bode diagram extracted by FRF method is also presented (just for non delay case). (a) The amplitude Bode is presented. (b) Shows the phase evolution for the different cases, including the PMs. Notice the low-frequency ranges of the system (x-axis) due to the emulated system inertia (10 s). Table I shows the stability values of these cases.

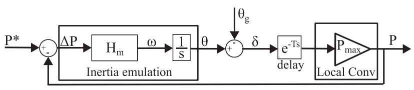

Fig. 8. Simplified model of SCAC with one converter.

As observed in the Bode diagram of Fig. 7 and the data presented in Table I, system stability is evident in the absence of communication delays, with a Phase Margin (PM) of 143.44 and an infinite Gain Margin (GM). When the limiting delay (d_2) is introduced, the system is positioned at the stability boundary, featuring a GM of 1.001 and a PM of 0.0038. Additionally, upon the introduction of the SP, the system regains its stability margin, displaying a GM of 6.86 and a PM of 97.7.

Taking advantage of the stability analysis conducted in the baseline case, a brief assessment of the system's stability sensitivity has been carried out. Critical parameters such as inertia (H), damping (τ), and droop slope (K_p) were varied across three different scenarios: A) without delay, B) with a limiting delay, and C) limiting delay but employing SP as a compensation method. These variations are reflected in Fig. 9. Furthermore, the aim of this analysis is to emphasize the significance of certain elements in the control system, demonstrating how they influence the variation of stability margins.

Leveraging Fig. 9 and Table I, it can be observed that, in the case A) without delays, the modification of H values a) causes the system to become more underdamped but faster as its value decreases. Increasing the value of τ b) results in a more overdamped and slower system, while the variation of K_p c) mainly affect to the position of the zeros, moving the root locus to the right, as K_p is increasing. In case B), the system behaves similarly, but with eigenvalues shifted to the right. It is even noticeable that, by increasing H and decreasing τ, the dominant poles can lead the system to the stability margin, as detailed in Table I. In case C), after delay compensation with SP, the significant eigenvalues return to the negative semi-axis, ensuring system stability.

IV. RESULTS

In this section some results are presented to validate the proposed compensation method, presenting different working modes of the system. Those operations are tested in both local Simulink simulations and real-time experimental proofs through Speedgoat emulator. Real-time tests are based on Fig. 3, where two 30 kW bidirectional dc/dc converters (CNG) from Cinergia S.L are used. In this case, CNG-2 has three strings working as power sources to emulate the power demand from the control system, which will receive the commands from the simulation (P_{ref1}, Q_{ref1}, P_{ref2}, Q_{ref2}). Those setpoints are sent and written in CNG-2 through MODBUS TCP. The energy computed by the control system will be obtained from CNG-1, which works as a battery emulator in each string, which is running in battery emulation mode to replicate the SCAC idea. As it was stated in Section III, a HIL system is used for real-time simulation.

For the case of communication delays between the central controller and the local units, the same variable time delay used in the local simulations (computed in Section III) are used for experimental tests. However, due to the CNG converter's internal delay in the processing of the power references and integration windows used for the calculation of the active and reactive power, additional delays are added to the control system (20 ms for active power and 400 ms for reactive power). These delays are also included in the model used by the Smith predictor to achieve better results.

This is a critical step, as the Smith predictor will also tackle the additional delays present in a real implementation.

For these tests, grid, and VSG models are taken from [4], where the SCAC idea was first published. In this case, the model includes three DEGs connected to a grid and considers a battery locally connected per converter, which is the element that provides/absorbs energy for frequency support. In this case,

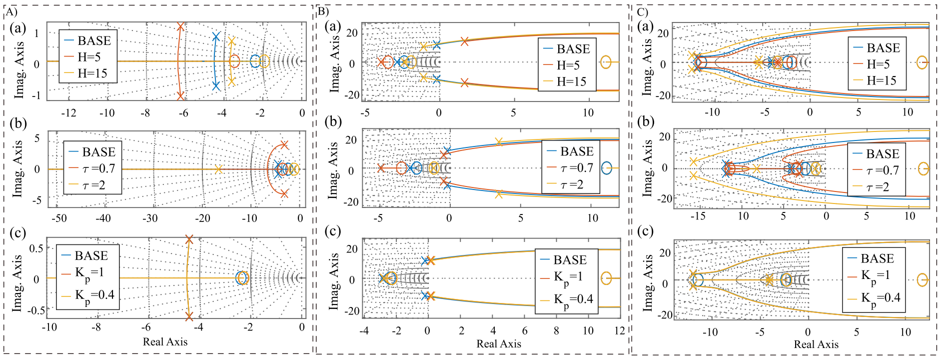

Fig. 9. Root locus of control system. Base case parameters shown in Table II. (a) Z-P map without delay. (b) Z-P map with delay. (c) Z-P map with SP compensation delay. In the first row of the figure (a), the inertia (H) is varied. In (b) the damping (τ), and in (c) the droop slope (K_p). In Table I the improved values are bold.

TABLE II
SCAC Parameters and Set-Points for the Simulation

Variable	$H\ (s)$	τ	K_p	$Sn\ (VA)$	$V_g\ (V)$
Value	10	0.98	0.1	6000	400
Variable	$f_g\ (Hz)$	$R_v\ (\Omega)$	$X_v\ (\Omega)$	$P_{set}\ (W)$	$Q_{set}\ (Var)$
Value	50	8	0.48	4000	2000

feeder impedance is considered, demonstrating that the system could work in a real implementation with real feeders.

Fig. 10 shows an overview of the different tests that are going to be evaluated, showing several operation modes to be validated. Going from a simple active and reactive power reference tracking to a power support operation mode, depending on the grid operator requirements modifying the power exchange with the grid. Besides frequency support capability, by injecting/absorbing energy through an ESS, validating the disturbance rejection capability, which is one of the main purposes of the system. Also the phase-jump reaction of the system and the islanding mode operation are analysed in this paper, to show other extra operations of the system. The cases I, II and III can be seen in Fig. 11, but in terms of power signals in the form of a complete simulation. Fig. 11(a) shows I, II, and III working modes in terms of active power. Fig. 11(b) depicts the behavior in Case I, injecting the required power by the global controller. Fig. 11(c), depicts Case II, for active power management. Besides, Fig. 11(d) and (e) show Case III, which is the injected power when a frequency drop appears in the grid, trying to reduce the frequency variation. These working operations will be explained in more detail in the following subsections. Worth noting that power is oddly shared among the three converters in the next section, providing a distribution shown in Fig. 12, for each DEG. Simulation parameters are given in Table II.

Previous simulation is performed by using an ideal grid. However, in order to validate and demonstrate how the SCAC system works, the following simulations will be performed by using a weak grid formed by a simple synchronous generator (with real frequency variations), with a limited power (300 kW) and inertia (0.116 kgm^2). In these simulations, the five cases from Fig. 10 are validated: I) active and reactive power injection, II) supporting frequency changes, III) grid operator active power reference tracking, IV) phase angle jump and V) islanding operation.

A. Case I

Considering what is accounted in Figs. 10(b) and 11, active and reactive power setpoints are established in order to control the power exchange with the grid. This principle is the basis for the other two working modes, showing how the SCAC can manage the required power by the global controller. This operation is tested by a simple local simulation, and also by a real-time simulation. Besides, these power injections are varied by adjusting the virtual admittance in control as Fig. 12 shows, where the unit admittance is divided in 3, and it varies during time.

1) Local Simulation: As it can be seen in Fig. 13(a), the power setpoint is reached, sharing the energy among the DEGs, regarding the power distribution between the DEGs shown in Fig. 12. The same happens with the reactive power in b).

2) Real-Time Experimental Test: As it was aforementioned, the control system is tested in real-time by using the Speedgoat simulator and CNG converters. The experimental results are presented in Fig. 14. As it can be seen active and reactive power are tracked perfectly, quite similar to local results. It is important to note that there is a different delay between active and reactive power, which has to do with the integration window from each variable in the power converter used in the HIL system [13]. In case of c), the different steps that appear in the read power are directly the delay of the integration window for active power. Nevertheless, those delays are tackled by the Smith predictor making the system controllable and stable. The difference in the ripple between the local simulation and the real-time is because

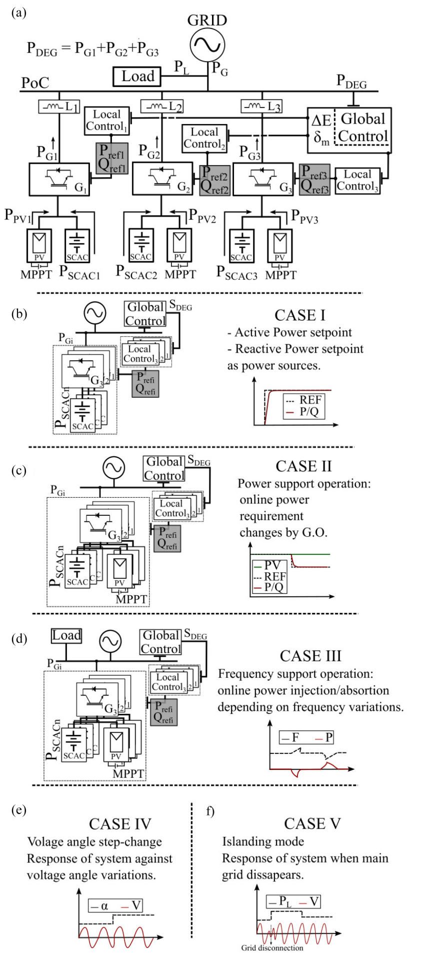

Fig. 10. (a) Power system scheme with three DEGs, showing global and local controllers, battery (SCAC) and PV panels. (b) Working mode I: Active and reactive power setpoints by each DEG, controlled by the SCAC. (c) Working mode II: Power support operation, taking into account grid operator requests. (d) Working mode III: Frequency support operation by power management depending on frequency variations. (e) Working mode IV: Voltage angle step-change. (f) Working mode V: Islanding mode.

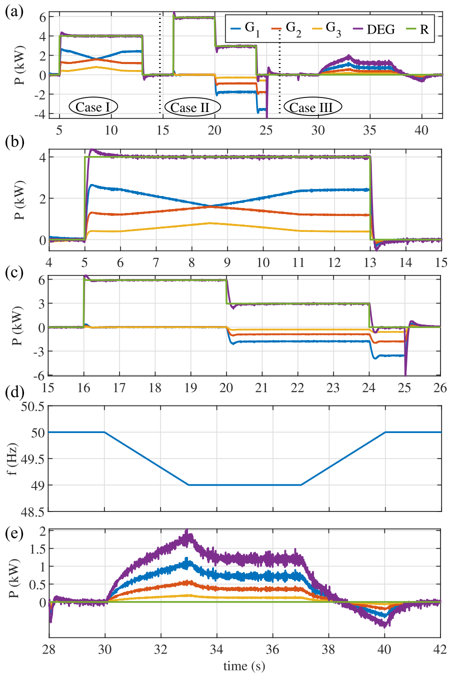

Fig. 11. (a) Active power management for all working modes in each DEG, taking into account the power-sharing between them. Legend G_1 is the first power converter, G_2 is the second power converter, G_3 is the third power converter, DEG is the total power injected by the power plant and R is the power reference. Case I shows the Active and reactive power setpoints by each generator, controlled by the SCAC. Case II shows the power support operation. Case III shows the frequency of support operation. (b) Zoom of case I for active power injection. (c) Zoom of Case II for active power management. (d) Grid frequency variation. (e) Zoom of Case III for Battery power injection for compensating frequency change.

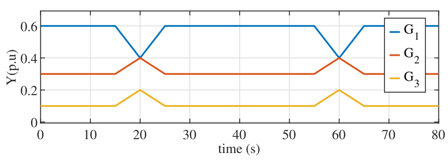

Fig. 12. Virtual admittance variation for Case I and Case II from this section, in order to modify the output power of each converter. G_1, G_2 and G_3 is the designation of each power converter, as in Fig. 10.

the signals read by MODBUS TCP do not have the ripple data. Although the power with ripple is sent, the converter used for the experimental tests filters the component.

B. Case II

This case aims to demonstrate the main operation mode of the SCAC system. As it was above-mentioned, SCAC system adds virtual inertia capabilities, helping to reduce any frequency disturbance in the grid. Two frequency variations (see Fig. 15(a)) are induced by forcing some abrupt load changes (8.5 kW at 12 and −12 kW 18 s) to observe the dynamic behavior of the control system.

1) Local Simulation: In Fig. 15, the response of the system is demonstrated, when a frequency variation is forced due to

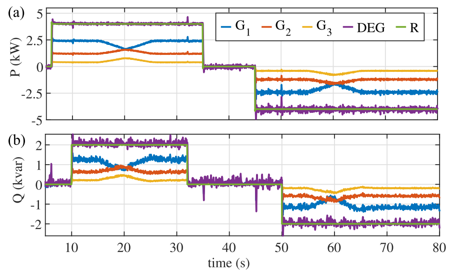

Fig. 13. Simulation validation: (a) Active power reference tracking injected to the grid, taking into account the power-sharing between DEGs. (b) Reactive power reference tracking injected to the grid, taking into account the power-sharing between DEGs. G_1, G_2 and G_3 is the designation of each power converter. DEG is the power developed by the power plant, as Fig. 10 shows. R is the reference power.

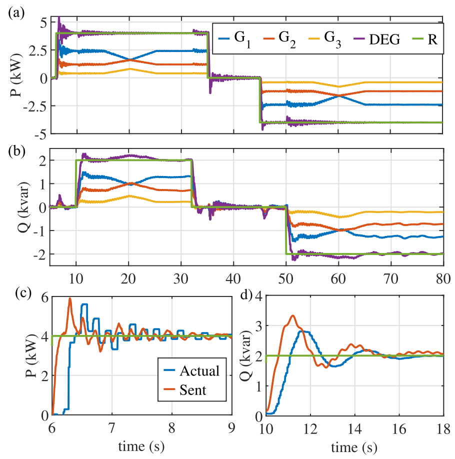

Fig. 14. Experimental validation: (a) Active power command, total power injected to grid and power injected by each converter. (b) Reactive power injected to the grid, showing the command and the actual reactive power. The same legends as Fig. 13 are used in this plot. (c) and (d) Zoomed active and reactive power values and sent references. $Actual$ is the power read by MODBUS TCP. $Sent$ is the power sent by MODBUS TCP to the converter.

a load-step change. Fig. 15(a) shows the frequency variation by using the SCAC system connected to the grid (showing the frequency with and without SCAC system). With SCAC system, the frequencies that appears are for two different rated power of the SCAC system. So frequency is forced to change at 12 s. In case of using the SCAC system, the ESS will inject active power (Fig. 13(a)) to the system in order to help the grid to increase its frequency, as it can be seen in b). On the other hand, if a suddenly frequency increase appears, as it can be seen at 18 s, the ESS-SCAC will absorb power from the system to decrease the frequency. Therefore, the power injection/absorption by the

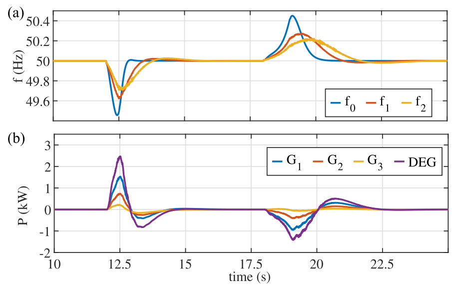

Fig. 15. Simulation: (a) Frequency variation of a weak grid due to a power change demand (with and without SCAC), modifying the installed power in the power plant. The higher power the lower frequency variation (f_0 is for the case without SCAC, f_1 is for the case with SCAC and $S_n = 6$ kVA, and f_2 is for the case with SCAC and $S_n = 10$ kVA. (b) Power injected by each DEG, to mitigate the frequency variation from the case f_1 of b). G_1, G_2 and G_3 are the designations of each power converter and DEG is the power of the total power plant, as Fig. 10 shows.

SCAC system will depend on the inertia emulated and also the power installed in their ESS. It can be concluded from [13], the more power installed in the system, the lower the frequency variation will be.

2) Real-Time Experimental Test: In the case of real-time simulation, the SCAC system has been emulated by using the battery module from CNG. Those results are presented in Fig. 16. As it can be seen it works as the local simulation, when a frequency dip appears (Fig. 18(a)), DEGs inject power trying to reduce the frequency variation, respecting the power-sharing between converters (Fig. 18(b)). In this case, as a battery emulator is used, the SOC state of each battery is presented in c), showing how the battery is charged or discharged.

C. Case III

This operation mode is controlled by the DEG operator (central controller), in order to reduce or increase the power injected by the power plant, depending on the grid requirements, as long as the ratings of the power plant are not exceeded. This means that if a power change is requested by the grid operator, the power injected will vary, taking into account that the RES are working normally at their maximum power point (MPP), and the excess or lack of power regarding the new power command will be managed by the SCAC-ESS. Once the grid operator's setpoint returns to normal state, the storage system would stop absorbing energy, returning to zero power if there are not frequency changes. Another possible scenario is that the storage system reaches its maximum capacity and it cannot absorb more energy. This would mean that the PV string has to be taken out of its maximum power point to comply with the conditions of the grid operator.

1) Local Simulation: The aforementioned effect can be observed in Fig. 17, where at t = 40 s, grid operator active power reference varies (P_{DEG}, as shown in Fig. 15(a), forcing to inject less power from the DEG system. In this situation, either an

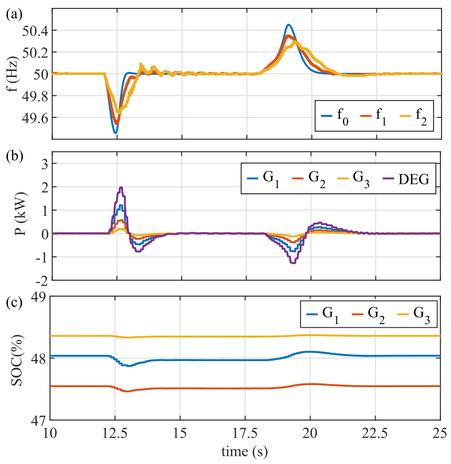

Fig. 16. Experimental validation: (a) Frequency variation of a weak grid due to a power change demand (with and without SCAC), modifying the installed power in the power plant. The higher power the lower frequency variation (f_0 is for the case without SCAC, f_1 is for the case with SCAC and $S_n = 6$ kVA, and f_2 is for the case with SCAC and $S_n = 10$ kVA. The same legends than Fig. 15 are used in this plot. (b) Power injected by each DEG, to mitigate the frequency variation from the case f_1 of (a). The same legends as Fig. 15 are used in this plot. (c) State of Charge (SOC) of each ESS-SCAC emulated in CNG. The same legends than Fig. 15 are used in this plot. For SOC information, colors match.

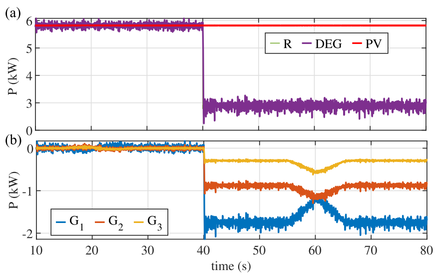

Fig. 17. Simulation: (a) Power injected to the grid. At 40 s, the required grid power changes to 2.4 kW. R is the power reference, DEG is the total power injected by the power plant, and PV is the power developed by the PV array. (b) ESS-SCAC power absorption to obtain the required 2.4 kW power demand by the PoC. G_1, G_2 and G_3 is the designation of each power converter, as Fig. 10 shows.

inverter curtailment or a charging of the ESS is required. In this case, the power set-point has been reduced by 2.4 kW, and as the PV system is working at its MPP, the ESS-SCAC will absorb the energy difference. However, in case the ESS-SCAC reach their maximum capacity, the PV arrays will have to be moved out of their maximum power point, in order to comply with TSO requirements.

2) Real-Time Experimental Test: The same results are obtained in real-time simulations as can be seen in Fig. 18. When

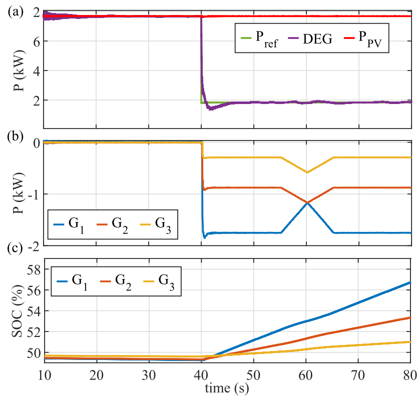

Fig. 18. Experimental validation: (a) Power injected to the grid, where at 40 s, the power required by the grid changes to 2.4 kW. (b) Power absorbed by the ESS-SCAC emulated with CNG to obtain the required power. c) ESS-SCAC state of charge (SOC) increases due to the power absorbed by the SCAC system. The same legends than Fig. 17 are used in this plot. For SOC information, the colors match with the number of generators from Fig. 17.

there is a power setpoint requirement by the global controller, the ESS-SCAC absorbs the extra power, charging the batteries as can be seen in c). If the opposite were the case, the batteries would be discharged.

D. Case IV

The conducted simulation aims to illustrate the operation of the SCAC system in the presence of a phase-jump in the grid voltage. In this specific test, a phase jump of 50 deg. Has been triggered. Variable delay from Fig. 4 has been considered for this test. Fig. 19 visually depicts this event. As observed, when the event occurs at 6 s (see Fig. 19(a)), there is a decrease in the frequency detected by the converter (see b). In response to this variation, the inertia emulation system takes the task of injecting active power, as it can be seen in c), to actively mitigate the disturbance, working towards reducing the discrepancy until the event completely dissipates. This detailed assessment not only provides a deeper understanding of the SCAC system's behavior under specific conditions but also emphasizes the effectiveness of the implemented strategy in maintaining stability and the continuity of electrical supply in the face of network disturbances.

E. Case V

In case V, the objective is to showcase the functionality of the SCAC control system in island mode, demonstrating its ability to create a proper grid, thus providing power to the loads connected to that grid. The converters will power the loads assuming different weights to their power injection (0.6 for G_1, 0.1 for G_2, and 0.3 for G_3). As it can be seen in Fig. 20(a) the grid is created, starting to feed the connected loads by the VSG converter (see b). The delivered power (see Fig. 20(c)) will vary with the load connected to the microgrid.

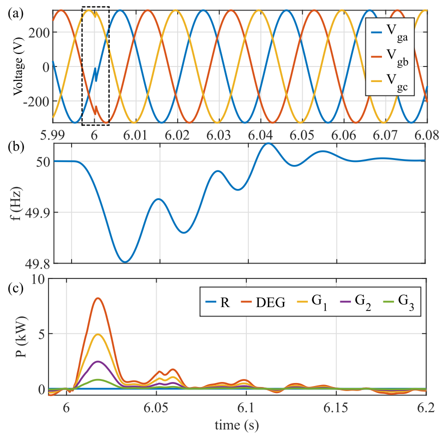

Fig. 19. (a) Grid voltage evolution with angle-step at 6 s. (b) Frequency evolution due to the voltage angle-step. (c) Power injection caused for the frequency variation.

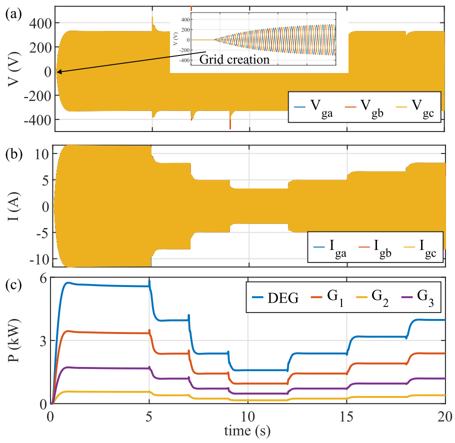

Fig. 20. (a) Grid voltage creation and evolution with different load changes. (b) Feeding current by SCAC converter in islanding mode. (c) Power injected by SCAC with some load variations.

For this case, the reactive power control loop depicted in Fig. 1(c) is employed, in order to add grid forming features to the system. To achieve this, a proportional (P) gain of 0.05 has been utilized, alongside a Proportional-Integral (PI) controller with a P value of 0.27 and an I value of 8. This case has been tested with a constant delay of 75 ms. This scenario underscores the robustness of the SCAC system when operating autonomously, ensuring the stability of the electrical supply even in instances of disconnection from the main grid. The efficient management of loads, considering the distinct characteristics of each converter, highlights the versatility and effectiveness of the system in varied environments.

V. Conclusion

This paper proposed a method for the implementation of the aggregated VSG concept in industrial converters by removing access to internal instantaneous variables (current/voltage) and replacing them with a reconstruction technique from RMS values obtained by communications. Considering communications, the effect of a stochastic delay has been addressed, measuring the magnitude of the delay in a MODBUS TCP communication protocol and then employing a delay compensation mechanism to mitigate its effect on the control system performance. Besides, the stability of the system with constant communication delays has been studied, showing that the system remains stable up to 75 ms, although it does not have good dynamics, but the response is significantly improved using the Smith predictor compensation. Furthermore, simulation and experimental results show a satisfactory response with the considered constant and variable delay, in which the effect of internal computational delay and integration windows have been also considered. For that, different scenarios were considered, to test different operation modes, such as Case I, II and III, and they were validated in local and in real-time simulations. In case of Case IV and V, just local simulations. Both reference tracking and disturbance rejection mechanisms have been considered for the system's overall performance evaluation.

References

[1] A. G. Olabi et al., "Wind energy contribution to the sustainable development goals: Case study on London array," *Sustainability*, vol. 15, no. 5, 2023, Art. no. 4641. [Online]. Available: https://lutpub.lut.fi/handle/10024/163284
[2] H. Bevrani, B. François, and T. Ise, *Microgrid Dynamics and Control*. New York, NY, USA: Wiley, 2017.
[3] H. Bevrani, T. Ise, and Y. Miura, "Virtual synchronous generators: A survey and new perspectives," *Int. J. Elect. Power Energy Syst.*, vol. 54, pp. 244–254, 2014.
[4] C. Verdugo, A. Tarraso, J. I. Candela, J. Rocabert, and P. Rodriguez, "Centralized synchronous controller based on load angle regulation for photovoltaic power plants," *IEEE Trans. Emerg. Sel. Topics Power Electron.*, vol. 9, no. 1, pp. 485–496, Feb. 2021.
[5] W. Zhang, A. M. Cantarellas, J. Rocabert, A. Luna, and P. Rodriguez, "Synchronous power controller with flexible droop characteristics for renewable power generation systems," *IEEE Trans. Sustain. Energy*, vol. 7, no. 4, pp. 1572–1582, Oct. 2016.
[6] W. Zhang, A. Luna, I. Candela, J. Rocabert, and P. Rodriguez, "An active power synchronizing controller for grid-connected power converters with configurable natural droop characteristics," in *Proc. IEEE 6th Int. Symp. Power Electron. Distrib. Gener. Syst.*, 2015, pp. 1–7.
[7] C. Verdugo, A. Tarraso, J. I. Candela, J. Rocabert, and P. Rodriguez, "Synchronous frequency support of photovoltaic power plants with inertia emulation," in *Proc IEEE Energy Convers. Congr. Expo.*, 2019, pp. 4305–4310.
[8] Q.-C. Zhong and G. Weiss, "Synchronverters: Inverters that mimic synchronous generators," *IEEE Trans. Ind. Electron.*, vol. 58, no. 4, pp. 1259–1267, Apr. 2011.
[9] M. Shadoul, R. Ahshan, R. S. AlAbri, A. Al-Badi, M. Albadi, and M. Jamil, "A comprehensive review on a virtual-synchronous generator: Topologies, control orders and techniques, energy storages, and applications," *Energies*, vol. 15, no. 22, 2022, Art. no. 8406.
[10] Y. Hirase, K. Abe, K. Sugimoto, and Y. Shindo, "A grid-connected inverter with virtual synchronous generator model of algebraic type," *Elect. Eng. Jpn.*, vol. 184, no. 4, pp. 10–21, 2013.

[11] U. Tamrakar, D. Shrestha, M. Maharjan, B. P. Bhattarai, T. M. Hansen, and R. Tonkoski, “Virtual inertia: Current trends and future directions,” *Appl. Sci.*, vol. 7, no. 7, 2017, Art. no. 654.

[12] A. Tarrasó, C. Verdugo, N. B. Lai, J. I. Candela, and P. Rodriguez, “Synchronous power controller for distributed generation units,” in *Proc. IEEE Energy Convers. Congr. Expo.*, 2019, pp. 4660–4664.

[13] D. D. Rivero, P. G. Fernández, C. Blanco, and A. Navarro-Rodríguez, “Control of aggregated virtual synchronous generators including communication delay compensation,” in *Proc. IEEE Energy Convers. Congr. Expo.*, 2022, pp. 1–7.

[14] I. Modbus, “Modbus application protocol specification v1. 1a,” North Grafton, Massachusetts, 2004. [Online]. Available: www.modbus.org/specs.php

[15] S. Alliance, “Sunspec specification - sunspec der information model specification,” 2019. [Online]. Available: https://sunspec.org/

[16] K. E. Martin, “Synchrophasor measurements under the IEEE standard C37.118.1-2011 with amendment C37.118.1a,” *IEEE Trans. Power Del.*, vol. 30, no. 3, pp. 1514–1522, Jun. 2015.

[17] H. S. Wang and N. Moayeri, “Finite-state Markov channel-a useful model for radio communication channels,” *IEEE Trans. Veh. Technol.*, vol. 44, no. 1, pp. 163–171, Feb. 1995.

[18] Z. Chen, D. Boroyevich, R. Burgos, and F. Wang, “Characterization and modeling of 1.2 Kv, 20 A SiC MOSFETs,” in *Proc. IEEE Energy Convers. Congr. Expo.*, 2009, pp. 1480–1487.

[19] D. Gross, *Fundamentals of Queueing Theory*. New York, NY, USA: Wiley, 2008.

[20] G. Villa, S. Saeed, P. García, C. Gómez-Aleixandre, and R. Georgious, “Compensation alternatives for power sharing mismatch in multiport DC–DC–AC converters,” vol. 57, no. 6, pp. 6221–6236, Nov.–Dec. 2021, doi: 10.1109/TIA.2021.3115721.

[21] A. Ghanaim, G. A. Borges, and G. Frey, “Estimating delays in networked control systems using colored petri nets and Markov chain models,” in *Proc. IEEE Conf. Emerg. Technol. Factory Automat.*, 2009, pp. 1–6.

[22] A Mirzal, “Delay compensation using the smith predictor: A brief review with numerical examples,” *Int. J. Comput.-Aided Mech. Des. Implementation*, vol. 3, no. 1, pp. 1–8, 2017.

[23] T. Matiakis, S. Hirche, and M. Buss, “The scattering transformation for networked control systems,” in *Proc. IEEE Conf. Control Appl.*, 2005, pp. 705–710.

[24] T. Matiakis, S. Hirche, and M. Buss, “Independent-of-delay stability of nonlinear networked control systems by scattering transformation,” in *Proc. Amer. Control Conf.*, 2006, Art. no. 6.

[25] M. Lu, X. Wang, P. C. Loh, F. Blaabjerg, and T. Dragicevic, “Graphical evaluation of time-delay compensation techniques for digitally controlled converters,” *IEEE Trans. Power Electron.*, vol. 33, no. 3, pp. 2601–2614, Mar. 2018.

[26] S. Bibian and H. Jin, “Time delay compensation of digital control for DC switchmode power supplies using prediction techniques,” *IEEE Trans. Power Electron.*, vol. 15, no. 5, pp. 835–842, Sep. 2000.

[27] V. Miskovic, V. Blasko, T. Jahns, A. Smith, and C. Romenesko, “Observer based active damping of LCL resonance in grid connected voltage source converters,” in *Proc. IEEE Energy Convers. Congr. Expo.*, 2013, pp. 4850–4856.

[28] R. Kennel, A. Linder, and M. Linke, “Generalized predictive control (GPC)-ready for use in drive applications?,” in *Proc. IEEE 32nd Annu. Power Electron. Specialists Conf.*, 2001, pp. 1839–1844.

[29] K. C. Konjerla, “FRF based experimental–analytical dynamic substructuring using transmission simulator,” 2016. [Online]. Available: https://www.diva-portal.org/smash/record.jsf?dswid=-9969&pid=diva2%3A1057263

Daniel del Rivero (Graduate Student Member, IEEE) was born in Avilés, Spain. He received the B.Sc. degree in electrical engineering and the M.Sc. degree in electrical energy conversion and power systems, from the University of Oviedo, Oviedo, Spain, in 2016 and 2018, respectively. He also undertook an Internship with the Luxembourg Institute of Science and Technology (LIST), Esch-sur-Alzette, Luxembourg, in 2023. From 2018 to 2020, he focused on railway traction systems before transitioning to his doctoral studies in energy and process control at the University of Oviedo. Throughout his academic journey, he has been specialized on control systems with delayed communications and real-time simulations for microgrid control, renewable energy integration, and power quality enhancement.

Pablo García (Senior Member, IEEE) was born in Luanco, Asturias, Spain. He received the M.S. and Ph.D. degrees in electrical engineering from the University of Oviedo, Gijón, Spain, in 2001 and 2006, respectively. In 2004, he was a Visiting Scholar with the University of Wisconsin-Madison, Madison, WI, USA. In 2013, he was a Visiting Scholar with The University of Nottingham, Nottingham, U.K. He is currently a Full Professor with the Department of Electrical, Electronics, Communications and Systems Engineering, University of Oviedo. Since 2022, he has been with the Spanish Research Agency as the Manager for international projects in the Energy and Transport division area. He is the coauthor of more than 40 journal papers and more than 80 international conference papers. He has been the Principal Investigator of 50 projects with companies, one European H2020, and four national funded projects. He is the cofounder of the ENFASYS startup, focused on the development of solutions for the integration of energy storage in distribution and generation applications. His research interest includes control of grid-tied power converters for distributed resources integration and particularly for the control of grid-tied battery energy storage systems, parameter estimation, optimization of distributed resources, and digital signal processing for real-time embedded systems. Dr. García was the recipient of the 2005 IEEE Transactions on Industry Applications, Third Place Prize Paper Award, three IEEE Industry Applications Society Conference prize paper awards in 2006, 2010, and 2016, respectively and one EPE Conference Award in 2018 and was also a fellowship for the national research and training program by the Ministry of Science and Technology in Spain, from 2002 to 2006. He is a member of the LEMUR research group.

Cristian Blanco (Senior Member, IEEE) was born in Villablino, Leon (Spain). He received the B.S. degree in telecommunications engineering and the M.S. and Ph.D. degrees in electrical engineering from the University of Oviedo, Gijon, Spain, in 2010, 2011, and 2015, respectively. The Regional Ministry of Education and Science of Asturias awarded him a fellowship for the Personnel Research Training Program in 2011. From September 2012 to February 2013, he was a Ph.D. Guest with Aalborg University, Denmark. From July 2019 to December 2019, he was a Visiting Faculty with The University of British Columbia, Vancouver, BC, Canada. He is currently an Associate Professor with the Department of Electrical, Computer, and Systems Engineering, University of Oviedo. He is a member of the LEMUR Research Team. His research interests include modeling and control of islanded and grid-connected converters including storage systems, hybrid AC/DC microgrids, energy management systems, and hybrid power plants with energy storage capabilities. He was the recipient of an IEEE Energy Conversion Congress and Exposition Second Prize Paper Award, in 2013, and the University of Oviedo Outstanding Ph.D. Thesis Award, in 2016.

Ángel Navarro-Rodríguez (Member, IEEE) received the B.Sc. degree in telecommunications engineering (with Hons.) from the University of Castilla La-Mancha, Spain, in 2012, the M.Sc. degree in electrical energy conversion and power systems, and the Ph.D. degree (*cum laude*) in energy and process control from the University of Oviedo, Oviedo, Spain, in 2014 and 2019, respectively, granted by the government of Principado de Asturias. He has been an Assistant Professor with the Department of Electrical, Electronics, Communications, and Systems Engineering, University of Oviedo since 2019. During 2016–2017, he was a Visitor Researcher with the PEMC Research Group, The University of Nottingham, Nottingham, U.K. Between 2022 and 2023, he was a Visitor Researcher with the Chair of Power Electronics in the University of Kiel, Kiel, Germany. He has been a part of the LEMUR Research Group, University of Oviedo since 2014. He has authored or coauthored 15 IEEE journals and 30 IEEE conferences. His current research interests include microgrids control and modelling, grid-tied converters, energy storage systems, control systems applied to electrical energy conversion, sustainable transportation and electric traction, power quality, renewable energies integration, grid modernization, and smart grids. Dr. Navarro-Rodríguez was the recipient of the Outstanding Young EPE Member Award in 2018 and the University of Oviedo Outstanding Ph.D. Thesis Award in 2020.

Appendix C

Conference Publications

C.1 Control of Aggregated Virtual Synchronous Generators Including Communication Delay Compensation.

Control of Aggregated Virtual Synchronous Generators Including Communication Delay Compensation

Daniel del Rivero, dept. Electrical Engineering, University of Oviedo, Gijón, Spain, riverodaniel@uniovi.es

Pablo García Fernández, dept. Electrical Engineering, University of Oviedo, Gijón, Spain, garciafpablo@uniovi.es

Cristian Blanco, dept. Electrical Engineering, University of Oviedo, Gijón, Spain, blancocristian@uniovi.es

Ángel Navarro-Rodríguez, dept. Electrical Engineering, University of Oviedo, Gijón, Spain, navarroangel@uniovi.es

***Abstract*—In this paper, a new method for the delay compensation when using an aggregation of virtual synchronous generators is proposed. Lack of inertia in power converters can potentially provoke stability issues that can be mitigated by the use of virtual inertia techniques. Among those, the Virtual Synchronous Generator (VSG) concept has received strong impulse in the last years. This paper is focused on the idea of using the distributed VSG concept in a renewable power plant, in which a single Synchronous Central Control (SCAC) is used for the power control exchange at the Point of Common Coupling (PCC), while distribution control units are employed for the local inverter control. This idea, already discussed in the literature, is in here extended to consider the implementation on industrial string-level commercial power converters, recalling the importance of accessible measurements and communication delays. In order to validate the proposal, firstly communication delays are measured and modelled. Following, simulations with different SCAC operating modes are conducted, and finally experimental results with commercial converters are presented.**

***Index Terms*—Virtual Synchronous Generator, Communication delay, Smith predictor**

I. Introduction

Currently, worldwide power generation is going towards a more sustainable and green approach, thanks to use distributed energy generation (DEG) plants based in renewable energy sources (RES), following a decline of fossil fuels due to their high environmental cost (greenhouse emissions, lack of source material, etc). Furthermore, most used RES, such as photovoltaic (PV) and wind generation are getting cheaper, providing a better levelized cost of energy (LCOE) indexes [1]. However, the inclusion of this kind of generation systems potentially provokes a weaker power system, mainly due to the inertia reduction currently given by synchronous generators with a rotating mass, to a power converter-based system with no (or barely) inertia [1]–[3]. This issue potentially leads to stability problems in the power grid, since power converters have neither inertia nor damping. When considering massive inclusion of DEG, with aggregated sizes compared to conventional power plants, it is now recognized that grid-forming and/or grid-supporting services have to be considered in the design [4]–[6]. This is where the VSG approach arises. This control technique allows to emulate the dynamic properties of a real or arbitrary synchronous generator (SG) for the power electronics-based DEG/RES units [2] [3].

The virtual inertia concept is implemented by using energy storage systems (ESS) along power converters and a suitable control mechanism, providing certain amount of inertia for given (usually in the range of ms to few dozens of seconds). Thus, VSG creates the basis for future large-scale implementation in RES systems without compromise the stability of the system. In [1]- [7] several VSG techniques are presented. Nevertheless, in this paper the strategy presented in [4] and [7] is followed.

The Synchronous Central Control (SCAC) strategy proposes to simultaneously drive several converters, emulating an unique SG in the point of common coupling (PCC), giving rise to an aggregated VSG. This concept introduces the idea of a single virtual rotor, emulated at the PCC, where the electromechanical model of the SG is considered (central control architecture). Therefore, the inertia and damped response are emulated at the PCC. This control structure makes possible to control the exchange of power (both active and reactive) by the system operator at the PCC, regardless of the distances among the local converters, being able to distribute the energy to be delivered under different operation modes (power and frequency support), by each of them independently. A more detailed explanation can be found in the literature, where both, central and local control systems are detailed [7].

Fig. 1 shows a scheme for a n-converters structure, where a central controller which commands the local controllers at each converter is considered. As it can be seen in the shown dynamic model and control loops, it is possible to control the exchanged active and the reactive power independently. The key control system is implemented in the central controller, where the inertia is emulated by the swing equation of a virtual

This work was supported in part by the European Union's H2020 Research and Innovation program under Grant Agreement No 864459 (UE-19- TALENT-864459) and by the Spanish Ministry of Innovation and Science under Grant MCI-20-PID2019-111051RB-I00 funded by MCIN/AEI/10.13039/501100011033.

978-1-7281-9387-8/22/$31.00 ©2022 IEEE

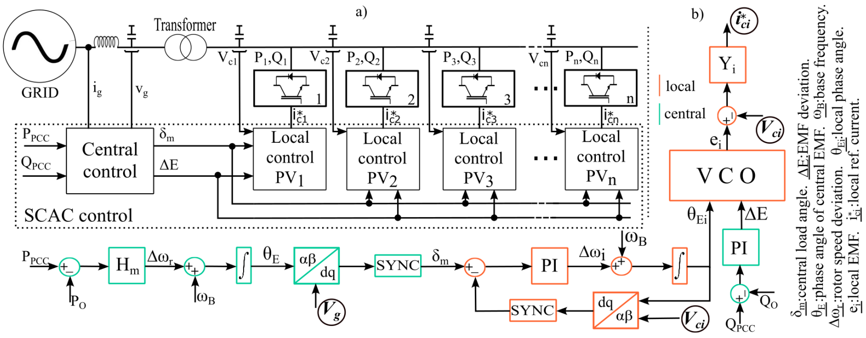

Fig. 1. a) SCAC scheme for n-converters. b) Simplified Local control scheme. Light green control loop is implemented in the central controller. Orange control loop is implemented in the local controller.

synchronous generator,(1) and (2).

$$\frac{\mathrm{d}\delta_{sm}}{\mathrm{d}t} = \Delta\omega_r \tag{1}$$

$$J\frac{\mathrm{d}\Delta\omega_r}{\mathrm{d}t} = \frac{P_m - P_e}{\omega_B|} - D\Delta\omega_r = \frac{\Delta P}{\omega_B} - D\Delta\omega_r \tag{2}$$

Where δ_{sm} is the power angle, $\Delta\omega_r$ is the angular speed deviation of the rotor, J is the SG inertia, P_m is the mechanical power, P_e is the electrical power, D is the damping constant and ω_B is the base frequency. In [5] the electromechanical control has been studied and a frequency analysis has been considered to obtain the power loop control H_M (3), being k_p, k_i and K_D designed according to the required inertia constant and frequency droop slope, respectively.

$$H_M = \frac{\Delta\omega_r}{\Delta_P} = \frac{k_p + k_i s}{s + k_D}\begin{cases} k_p = \frac{\omega_n^2}{P_{max}} \\ k_D = \frac{\omega_n^2 D}{P_{max}} \\ k_i = \frac{2P_{max}\xi\omega_n - \omega_n^2 D}{P_{max}^2} \\ w_n = \sqrt{\frac{P_{max}\omega_B}{2HS_N}} \\ H = \frac{J\omega_B^2}{2S_N} \end{cases} \tag{3}$$

In (3), H is the inertia constant, P_{max} is the maximum active of the converter, S_N is the nominal power, ω_n is the natural frequency and ξ is the damping factor.

However, this control system assumes there is access to the converter internal time-domain variables and control-loops (current/voltage). In case of already existing installed commercial converters, only active and reactive power set-points are usually externally available, typically through a communications interface. Hence, an adaptation of this control is needed for a more extensive application. For that, MODBUS TCP is proposed as the communication system due to its large widespread as the preferred solution in industrial installations [8]. In the following sections, it is proposed a modification of the control system architecture according to the previous motivation based on a communication-based implementation. The proposed control system is initially validated by local simulation and then, by using a real-time hardware controller with commercial converters. A focus on the effect and modelling of the communication delays (measuring actual delays in MODBUS TCP systems) and their compensation are the main paper contribution.

II. Proposed control system

Most of the VSG strategies integrate their controllers as a firmware add-on in each converter. However, as it has been aforementioned, in case of the SCAC approach, it requires to have access to different control actions and sensors measurements (current, voltages). In this paper, it is intended to change the control structure to have an approach that can be applied to already existing commercial converters, by requiring only access to active and reactive powers set-points and measurements obtained from MODBUS TCP communications and the dictionary variables included in the SunSpec DER specification [9]. Thus, this proposal will not include unnecessary measurement elements, such as additional voltage and current sensors, which would increase the difficulty and cost of the implementation. Hence, this approach, makes the proposal appealing for the standardization of the VSG concept for a massive implementation in future and existing DEG's. The needed communication-based readings are the RMS voltage, frequency as well as active and reactive power values from each converter.

For the application of this concept, instantaneous voltage signals for each converter and PCC are built from the RMS values as shown in Fig.2.a), b). Those signals are used as feedback variables in the control system (as a replace of bold and circled variables in the original scheme shown in Fig. 1b). Besides, as it was mentioned above, commercial converters typically require power set-points. However, for the implementation of the VSG concept, current commands computed from the control system are needed instead. In

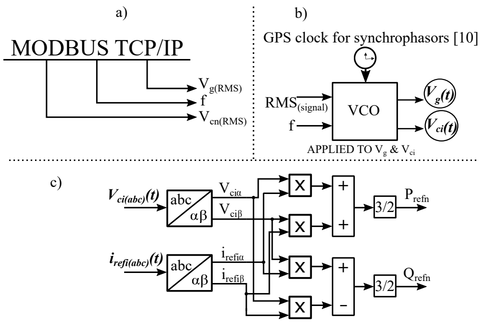

Fig. 2. a) MODBUS TCP frequency and RMS voltage. b) instantaneous values from the RMS voltage, frequency and clock signal obtained by a VCO (Voltage Controller Oscillator) [10]. c) Active and reactive reference power calculation.

this proposal, the power references are obtained from the reconstructed voltage signals and the current references as shown in Fig. 2c) in the $\alpha - \beta$ reference frame.

III. Delay Compensation

In the proposed renewable power plant application, each converter control unit connects with the central controller through MODBUS TCP communications. Considering MODBUS TCP is not a real-time protocol, and depending on the number of elements in the bus and the distance, a variable delay will often occur in the communication between the central controller and each of the distributed units. These delays directly affect the control actions sent from the central controller and the provided feedback information, thus compromising the performance of the close-loop system. In the following subsections, the delay distribution will be modelled, as well as a method for compensating the delay is presented.

A. Delay modelling

In the literature, there are several proposals to model random delays. One of those is based on the Markov chain [11], [12]. Markov chain is a stochastic model which describes in a discrete way some possible states or events (in this case delays). Those possible events have a probability which depends only on the state attained in the previous event. However, for this paper the communication delay has been measured in the laboratory in order to model the communication delays that are available in the local network through MODBUS TCP communication protocol. For this, a 30 kW bidirectional dc/dc converter (CNG) from CINERGIA SL (as the one shown in Fig. 4) has been used. This power supply can operate as voltage/current/power source and also includes different emulation units, such as batteries and PV panels. It will be used for the experimental tests in section V. For performing the measurements a hardware-in-the-loop (HIL) system has been used (SPEEDGOAT target machine), with the aim to act as a communication gateway between the control system on Matlab and the converters in a real-time simulation. Those elements are also shown in Fig. 4.

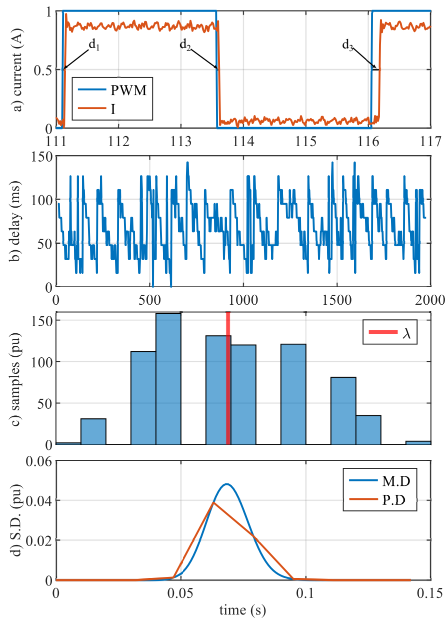

Fig. 3. a) Instantaneous delay measurement in the lab (PWM is the sent reference signal and I is the actual current the converter develops). b) Delay histogram from experimental tests. c) Time variation of delay. d) Probability density function of the communication delay (M.D) in comparison to Poisson distribution (P.D) with λ of 68 ms.

In order to measure the delay, a digital square reference signal of 0.25 Hz has been sent simultaneously to the current converter set-point (both are measured by an oscilloscope). Both signals can be seen at Fig. 3a), where a variable delay between them can be seen. In fact, that delay varies between a much wide range, as it can be seen at Fig. 3b), with a mean value of around 68 ms. In Fig. 3c), time variation of the delay during all the experiment can be easily appreciated. Taking into account the shape of the delay variation obtained during the test, and considering proposed queuing theory delay models [13], [14] in a communication network, a Poisson distribution as expressed in (4) is selected for the delay modelling. In (4), λ parameter allows the calculation of the distribution for each delay case ($X = k$).

$$f(k, \lambda) = Pr(X = k) = \frac{\lambda^k e^{-\lambda}}{k!}; \lambda > 0; k = 0, 1, 2... \quad (4)$$

By using the Poisson distribution, the distribution from Fig. 3.d) is obtained.

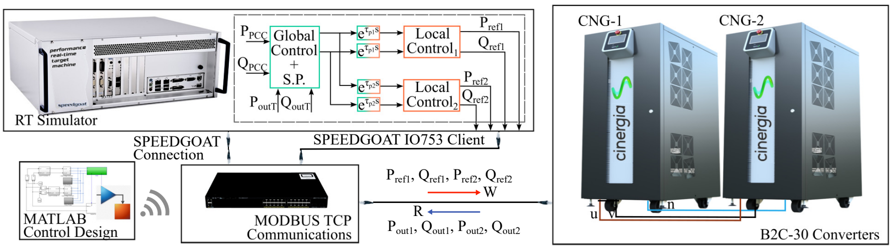

Fig. 4. Setup for HIL experimental tests. The the control design is made on Matlab and executed in the real-time Speedgoat target. The converters are controlled by writing/reading published MODBUS/TCP variables.

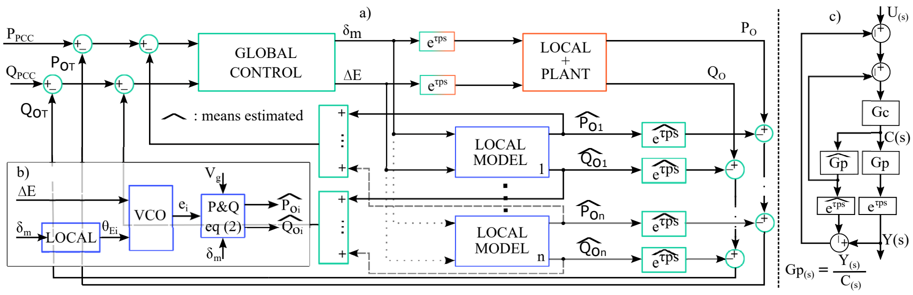

Fig. 5. a) Global SP architecture for n-converters (light green block for global control and orange for local control) [12]. b) Local model for each converter (blue blocks) emulated in global controller. c) Basic Smith predictor structure.

B. Delay compensation. The Smith predictor

Several delay compensation methods have been studied, such as the Smith predictor (SP) and their modifications [15] [16], as well as scattering transformation [17] [18]. The Scattering Transformation, is a method that passivates the control systems in order to mitigate the delay effects and contribute to the stabilization. However, for this paper, the Smith predictor is selected due to its simplicity and correct operation. It is field of current research alternative delay compensation methods more suitable for the stochastic nature of communication-based delays. The Smith predictor removes the delay component from the system's control loop by using a model of the delay structure, as well as a fairly exact modeling of the system plant.

In the SCAC system, the delay is presented in the control actions sent to the local converters. The Smith predictor compensates the plant delay, through an plant model ($\widehat{G_p}$) and an estimated delay ($\widehat{e^{tps}}$). Plant model shall be the one between the control actions (δ_m, ΔE) and the output (P_{out}, Q_{out}) (see Fig. 5a). However, for the proposed communications-based control system finding the transfer model is not an easy task. The proposed solution is to execute a replica of the local control in the central controller for each converter. Fig. 5c) shows the simulated plant for SP which is considered as the affected plant by the delay. Besides, δ_m and e_i outputs of the emulated local model are used for computing the output power using the power equations (5). Finally, the error between the predicted active and reactive power and the values given by the local control units is used to compensate the delay (see Fig. 5).

$$P_i = \frac{E_i V_i}{X_i} sin(\delta_m);\ Q_i = \frac{V_i}{X_i}(Ecos(\delta_m) - V_g) \quad (5)$$

IV. Simulation Results

Simulation results are presented for validating the proposed compensation method. For these tests, grid and VSG models are taken from [4], where the SCAC idea was first published. In this case, the model includes two DEGs connected to a grid and considering a battery locally connected, which is the element providing/absorbing energy for frequency support, and no-feeder impedance is considered in the simulations. In this first simulation, power is oddly shared between the two converters, providing the first converter 60 %, and the second one the remaining 40 %. Active and reactive power set points are established in order to control the power exchange with the grid. Disturbance rejection capability is analyzed by including a variation in the grid frequency. Simulation parameters are given in Table I.

TABLE I
SCAC PARAMETERS AND SET-POINTS FOR THE SIMULATION.

Variable	$H\ (s)$	τ	$Sn\ (VA)$	$V_g\ (V)$	$f_g\ (Hz)$
Value	10	1	2000	400	50
Variable	$R_v\ (\Omega)$	$X_v\ (\Omega)$	$P_{set}\ (W)$	$Q_{set}\ (Var)$	
Value	8	0.48	2000	2000	

The first simulation results considering variable delay compensation are present in Fig. 6. In there, both the operation under reference tracking for active and reactive power set-points variations as well as the disturbance rejection capability when a grid frequency variation is forced is demonstrated. As it can be seen in Fig. 6a), b), the control system works properly, delivering the required active and reactive power to the grid with a sharing between both DEG's when the SP concept is applied. Otherwise, if no delay compensation is present, the system becomes unstable, as it can be seen in Fig. 6d). Under a grid-frequency variation (see Fig. 6d)), the DEG's maintain their power injection while the batteries try to compensate for the frequency drop, by increasing the power injected to the grid (see Fig. 6e)). Otherwise, if the grid frequency increases, the opposite effect can be seen. Furthermore, different time delays have been applied for each local converter and also for SP estimation. Fig. 6f) shows the time delay distribution for each converter.

Previous simulation works without problems with an ideal grid. However, in order to validate and demonstrate that SCAC system works as it must, two simulations are included, where the SCAC system is connected to a weak grid formed by a simple synchronous generator (with real frequency variations), with a limited power and inertia. In these simulations, two system operating modes are validated: 1) supporting frequency changes, and 2) grid operator active power reference tracking.

A. Frequency support

This simulation aims to demonstrate the main operation mode of the SCAC system. As it was above-mentioned, SCAC system adds virtual inertia capabilities, helping to reduce any frequency disturbance in the grid. Several frequency variations are induced by forcing some abrupt load changes (at 15, 25 and 36 s from Fig. 7a), power variations can be observed) in order to observe the dynamic behavior of the control system. In Fig. 7b) frequency variation by using the SCAC system connected to the grid (with several installed power converters), and the frequency variation by feeding the load by only the grid are shown. As it can be seen in Fig. 7a), a load change is forced at 15 s, absorbing power from the system, and forcing the frequency to decrease. In case of having the SCAC system (blue and red traces in Fig. 7c)), the ESS will inject power to the system in order to help the grid to increase its frequency (blue and red traces in Fig. 7b)). On the other hand, if a suddenly load decrease appears, as it can be seen at 36 s, frequency increases, making the ESS-SCAC to absorb power from the system in order to decrease the frequency. Furthermore, this power injection/absorption by the SCAC system will depend on the inertia emulated and also the power

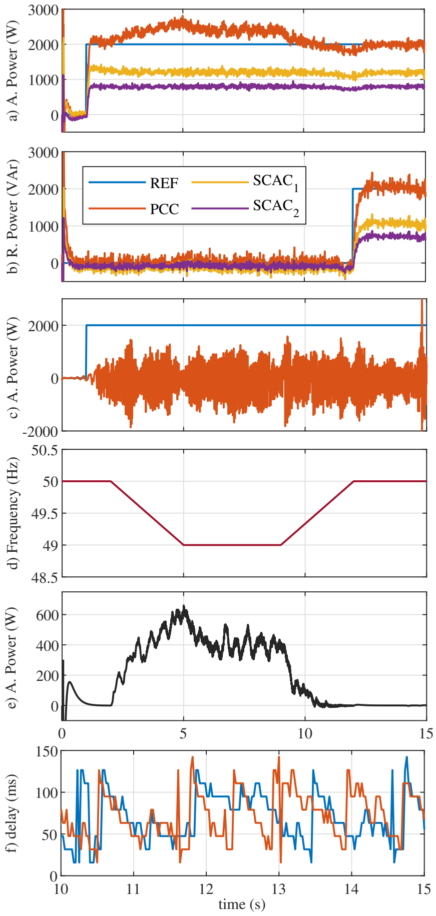

Fig. 6. a) Active power at the grid and the two converters. b) Reactive power at the grid and the two converters. c) Uncontrolled system without the SP compensation. Active power is divided by 1000 for allowing its representation. d) Grid frequency variation. e) Battery power injection for compensating frequency change. f) Variable delay for each converter and SP.

installed in its ESS. As an example, the simulated SCAC power is tripled, being noticeable lower the frequency variation (see Fig. 7b)), and hence higher the power injection/absorption by the ESS as it can be seen in Fig. 7b).

B. Power support

This operation mode is controlled by DEG operator (central controller), in order to reduce or increase the power injected by the power plant, depending on the grid requirements, as long

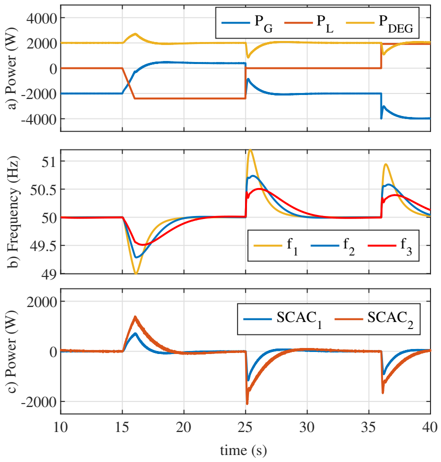

Fig. 7. a) Frequency variation of a weak grid due to a sudden load variation (f_1 only grid with load, f_2 grid with load and 2 kVA SCAC system and f_3 grid with load and 6kVA SCAC system. b) 2 kVA ESS-SCAC power and 6 kVA ESS-SCAC power. c) Active power from grid, load and 6 kVA DEG-SCAC system.

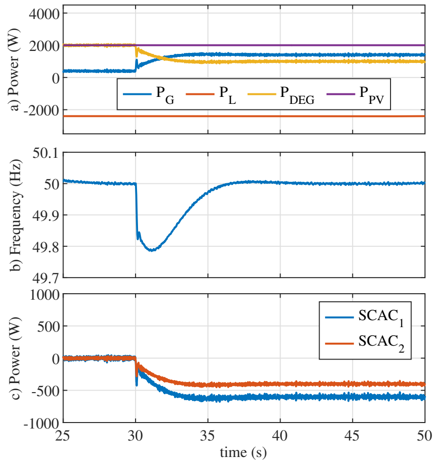

Fig. 8. a) Frequency variation of a weak grid due to a power change demand. b) ESS-SCAC power absorption to obtain the required 1 kW power demand by the PCC. c) Active power from grid, load and 6 kVA DEG-SCAC system.

as the ratings of the power plant are not exceeded. This means that if a power change is requested by grid operator, the power injected will vary, taking into account the RES are working normally at their maximum power point (MPP), and the excess or lack of power regarding the new power command will be managed by the SCAC-ESS. This effect can be observed in Fig. 8, where at certain moment (t=30 s), grid operator active power reference varies (P_{DEG} at Fig. 8a)), forcing to inject less power from the DEG system. In this situation either an inverter curtailment or a charging of the ESS is required. In this case, the power set-point has been reduced by 1 kW, and as the PV system is working at its MPP, the ESS-SCAC will absorb the energy difference.

V. Experimental results

In this section, experimental results of the proposed system will be shown and explained in order to demonstrate the control system works as it has been presented in the simulations. For these experimental results, two 30 kW bidirectional dc/dc converters (CNG) from CINERGIA SL will be used (as shown in Fig. 4). In this case, CNG-2 has two strings working as a power source to emulate two different converter strings, which will receive the commands from the simulation (P_{ref1}, Q_{ref1}, P_{ref2}, Q_{ref2}). Those setpoints are sent and written in CNG-2 by sending them through MODBUS TCP. The power developed will be inject the power to CNG-1, which is working as parallel voltage source in all its terminals. Power readings from communication channel will be used for feedback-control loop. As it was stated in III, a HIL system is used for the real-time simulation. Besides, for the control implementation, the CNG mains RMS-voltages are read and used for the reconstruction of the grid instantaneous voltage used in the control system, as shown in Fig. 2. The need of GPS clock for the synchrophasors calculations is here not needed as a single HIL system is used for the reconstruction.

For the case of communication delays between the central controller and the local units, the same variable time delay used in the simulation has been employed here. However, due to the CNG converters internal delay in the processing of the power references and integration windows used for the calculation of the active and reactive power, additional delays are added to the control system (20 ms for active power and 400 ms for reactive power). These delays are also included in the model used by the Smith predictor in order to achieve better results. It is considered this to be a remarkable result since most of the commercial power units will include similar additional delays.

In Fig. 9, the experimental results are depicted, where two local DEG converters are emulated with CNG, providing different power sharing, as performed in Section IV.A. Those results are obtained from the HIL system, being the power readings from MODBUS TCP the actual power injected by CNG. As it can be seen, a power set-point is applied at 3 s, sharing the power injected by both inverters in a 60 % and 40 % ratio. In the case of reactive power, it is only controlled by a single converter, injecting 2 kVAr at 14 s.

Furthermore, as it can be seen in Fig. 9b) and c), there is a different delay between active and reactive power, which has

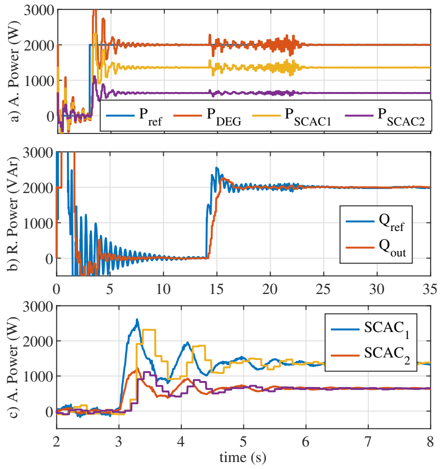

Fig. 9. a) Active power command, total power injected to grid and power injected by each converter. b) Reactive power injected to grid, showing the command and the actual reactive power, showing a small delay, due to the integration window. c) Active powers commands and actual power injected by converter, with a small delay due to the integration window. Same power than a) with a tiny zoom.

to do with the integration window from each variable. Nevertheless, those delays are overcome with the Smith predictor, making the system controllable and stable.

VI. Conclusion

This paper has proposed a method for the implementation of the aggregated VSG concept in industrial converters by removing access to internal instantaneous variables (current/voltage) and replacing them by a reconstruction technique from RMS values obtained by communications. Considering communications, the effect of a stochastic delay has been addressed, measuring the magnitude of the delay in a MODBUS TCP communication protocol and then employing a delay compensation mechanism for mitigating its effect in the control system performance. Simulation and experimental results show a satisfactory response with the considered variable delay, in which the effect of internal computational delay and integration windows have been also considered. Both reference tracking and disturbance rejection mechanisms are considered for the system overall performance evaluation.

References

[1] F. Durakovic, "Levelized cost of electricity of renewable energy technologies as a criterion for project prioritization," 2021.

[2] H. Bevrani, B. François, and T. Ise, *Microgrid dynamics and control*. John Wiley & Sons, 2017.

[3] H. Bevrani, T. Ise, and Y. Miura, "Virtual synchronous generators: A survey and new perspectives," *International Journal of Electrical Power & Energy Systems*, vol. 54, pp. 244–254, 2014.

[4] C. Verdugo, A. Tarraso, J. I. Candela, J. Rocabert, and P. Rodriguez, "Centralized synchronous controller based on load angle regulation for photovoltaic power plants," *IEEE Journal of Emerging and Selected Topics in Power Electronics*, vol. 9, no. 1, pp. 485–496, 2020.

[5] W. Zhang, A. M. Cantarellas, J. Rocabert, A. Luna, and P. Rodriguez, "Synchronous power controller with flexible droop characteristics for renewable power generation systems," *IEEE Transactions on Sustainable Energy*, vol. 7, no. 4, pp. 1572–1582, 2016.

[6] W. Zhang, A. Luna, I. Candela, J. Rocabert, and P. Rodriguez, "An active power synchronizing controller for grid-connected power converters with configurable natural droop characteristics," in *2015 IEEE 6th International Symposium on Power Electronics for Distributed Generation Systems (PEDG)*. IEEE, 2015, pp. 1–7.

[7] C. Verdugo, A. Tarraso, J. I. Candela, J. Rocabert, and P. Rodriguez, "Synchronous frequency support of photovoltaic power plants with inertia emulation," in *2019 IEEE Energy Conversion Congress and Exposition (ECCE)*. IEEE, 2019, pp. 4305–4310.

[8] I. Modbus, "Modbus application protocol specification v1. 1a," *North Grafton, Massachusetts (www. modbus. org/specs. php)*, 2004.

[9] S. Alliance, "Sunspec specification - sunspec der information model specification," https://sunspec.org/, 2019.

[10] K. E. Martin, "Synchrophasor measurements under the ieee standard c37. 118.1-2011 with amendment c37. 118.1 a," *IEEE Transactions on Power Delivery*, vol. 30, no. 3, pp. 1514–1522, 2015.

[11] Z. Chen, D. Boroyevich, R. Burgos, and F. Wang, "Characterization and modeling of 1.2 kv, 20 a sic mosfets," in *2009 IEEE Energy Conversion Congress and Exposition*. IEEE, 2009, pp. 1480–1487.

[12] H. S. Wang and N. Moayeri, "Finite-state markov channel-a useful model for radio communication channels," *IEEE transactions on vehicular technology*, vol. 44, no. 1, pp. 163–171, 1995.

[13] D. Gross, *Fundamentals of queueing theory*. John Wiley & Sons, 2008.

[14] G. Villa Fernández, *Dynamic analysis and development of distributed control systems in power cells and multiport converters for grid integration of distributed resources*. PhD, University of Oviedo, Spain, 2022.

[15] A. Ghanaim, G. A. Borges, and G. Frey, "Estimating delays in networked control systems using colored petri nets and markov chain models," in *2009 IEEE Conference on Emerging Technologies & Factory Automation*. IEEE, 2009, pp. 1–6.

[16] A. Mirzal, "Delay compensation using the smith predictor: a brief review with numerical examples," *International Journal of Computer-aided Mechanical Design and Implementation*, vol. 3, no. 1, pp. 1–8, 2017.

[17] T. Matiakis, S. Hirche, and M. Buss, "The scattering transformation for networked control systems," in *Proceedings of 2005 IEEE Conference on Control Applications, 2005. CCA 2005.* IEEE, 2005, pp. 705–710.

[18] ——, "Independent-of-delay stability of nonlinear networked control systems by scattering transformation," in *2006 American Control Conference*, 2006, pp. 6 pp.–.

C.2 Integration of Ramp-Rate Compensation in a Distributed Virtual Synchronous Generator Schema for Hybrid PV Plants.

Integration of Ramp-Rate Compensation in a Distributed Virtual Synchronous Generator Schema for Hybrid PV Plants

Daniel del Rivero
dept. of Electrical Engineering
University of Oviedo
Gijón, Spain
riverodaniel@uniovi.es

Irene Peláez
Enfasys Enineering
Gijón, Spain
irene.pelaez@enfasys.es

Pablo García Fernández
dept. of Electrical Engineering
University of Oviedo
Gijón, Spain
garciafpablo@uniovi.es

Cristian Blanco
dept. of Electrical Engineering
University of Oviedo
Gijón, Spain
blancocristian@uniovi.es

Ángel Navarro-Rodríguez
dept. of Electrical Engineering
University of Oviedo
Gijón, Spain
navarroangel@uniovi.es

***Abstract*—In this paper, the integration of a PV ramp-rate compensation is presented, taking advantage of behaviour of an aggregated virtual synchronous generator (VSG) method. This method can be used for virtually increasing the inertia of the power converters connected to a grid, reducing potential stability issues, as well as enhancing the behaviour of a PV power plant during transients, such as cloud passing or temperature variation, avoiding sudden reduction in the power injection to the grid, complying with grid requirements. The proposal is validated by simulation tests. Furthermore, a little economical study based in LCoE index is done in order to analyze if it is worth including this method in an application with VSG, considering parameters and generation of a real PV plant.**

***Index Terms*—Virtual Synchronous Generator, Communication delay, Smith predictor, Ramp-rate Compensation**

I. Introduction

Currently, the usage of distributed energy generation (DEG) is increasing, which are based on renewable energy sources (RES), trying to decline the usage of fossil fuels due to their high environmental cost (greenhouse emissions, lack of source material, etc). So, power generation is going towards a more green and sustainable generation. That kind of RES, such as photovoltaic (PV) or wind generation, are getting cheaper, providing a better Levelized Cost of Energy (LCOE) indexes [1], being controlled in a fairly easy and cheap way.

One of the most important energy resources (in terms of installed power along the power systems) is photovoltaic solar energy. Nevertheless, this kind of generation systems provokes a weaker power system due to the inertia reduction, which is currently given by synchronous generator with rotating mass, whereas the power converter-based system barely has no inertia [1]–[3].

Since power converters lack both inertia and damping, this problem could affect the power grid stability, and it is here where the Virtual Synchronous generator approach arises. This control technique allows to emulate the dynamic properties of a real or arbitrary synchronous generator (SG) for the power electronics-based DEG/RES units [2] [3]. Thus, the virtual inertia concept is implemented by using energy storage systems (ESS) along power converters, and a suitable control mechanism, providing certain amount of inertia for given (usually in the range of ms to few dozens of seconds). Thus, VSG creates the basis for future large-scale implementation in RES systems without compromise the stability of the system.

However, the lack of inertia in the power converters is not the only problem that a RES can suffer. The energy that comes from renewable resources typically have an intermittent behaviour, which depends on the surrounding weather conditions. This is the case in PV systems, where the irradiance and temperature can vary abruptly causing a corresponding variation in the delivered power. These issues can be the perfect mix for having severe power quality (PQ) problems. Specially for very fast fluctuations, where the transmission system operator (TSO) has an extremely limited response capacity and the power fluctuations exceed the permitted limits, giving rise to frequency or even voltage stability problems [4]–[6].

In order to mitigate those problems, TSO's have developed different regulations in their grid codes by tying down the maximum permitted rate of change for PV collectors. There is not a common rule for all of them, in fact, nowadays there are some TSO's which do not contemplate this problem in their grid codes. However, in some countries like Mexico, which has the most restrictive scenario [7], the ramp rate

This work was supported by Grant MCINN-22-TED2021-129796B-C21 funded by MCIN/AEI /10.13039/501100011033, by the European Union NextGenerationEU/ PRTR and by the Principality of Asturias, FICYT, FEDER funds under Grant SV-PA-21-AYUD/2021/57546.

979-8-3503-1644-5/23/$31.00 ©2023 IEEE

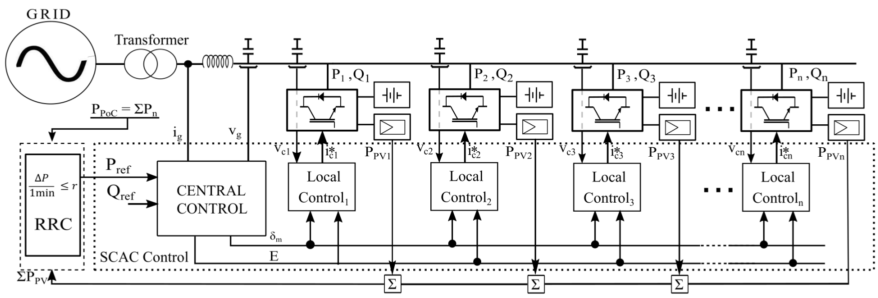

Fig. 1. Virtual synchronous generator scheme with n-PV plants and batteries, working with a ramp-rate compensation method.

TABLE I
RR RESTRICTIONS FOR RELEVANT COUNTRIES AND REGIONS. ORDERED FROM MORE TO LESS RESTRICTIVE.

Mexico	Atlanta (USA)	Puerto Rico (USA)	Germany
$1\%/min$	$3.3\%/min$	$10\%/min$	$10\%/min$

(RR) limit is set to $1\%/min$. This means that the PV power only can vary 1% of this rated power from one minute to the next one. Other countries such as Puerto Rico [8] or Germany [6] grid codes, are a bit less restrictive. Table I shows a summary for some relevant countries and regions. Other TSO's are also concerned about this matter, with even more restrictive ramp rates [9]. The RR limit of $10\%/min$ will be the basis for the development of this paper. In order to allow ramp-rate limitations, PV collectors are required to have some additional reserve power. This can be achieved by local energy storage systems (ESS). The most used technology being Li-ion batteries thanks to their technical development, performance and continuous decrease in prices [10]. These ESS solutions allow to absorb or inject power rapidly in order to compensate the possible ramp-rate violation.

For traditional PV ramp-rate control strategies, there are normally two types, which are the classical ramp-rate control [4] and the moving average filter [11], although other kind of techniques are being developed currently. For this paper, the classical RR strategy is proposed for eliminating these kind of fluctuations

The RR mitigation design is an economic decision having which need to be carried out during the PV collector design stage to properly size the ESS meeting the RR requirements. As explained, the RR constraints depend on the country-level or region-level grid-code directives. In the case RR violations occur, penalty fees will be applied to the PV plant operator.

Taking into account what has been discussed above, it is crucial to carry out an economic study in order to verify not only the effectiveness of these systems to reduce RR penalties, but also to size them in an optimal direction. For this, LCoE is often used. It represents the sum of the costs of an energy generation asset during its lifetime.

So in this paper, the integration of a RR method within an aggregated VSG will be implemented. The proposal includes an adaptive weight distribution technique for the ESS power delivery based on a variable virtual admittance technique. The proposal is analyzed from a techno-economic perspective by using the LCoE as an indicator.

.

In the following sections, the main content of the paper will be developed. In Section II, the explanation of the smoothing method using for compensating the ramp variations will be explained. In Section III, the explanation about how the VSG control system is operated together with the ramp-rate compensation method is explained. Simulation results will be presented in order to validate the idea in Section IV. Following, in Section V, the use of the LCoE for determining the economical impact of the proposed control system is included. Finally, in Section VI, the main conclusions of the article will be exposed.

II. RAMP RATE METHODS

Currently, there is no consensus on the calculation method to obtain the RR violation from the TSO side, so different ramp-rate calculation methods are reported. Literature collects different approaches to overcome the RR violations, such as: moving average (MA), which is the most extensively used; exponential moving average (EMA); or method based on low-pass-filters (LPF) [6]. Additionally, it has to be considered that the method can be dependent on the grid code from the country where the plant is installed.

The RR violation range can be computed by using instantaneous values or per minute values. However, for the development of this paper a system similar to Puerto Rican or Germany grid codes, with a maximum variation of 10%/min is used. In these grid codes, the RR violation is calculated with a time window of 60 s, according to (1). It is important to note that 10% is calculated for the total amount of installed power of the PV collectors.

$$RR(t) = \frac{P_{PoC}(t) - P_{PoC}(t-60)}{t(t) - t(t-60)} \tag{1}$$

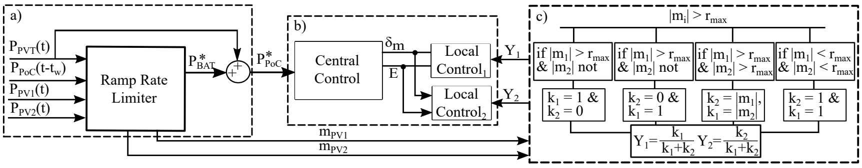

Fig. 2. a) Ramp-rate limiter algorithm, as presented in Section II. b) SCAC controller. c) Virtual admittance calculator, where the algorithm in Section II is implemented.

where $P_{PoC}(t)$ and $t(t)$ are the grid power and time at the current instant and the index $(t-60)$ represents the time interval 60 seconds ago.

The proposed strategy attenuates the fluctuations of the power injected into the grid (P_{PoC}) during a predefined time window (normally 1 minute), evaluating the PV power variation in order to inject or absorb power when the predefined RR limit (r_{max}) is exceed. This strategy allows direct control of the ramp rate in contrast to other techniques. This will allow injecting or absorbing power from the ESS when it is strictly necessary, resulting in a lower cycling of the batteries [4].

a) Description of the method: As it was aforementioned, TSOs normally impose the time window (t_w) for deciding if there is a violation or not. However, a quicker RR evaluation is in here considered by using a lower time window ($t_w = 12$ s). The algorithm is executed at half the window size (t_s = 6 s), thus allowing to obtain the values of $P_{PV}(t)$ and $P_{PoC}(t-t_w)$ to be compared against the ramp rate limit [12], [13].

The method can be summarized in the following statements:

- If P_{PV} increases too fast, the ESS will absorb the excess of power ($P_{bat} < 0$), so P_{PoC} will comply to the maximum ramp rate.
- Otherwise, if P_{PV} decreases too fast, in this case the battery will deliver the lack of power ($P_{bat} > 0$) so P_{PoC} will comply to the minimum ramp rate.
- If $P_{PV}(t) - P_{PoC}(t-t_w)$is within the ramp rate limitation, the battery will not inject power ($P_{bat} = 0$).

In this paper, the investigation is directed to incorporate the RR compensation strategy within a VSG control scheme while evaluating the performance of the RR compensation method simultaneously with the VSG control when grid-frequency deviations occur.

III. VSG-based ramp-rate compensator

VSG approaches arise to mitigate lack of inertia in modern high-populated DER grids, emulating the dynamics of a real or arbitrary synchronous generator (SG) in a power converter [2], [3]. That virtual inertia is normally implemented through ESS along power converters and a suitable control mechanism, providing certain amount of inertia for a given time.

For this paper, the Synchronous Central Control (SCAC) strategy is used, which proposes to simultaneously drive several converters, emulating an unique SG in the Point of Coupling (PoC), giving rise to an aggregated VSG [14], [15]. This concept introduces the idea of a single virtual rotor emulated at the PoC, where the electromechanical model of the SG is considered, emulating the inertia and damping response at the PoC. This structure makes possible to control the power exchange (both active and reactive power) by the TSO, for injecting/absorbing power or for frequency support from an external control system (see Fig. 1), regardless of the distances among local converters due to the use of the virtual admittance concept [14]. This is the key point for the implementation of RR mechanisms, because through a simple power set-point (calculated by the RR method), the power ramps at the PoC can be smoothed easily without losing the ability of frequency compensation. The integration of both control systems is depicted in Fig. 2, where the RR limiter block is connected to the SCAC controller as it has been aforementioned. Furthermore, the virtual admittance concept, that determines the proportion of power each converter can deliver, can be used for a local adaptive ramp compensation at each PV collector. This is implemented by modifying the value of the admittance depending on the local RR violations. Fig. 2 c), shows a flowchart for the admittance calculation considering two converters. It can be described as:

- If the slope for one PV panel exceeds the limit (r_{max}), and the other not, during this event, the total amount of power is delivered by the local converter. The local converter is the converter which is close to the PV generation where the ramp is violated.
- If none PV panel surplus the limit, the admittances are set fairly (k_n = 1).
- Otherwise, if both converters exceed the limits, the calculation is done by weighting the slopes ($k_n = |m_n|$).
- In case of having more than two converters, the algorithm can be calculated using a small truth table (1-0) to select the cases in a simple way.

This variable virtual admittance concept is following evaluated in the simulation results sections. In Section V, the cost-effectiveness of this method is also evaluated using the proposed LCoE metric.

IV. Simulation Results

Simulation results are presented in this section. Grid and VSG models are taken from [14], where the SCAC idea was first published. In this case the model includes two PV DEGs connected to a grid, considering a battery locally connected

TABLE II
SCAC PARAMETERS AND SET-POINTS FOR THE SIMULATION.

Variable	Value	Variable	Value
$H(s)$	10	τ	1
S_n (kVA)	20	Z_v	$8.014\angle 3.4$
Pn_{PV}/PV $(kW$	28	r_{max} $(\%/min)$	10

to each one. This element will provide/absorb energy for RR compensation and for frequency support. The simulated system is similar to the one shown in Fig. 1, but considering two PV collectors and their respective ESS.

The PV profile is extracted from a real plant in Oruro, Bolivia, down-scaled for simulation and final paper validation. However, the simulation is done in per unit (pu) values, so it can be scaled to any value. The base power is 56 kW, for the PV installation. Those profiles are displaced 20 minutes in order to emulate the cloud evolution in the sky of a larger solar plant. Taking into account the RR violation is at PoC level, the RR limit is 10%. Main simulation parameters are given in Table II.

a) Ramp rate simulation: In this subsection the classical ramp rate strategy is applied in order to smooth the ramps of the PV collector. A small zoom of the PV profiles for each PV collector are presented in Fig. 3 a). In Fig. 3 b), the power injected at the PoC is depicted. The resulting power without the RR compensation method is labelled as P_{Gr}, while the corrected one is P_{Gc}. As it was explained in Section II, the algorithm compensates the ramps when they exceed the ramp limitation. In Fig. 3 c) the limits (yelow and purple discontinue lines) , the ramp for total PV power r_{pv} and the ramp for PoC power r_G are depicted. It can be seen r_G is within the limits. Fig. 3 d) shows the power injection by each battery. As it has been told, these batteries will inject more or less power depending on the PV collector that violates the ramp conditions represented in Fig. 3 e), that considers the $10\%/min$ limit with respect to the nominal power of each of them. So, the virtual admittance values will vary (see Fig. 3f)).

b) Frequency compensation by VSG: In this subsection, a grid frequency variation is forced, in order to see the simultaneous operation with the ramp controller. As it can be seen in Fig. 4, even when a frequency variation appears (see a)), the power ramps are compensated by the ramp-rate violation. Fig. 4b) shows the ramp evolution that during the frequency event violates the restriction. Fig. 4c) depicts the power evolution of each ESS. However, the SCAC prioritizes the frequency compensation. In Fig. 4 d), the ramp rate variation are shown in Fig. 2. Those PV ramp power variations are used for computing the admittance weights which manage the injected power by the ESS.

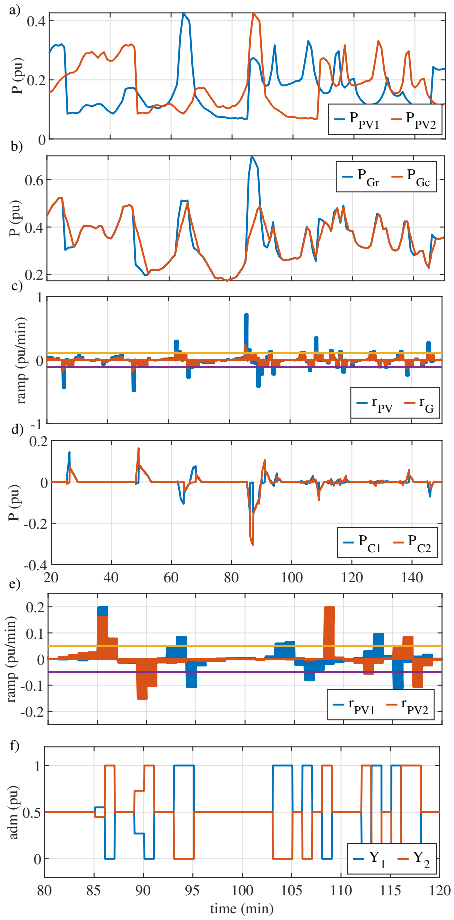

Fig. 3. a) Active power injected by each PV collector. b) P_{PoC} injected to grid. P_{Gc} is by applying the ramp rate compensation (ΣP_{PVn}) and P_{Gr} without. c) power ramp for PV power (r_{PV}), and ramp for P_{PoC} (r_G) and the limits. d) Injected power for each battery (P_{C1} and P_{C2}). e) Power ramps for each PV collector and the limits. f) Virtual admittance calculation for each converter. Y_1 is the admittance calculated for P_{C1}. Y_2 is the admittance calculated for P_{C2}. e) and f) have a small to better see the variation of ramp and admittance.

V. Levelized Cost of Energy

The inclusion of a RR mitigation strategy is mainly an economical decision that must be taken during the design stage of the PV plant. So, it is critical to determine the size of the ESS in order to meet the requirements for RR compensation, keeping the cost as low as possible.

The LCoE index will be determined for this application, considering the incorporation of the RR method described in Section IV by means of using a variable admittance compensating the RR violation locally. Also, same index will be obtained with the incorporation of the RR method but maintaining a constant admittance and delivering the same

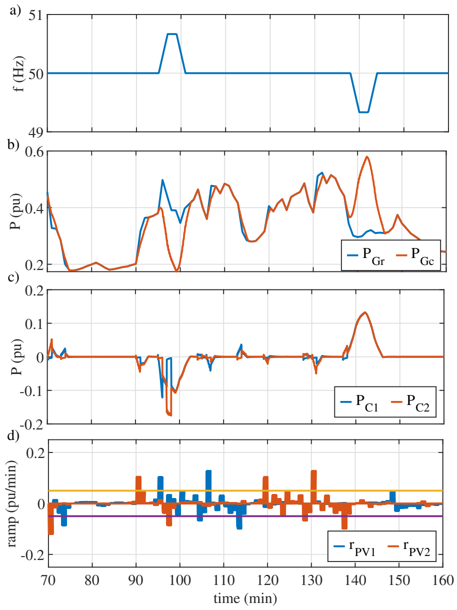

Fig. 4. a) Positive grid frequency variation at 94 min and negative grid frequency variation at 138 min. b) P_{PoC} injected to grid. P_{Gc} is the PoC injected power by applying the ramp rate compensation and P_{Gr} without, trying to compensate the frequency variation. c) Injected power for each battery (P_{c1} and P_{c2}). d) RR variation at each PV collector to calculate the Y admittance.

TABLE III
LCoE TERMS.

Type	I [€/kW]	$O\&M$ [€/kW/year]	N [year]	C_{dis} C_{ch}	η [%]
$PV_{utility}$	800	11.5	25	-	[18]
LFP	400	8.2	12	$1.2-1$	92

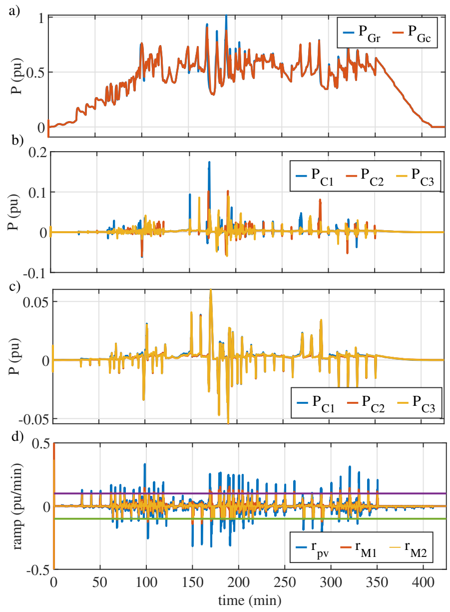

Fig. 5. a) Power profile with and without ramps. P_{Gr} is the power with RR correction, and P_{Gc} is the power without RR correction. Data in pu. For analysis lets assume a 50MW base power. b) Power demand of batteries for case with varying admittance. P_{C1}, P_{C2}, P_{C3} is the power injected for each converter respectively. c) Power demand of batteries for case with constant admittance. P_{C1}, P_{C2}, P_{C3} is the power injected for each converter respectively. Same power for all of them. d) Ramp violations for the PV power injection without RR (r_{pv}), with RR at constant admittance (r_{G1}), and varying admittance (r_{G2}).

energy of all ESS. Finally, the LCoE is obtained considering the non-inclusion of any compensation method. With these indexes, in summary, the proposed metric looks for a trade off between ESS operation, installation costs and the penalization costs because of RR violations.

With the aim to obtain the LCoE index, some parameters must be computed, considering the characteristics of the system. In order to analyse the minimum required ESS, the associated PV plant costs, C_{PV},(2), and the ESS, C_{ESS} (3), are considered in the $LCoE$ (4) [16]. CP_V includes the annual investment cost (I_{PV}) considering the PV plant investing stage, the fixed operation and maintenance costs ($O\&M$) and the annual charge due to RR violations (RR_c). The charge associated with the violation of the RR is estimated to be $10cents/s/MWp$, where MWp is the installed power of the plant [17]. So taking into account the maximum power of this plant, it corresponds to 5 €/s [17].

C_{ESS} considers the energy storage installation cost (I_{ESS}) which includes the associated cost of the ESS power conversion stage, considering a dc-link coupling mechanism, common cost for grid connection among others [1], [5], and its $O\&M$ annual costs. In the present case I_{ESS} investments are assumed to be during the first year of operation. However, $O\&M$ are paid with some interests.

$$C_{PV} = \sum_{k=1}^{k=N_{PV}} \frac{I_{PV} + O\&M_{PV} + RR_c}{(1+r)^k} \tag{2}$$

$$C_{ESS} = \sum_{k=1}^{k=N_{PV}} \frac{I_{ESS} + O\&M_{ESS} + Ch_{ESS}}{(1+r)^k} \tag{3}$$

$$LCoE = \frac{C_{PV} + C_{ESS}}{\sum_{k=1}^{k=N_{PV}} \frac{E_{grid}(1-d)^k}{(1+r)^i}} \tag{4}$$

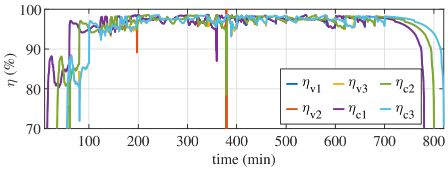

Fig. 6. Computed efficiency taking into account the efficiency curve of the power converter used for each PV string and ESS. η_{v1}, η_{v2}, η_{v3} are the efficiency for P_{C1}, P_{C2} and P_{C2} taking into account variable admittance. Average efficiencies are 87.2885%, 87.2871% and 87.2815% respectively. η_{c1}, η_{c2}, η_{c3} are the efficiency for P_{C1}, P_{C2} and P_{C2} taking into account constant admittance. Average efficiencies are 87.2471%, 87.2195% and 87.2533% respectively.

The discount rate r considered in (4) is 4% [19]. N is the technology lifespan and E_{grid} is the grid energy injected in the year base-case presented. Furhtermore, the PV system is expected to degrade each year at a rate d equal to 0.8% [20]. Regarding battery technology, a LFP cathode battery is assume for the application, because it has a cheaper price in terms of energy. Table III shows the LCoE parameters for the PV and the battery.

To calculate the LCoE, a daily the profile shown in Fig. 5 a) will be assumed and repeated along the years used for the economic study. This power profile is the same than the one in Section IV, but extended for a complete day, with a total energy production of around 7 hours. The data is calculated in pu, but for the analysis, a base power of 50 MW will be assumed, for the entire power plant. In this case, the simulated system replicates the one in Section IV, but using three PV strings, converters and their respective ESS. In addition, in order to observe the behavior of the system operating at constant admittance and at variable admittance, the results of power injection by each one of the converters are presented in Fig. 5 b) and c). It can be seen in b) that the power at variable admittance changes as needed, and in c) it is the same for all converters. In addition, it can be seen in Fig. 5 d) how the ramps of the PV collectors vary, violating the 10% norm, and by introducing the compensation method, these violations drop drastically.

The data from Fig. 5 b) and c), beside the power injected by each PV string is used for calculating the power injected to the grid. However that power is ideal without considering power converters. So the total amount of power generated by the PV system beside the efficiency of both methods (variable and constant admittances) will be computed taking into account the efficiency curve of the power converter from [18], assuming that the efficiency (η) curve belongs to the power inverter and DC/DC converter. Then, η is calculated in Fig. 6, for each PV string and battery. Table IV show the average η values, showing a best performance in the variable admittance case. Note that in this case feeder impedance is considered.

It must be accounted this example is only for demonstration purposes, so the batteries are sized taking into account the energy demand of each day. Taking into account these data, and by using the aforementioned formulas the LCoE can be computed approximately. Table V shows the calculation results of the LCoE, taking into account the data from Fig. 5. As can be seen in the Table IV, the ramp-rate violations (RR_c) are reduced by 90% and 80% using a variable RR and constant RR admittance method respectively, with respect to no use none. Having a lower expense for ramp violations, as well as less time breaking the rule. The variable admittance method is more economical by calculating the LCoE index. Also, as explained, Y_v is more efficient. From here it arises an interesting optimization problem for the calculation of the Y_v value. Depending on the line impedances connecting each collector to the PoC and the ramp violation location, the Y_v should be optimally calculated. This is concern of future research by the authors.

TABLE IV
EFFICIENCY RESULTS FOR VARIABLE (Y_v) AND CONSTANT (Y_c) ADMITTANCE METHODS.

Y_v			Y_c		
η_{v1}	η_{v2}	η_{v3}	η_{c1}	η_{c2}	η_{c3}
87.48	87.42	87.39	87.34	87.37	87.36

TABLE V
ECONOMICAL RESULTS FOR THE APPLICATION WITHOUT RR COMPENSATION, WITH RR AND CONSTANT ADMITTANCE (Y_c), AND RR WITH VARYING ADMITTANCE (Y_v).

Cases	ESS [MW]	$LCOE$ [€/MWh]	t_{RR} [s]	RR_c [M€]
PV		74.22	841	30711
PV+ESS+Y_c	4.95	57.61	161.5	5897
PV+ESS+Y_v	5.61	56.44	89.23	3257

VI. CONCLUSION

This paper has proposed the inclusion of a ramp-rate compensation method within an aggregated virtual synchronous generation technique, fulfilling both working principles. Simulation results are presented showing a satisfactory response for both operation modes. Furthermore, an economical study has been conducted, taking into account the LCoE figure. It has been demonstrated that the ramp-compensation technique implies a real saving of money, especially when handling larger amounts of energy. Even in the absence of a more in-depth study, it is considered that the proposed method, based in variable admittances is more economical than using classical constant approach. Moreover, during the efficiency analysis performed to be used in the LCoE calculation, it has been demonstrated that the variable admittance method has a higher efficiency for a given converter.

REFERENCES

[1] F. Durakovic, "Levelized cost of electricity of renewable energy technologies as a criterion for project prioritization," 2021.
[2] H. Bevrani, B. François, and T. Ise, *Microgrid dynamics and control*. John Wiley & Sons, 2017.
[3] H. Bevrani, T. Ise, and Y. Miura, "Virtual synchronous generators: A survey and new perspectives," *International Journal of Electrical Power & Energy Systems*, vol. 54, pp. 244–254, 2014.

[4] A. Gonzalez-Moreno, J. Marcos, I. de la Parra, and L. Marroyo, "A pv ramp-rate control strategy to extend battery lifespan using forecasting," *Applied Energy*, vol. 323, p. 119546, 2022.
[5] I. Peláez Acedo, C. Blanco Charro, A. Suárez González, Á. Navarro Rodríguez, P. García Fernández *et al.*, "Levelized cost of energy optimization in hybrid pv plants by energy storage for ramp-rate control operation," in *2021 IEEE energy conversion congress and exposition, ecce 2021-proceedings*, 2021.
[6] J. Martins, S. Spataru, D. Sera, D.-I. Stroe, and A. Lashab, "Comparative study of ramp-rate control algorithms for pv with energy storage systems," *Energies*, vol. 12, no. 7, p. 1342, 2019.
[7] D.-D. O. de la Federación, "Resolución por la que la comisión reguladora de energía expide las reglas generales de interconexión al sistema eléctrico nacional para generadores o permisionarios con fuentes de energías renovables o cogeneración eficiente. consultado el 20 de marzo de 2018," 2012.
[8] V. Gevorgian and S. Booth, "Review of prepa technical requirements for interconnecting wind and solar generation," National Renewable Energy Lab.(NREL), Golden, CO (United States), Tech. Rep., 2013.
[9] R. Piwko *et al.*, "Interconnection requirements for variable generation," *North American Electric Reliability Corporation (NERC), Atlanta, GA, USA, Tech. Rep*, vol. 19, 2012.
[10] D. Cormode, A. Lorenzo, W. Holmgren, S. Chen, and A. Cronin, "The economic value of forecasts for optimal curtailment strategies to comply with ramp rate rules," in *2014 IEEE 40th Photovoltaic Specialist Conference (PVSC)*. IEEE, 2014, pp. 2070–2075.
[11] J. Marcos, I. De la Parra, M. García, and L. Marroyo, "Control strategies to smooth short-term power fluctuations in large photovoltaic plants using battery storage systems," *Energies*, vol. 7, no. 10, pp. 6593–6619, 2014.
[12] E. Bullich-Massagué, M. Aragüés-Peñalba, A. Sumper, and O. Boix-Aragones, "Active power control in a hybrid pv-storage power plant for frequency support," *Solar Energy*, vol. 144, pp. 49–62, 2017.
[13] D. Lin, X. Li, S. Ding, and Y. Du, "Strategy comparison of power ramp rate control for photovoltaic systems," *CPSS Transactions on Power Electronics and Applications*, vol. 5, no. 4, pp. 329–341, 2020.
[14] C. Verdugo, A. Tarraso, J. I. Candela, J. Rocabert, and P. Rodriguez, "Centralized synchronous controller based on load angle regulation for photovoltaic power plants," *IEEE Journal of Emerging and Selected Topics in Power Electronics*, vol. 9, no. 1, pp. 485–496, 2020.
[15] D. Del Rivero, P. G. Fernández, C. Blanco, and Navarro-Rodríguez, "Control of aggregated virtual synchronous generators including communication delay compensation," in *2022 IEEE Energy Conversion Congress and Exposition (ECCE)*, 2022, pp. 1–7.
[16] C. S. Lai and M. D. McCulloch, "Sizing of stand-alone solar pv and storage system with anaerobic digestion biogas power plants," *IEEE Transactions on Industrial Electronics*, vol. 64, no. 3, pp. 2112–2121, 2017.
[17] D. Cormode, A. Lorenzo, W. Holmgren, S. Chen, and A. Cronin, "The economic value of forecasts for optimal curtailment strategies to comply with ramp rate rules," in *2014 IEEE 40th Photovoltaic Specialist Conference (PVSC)*, 2014, pp. 2070–2075.
[18] W. E. Boyson, G. M. Galbraith, D. L. King, and S. Gonzalez, "Performance model for grid-connected photovoltaic inverters." Sandia National Laboratories (SNL), Albuquerque, NM, and Livermore, CA …, Tech. Rep., 2007.
[19] D. Lin, X. Li, S. Ding, and Y. Du, "Strategy comparison of power ramp rate control for photovoltaic systems," *CPSS Transactions on Power Electronics and Applications*, vol. 5, no. 4, pp. 329–341, 2020.
[20] D. C. Jordan, S. R. Kurtz, K. VanSant, and J. Newmiller, "Compendium of photovoltaic degradation rates," *Progress in Photovoltaics: Research and Applications*, vol. 24, no. 7, pp. 978–989, 2016.

C.3 Control of Green Hydrogen Production on Isolated Hybrid Solar Plants Considering the Effect of Communications.

Control of Green Hydrogen Production on Isolated Hybrid Solar Plants Considering the Effect of Communications

Daniel del Rivero
dept. of Electrical Engineering
University of Oviedo
Gijón, Spain
riverodaniel@uniovi.es

Ángel Navarro-Rodríguez
dept. of Electrical Engineering
University of Oviedo
Gijón, Spain
navarroangel@uniovi.es

Carlos Gómez-Aleixandre
dept. of Electrical Engineering
University of Oviedo
Gijón, Spain
gomeztcarlos@uniovi.es

Cristian Blanco
dept. of Electrical Engineering
University of Oviedo
Gijón, Spain
blancocristian@uniovi.es

Pablo García
dept. of Electrical Engineering
University of Oviedo
Gijón, Spain
garciafpablo@uniovi.es

Pedro Rodriguez
Luxembourg Institute Science and Technology (ICES)
Technical University of Catalonia (SEER)
University of Luxembourg (SnT)
pedro.rodriguez@list.lu

***Abstract*—This paper investigates the feasibility and operational considerations of green hydrogen production in islanded hybrid photovoltaic (PV) plants. These plants operate exclusively during daylight hours, using solar energy as the main source. To mitigate power fluctuations in PV generation, a battery energy storage system (BESS) is integrated to supplement the plant's power during periods of low solar irradiation. Key considerations include the operation of power converters via communication links, specifically addressing the challenges associated with communication delays. These delays will be managed to minimise their impact on system stability. In this study, voltage commands will be sent remotely and used to calculate power references locally to feed the loads. Additionally, the challenges that arise when working with commercial converters that only allow the reception of active and reactive power commands are highlighted. Strategies are discussed to maintain system stability and optimise the performance of the hybrid plant, ensuring efficient and reliable operation. This work contributes to the technical knowledge necessary for the development green hydrogen production through distributed generation plants.**

***Index Terms*—Electrolyzer, Green Hydrogen, Virtual Synchronous Generator, Communication delay, Smith predictor**

I. Introduction

The utilization of solar photovoltaic (PV) energy for green hydrogen production emerges as a key solution in the quest for a cleaner and more sustainable energy matrix. This innovative method involves using PV plants to drive water electrolysis processes, yielding green hydrogen devoid of carbon emissions, thus contributing significantly to mitigating greenhouse effects [1], [2]. Green hydrogen finds versatile applications across various sectors. It plays an important role in transportation, where it can power fuel cell vehicles, offering a zero-emission alternative to traditional fossil fuels. In the industrial sector, green hydrogen can serve as a feed-stock for various chemical processes, reducing the carbon footprint of manufacturing operations. Moreover, in power generation, green hydrogen can be used in fuel cells or combined with natural gas to enhance the sustainability of the energy mix [3], [4] The process of producing green hydrogen leverages renewable energy sources and abundant water resources, ensuring long-term energy security and diversification [5]. This is particularly important in the current context of finite fossil fuel reserves and the need for energy systems that are resilient to geopolitical and environmental uncertainties. Furthermore, because of the growing concern about climate change and the urgent need to reduce greenhouse gas emissions. Therefore, the green hydrogen production and utilization align with global efforts to transition towards a cleaner and more sustainable economy, reducing greenhouse gas emissions.

This paper proposes a control scheme for the production of green hydrogen by using solar energy, primarily through an isolated hybrid microgrid comprising PV generation and battery energy storage systems (BESS), where one converter is fed by a battery and the other is assumed to be fed by a hybrid PV with dc coupling. This microgrid considers a central controller, which remotely controls the entire power plant, taking into account the different limitations due to the variability of the solar production. In Section II, the system plant is described, where the central controller will manage the power distribution among the converters, via local controllers.

The present work has been partially supported by the Spanish Ministry of Economy and Competitiveness funded by MCIN/AEI/10.13039/501100011033 under Grants MCINN-23-PID2022-139479OB-C22, MCINN-22-TED2021-129796B-C21, in part by the European Union NextGenerationEU/PRTR and by the Principality of Asturias, FICYT, FEDER funds under Grant SV-PA-21-AYUD/2021/57546. Also this work was supported partially funded by EV-Hubs – Spanish Research Agency - PID2022-142372OB-C21, and the European Commission under project iSTENTORE HORIZON-CL5-2022-D3-01 with ID-101096787 and We-Forming HORIZON-CL5-2022-D4-02-04 with ID-101123556.

Considering the isolated condition, grid-forming operation is considered by the PV and BESS power converter control, while the electrolyzer is the system main load, neglecting any other ancillary load. With this setup, detailed in Section III, it is underscored the importance of the Virtual Synchronous Generator (VSG) architecture in maintaining the grid stability while adapting power reference to available resources.

Additionally, the control is communications-based, which reduces the number of sensors which requires addressing communications delays and signal reconstruction challenges [6], [7]. As this control system is communication-based, it is needed a way to compensate possible delays that can appear in the system, in order to ensure the stability of the system. Moreover, the electrolyzer will feature a droop control, discussed in Section III alongside the VSG system, to adjust energy consumption based on grid power limitations. Finally, Section IV will present simulation results to enhance understanding of the discussed concepts. Finally, Section V is concluding the paper.

II. System Description

This section provides a description of the different components of the microgrid system, considering PV generation, BESS and the electrolyzer system. Those elements are depicted in Fig. 1.

The figure shows different control layers distinguishing between external and internal control. Starting with the external control layers, the central controller located at the point of connection (PoC) between the two distributed generators and the electrolyzer, whose functionalities will be explained in Section III and also explained in [7], [8], will calculate the polar voltage values. Those values will be sent via MODBUS TCP, to the local controllers associated to each converter. There, the received commands feed a virtual impedance model that calculates the Active and Reactive power setpoints for the inner loops of the converter, and inject the necessary power into the grid.

The considered power plant is based on a hybrid PV plant, with dc-coupled BESS, and an inverter based BESS. In here is remarkable also the fact that an ac grid is used to interconnect the electrolyzer with the energy resources. Although a DC grid interconnection would present clear benefits for this application, nowadays there are not suitable commercial alternatives for DC connection of hybrid PV plants.

In the proposed system, to mitigate the additional installation costs associated with measurement sensors (see Fig. 2 a)), internal variables accessible within the converters (such as frequency, RMS voltages, active and reactive power) will be leveraged. These variables can be transmitted via communication protocols, enabling their reconstruction and integration into the control system (see Fig. 2 b)). Such variables are standardized and included in the SunSpec DER specification [9].

The power converters are driven by the local controllers, which deliver the active and reactive power commands (see Fig. 2 c)). These power set-points are calculated assuming as a main constraint the use of commercial inverters, only relying on external calculated active and reactive power commands. For that, as it can be seen in the figure, the output voltage of each converter, and the reference current calculated by the local controllers are used.

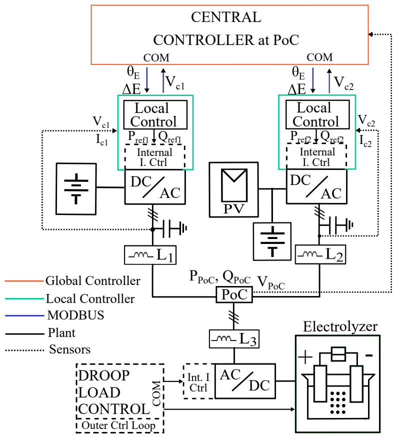

Fig. 1. Topology of the proposed green hydrogen generation system (GHGS), with PV generation and dc-coupled BESS operating in grid-forming to create the grid that feeds the electrolyzer.

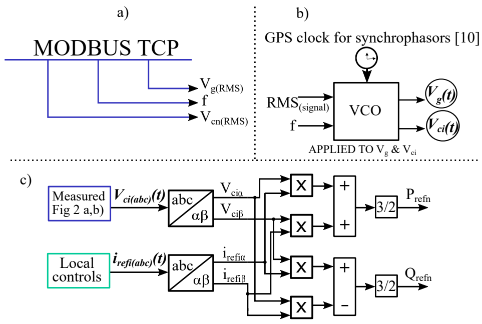

Fig. 2. a) MODBUS TCP frequency and RMS voltage. b) instantaneous values from the RMS voltage, frequency, and clock signal obtained by a VCO (Voltage Controller Oscillator) [10]. c) Active and reactive reference power calculation.

These converters are strategically distributed at varying distances from the PoC, collectively forming a resilient and adaptable grid which is important for the operation of the electrolyzer. This integrated approach ensures seamless operation and scalability while minimizing costs associated with additional sensors and hardware.

The central controller serves as the nerve center, dynamically adjusting the frequency and voltage references, that will

TABLE I
SYSTEM PARAMETERS

Variable	Value	Variable	Value	Variable	Value
V_g	400 V	C_{filter}	200 μF	H	10 s
S	8 kVA	R_p	0.01	τ	1
f	50 Hz	R_v	2.2918Ω	L_v	0.0218 H
y_1	0.6	y_2	0.4	I_v	$2\pi 2$
L_1	$10\mu H$	L_2	$10\mu H$	L_3	$10\mu H$
R_1	$10\mu\Omega$	R_2	$10\mu\Omega$	R_3	$10\mu\Omega$

be used in the local controllers for computing the power references based on real-time generation levels. For that, the control system will employ a distributed VSG architecture, based in Synchronous Central Angle Controller (SCAC), which could control multiple converters, emulating a single synchronous generator at the PoC, resulting in an aggregated VSG [6], [7] creating, in this case, an isolated grid. The main simulation parameters are shown in Table I, where S is the rated power of the converters, H is the emulated inertia, R_p is the droop slope (δ_f/δ_P), τ is the damping factor, R_v and L_v are the resistance and inductance of the virtual admittance respectively. y_1 and y_2 the corresponding weights of the virtual admittances for each converter and I_v is the gain of the integral voltage controller. Also the parameter of the lines are included.

In the case of the load, which has been explained to be an electrolyzer used for the generation of green hydrogen, it is noted to have relatively slow dynamics and its behaviour can be varied depending on the energy available in the system. The operating dynamics of the electrolyzer is characterised by a time constant of 2.85 s. This value has been derived from the dynamic model of an electrolyzer, as detailed in [11], [12]. This dynamic model is based on the Randles-Warburg electrical equivalent circuit, which is widely used to represent the electrochemical behaviour of electrolyzers.

Furthermore, the inclusion of a VSG method not only assists in establishing a grid with a certain level of inertia, thereby enhancing system stability, but also enables automatic adjustment of the energy consumed by the electrolyzer based on voltage and frequency readings, through the incorporation of a dual droop system. These considerations will be further expanded upon in Section III.

III. Control System

The proposed control system is based on a distributed VSG concept for driving the PV and BESS converters, taking into account the possible communication delays can appear in the system, whilst a dual power-frequency and power-voltage droop control are used at the electrolyzer level. The main idea is to make a functional grid-forming control system in the generation units and a flexible controller at the load units, so the hydrogen production can be adapted to the generation levels, thus helping in the system stability.

A. Virtual Synchronous Generator

Considering what has been explained previously, the control system represented in Fig. 3 is applied to drive the entire

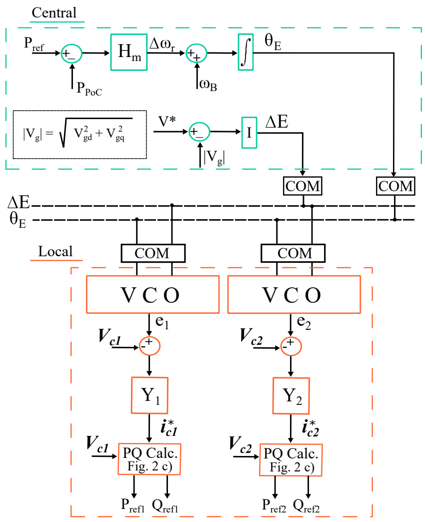

Fig. 3. SCAC control structure for grid-forming converters. Light Blue: Global controller. Light Orange: Local controllers.

power plant. This control structure is based on the SCAC-VSG scheme, which simultaneously drives several converters, emulating a unique Synchronous Generator (SG) in the PoC, giving rise to an aggregated VSG. This concept presents the idea of a single virtual rotor, emulated at the PoC, where the electromechanical model of the SG is considered (central control architecture). Hence, the SG inertia and damping response are emulated at the PoC. In the case of this paper, it is based on 2-aggregated power converters, however it can be expanded to n-converters.

In recent research, the SCAC system of this article has been implemented in grid-feeding/supporting systems. However, in this paper, modifications have been implemented in the voltage calculation loop to adapt it to a grid-forming control structure. The proposed control system alternative replace the reactive power droop control loop by the direct calculation of the stators' voltage module. In this manner, the voltage magnitude in PoC can be manipulated through an integral controller [7], [13].

As can be seen in the Fig. 3, the stator voltage is sent from the central controller in polar coordinates (stator angle θ_e and voltage magnitude ΔE) to each of the converter's local controllers, via MODBUS TCP. Those voltage components are obtained from the PoC voltage loop, and the VSG dynamic model. These polar voltage components are used to drive the Voltage Controlled Oscillator (VCO), computing the local stator voltage, which, subtracted from the voltage at the converter terminals, gives the voltage drop across the virtual impedance of the VSG. By using the virtual admittance concept, the

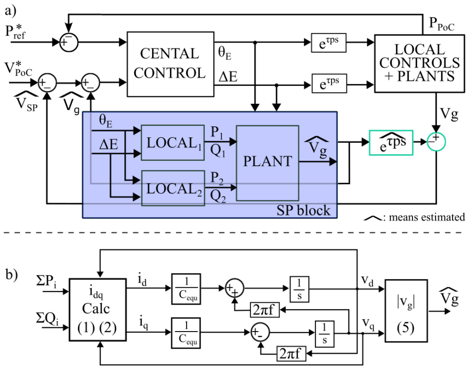

Fig. 4. a) Central controller with S.P architecture for 2-converters with voltage delay compensation [7]. b) Voltage at PoC estimation for SP.

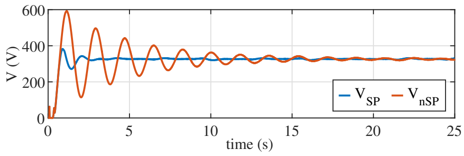

Fig. 5. Grid voltage envelope created by microgrid at PoC with and without SP, by using a delay of 300 ms.

reference current to drive the converter are obtained. These admittances (Y_i) can be used to select the weight of the power share in each of the converters.

At the local converter control system, these values are transformed into active and reactive power set-points, as illustrated in Fig. 3. Finally, these set-points are sent to the internal converter control, responsible of the close-loop reference tracking.

As mentioned before, this system is designed for an application where instantaneous voltage and current readings from the converters are not available, necessitating control and readings through communications. The available measurements by the communication link are the terminal RMS voltage at each converter, grid frequency and active and reactive power (see Fig. 2 a). As instantaneous voltage values are needed for the control system, these must be reconstructed from RMS and frequency values, as shown in Fig. 2 b).

B. Communication delays treatment

Since the system is based on communications, it will be subject to communication delays that may cause the control system to become unstable, thus necessitating compensation. Therefore, the Smith predictor (SP) compensation method [14] has been chosen, as depicted in Fig. 4 a). It illustrates that the angle and voltage computed by the central controller are subject to delays, and by employing a model of the local control and plants, these delays can be compensated for. The delay compensation will be carried out only for the voltage control loop, and not at the active power control loop. This is because although it is a variable load, which will depend on the existing generation level, this variation is very slow and does not have much effect on the control system. In order to do so, as it can be seen in 4, two replicas of the local controllers are used in the SP, using the scheme from Fig. 4 b), in order to estimate the voltage at the PoC. Those replicas are used to calculate the active an reactive set-points of each converter. The references are transformed into currents by using (1) and (2). However, the voltage value that will be used for the calculation is the estimated voltage at PoC that comes from equations (3) and (4). Once this is done, (5) is used to calculate the voltage module to be used in the SP compensation.

Although the system stability withstands relatively high values of the communication delay without compensation, increased delay values have been used to test the system behavior under certain conditions that can show-up in a real application. Fig. 5 shows the evolution of the voltage envelope by using a delay of 300 ms, by applying S.P. or without. As it can be seen, a noticeable compensation effect clearly improves the transient response when the SP is considered.

$$i_d = \frac{2(Pv_d + Qv_q)}{3(v_d^2 + v_q^2)} \tag{1}$$

$$i_q = \frac{2(Pv_q - Qv_d)}{3(v_d^2 + v_q^2)} \tag{2}$$

$$\frac{dv_d}{dt} = \frac{id}{C_{equ}} + \omega v_q \tag{3}$$

$$\frac{dv_q}{dt} = \frac{iq}{C_{equ}} - \omega v_d \tag{4}$$

$$|V_g| = \sqrt{v_d^2 + v_q^2} \tag{5}$$

C. Droop Control of Electrolyzer

As mentioned above, a minor adaptation is implemented in the control system of the electrolyzer to obtain a better adaptability of the energy to the power available in the grid. It is known that this type of load is mainly constant, in order to get the greater amount of hydrogen, but it is expected to vary according to the demand and the power available in the grid. There are different kind of controllers to make the electrolyzer behaving as a flexible load as in [15]. However in this case,

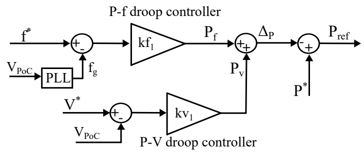

Fig. 6. Proposed dual-droop controller.

a dual frequency and power voltage droop is implemented [16], as shown in Fig. 6. A dual droop has been selected to make the system more flexible to any variation in generation, allowing operation, although more variable, also more stable. These droops come into effect when the frequency or voltage of the grid changes due to a mismatch between the power generated and consumed, resulting from a decrease in the power generated by any of the converters. In normal situations, when there is no significant frequency or voltage variation, the implemented scheme remains inactive. However, when the available power decreases, both frequency and voltage drop, leading to a reduction in the electrolyzer's power consumption.

This adjustment is critical to ensure grid stability while sustaining hydrogen production, allowing the electrolyzer to operate as a flexible load. The droop control parameters in this system are kf_1 = 100 W/V and kv_1 = 600 W/Hz. These parameters have been selected to enable proper system operation. In future research, more realistic and studied droop values will be explored to optimise the performance of the system.

The principle of operation of this dual droop controller will be demonstrated in Section IV, where detailed results and analysis will be presented. This adaptation allows a dynamic response to power variations, ensuring that the electrolyzer effectively contributes to the stability of the power system. By adjusting consumption according to power availability, the system increases resilience to unforeseen fluctuations in power generation.

IV. Simulation Results

In this section, simulation results are presented in order to demonstrate the performance of the proposed system. The results are presented with a reference frame set by a base scenario in which the generation capability is enough to supply the load. From there, applying limitations in the generation capability, the effect of the the dual V-f droop to improve system stability. All the simulation results are presented, taking into account a communication delay between the central and local controller of 160 ms, which is in the range of typical values found in industrial applications.

A. Base case. Normal operation

The simulation results of the nominal operation of the system are depicted in Fig. 7. In this simulation, the hybrid PV is used for creating the ac grid to feed the electrolyzer. Fig. 7 a) shows the three-phase grid voltage established by the two converters. In this simulation, these two converters share the power delivered to the load by using different weights in their control, with 0.6 pu for converter 1 and 0.4 pu for converter 2. The virtual admittance values are updated based on the selected sharing weights, as explained in [7]. As it can be seen in Fig. 7 b) and c), the electrolyzer starts to demand power, so the power converters start to inject the shared power to feed the load.

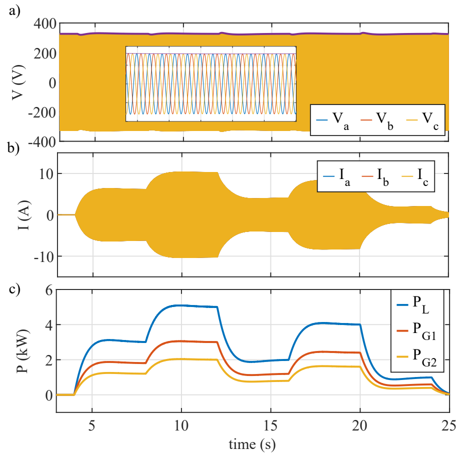

Fig. 7. Nominal operation: a) PoC voltage. b) Injected current by converters. c) Injected power by converters with weights between both of 0.6 and 0.4, converter 1 and converter 2 respectively.

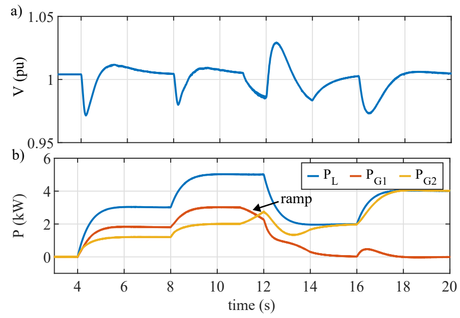

Fig. 8. Limitation case: a) PoC voltage magnitude. b) Load power and power supplied with a weight distribution of 0.6 and 0.4. When a PV ramp appears, the ESS compensates the lack of PV power.

B. Limited generation case

This simulation presents the common case where the power of one of the converters is limited for various reasons. In this particular case, a drop in the generation of converter 1, which corresponds to the PV-hybrid converter, is considered. This generation drop occurs due to a ramp-down event, which can be triggered by varying environmental conditions, such as passing clouds or a sudden drop in temperature.

As depicted in Fig. 8 a) shows the voltage created by the microgrid, which barely varies in this case and in b), when the ramp-down event in generator 1 appears at 11 s. Under those circumstances, the BESS plays an important role, compen-

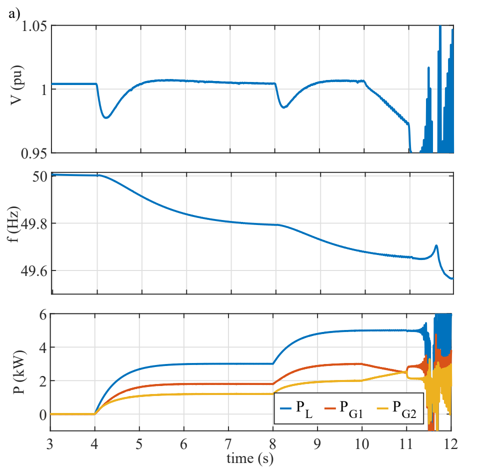

Fig. 9. Unstable case: a) Module of voltage, which is unstable when the generators have a lack of power to feed the load. b) Load and converter powers with a ramp in PV generation, which is too big, making the system unstable.

sating the generation decrease of the PV-hybrid converter by increasing its energy injection to maintain supply to the load. This dynamic response of the batteries is essential to ensure stability and continuity of power supply in situations where primary generation is intermittent or undergoes significant fluctuations.

C. Unstable case

In this case, shown in Fig. 9, the main reason for the implementation of the dual droop concept in the electrolyzer is demonstrated. This idea becomes essential in scenarios where there is a very abrupt ramp in the solar generation, or when the battery cannot deliver the necessary balancing power to the system due to its own limitations, such as being partially discharged.

In such circumstances, the system cannot meet the power demand, leading to instability. This situation can be clearly seen in Fig. 9. In a), the system voltage up to the point of instability is shown, illustrating how abrupt fluctuations can affect system stability. In b), the power injected or absorbed by each of the power converters is shown, providing a detailed view of how each component of the system responds to variations in generation and demand.

The implementation of the dual droop concept in the electrolyzer mitigates these instability issues. By dynamically adjusting the operation of the electrolyzer in response to sudden changes in solar generation or battery capacity, the system can maintain a more stable and reliable power supply, as will be demonstrated in the next subsection.

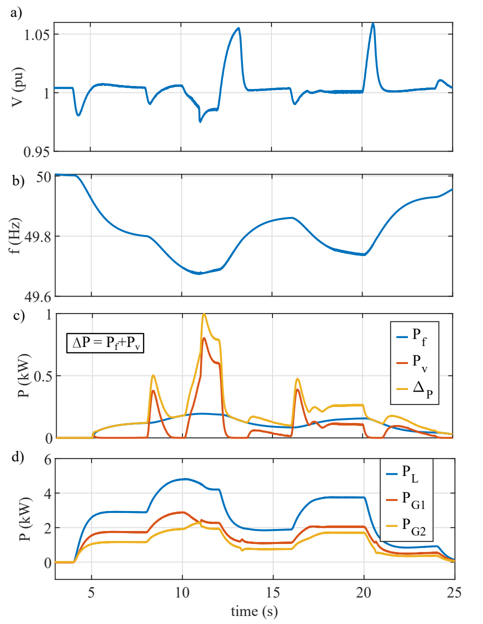

Fig. 10. Ramp limitation with electrolyzer droop controller: a) Module of voltage at load level used for droop control. b) PV panel ramp generation in converter 1, compensating the power for the battery and reducing the load power as a flexible load. c) frequency variation used for droop control. d) Δ_P which is subtracted to the load set-point, in order to keep the stability of the system.

D. Ramp limitation with droop controller

To mitigate the unstable operating region, the proposed dual droop control is introduced. The results of this implementation are shown in Fig. 10, where the effect of the dual frequency and voltage droop can be observed.

As mentioned before, the inclusion of this droop is used to safeguard the grid stability by adjusting the load consumption as a flexible load when one or more converters cannot deliver the required power to the load. In Fig. 10, several key aspects of this process are presented.

In a), the system voltage variation is observed. This variation is critical to understanding how fluctuations in generation or consumption affect voltage stability. In b), the frequency variation of the grid is depicted. Frequency fluctuations are equally important, as they can indicate instabilities in generation or power demand. These voltage and frequency variations are read by the electrolyzer, which feeds them into the droop controller to modify the load consumption. This mechanism allows the electrolyzer to act adaptively, responding to changing system conditions to maintain stability. In c), the powers calculated by the system can be seen. These powers are

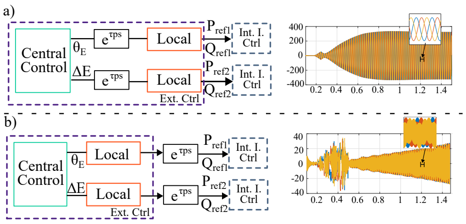

Fig. 11. a) Control structure sending θ_e and ΔE, computing power set-points in local controllers at converter level. b) Control structure sending active and reactive power from global controller.

subtracted from the power limit of the electrolyzer, which allows the consumption to be adjusted precisely according to the current operating conditions.

Finally, in Fig. 10 d), the effect of a ramp on the PV generation is depicted. This ramp alters both the grid voltage and frequency, which in turn modifies the power command of the electrolyzer. This adaptive behaviour is crucial to maintain grid stability in the face of rapid and unexpected fluctuations in renewable energy generation.

The implementation of dual droop control proves to be an effective strategy for managing system stability in the presence of significant variations in generation and consumption. By allowing dynamic adjustments in load consumption, it ensures that the system can operate stably and efficiently, even under challenging conditions.

E. Additional considerations

One of the critical points for the correct system operation, was the selection of the references sent from the central controller to the local controllers. Two alternatives approaches can be used, as shown in Fig. 11: 1) polar coordinates (ΔE and θ_e) or, 2) rectangular coordinates (P_{ref}, Q_{ref}). A preliminary numerical evaluation has been carried out under the simulation environment for the two options. The obtained results are shown, respectively, in Fig. 11 a) and b). As it can be seen, the use of polar coordinates leads to an stable operation, whereas the rectangular ones can not guarantee it. Not obvious reasons have been found about this behavior, being currently under study.

V. Conclusion

This paper has proposed a centralised control structure based on distributed VSGs to operate multiple converters, creating a stable network for green hydrogen production. The implementation of this system is based on the use of communications for the integration with the local converter control system. This approach reduces the need for physical sensors, but introduces the challenge of communication delays.

The delay effect has been addressed by compensation techniques to improve the stability of the control system, using the Smith predictor. In addition, a local dual droop control has been incorporated at the electrolyzer side, which allows that in an event of a generation variation, due to an energy mismatch, the energy consumption of the electrolyzer varies taking into account variations in voltage and frequency, acting as a flexible load.

In addition, several possibilities have been tested in global control, such as sending voltage levels in rectangular coordinates to a local controller or sending the reference power directly from the global controller, taking into account communication delays. It is only stable when the voltage is sent and not the power, for no obvious reason. This behavior is currently under study.

References

[1] S. E. Hosseini and M. A. Wahid, "Hydrogen from solar energy, a clean energy carrier from a sustainable source of energy," *International Journal of Energy Research*, vol. 44, no. 6, pp. 4110–4131, 2020.

[2] L. Palma, B. Molina, and A. Díaz, "Design and sizing of power conversion system with energy storage for improved pv-electrolyzer energy coupling," in *2023 International Conference on Clean Electrical Power (ICCEP)*, 2023, pp. 784–788.

[3] D. Guilbert, M. Zasadzinski, H. Rafaralahy, and L. Boutat-Baddas, "Modeling of the dynamic behavior of a pem electrolyzer," in *2022 10th International Conference on Systems and Control (ICSC)*, 2022, pp. 78–84.

[4] C. Wang, Y. Hao, G. Han, C. Zhou, and C. Wang, "Coordinated scheduling of integrated energy systems with hydrogen electrolyzer units," in *2022 IEEE/IAS Industrial and Commercial Power System Asia (ICPS Asia)*, 2022, pp. 546–550.

[5] X. Yan, X. Zhang, C. Gu, and F. Li, "Power to gas: addressing renewable curtailment by converting to hydrogen," *Frontiers in Energy*, vol. 12, pp. 560–568, 2018.

[6] C. Verdugo, A. Tarraso, J. I. Candela, J. Rocabert, and P. Rodriguez, "Centralized synchronous controller based on load angle regulation for photovoltaic power plants," *IEEE Journal of Emerging and Selected Topics in Power Electronics*, vol. 9, no. 1, pp. 485–496, 2020.

[7] D. d. Rivero, P. García, C. Blanco, and Navarro-Rodríguez, "Control of aggregated virtual synchronous generators for pv plants considering communication delays," *IEEE Transactions on Industry Applications*, pp. 1–13, 2024.

[8] W. Zhang, A. M. Cantarellas, J. Rocabert, A. Luna, and P. Rodriguez, "Synchronous power controller with flexible droop characteristics for renewable power generation systems," *IEEE Transactions on Sustainable Energy*, vol. 7, no. 4, pp. 1572–1582, 2016.

[9] S. Alliance, "Sunspec specification - sunspec der information model specification," https://sunspec.org/, 2019.

[10] K. E. Martin, "Synchrophasor measurements under the ieee standard c37. 118.1-2011 with amendment c37. 118.1 a," *IEEE Transactions on Power Delivery*, vol. 30, no. 3, pp. 1514–1522, 2015.

[11] M. Rubio, A. Urquia, and S. Dormido, "Diagnosis of pem fuel cells through current interruption," *Journal of Power Sources*, vol. 171, no. 2, pp. 670–677, 2007.

[12] C. A. Martinson, G. Van Schoor, K. Uren, and D. Bessarabov, "Characterisation of a pem electrolyser using the current interrupt method," *International journal of hydrogen energy*, vol. 39, no. 36, pp. 20 865–20 878, 2014.

[13] H. Bevrani, B. François, and T. Ise, *Microgrid dynamics and control*. John Wiley & Sons, 2017.

[14] A. Mirzal, "Delay compensation using the smith predictor: a brief review with numerical examples," *International Journal of Computer-aided Mechanical Design and Implementation*, vol. 3, no. 1, pp. 1–8, 2017.

[15] B. Guha, R. Jain, and S. Veda, "Bulk grid frequency support using electrolyzers," in *2020 IEEE Industry Applications Society Annual Meeting*. IEEE, 2020, pp. 1–5.

[16] S. Akkari, J. Dai, M. Petit, and X. Guillaud, "Interaction between the voltage-droop and the frequency-droop control for multi-terminal hvdc systems," *IET Generation, Transmission & Distribution*, vol. 10, no. 6, pp. 1345–1352, 2016.

C.4 Real-Time Cosimulation of Power Systems Integration of eMEGASIM and ePHASORSIM Using OPAL-RT Simulators.

Real-Time Cosimulation of Power Systems: Integration of eMEGASIM and ePHASORSIM Using OPAL-RT Simulators

Daniel del Rivero
dept. Electrical Engineering
University of Oviedo
Gijón, Spain
riverodaniel@uniovi.es

Shailendra Singh
Luxembourg Institute of
Science and Technology (LIST)
Luxembourg
shailendra.singh@list.lu

Pablo García
dept. Electrical Engineering
University of Oviedo
Gijón, Spain
garciafpablo@uniovi.es

Pedro Rodríguez
Luxembourg Institute of
Science and Technology (LIST)
Luxembourg
pedro.rodriguez@list.lu

***Abstract*—This article presents a real-time cosimulation between two OPAL-RT simulators, utilizing the eMEGAsim system for simulations in the time domain and the ePHASORsim system for simulations in the phasor domain. It focuses on simulating a distributed Virtual Synchronous Generator control system with real power converters connected to a power system, facilitated by the interface through a high-speed DOLPHIN communication cable. The control system and interface configuration for cosimulation are detailed, along with the results obtained from the simulations. This real-time cosimulation approach provides an effective tool for the analysis and development of control systems in power environments.**

***Index Terms*—Virtual Synchronous Generator, Real-time simulation, Co-simulation, OPAL-RT**

I. Introduction

In recent years, there has been a significant increase in the number of power converters and generation elements, such as photovoltaic (PV) systems, wind generation, offering improved Levelized Cost of Electricity (LCOE) indices [1]. These new Distributed Energy Generation (DEG) facilities are mainly based on Renewable Energy Sources (RES). This surge implies a gradual replacement of conventional generation plants with renewable generation systems. While this shift aids in reducing pollution levels, greenhouse gas emissions going to a more environmentally friendly approach [2]. However, it also poses additional challenges in power systems that must be addressed. These emerging challenges arise from the increase in the weakness of energy systems, resulting from the decrease in the inertia present in the network, traditionally provided by Synchronous Generators (SG) with rotating mass, compared to the inertia provided by systems based on power converters, which is significantly lower or absent [1], [3], [4]. The absence of both inertia and damping in power converters can threaten the stability of the power grid. Consequently, various control strategies are imperative to counteract this inertia reduction and, to some extent, emulate the behavior of synchronous generators [5]. Considering this, it's now acknowledged that the design of grid-forming and grid-supporting services is crucial, especially with the substantial integration of Distributed Energy Generation (DEG) units, whose aggregated capacities rival traditional power plants [6]–[8]. This is where the concept of Virtual Synchronous Generator (VSG) approach arises. For the power electronics-based DEG/RES units, this control strategy allows for the emulation of dynamic characteristics, addressing the aforementioned challenges [3], [4].

The virtual inertia concept is realized through the integration of energy storage systems (ESS), power converters, and appropriate control mechanisms, which contribute a specific amount of inertia typically ranging from milliseconds to several seconds. This establishes the foundation for extensive integration of Virtual Synchronous Generators (VSG) into Renewable Energy Systems (RES) without compromising system stability. While various VSG techniques have been explored in literature [1], [6], [7], this paper adopts the strategy outlined in references [6] and [9].

The Synchronous Central Control (SCAC) strategy proposes synchronizing multiple converters to emulate a single synchronous generator (SG) at the point of connection (PoC), creating an aggregated Virtual Synchronous Generator (VSG). This approach introduces the concept of a unified virtual rotor, emulated at the PoC, where the electromechanical model of the SG is considered (central control architecture). Consequently, inertia and damped response are replicated at the PoC. This control structure enables the system operator to manage power exchange (both active and reactive) at the PoC, regardless of the distances between local converters, allowing for energy distribution under various operation modes (e.g., power and frequency support) independently for each converter. Further details on both central and local control systems can be found in the literature [9], [10].

This inertia emulation control system will be incorporated into the control system of switched power converters connected to real high-power grids. However, accurately emulating its behavior through traditional offline simulations is not

The present work has been partially supported by the Spanish Ministry of Economy and Competitiveness funded by MCIN/AEI/10.13039/501100011033 under Grants MCINN-23-PID2022-139479OB-C22, MCINN-22-TED2021-129796B-C21, and in part by the European Union NextGenerationEU/PRTR.

feasible, as simulating such large systems can lead to numerical problems like runtime and convergence errors, especially when detailed models are used. Therefore, to test it, real-time simulations are proposed to enhance accuracy. These types of simulations are commonly used to employ real hardware to improve system accuracy, with rapid control prototyping, as well as to utilize detailed models for large-scale electrical grids research.

This paper utilizes the real-time simulation OPAL-RT to perform real-time simulation of power grids with integrated power converters. As the number of inverters increases, so does the calculation time, potentially reaching the limit for real-time operation. To accelerate calculations, two approaches are proposed: parallel computing, where the main calculation system is divided into subsystems, and the use of acceleration elements from the OPAL-RT library, such as the ARTEMiS toolbox. Additionally, two extended methods are introduced to further speed up simulations: co-simulation [11], which combines detailed equivalent models (DEM) or average value models (AVM) with phasor models (PM) [12], [13]. The OPAL-RT simulation modules ePHASORSIM and eMEGASIM can simulate large-scale overlapping grids in the phasor domain and DEM power converters, respectively, and interacting between them. Thus, this paper will be focused on the co-simulation strategy, where a real power system will be simulated in real time by using PM, and this will interact with real models of power converters in order to check their interaction and proper functioning of the control system, allowing the obtaining of certain phasor results, with certain dynamics included by the time-domain simulation, and vice versa. Furthermore, a small explanation about how to perform these kind of simulation is done in section III. The results of the real-time simulation will be demonstrated through some simulations in section IV.

II. Models

In this section, the employed systems for real-time simulations (VSG and KUNDUR2AREA) are described. These systems will be elucidated by focusing on their most representative parameters, aiming for simple understanding.

A. VSG converter

The power converters to be used for simulation in the time domain are controlled by an inertia emulation system called SCAC. This system will control two battery converters distributed in a microgrid connected to a KUNDUR grid. Both converters have the same power, filters, and transformers, but are located at different distances from the connection point, considering different feeder impedance. This control system features a virtual admittance (Y_i) characteristic that can be utilized to distribute the injected power generation among different converters, depending on their respective rated power. This is done by applying different weights on the admittance. Fig. 2 illustrates a schematic of the distribution of these systems (a), as well as the control system implemented within

TABLE I
Power converter and VSG parameters.

POWER CONVERTER				VSG	
Variable	Value	Variable	Value	Variable	Value
Converter				Control system	
$Power$	100 kVA	V_{DC}	750 V	H	10 s
f_{sw}	3.150 kHz	V_{AC}	400	S_n	200 kVA
Filter				K_p	0.1
L_{f1}	777 μH	R_d	0.5 Ω	τ	1
L_{f2}	200 μH	C	66 μF	f	50 Hz
Transformer				R_v	1.5 Ω
V_1	400 V	V_2	20 kV	X_v	0.7709 Ω
Lines				Y_1	0.4 %
L	0.76 H/km	R	0.61 Ω/km	Y_2	0.6 %
$Line_1$	0.6 km	$Line_2$	1 km	V_g	400 V

TABLE II
KUNDUR 2 AREAS PARAMETERS

Generator Parameters			
X_d=1.8	X_q=1.7	X_l=0.2	X'_d=0.3
X'_q=0.55	X''_d=0.25	X''_q=0.25	R_a=0.0025
T'_{d0}=8.0 s	T'_{q0}=0.4 s	T''_d=0.03 s	T''_{q0}=0.05 s
A_{Sat}=0.015	B_{Sat}=9.6	Ψ_{T1}=0.9	k_D = 0
H=6.5 (for G_1 and G_2)		H=6.174 (for G_3 and G_4)	
Line Parameters			
Impedances	r=0.0001pu/km	x_L=0.001pu/km	b_C=0.00175pu/km
Powers and voltages			
G_1	P=8 pu	Q=2.86 pu	E_t=1.03∠20.2°
G_2	P=8 pu	Q=4.28 pu	E_t=1.01∠10.5°
G_3	P=7.16 pu	Q=2.48 pu	$E_t = 1.03\angle-6.8°$
G_4	P=7 pu	Q=3.49 pu	$E_t = 1.01\angle-17°$
Bus 7	P_L=8.56 pu	Q_L=0.59 pu	Q_c=0 pu
Bus 8	P_L=2.99 pu	Q_L=0.59 pu	Q_c=0 pu
Bus 13	P_L=22.73 pu	Q_L=1.15 pu	Q_c=0 pu
BASE			
S	100 MVA	V	20 kV

it [10] in b). Furthermore, in Table I, the different parameters for the converter simulation are described.

B. Kundur 2 Areas model

The grid employed for the phasor simulation is known as the 2-area Kundur system. This system emulates the electrical grid with two distinct areas, each resembling real-world power systems. These areas are interconnected by a weak tie, mimicking the connections found in actual power networks. Within each area, there are two power units, each boasting a rating of 900 MVA and operating at 20 kV. In addition, transmission lines are working at 230 kV. This setup reflects the typical configuration of power generation units in large-scale electrical grids. For further details and specifications of this system, please refer to the provided reference [14], also in Table II, the main parameters of the grid are presented. The simulated converters in eMEGASIM are included in the model within the bus 8 of Fig. 3.

III. Simulation process

Two OP5600 simulators have been used for simulations, as shown in Fig. 1, controlled by Matlab version 2017a and OPAL RT-LAB version 2019.2.3.176. Each simulator will run a different type of simulation. In the case of the OP5600 slave, the simulation will run on eMEGASIM, and in the

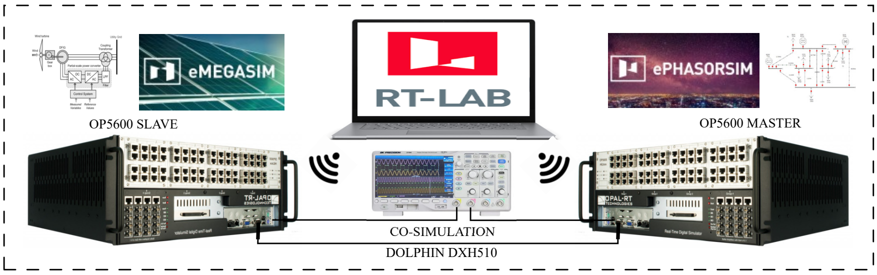

Fig. 1. Co-simulation structure with both simulators. Each of them will simulate one part of the system. The Master will simulate the ePHASORSIM simulation, and the slave will simulate the eMEGASIM simulation.

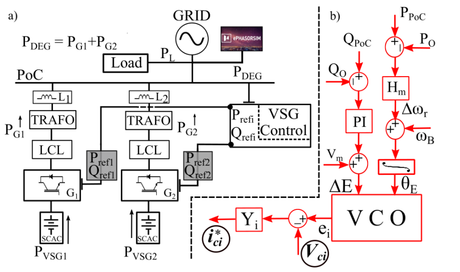

Fig. 2. a) Power converter distribution scheme connected to grid simulated by ePHASORSIM. b) SCAC control system [10].

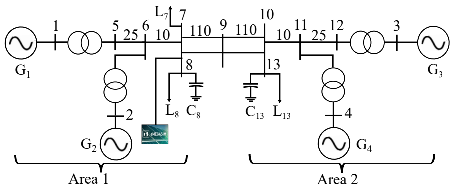

Fig. 3. Kundur's two-area system used for simulating the power grid with ePHASORSIM. Example 12.6 in [14]. The distances between buses are in km.

case of the master, the simulation will run on ePHASORSIM. Both simulations will be synchronized using the DOLPHIN $DXH510$ communication cable. As is depicted in Fig. 4 a), to perform any simulation on any of the simulators, it is needed to follow the model structure. The model in each simulator, must include a subsystem called "SM_NAME", where M, besides S indicates that it is the master model, and slave model respectively. From here, the monitoring signals will go to "SC_NAME", where the real-time signals can be monitored. Furthermore, this same system can also be used as a simulation control, sending different setpoints to the simulated model, changing parameters in real time. Considering this, a brief explanation of each simulator as well as the interface is performed in this section, to merge both in an unique model of co-simulation, explaining the procedure.

A. *eMEGASIM*

EMEGASIM is a real time simulator from OPAL-RT Technologies. This simulator is a tool specifically designed for the analysis and simulation of power systems in real time. With the ability to simulate complex electric power systems, including distribution grids, transmission systems and renewable energy generation, eMEGASIM is widely used in research, development and validation of electric power technologies [15]. It is important to highlight, that for performing a real-time simulation its mandatory to use a discrete simulation with the POWERGUI block.

B. *ePHASORSIM*

EPHASORSIM is a real-time simulator also developed for OPAL-RT Technologies. This simulator is used for carrying out real-time simulation of electrical power systems based on phasors [16]. It allows to model and analyse those system in large-scale, including transmission and distribution lines, as well as including different generation elements. This tool can be crucial in the research and development of different technologies. To perform a simulation in ePHASORSIM, the model of the grid must be included in the ".xls" template with the input and outputs of the system, and a ".raw" file with all the characteristics of the system, and it must be included in the solver RT-LAB block to work (this configuration will depend on the simulator version). The model initialization block is important to include all the simulation characteristics and parameters of both simulations. In Fig. 4 a), a scheme example is shown.

C. *Dolphin interface*

Dolphin interface ($DXH510$) is a technology used for real-time simulations, as the OPAL-RT simulators, in order to facilitate the co-simulation of complex systems. This interface builds a bridge between different simulators, allowing the

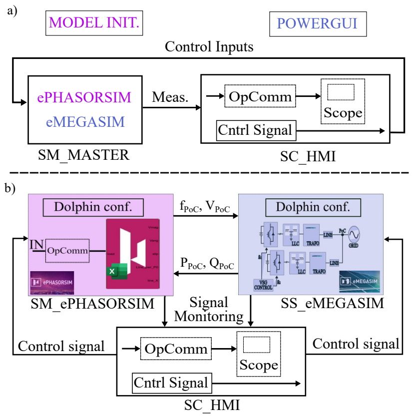

Fig. 4. a) Real-time simulation structure for eMEGASIM or ePHASORSIM, using POWERGUI and Model Initialization blocks respectively. b) Co-simulation structure with a Master subsystem based in ePHASORSIM and a Slave subsystem based in eMEGASIM. Both subsystem will share data through the Dolphin interface. Furthermore, the SC_HMI block will monitor some signals, and also it will send some set-points to the simulators.

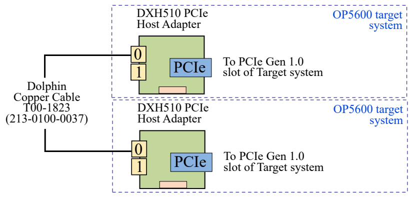

Fig. 5. Connection between the two OP5600 real-time simulator.

synchronization of data between them. In OPAL-RT context, $DXH510$ is used for integrating real-time control systems with models of electrical power systems. To configure Dolphin, it is important to make the physical connection between both simulators correctly, following the instructions provided in the OPAL-RT manuals. A small scheme of the connection is depicted in Fig. 5.

D. Co-simulation

In order to carry out the co-simulation between the two simulators, specific steps must be followed. First, for the system addressed in this article, the structure depicted in Fig. 4 b) will be followed. In this environment, the master simulator is implemented in ePHASORSIM, which exchanges data with the slave simulator in eMEGASIM through the Dolphin interface, as previously mentioned. Due to both systems are set in parallel, a memory block it is needed at the output of each subsystem to allow a propper simulation.

The signals from both systems are monitored by the HMI subsystem, which sends the setpoints to both simulators. As shown in Fig. 4 b), to construct the power grid voltage in eMEGASIM and feed the simulation in the time domain, V_8 is read from bus 9, as well as the frequency at that point. In addition, the power injected to the PoC is sent to the PM to interact with the simulation.

In order to be able to run the simulation in real time, in addition to the configurations made so far, it is important to transfer the corresponding cluster information file, known as ”dishosts.conf”, to each of the ”etc/dis/” directories of both simulators. This configuration file is used to set some global interconnection properties and the position of each node within the interconnection topology used. It is crucial to use the same file on both simulators and to make sure that the IP addresses used in the file match the IP addresses of the simulators. Once this is done, the simulation can be run following the next steps:

1. Lunch RT-LAB 2019.2.3.176 in admin mode.
2. Check the Target number: $PFXXX - XXX - S01$ ($OPAL2$) and $PFXXX - XXX - S02$ ($OPAL1$) for both simulators.
3. Check the RT-LAB Version 2019.2.3.176 is installed in both targets.
4. Set the Real-time simulation mode to Hardware synchronized and Real-time communication link type to Dolphin under Execution Properties tab.
5. Assign the subsystems SM_ePHASORSIM to $OPAL2$ and SS_eMEGASIM to $OPAL1$. Make sure that XHP mode is enable for both nodes.
6. Load the model in RT-LAB and check the display tab for compilation.
7. Once the model is successfully loaded with no errors, execute the model.

IV. Simulation Results

In this section, some results obtained from the co-simulation between both simulators are presented, showing three scenarios such as: A) Power support, B) Frequency support and C) Voltage support. In each of them, the power converter is connected to the bus 8.

A. Power support

In this first scenario, the active and reactive power setpoints are set in order to control the power injected into the grid. To demonstrate one of the main features of the co-simulation, a phasor simulation has been performed in which only the bus voltages are shown. In ePHASORSIM, the load is modified without dynamics at the same timing, achieving practically same results in steady state as when introducing dynamics. This can be seen in Fig. 6 a) and b). In addition, Table III presents the steady-state results of p.u. voltages for three specific cases, using only phasor simulation and cosimulation: 1) when no power is injected, 2) when 100 kW of active power is injected, and 3) when 50 kVar of reactive power is injected. The result of this comparison is assumed to be the same for the other scenarios.

Fig. 6 a) and b) show the different mains voltages in p.u., with special attention to V_8, which is the voltage at

TABLE III
PHASOR VOLTAGES WITH PHASOR SIMULATION AND WITH COSIMULATION, ADDING CONVERTER DYNAMICS FOR CASES A AND B.

	Voltage		V_1	V_2	V_3	V_4	V_5	V_6	V_7	V_8	V_9	V_{10}	V_{11}	V_{12}
A	Phasor	1)	1.03	1.01	1.03	1.01	0.9921	0.9484	0.9138	0.9146	0.93	0.9593	0.9975	0.8785
		2)	1.0444	1.0243	1.0444	1.0243	1.0067	0.9618	0.9246	0.9255	0.9388	0.9714	1.0114	0.8775
		3)	1.0381	1.0183	1.038	1.0179	1.0029	0.9621	0.9304	0.9313	0.9364	0.9669	1.0057	0.8829
	Cosim	1)	1.03	1.01	1.03	1.01	0.9921	0.9484	0.9137	0.9145	0.93	0.9594	0.9976	0.8783
		2)	1.0443	1.0242	1.0442	1.0242	1.0065	0.9615	0.9245	0.9253	0.9387	0.9712	1.0112	0.8776
		3)	1.0379	1.0181	1.0377	1.0177	1.0027	0.962	0.9302	0.9311	0.9362	0.9667	1.0055	0.8830
B	Phasor	1)	1.0303	1.0103	1.0304	1.0104	0.9924	0.9488	0.9142	0.915	0.9304	0.9597	0.9978	0.8788
		2)	1.0141	0.994	1.0141	0.9942	0.9741	0.9292	0.8938	0.8959	0.9183	0.9449	0.9816	0.8738
		3)	1.0307	1.0107	1.0307	1.0107	0.9927	0.9491	0.9145	0.9153	0.9307	0.96	0.9961	0.8792
	Cosim	1)	1.0303	1.0103	1.0304	1.0104	0.9924	0.9487	0.914	0.914	0.9302	0.9596	0.9977	0.8786
		2)	1.014	0.994	1.014	0.994	0.974	0.929	0.8937	0.8957	0.9182	0.9448	0.9814	0.8736
		3)	1.0306	1.0106	1.0306	1.0106	0.9926	0.9490	0.9144	0.9151	0.9306	0.959	0.996	0.879

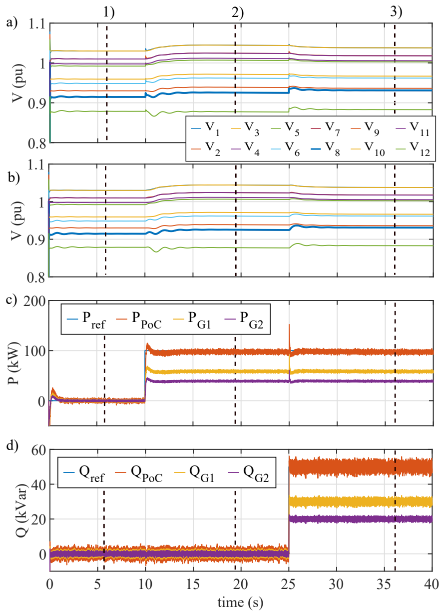

Fig. 6. a) Voltages in p.u. of all buses of KUNDUR2AREA model without cosimulation, just phasor simulation. b) Voltages in p.u. of all buses of KUNDUR2AREA model with cosimulation, introducing the dynamics of c) and d). c) Active power injection of VSG system. d) Reactive power injection of VSG system.

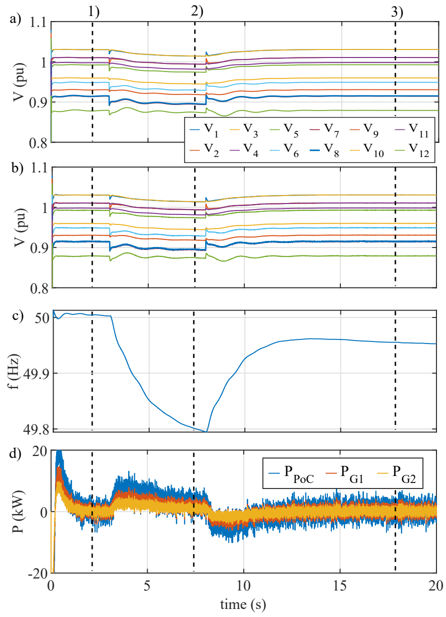

Fig. 7. a) Voltages in p.u. of all buses of KUNDUR2AREA model without cosimulation, just phasor simulation. b) Voltage in p.u. of all buses of KUNDUR2AREA model. c) Frequency variation provoked by a load change. d) Active power injection of VSG system.

the connection point of the power converter and is used to construct the local three-phase voltage used in eMEGASIM. As can be seen in Fig. b) and c), the injection of 100 kW of active power at 10 s and 50 kVar of reactive power at 25 s into the grid increases the voltage. As it was aforementioned, the power is oddly shared between the two converters, providing the first converter 60 %, and the second one the remaining 40 %, by means of the virtual admittance weights.

B. Frequency support

In this scenario a frequency variation is forced by a load variation in the grid. As case A, to demonstrate one of the main features of the co-simulation, a phasor simulation has been performed in which only the bus voltages are shown. Fig. 7 a) shows the voltage of each buses in a phasor simulation and b) in a co-simulation, with a special focus in V_8, which is the voltage where power converter is connected. However, in this case the dynamics does not change in excess, because

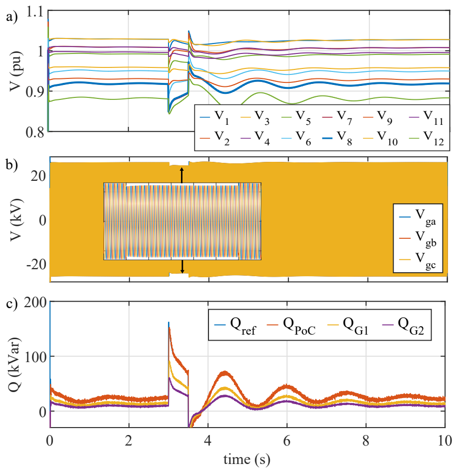

Fig. 8. a) Voltage in p.u. of all buses of KUNDUR2AREA model, where a 0.85 p.u. voltage sag appears. b) Actual voltage at the PoC in Volts. c) Reactive power injection due to the voltage variation.

the power injected in comparison with the grid power is very small. Table III shown the stationary voltage at different point, seeing that the final results are the same. There is a generalized decrease in voltage in the network, which also causes a reduction in frequency in it, as it is seen in c), where a negative frequency variation appears, which provokes that the VSG system injects some active power in order to try to compensate the variation, as it can be seen in d).

C. Voltage support

In this scenario, a voltage sag is induced in the power grid at 3 s with a duration of 0.5 s, aiming to verify the operation of the VSG control system. The control system until now had behaved like a grid feeding, however for voltage compensation, a Q-V droop must be included in the reactive loop, in order to inject reactive energy for voltage compensation, behaving as a grid-supporting controller. The Q-V droop used for this implementation following the equation (1).

$$V = (0.95 - \frac{0.95 - 0.85}{20 \cdot 10^4}(Q + 20 \cdot 10^4)) \cdot 400 \qquad (1)$$

As it can be seen in Fig. 8 a), the voltage evolution of all important buses are shown. Taking into account the bus under study, which is V_8. In Fig. 8 b), the three-phase PoC voltage is shown. As the Q-V droop controller is implemented, the system follows (1) to inject reactive power into the system to attempt to compensate for the voltage drop, as evident in Fig. 8c).

V. Conclusion

In this paper, the procedure for conducting a co-simulation between two OPAL-RT simulators is described. It considers the utilization of eMEGASIM (for detailed system simulation in the time domain) and ePHASORSIM (for phasor domain system simulation) together, enabling the simulation of large systems that would otherwise require significant real-time resource consumption, being able to add some dynamics to the phasor simulation. A small comparison between phasor simulation and cosimulation is done in cases A and B. Three base scenarios have been simulated: A) injecting arbitrary power into the grid; B) injecting active power for frequency compensation; C) injecting reactive power for voltage compensation.

For future work, the development of the simulated models can be extended to consider different contingencies and the grid-forming operation of the power converter under isolated bus conditions.

References

[1] F. Durakovic, "Levelized cost of electricity of renewable energy technologies as a criterion for project prioritization," 2021.

[2] C. A. Ogunbode, R. Doran, and G. Böhm, "Exposure to the ipcc special report on 1.5 c global warming is linked to perceived threat and increased concern about climate change," *Climatic Change*, vol. 158, pp. 361–375, 2020.

[3] H. Bevrani, B. François, and T. Ise, *Microgrid dynamics and control*. John Wiley & Sons, 2017.

[4] H. Bevrani, T. Ise, and Y. Miura, "Virtual synchronous generators: A survey and new perspectives," *International Journal of Electrical Power & Energy Systems*, vol. 54, pp. 244–254, 2014.

[5] A. Fernández-Guillamón, E. Gomez-Lazaro, E. Muljadi, and Molina-Garcia, *A Review of Virtual Inertia Techniques for Renewable Energy-Based Generators*, 05 2020.

[6] C. Verdugo, A. Tarraso, J. I. Candela, J. Rocabert, and P. Rodriguez, "Centralized synchronous controller based on load angle regulation for photovoltaic power plants," *IEEE Journal of Emerging and Selected Topics in Power Electronics*, vol. 9, no. 1, pp. 485–496, 2020.

[7] W. Zhang, A. M. Cantarellas, J. Rocabert, A. Luna, and P. Rodriguez, "Synchronous power controller with flexible droop characteristics for renewable power generation systems," *IEEE Transactions on Sustainable Energy*, vol. 7, no. 4, pp. 1572–1582, 2016.

[8] W. Zhang, A. Luna, I. Candela, J. Rocabert, and P. Rodriguez, "An active power synchronizing controller for grid-connected power converters with configurable natural droop characteristics," in *2015 IEEE 6th International Symposium on Power Electronics for Distributed Generation Systems (PEDG)*. IEEE, 2015, pp. 1–7.

[9] C. Verdugo, A. Tarraso, J. I. Candela, J. Rocabert, and P. Rodriguez, "Synchronous frequency support of photovoltaic power plants with inertia emulation," in *2019 IEEE Energy Conversion Congress and Exposition (ECCE)*. IEEE, 2019, pp. 4305–4310.

[10] D. d. Rivero, P. García, C. Blanco, and Navarro-Rodríguez, "Control of aggregated virtual synchronous generators for pv plants considering communication delays," *IEEE Transactions on Industry Applications*, pp. 1–13, 2024.

[11] F. Plumier, C. Geuzaine, and T. Van Cutsem, "A multirate approach to combine electromagnetic transients and fundamental-frequency simulations," 07 2013.

[12] N. Mohan, W. Robbins, T. Undeland, R. Nilssen, and O. Mo, "Simulation of power electronic and motion control systems-an overview," *Proceedings of the IEEE*, vol. 82, no. 8, pp. 1287–1302, 1994.

[13] T. Demiray, "Simulation of power system dynamics using dynamic phasor models," Ph.D. dissertation, ETH Zurich, 2008.

[14] P. Kundur, "Power system stability," *Power system stability and control*, vol. 10, pp. 7–1, 2007.

[15] O.-R. Technologies, "eMEGASIM," Recovered from: https://www.opal-rt.com/products/emegasim/, s.f.

[16] ——, "ePHASORsim," Recovered from: https://www.opal-rt.com/products/ephasorsim/, s.f.